CHAPTER 3
REACTOR

TABLE OF CONTENTS

			PAGE
3.0	**REACTOR**		3.1-1
3.1	**GENERAL DESIGN SUMMARY**		3.1-1
3.2	**DESIGN BASIS**		3.2-1
	3.2.1 PERFORMANCE OBJECTIVES		3.2-1
	3.2.2 DESIGN OBJECTIVES		3.2-1
	3.2.3 DESIGN LIMITS		3.2-1
		3.2.3.1 Nuclear Design Limits	3.2-1
		3.2.3.2 Reactivity Control Design Limits	3.2-2
		3.2.3.3 Thermal and Hydraulic Design Limits	3.2-2
		3.2.3.4 Mechanical Design Limits	3.2-2
		3.2.3.5 Fuel Assembly Design Limits	3.2-3
		3.2.3.6 Control Element Assembly Design Limits	3.2-4
	3.2.4 REFERENCES		3.2.5
3.3	**MECHANICAL DESIGN**		3.3-1
	3.3.1 SUMMARY		3.3-1
	3.3.2 CORE MECHANICAL DESIGN		3.3-1
		3.3.2.1 Fuel Rod Mechanical Design	3.3-1
		3.3.2.2 Burnable Poison Rod Mechanical Design	3.3-2
		3.3.2.3 Fuel Assembly Mechanical Design	3.3-3
		3.3.2.4 Control Element Assembly Mechanical Design	3.3-6
		3.3.2.5 Neutron Source Design	3.3-9
		3.3.2.6 Guide Tube Flux Suppressor Design	3.3-9
		3.3.2.7 Test Capsule Assembly Design	3.3-9
		3.3.2.8 ZIRLO Cladding (Westinghouse Fuel)	3.3-10
		3.3.2.9 M5 Cladding (AREVA/Framatome Fuel)	3.3-11
		3.3.2.10 Axial Blankets	3.3-11
		3.3.2.11 Radial Enrichment Zoning	3.3-11
	3.3.3 REACTOR INTERNAL STRUCTURES		3.3-11
		3.3.3.1 Core Support Assembly	3.3-12
		3.3.3.2 Core Support Barrel	3.3-12
		3.3.3.3 Core Support Plate and Support Column	3.3-13
		3.3.3.4 Core Shroud	3.3-13
		3.3.3.5 Flow Skirt	3.3-13
		3.3.3.6 Upper Guide Structure Assembly	3.3-13
	3.3.4 CONTROL ELEMENT DRIVE MECHANISM		3.3-14
		3.3.4.1 Design	3.3-14
	3.3.5 REFERENCES		3.3-16
3.4	**NUCLEAR DESIGN AND EVALUATION**		3.4-1
	3.4.1 SUMMARY		3.4-1

CHAPTER 3
REACTOR

TABLE OF CONTENTS

			PAGE
3.4.2	REACTIVITY AND CONTROL REQUIREMENTS		3.4-1
	3.4.2.1	Fuel Temperature Coefficient	3.4-2
	3.4.2.2	Moderator Temperature Coefficient	3.4-2
	3.4.2.3	Moderator Pressure Coefficient	3.4-3
	3.4.2.4	Moderator Void Coefficient	3.4-3
	3.4.2.5	Power Coefficient	3.4-3
3.4.3	SHUTDOWN REACTIVITY CONTROL		3.4-4
	3.4.3.1	Shutdown Reactivity Margin	3.4-4
	3.4.3.2	Power Defect	3.4-5
	3.4.3.3	Control Element Assembly Bite and Power Dependent Insertion Limits	3.4-5
	3.4.3.4	Shutdown Conditions	3.4-6
3.4.4	CONTROL ELEMENT ASSEMBLY PATTERN, OPERATIONS, AND WORTHS		3.4-6
3.4.5	REACTIVITY INSERTION RATES		3.4-7
3.4.6	POWER DISTRIBUTION		3.4-7
	3.4.6.1	General	3.4-7
	3.4.6.2	Objective	3.4-7
	3.4.6.3	Fuel Management and Operations	3.4-7
	3.4.6.4	Power Peaking Limits	3.4-8
	3.4.6.5	Power Distribution Monitoring Capability	3.4-8
3.4.7	REACTOR STABILITY		3.4-8
	3.4.7.1	General	3.4-8
	3.4.7.2	Method of Analysis	3.4-9
	3.4.7.3	Radial Stability	3.4-9
	3.4.7.4	Azimuthal Stability	3.4-10
	3.4.7.5	Axial Stability	3.4-10
	3.4.7.6	Detection and Control of Oscillations	3.4-10
3.4.8	NEUTRON FLUX AT PRESSURE VESSEL		3.4-10
3.4.9	ANALYTICAL METHODS		3.4-11
	3.4.9.1	General	3.4-11
	3.4.9.2	Coarse-Mesh Diffusion Calculations - Westinghouse only	3.4-12
	3.4.9.3	Power Distribution Monitoring	3.4-12
3.4.10	REFERENCES		3.4-13
3.5	**THERMAL AND HYDRAULIC DESIGN AND EVALUATION**		3.5-1
3.5.1	GENERAL		3.5-1
	3.5.1.1	Cycle Summaries	3.5-1

CHAPTER 3
REACTOR

TABLE OF CONTENTS

			PAGE
3.5.2	THERMAL AND HYDRAULIC DESIGN BASES		3.5-12
	3.5.2.1	Minimum Departure from Nucleate Boiling Ratio	3.5-12
	3.5.2.2	Fuel Design Basis	3.5-12
	3.5.2.3	Hydraulic Stability	3.5-13
3.5.3	STATISTICAL COMBINATION OF UNCERTAINTIES		3.5-13
3.5.4	REACTOR HYDRAULICS		3.5-13
	3.5.4.1	Coolant Flow	3.5-13
	3.5.4.2	Pressure Losses	3.5-14
	3.5.4.3	Partial Flow Operation	3.5-14
3.5.5	MAXIMUM CORE TEMPERATURE		3.5-14
3.5.6	DEPARTURE FROM NUCLEATE BOILING		3.5-15
	3.5.6.1	Design Approach to Departure from Nucleate Boiling	3.5-15
	3.5.6.2	Evaluation of Margin to DNB	3.5-15
3.5.7	VAPOR FRACTION		3.5-15
3.5.8	THERMAL AND HYDRAULIC EVALUATION		3.5-16
	3.5.8.1	Statistical Analysis of Hot Channel Factors	3.5-16
	3.5.8.2	Fuel Temperature Conditions	3.5-16
	3.5.8.3	Flow Stability	3.5-16
	3.5.8.4	AREVA/Framatome Fuel Assemblies	3.5-16
3.5.9	REFERENCES		3.5-17
3.6	**ORIGINAL FUEL DESIGN EVALUATION**		3.6-1
3.6.1	FUEL DESIGN AND ANALYSIS		3.6-1
3.6.2	ANALYSIS OF BURNUP AND LINEAR HEAT RATINGS		3.6-2
3.6.3	SUMMARY OF PERTINENT FUELS IRRADIATION INFORMATION		3.6-3
	3.6.3.1	High Linear Heat Rating Irradiations	3.6-3
	3.6.3.2	Shippingport Blanket Irradiations	3.6-3
	3.6.3.3	NRX Irradiations (AECL - Canada)	3.6-4
	3.6.3.4	Saxton Irradiations	3.6-4
	3.6.3.5	Vallecitos Boiling Water Reactor - Dresden	3.6-4
	3.6.3.6	Large Seed Blanket Reactor Rods	3.6-5
	3.6.3.7	Central Melting in Big Rock	3.6-5
	3.6.3.8	Peach Bottom 2	3.6-5
3.6.4	EVALUATION		3.6-6
3.6.5	REFERENCES		3.6-6
3.7	**SUPPLEMENTARY FUEL DESIGN AND EVALUATION**		3.7-1
3.7.1	FUEL ROD DESIGN EVALUATION		3.7-1
	3.7.1.1	Mechanical Design Evaluation	3.7-1
	3.7.1.2	Fuel Thermal Design Evaluation	3.7-3

CHAPTER 3
REACTOR

TABLE OF CONTENTS

			PAGE
	3.7.1.3	License Conditions with RODEX2 Methodology	3.7-8
3.7.2	DESIGN EVALUATION OF OTHER FUEL ASSEMBLY COMPONENTS		3.7-9
	3.7.2.1	Burnable Poison Rod Design Evaluation	3.7-9
	3.7.2.2	CEA Guide Tube Evaluation	3.7-9
3.7.3	DEMONSTRATION PROGRAMS		3.7-10
	3.7.3.1	Introduction	3.7-10
	3.7.3.2	CE/EPRI Fuel Performance Evaluation	3.7-10
	3.7.3.3	CE Irradiation of Test Fuel Rods	3.7-11
	3.7.3.4	SCOUT Program	3.7-11
	3.7.3.5	PROTOTYPE Program	3.7-11
	3.7.3.6	Materials Surveillance Specimens	3.7-12
	3.7.3.7	Prototype CEA	3.7-12
	3.7.3.8	ANF Demonstration Assemblies	3.7-12
	3.7.3.9	Erbium Demonstration Assemblies	3.7-12
	3.7.3.10	Test Capsule Assemblies	3.7-13
	3.7.3.11	Lead Fuel Assemblies for Unit 2 Cycle 11	3.7-13
	3.7.3.12	Batch 1RT Lead Fuel Assemblies	3.7-13
	3.7.3.13	Framatome and Westinghouse Lead Fuel Assemblies for Unit 2 Cycle 15	3.7-14
3.7.4	CHRONOLOGY OF FUEL EXPERIENCE		3.7-15
	3.7.4.1	Unit 1	3.7-15
	3.7.4.2	Unit 2	3.7-27
3.7.5	REFERENCES		3.7-35

CHAPTER 3
REACTOR

LIST OF TABLES

TITLE		PAGE
3.2-1	PRIMARY STRESS LIMITS FOR CRITICAL REACTOR VESSEL INTERNAL STRUCTURES	3.2-6
3.3-1	UNIT 1 BATCH-RELATED DATA	3.3-17
3.3-2	UNIT 2 BATCH-RELATED DATA	3.3-37
3.3-3	BURNABLE POISON ROD DATA	3.3-55
3.3-4	CONTROL ELEMENT ASSEMBLY DATA	3.3-57
3.3-5	CORE RELATED DATA	3.3-59
3.4-1	NUCLEAR PARAMETERS	3.4-15
3.4-2	CEA REACTIVITY WORTH AND ALLOWANCES, (% $\Delta\rho$)	3.4-17
3.5-1	DELETED	3.5-18
3.5-2	REACTOR COOLANT FLOWS IN BYPASS CHANNELS	3.5-19
3.5-3	DESIGN REACTOR PRESSURE LOSSES	3.5-20
3.6-1	TYPICAL PEAK BURNUP - MAXIMUM HEAT RELATIONSHIP	3.6-8
3.6-2	COMPARISON OF MAXIMUM HEAT RATINGS	3.6-9

CHAPTER 3
REACTOR

LIST OF FIGURES

FIGURE	
3.1-1	REACTOR VERTICAL ARRANGEMENT
3.3-1	REACTOR CORE CROSS-SECTION
3.3-2	FIRST CYCLE FUEL ROD
3.3-3	FUEL ROD
3.3-3A	FUEL ROD ASSEMBLY (Westinghouse)
3.3-3B	FUEL ROD DESIGN (UNIT 2 CYCLE 16)
3.3-3C	FUEL ROD DESIGN (UNIT 1 CYCLES 18, 19, & 20 AND UNIT 2 CYCLES 17 & 18)
3.3-4 sh 1	BURNABLE POISON ROD LOCATION (Sheets 1 - 25)
3.3-4 sh 2	
3.3-4 sh 3	
3.3-4 sh 4	
3.3-4 sh 5	
3.3-4 sh 6	
3.3-4 sh 7	
3.3-4 sh 8	
3.3-4 sh 9	
3.3-4 sh 10	
3.3-4 sh 11	
3.3-4 sh 12	
3.3-4 sh 13	
3.3-4 sh 14	
3.3-4 sh 15	
3.3-4 sh 16	
3.3-4 sh 17	
3.3-4 sh 18	
3.3-4 sh 19	
3.3-4 sh 20	
3.3-4 sh 21	
3.3-4 sh 22	
3.3-4 sh 23	
3.3-4 sh 24	
3.3-4 sh 25	
3.3-4 sh 26	
3.3-4 sh 27	
3.3-4 sh 28	
3.3-4 sh 29	
3.3-4 sh 30	
3.3-4 sh 31	
3.3-4 sh 32	
3.3-4 sh 33	
3.3-4 sh 34	
3.3-4 sh 35	
3.3-4 sh 36	
3.3-5	FUEL ASSEMBLY
3.3-6	FUEL ASSEMBLY HOLD DOWN
3.3-7	CANTILEVER TAB FUEL SPACER GRID

CHAPTER 3
REACTOR

LIST OF FIGURES

FIGURE	
3.3-7A	I-SPRING UNVANED SPACER GRID (TURBO)
3.3-7B	I-SPRING VANED SPACER GRID (TURBO)
3.3-8	CONTROL ELEMENT ASSEMBLY (CEA)
3.3-9A	WESTINGHOUSE/ABB-CE - CONTROL ELEMENT ASSEMBLIES
3.3-9B	AREVA/FRAMATOME - CONTROL ELEMENT ASSEMBLIES
3.3-10	CEA GROUP IDENTIFICATION
3.3-11	CORE ORIENTATION
3.3-12	PRESSURE VESSEL - CORE SUPPORT BARREL SNUBBER ASSEMBLY
3.3-13	CORE SHROUD ASSEMBLY
3.3-14	UPPER GUIDE STRUCTURE ASSEMBLY
3.3-15	CONTROL ELEMENT DRIVE MECHANISM (MAGNETIC JACK)
3.3-16	AREVA/FRAMATOME HTP FUEL ASSEMBLY, FUEL ROD, AND SPACER GRIDS
3.4-1	CYCLE 1 FUEL TEMPERATURE COEFFICIENT VS AVERAGE FUEL TEMPERATURE
3.4-2	CYCLE 1 POWER COEFFICIENT VS PERCENT OF FULL POWER (BEGINNING OF FIRST CYCLE)
3.4-3	FIRST CYCLE FUEL ASSEMBLY IDENTIFICATION BOTH UNITS
3.4-4	UNIT 1 CYCLE 24 CORE MAP
3.4-5	UNIT 2 QUARTER-CORE ASSEMBLY MAP
3.4-6	CYCLE 1 CORE POWER DISTRIBUTION, 2560 MWT (BEGINNING-OF-LIFE), NO XENON
3.4-7	UNIT 1 CYCLE 24 ASSEMBLY RELATIVE POWER DENSITY AT BOC, HFP, ARO, EQUILIBRIUM XENON
3.4-8	UNIT 2 ASSEMBLY RELATIVE POWER DENSITY AT BOC, HFP, ARO, EQUILIBRIUM XENON
3.4-9	CYCLE 1 CORE POWER DISTRIBUTION, 2560 MWT, 1000 MWD/MTU, EQUILIBRIUM XENON
3.4-10	UNIT 1 CYCLE 24 ASSEMBLY RELATIVE POWER DENSITY AT 10,000 MWd/MTU, HFP, ARO, EQUILIBRIUM XENON
3.4-11	UNIT 2 ASSEMBLY RELATIVE POWER DENSITY AT 10,000 MWd/MTU, HFP, ARO, EQUILIBRIUM XENON
3.4-12	CYCLE 1 CORE POWER DISTRIBUTION, 2560 MWT, END-OF-CYCLE, EQUILIBRIUM XENON
3.4-13	UNIT 1 CYCLE 24 ASSEMBLY RELATIVE POWER DENSITY AT EOC, HFP, ARO, EQUILIBRIUM XENON
3.4-14	UNIT 2 ASSEMBLY RELATIVE POWER DENSITY AT EOC, HFP, ARO, EQUILIBRIUM XENON
3.4-15	CORE POWER DISTRIBUTION – CEA GROUP 5 BEGINNING OF FIRST CYCLE, NO XENON
3.4-16	UNIT 1 CYCLE 24 ASSEMBLY RELATIVE POWER DENSITY WITH BANK 5 INSERTED TO PDIL AT BOC, HFP, EQUILIBRIUM XENON
3.4-17	UNIT 2 ASSEMBLY RELATIVE POWER DENSITY WITH BANK 5 INSERTED TO PDIL AT BOC, HFP, EQUILIBRIUM XENON

CHAPTER 3
REACTOR

LIST OF FIGURES

FIGURE	
3.4-18	CORE POWER DISTRIBUTION – CEA GROUP 5 END-OF-CYCLE 1, EQUILIBRIUM
3.4-19	UNIT 1 CYCLE 24 ASSEMBLY RELATIVE POWER DENSITY WITH BANK 5 INSERTED TO PDIL AT EOC, HFP, EQUILIBRIUM XENON
3.4-20	UNIT 2 ASSEMBLY RELATIVE POWER DENSITY WITH BANK 5 INSERTED TO PDIL AT EOC, HFP, EQUILIBRIUM XENON
3.4-21	CORE POWER DISTRIBUTION - PART LENGTH CEA (P-1), BEGINNING OF FIRST CYCLE, NO XENON
3.4-22	CORE POWER DISTRIBUTION - PART LENGTH CEA (P-1), BEGINNING OF FIRST CYCLE, EQUILIBRIUM XENON
3.4-23	AXIAL PEAK VS % CEA INSERTION (BEGINNING OF FIRST CYCLE)
3.4-24	AXIAL PEAK VS CEA INSERTION WITH PART LENGTH CEAs (END OF FIRST CYCLE)
3.4-25	NUCLEAR HEAT FLUX PEAK VS CEA INSERTION (BEGINNING OF FIRST CYCLE)
3.4-26	NUCLEAR HEAT FLUX PEAK VS CEA INSERTION WITH PART LENGTH CEAs (END OF FIRST CYCLE)
3.4-27	FIRST CYCLE POWER DEPENDENT CEA INSERTION LIMITS
3.4-28	Deleted
3.7-1	FRAMATOME LEAD FUEL ASSEMBLY

LIST OF ACRONYMS

ABB	Asea Brown Boveri, Inc.
ANF	Advanced Nuclear Fuel
AOO	Anticipated Operational Occurrence
APD	Axial Power Distribution
ARI	All Rods Inserted
ASI	Axial Shape Index
ASME	American Society of Mechanical Engineers
B&PV	Boiler and Pressure Vessel
BGE	Baltimore Gas and Electric Company
BOC	Beginning of Cycle
BOL	Beginning of Life
BPR	Burnable Poison Rods
CE	Combustion Engineering, Inc.
CEA	Control Element Assembly
CEDM	Control Element Drive Mechanism
CEDS	Control Element Drive System
CHF	Critical Heat Flux
CVCS	Chemical and Volume Control System
DBE	Design Basis Event
DNB	Departure from Nucleate Boiling
DNBR	Departure from Nucleate Boiling Ratio
ENDF	Evaluated Nuclear Data File
EOC	End of Cycle
EOL	End of Life
ESCU	Extended Statistical Combination of Uncertainties
ESFAS	Engineered Safety Feature Actuation Signal
FANP	Framatome Advanced Nuclear Power
FTC	Fuel Temperature Coefficient
GTFS	Guide Tube Flux Suppressor
HTP	High Thermal Performance
HMP	High Mechanical Performance
ICI	Incore Instrumentation
IFBA	Integral Fuel Burnable Absorber
LCO	Limiting Conditions for Operation
LEF	Lower End Fitting
LFA	Lead Fuel Assemblies
LHR	Linear Heat Rate
LOCA	Loss-of-Coolant Accident
LPD	Local Power Density
LSBR	Large Seed Blanket Reactor
LSSS	Limiting Safety System Setting
MDNBR	Minimum Departure from Nucleate Boiling Ratio
MRR	Most Reactive Rod
MTC	Moderator Temperature Coefficient

LIST OF ACRONYMS

NEM	Nodal Expansion Method
NRC	Nuclear Regulatory Commission
PCI	Pellet-Clad Interaction
PDF	Probability Distribution Function
PDIL	Power Dependent Insertion Limit
PLCEA	Part Length Control Element Assembly
PLHR	Peak Linear Heat Rate
PWR	Pressurized Water Reactor
RCS	Reactor Coolant System
RPS	Reactor Protective System
RSS	Root-Sum-Square
SAFDL	Specified Acceptable Fuel Design Limit
SCU	Statistical Combination of Uncertainties
SS	Stainless Steel
T-H	Thermal Hydraulics
TD	Theoretical Density
TM/LP	Thermal Margin/Low Pressure
UGS	Upper Guide Structure
UO_2	Uranium Oxide
VAP	Value Added Pellet
VBWR	Vallecitos Boiling Water Reactor
ZrB_2	Zirc Diboride

3.0 REACTOR

3.1 GENERAL DESIGN SUMMARY

Both of the Calvert Cliffs reactors are of identical design. Consequently, reference throughout this section is made to a single reactor and, unless otherwise noted, implies either Unit 1 or 2.

The reactor is of the pressurized water type, using two reactor coolant loops. A vertical cross-section of the reactor is shown in Figure 3.1-1. The reactor core is composed of 217 fuel assemblies and 77 Control Element Assemblies (CEAs).

The fuel assemblies are arranged to approximate a right circular cylinder with an equivalent diameter of 136" and an active height of 136.7".

The fuel assembly consists of 176 rods (pins) and 5 guide tubes. The pins may contain fuel and/or a neutron poison. The assembly is held together by spacer grids and is closed at the top and bottom by end fittings.

Lateral support and positioning of the fuel rods within an assembly is provided by spacer grids. The spacer grids are welded to five full-length guide tubes. The guide tubes provide channels which guide the CEAs over their entire length of travel and form the longitudinal structure of the assembly. In selected fuel assemblies the central guide tube houses incore instrumentation (ICI). Design characteristics of demonstration or lead fuel assemblies are discussed in Section 3.7.

The fuel is low enrichment uranium dioxide (UO_2) in the form of ceramic pellets clad in Zircaloy or ZIRLO for Westinghouse fuel (as part of an advanced cladding test program, some fuel pins in Batches 2NT, 1RT, 2TF, and 2TW utilize cladding other than Zircaloy or ZIRLO) tubes which are welded into a hermetic enclosure. Starting with Unit 2 Cycle 19 and Unit 1 Cycle 21, AREVA/Framatome fuel uses M5® alloy cladding. Initially the fuel was managed in a three-cycle, mixed central zone, fuel management plan (Figure 3.4-3). Starting with Unit 2 Cycle 8 and Unit 1 Cycle 10, the 24-month cycle core utilized low leakage fuel management. Starting with Unit 1 Cycle 11 and Unit 2 Cycle 10, low fluence fuel management is employed to reduce the fluence on the critical vessel weld. Low fluence fuel management includes replacement of fresh fuel located on the core flats with once or twice-burned fuel. In Unit 1 Cycle 11 and Cycle 12 low fluence fuel management also included the addition of Guide Tube Flux Suppressors (GTFSs) in selected assemblies near the periphery. Sufficient margin is provided to ensure that power peaks are minimized.

The reactor coolant enters the upper section of the reactor vessel, flows downward between the reactor vessel wall and the core barrel, passes through the flow skirt where the flow distribution is equalized and into the lower plenum. The coolant then flows upward through the core, removing heat from the fuel rods, exits from the reactor vessel and passes through the tube side of the vertical U-tube steam generators where heat is transferred to the secondary system. The reactor coolant pumps return the coolant to the reactor vessel.

The reactor internals support and orient the fuel assemblies, the CEAs, and the incore instrumentation and guide the reactor coolant through the reactor vessel. The reactor internals also absorb static and dynamic loads and transmit the loads to the reactor vessel flange. They will safely perform their functions during normal operating, upset, emergency, and faulted conditions. The internals are designed to safely withstand forces due to deadweight, handling, temperature and pressure differentials, flow impingement, vibration, and seismic acceleration.

Reactivity control is provided by two independent systems: (1) the Control Element Drive System (CEDS) which controls CEA motion, and (2) the Chemical and Volume Control System (CVCS) which is used to control the Reactor Coolant System (RCS) boric acid concentration.

Boric acid dissolved in the coolant is used as a neutron absorber to provide long-term reactivity control. In order to reduce the boric acid concentration required at Beginning of Life (BOL) operating conditions and lower power peaking, mechanically fixed burnable poison rods (BPRs) may be provided in certain fuel assemblies. Originally, the neutron poison was boron carbide which is dispersed in alumina pellets; the pellets are clad in Zirconium alloy to form rods which are similar to the fuel rods. Gadolinia and erbium oxide, mixed into fuel pellets, are also being used as a neutron burnable absorber. Beginning with Unit 2 Cycle 16 and Unit 1 Cycle 18 Zirc Diboride (ZrB_2), applied as a coating on the fuel pellets, was used as a neutron burnable absorber. Poison rods are also called shims. Beginning in Unit 2 Cycle 19 and Unit 1 Cycle 21, Gadolinia (Gd_2O_3) mixed into the fuel is used as the neutron burnable absorber.

The CEAs consist of five Inconel tubes filled with neutron absorbers. Four tubes are assembled in a square array around the central fifth tube. A spider joins the tubes at the upper end. The hub of the spider couples the CEA to the drive assembly. The CEAs are activated by magnetic jack Control Element Drive Mechanisms (CEDMs) mounted on the reactor vessel head.

The maximum reactivity worth of the CEAs and the associated reactivity addition rate are limited by system design to prevent sudden large reactivity increases. The design restraints are such that reactivity increases do not result in violation of the fuel damage limits, rupture of the reactor coolant pressure boundary, nor disruption of the core or other internals sufficient to impair the effectiveness of emergency cooling.

Control Element Assemblies are moved in groups to satisfy the requirements of shutdown, power level changes, and operational maneuvering. The control system is designed to produce power distributions that are within the acceptable limits of overall nuclear heat flux factor and Departure from Nucleate Boiling Ratio (DNBR). The Reactor Protective System (RPS) and administrative controls ensure that these limits are not exceeded.

In order to assure control of axial power distribution (APD), particularly in the event of axial xenon oscillation, eight CEAs designated as Part Length CEAs (PLCEA) were initially installed. They have since proved unnecessary and were removed along with their extension shafts. Control Element Assembly guide tube plugs were inserted into the locations previously occupied by the PLCEAs. They have also proved unnecessary and were removed before Unit 1 Cycle 8 and Unit 2 Cycle 7.

3.2 DESIGN BASIS

3.2.1 PERFORMANCE OBJECTIVES

The full-power thermal rating of the core is 2737 MWt. The physics, thermal and hydraulic information presented in this section is based on this power level.

3.2.2 DESIGN OBJECTIVES

The reactor core, together with its control systems and the RPS, is designed to function over its lifetime without exceeding fuel damage limits of excessive fuel temperature, cladding strain, and cladding stress (Section 3.2.3) during normal operating conditions and Design Basis Events (DBEs).

In the power operating range, the net effect of the prompt inherent nuclear feedback characteristics tends to compensate for a rapid increase in power. At the beginning of cycle (BOC) a slightly positive Moderator Temperature Coefficient (MTC) may occur. If power oscillations occur, their magnitude will be such that the fuel damage limits are not exceeded.

Reactivity control is provided by two independent systems: (1) the CEDS, and (2) the CVCS. The CEDS controls short-term reactivity changes and is used for rapid shutdown. The CVCS is used to compensate for long-term reactivity changes and can make the reactor subcritical without the benefit of the CEDS. The design of the core and the RPS prevents fuel damage limits from being exceeded for any single malfunction in either of the reactivity control systems.

The maximum reactivity addition rate from the withdrawal of the CEAs is limited by the core excess reactivity, CEA worth, and CEDS design. These limitations prevent sudden large reactivity increases. The design restraints are such that reactivity increases will not result in exceeding the fuel damage limits, rupture of the reactor coolant pressure boundary, or disruption of the core or other internals sufficient to impair the effectiveness of emergency cooling.

3.2.3 DESIGN LIMITS

3.2.3.1 Nuclear Design Limits

The design of the core is based upon the following nuclear limitations:

a. The limitation on fuel burnup is determined by material design, mechanical design and nuclear considerations. The mechanical integrity of the fuel remains satisfactory beyond the planned discharge burnup.

b. In the power operating range, the effect of the prompt inherent nuclear feedback characteristic [Fuel Temperature Coefficient (FTC)] compensates for rapid increases in power.

c. CEAs are moved in groups to satisfy the requirements of shutdown, power level changes and operational maneuvering. The control systems are designed to produce power distributions that are within the acceptable limits of overall Nuclear Heat Flux Factor (F_q^N) and DNBR. The RPS and administrative controls ensure that these limits are not exceeded.

d. Axial xenon oscillations, when they occur, will be manually controlled by regulating CEAs using information provided by the neutron flux detectors. The xenon oscillation period, about one day, allows ample time for operator action before the RPS trip setpoint is exceeded.

3.2.3.2 Reactivity Control Design Limits

The control system and operating procedures provide for adequate control of the core reactivity and power distributions such that the following limits are met:

a. Sufficient CEAs are withdrawn to provide an adequate shutdown reactivity margin;
b. The shutdown margin is maintained with the highest worth CEA assumed stuck in its fully withdrawn position;
c. The CVCS is capable of adding boric acid to the reactor coolant at a rate sufficient to maintain the shutdown margin during a RCS cooldown at the design rate following a reactor trip.

3.2.3.3 Thermal and Hydraulic Design Limits

The principal basis of the thermal and hydraulic design is to avoid thermally-induced fuel damage during normal operation, and Design Basis Event (DBE). It is recognized that there is a small probability of limited fuel damage in certain unlikely situations as discussed in Chapter 14.

The following corollary thermal and hydraulic design bases are established, but violation of either is not necessarily equivalent to fuel damage:

a. There is a high confidence level that Departure from Nucleate Boiling (DNB) is avoided during normal operation and DBEs. This is achieved by setting a design lower limit on the Minimum Departure from Nucleate Boiling Ratio (MDNBR) calculated according to the Asea Brown Boveri, Inc. (ABB)-NV correlation for each cycle. Starting with Unit 1 Cycle 17, the ABB-TV correlation was used. Starting with Unit 2 Cycle 19 and Unit 1 Cycle 21, the high thermal performance (HTP) correlation was used to determine DNBR for AREVA/Framatome fuel.
b. The melting point of the UO_2 fuel is not reached during normal operation nor during DBEs.

The RPS provides for automatic reactor trip before these design limits are exceeded.

Reactor internal flow passages and fuel coolant channels are designed to prevent hydraulic instabilities. Flow maldistributions are limited by design to be compatible with the specified thermal design criteria.

3.2.3.4 Mechanical Design Limits

The reactor internals are designed to perform their functions safely during steady state conditions and DBEs. The internals can safely withstand the forces due to deadweight, handling, system pressure, flow-induced pressure drop, flow impingement, temperature differential, shock, and vibration. The structural components satisfy stress values given in the American Society of Mechanical Engineers (ASME) Boiler and Pressure Vessel (B&PV) Code, Section III.

The following limitations on stresses or deformations are employed to ensure capability of a safe and orderly shutdown in the combined event of earthquake and major loss-of-coolant accident (LOCA). For reactor vessel internal structures, the

stress criteria are given in Table 3.2-1. The intent of the limits in this table is as follows:

a. Under design loading plus design earthquake forces the critical reactor vessel internal structures are designed within the stress criteria established in the ASME B&PV Code, Section III, Article 4;
b. Under normal operating loadings plus maximum hypothetical earthquake forces, the design criteria permits a small amount of local yielding;
c. Under normal operating loadings plus reactor coolant pipe rupture loadings plus maximum hypothetical earthquake forces, permanent deformation is permitted by the design criteria.

The following typical values are selected to illustrate the conservatism of this approach for establishing stress limits. Units are 10^3 lbs/in^2.

Material	S_y[(a)]	S_u	S_D	S_L
SA 106B	25.4	60.0[(b)]	25.4	36.9
SA 533B	41.4	80.0[(b)]	41.4	54.3
304 SS	17.0	54.0[(c)]	18.35	29.3
316 SS	18.5	58.2[(c)]	22.2	31.7

(a) From ASME B&PV Code, Section III, at 650°F
(b) Minimum value at room temperature, which is approximately the same at 650°F for ferritic materials
(c) Estimated

S_u = Minimum tensile strength of material at temperature
S_L = $S_y + (1/3)(S_u - S_y)$
S_y = Tabulated yield at temperature from ASME B&PV Code, Section III
S_D = Design stress

To properly perform their functions, the critical reactor internal structures are designed to satisfy the additional deflection limits described below, in addition to the stress limits given in Table 3.2-1.

Under normal design loadings plus design earthquake forces or normal operating loadings plus maximum hypothetical earthquake forces, deflections are limited so that the CEAs can function and adequate core cooling is maintained. Under normal operating loadings plus maximum hypothetical earthquake forces plus pipe rupture loadings, the deflection design criteria depend on the size of the piping break. If the equivalent diameter of the pipe break is no larger than the largest line connected to the main reactor coolant lines, deflections are limited so that the core is held in place, the CEAs function normally, and adequate core cooling is maintained. Those deflections which would influence CEA movement are limited to less than two-thirds of the deflection required to prevent CEA function. For pipe breaks larger than the above, the criteria are that the fuel is held in place in a manner permitting core cooling and that adequate coolant flow passages are maintained. For these major pipe break sizes, CEA insertability is not required to achieve shutdown because the rapid voiding during the ensuing blowdown and the subsequent refill with the borated safety injection water ensures adequate shutdown margin for the reactor. For the larger break sizes, critical components are restrained from buckling by further limiting the stress levels to two-thirds of the stress level calculated to produce buckling
.

3.2.3.5 Fuel Assembly Design Limits

The fuel assemblies are designed to maintain their structural integrity under steady state conditions, DBEs, normal handling loads, shipping stresses, and refueling loads. The design takes into account differential thermal expansion of fuel rods, thermal bowing of fuel rods and CEA guide tubes, irradiation effects, and wear of all components. Mechanical tolerances and clearances have been established on the basis of the functional requirements of the components. All components including welds are highly resistant to the corrosive action of the reactor environment.

The fuel rod design accounts for external pressure, differential expansion of fuel and clad, fuel swelling, clad creep, fission and other gas releases, thermal stress, pressure and temperature cycling, and flow-induced vibrations. The structural criteria are based on the following:

a. The maximum primary stress during steady state operation, expected transients, and depressurization is limited to two-thirds of the minimum yield strength of the material at operating temperature.
b. The predicted total strain of the cladding at the End of Life (EOL) is less than 1.0%.

AREVA/Framatome has performed the mechanical design analyses starting with the Unit 2 Cycle 19 and Unit 1 Cycle 21 fuel assembly design. These evaluations used the Nuclear Regulatory Commission (NRC)-approved mechanical analysis codes and methodology to demonstrate compliance with the NRC-approved design criteria. (References 1, 2, 3, and 4)

3.2.3.6 Control Element Assembly Design Limits

The CEAs are designed to maintain their structural integrity under all steady state conditions, DBEs and handling, shipping and refueling loads. Thermal distortion, mechanical tolerances, vibration and wear of the CEA are all accounted for in the design. Clearances and corresponding fuel assembly alignment are established so that possible accumulation of mechanical tolerances and thermal distortion will not result in frictional forces that could prevent reliable operation of the system. The structural criteria are based on limiting the maximum stress intensity to those values specified in Section III of the ASME B&PV Code.

The clearance between the CEA fingers and the guide tubes is designed for actuating within the prescribed time under steady state conditions, during DBEs, under maximum hypothetical earthquake, and temperature conditions in combination with various factors which cause a reduction in diametral clearance. These factors include adverse dimensional tolerances, bowing and twisting of CEA and guide tubes and possible enlargement of the poison rod diameter due to swelling of B_4C pellets at maximum burnup conditions. The design diametral change due to swelling of B_4C is based on the pellets being rigid and the high strength clad offers no restraint to pellet diametral growth.

The core is designed to limit deflections so that the core is held in place. The CEAs function and adequate core cooling is maintained even under:

a. Normal design loadings plus design earthquake forces;
b. Normal operating loadings plus maximum hypothetical earthquake forces plus a pipe break no larger than the equivalent diameter largest line connected to the main reactor coolant lines

If the equivalent diameter of the pipe break is larger than the largest coolant line, the core is designed so that fuel is held in place to permit core cooling and adequate coolant flow is maintained.

Those deflections which would influence CEA movement are limited to less than two-thirds of the deflection required to prevent CEA function. If the equivalent diameter of the pipe break is larger than condition b above, the core is designed so that the fuel is held in place in a manner permitting core cooling and that adequate coolant flow passages are maintained. For these major pipe breaks, CEA insertion is not required to achieve shutdown because the rapid voiding during blowdown and the refilling of the vessel with borated safety injection water ensures adequate shutdown margin for the reactor.

The speed at which the CEAs are inserted or withdrawn from the core is consistent with the reactivity change requirements during reactor operation (Chapter 7). For conditions that require a rapid shutdown of the reactor, the CEDM holding coils deenergize to allow the CEAs to drop into the core. The reactivity is reduced during such a CEA drop at a rate sufficient to prevent exceeding fuel damage limits. A CEA automatic drive-down capability after a reactor trip is not required. During a trip, the RPS opens the trip circuit breakers, deenergizing the CEDM holding coils allowing the CEAs to drop by gravity into the core. To drive down a CEA stuck in the fully withdrawn position, the operator must first clear the trip condition and manually close the trip circuit breaker. Therefore, a drive-down feature would introduce the possibility of a failure which would prevent power from being removed from the CEDM holding coils. The safety analysis (Chapter 14) assumes the CEA of highest reactivity worth sticks in the fully withdrawn position.

The CEDM pressure housings are an extension of the reactor vessel, providing a part of the reactor coolant boundary, and are, therefore, designed to meet the requirements of the ASME B&PV Code, Section III, Nuclear Vessels. Pressure and thermal transients as well as steady state loadings were considered in the design analysis.

3.2.4 REFERENCES

1. ANF-88-133(P)(A), Revision 0 and Supplement 1, “Qualification of Advanced Nuclear Fuels PWR Design Methodology for Rod Burnups of 62 GWd/MTU,” December 1991
2. XN-NF-82-06(P)(A), Revision 1 and Supplements 2, 4, and 5, “Qualification of Exxon Nuclear Fuel for Extended Burnup,” October 1986
3. BAW-10133(P)(A), Revision 1, Addendum 1 and Addendum 2, “Mark-C Fuel Assembly LOCA-Seismic Analysis,” October 2000
4. EMF-92-116(P)(A), Revision 0, Supplement 1 (P)(A), Revision 0, “Generic Mechanical Design Criteria for PWR Fuel Designs,” February 2015

TABLE 3.2-1

PRIMARY STRESS LIMITS FOR CRITICAL REACTOR VESSEL INTERNAL STRUCTURES

LOADING COMBINATIONS	ALLOWABLE STRESSES
Design Loading Plus Design Earthquake Forces	$P_m \leq S_m$ $P_b + P_L \leq 1.5S_m$
Normal Operating Loading Plus Maximum Hypothetical Earthquake Forces	$P_m \leq S_D$ $P_b \leq 1.5 \left(1 - \left(\frac{P_m}{S_D} \right)^2 \right) S_D$
Normal Operating Loadings Plus Maximum Hypothetical Earthquake Forces Plus Pipe Rupture Loadings	$P_m \leq S_L$ $P_b \leq 1.5 \left(1 - \left(\frac{P_m}{S_L} \right)^2 \right) S_L$

where:

LEGEND

P_m = Calculated Primary Membrane Stress, psi

P_b = Calculated Primary Bending Stress, psi

P_L = Calculated Primary Local Membrane Stress, psi

S_m = Tabulated Allowable Stress Limit at Temperature from ASME B&PV Code, Section III or ANSI B31.7, psi

S_y Tabulated Yield Strength at Temperature, ASME B&PV Code, Section III, psi

S_D = Design Stress, psi

S_D = S_y (for ferritic steels), psi

S_D = $1.2S_m$ (for austenitic steels), psi

S_L = $S_y + 1/3 (S_u – S_y)$, psi

S_u = Tensile Strength of Material at Temperature, psi

3.3 MECHANICAL DESIGN

3.3.1 SUMMARY

The reactor core and internals are shown in Figure 3.1-1. A cross-section of the reactor core and internals is shown in Figure 3.3-1. Mechanical design features of the reactor internals, the CEDMs and the reactor core are described below. Mechanical design parameters are listed in Tables 3.3-1, 3.3-2, 3.3-3, 3.3-4, and 3.3-5.

The fuel for Unit 2 is essentially identical to that of Unit 1. After the first cycle of Unit 1, a number of minor refinements (shown in Tables 3.3-1 and 3.3-2) were incorporated for the purpose of improving overall fuel performance. The principal changes are that the pellet density has been increased slightly and the overall pellet geometry modified. The increased pellet density, along with improvements in pellet microstructure, has the effect of improving the in-pile dimensional stability of the pellet, thereby lessening the adverse effect of in-pile densification on gap conductance and axial gap formation. The reduced pellet length-to-diameter (L/D) ratio and the use of chamfered pellets have the effect of reducing the severity of interaction between the pellets and the clad. Also, the fuel has been modified to permit replacement of fuel rods. These refinements represent standard practice among Combustion Engineering, Inc. (CE) reactors like the Calvert Cliffs design.

3.3.2 CORE MECHANICAL DESIGN

The core approximates a right circular cylinder with an equivalent diameter of 136" and an active height of 136.7". It consists of Zircaloy-4 or ZIRLO (as part of an advanced cladding test program, some fuel pins in Batches 2NT, 1RT, 2TF, and 2TW utilize other cladding materials) clad fuel rods containing slightly enriched uranium in the form of sintered UO_2 pellets. Starting with Unit 2 Cycle 19 and Unit 1 Cycle 21, AREVA/Framatome fuel uses the M5® alloy cladding. In addition, there are BPRs in certain fuel batches. The fuel rods are grouped into 217 assemblies. The enrichment of each batch of fuel is shown in Tables 3.3-1 and 3.3-2.

Short-term reactivity control is provided by 77 CEAs. The CEAs are guided within the core by the guide tubes which are integral parts of the fuel assemblies.

3.3.2.1 Fuel Rod Mechanical Design

The fuel rods consist of slightly enriched UO_2 cylindrical ceramic pellets. The first cycle fuel rod is shown in Figure 3.3-2. Recent Westinghouse fuel rod designs are shown in Figures 3.3-3A, 3.3-3B, and 3.3-3C. Originally, a round wire Type 302 stainless steel (SS) compression spring, and an alumina spacer disc were located at each end of the fuel column, all clad within a seamless Zircaloy-4 or ZIRLO tube with a Zircaloy-4 cap welded at each end. As part of an advanced cladding test program, some fuel pins in Batches 2NT, 1RT, 2TF, and 2TW utilize other cladding materials. Beginning with Unit 1 Cycle 12 and Unit 2 Cycle 11, the upper alumina spacer disc was removed. Beginning with the Unit 1 Cycle 16 Batch 1V rods manufactured at the Columbia facility, the lower alumina spacer disk was removed. The fuel rods manufactured by Hematite are evacuated and internally pressurized with helium to compensate for the pressure difference across the clad, minimizing clad collapse. The fuel rods built at Columbia are not evacuated prior to being pressurized with Helium. Helium, an inert gas, is chosen as the pressurizing medium because of its thermal conductivity. Cladding creep-collapse time for fuel was analyzed for each cycle until Unit 1 Cycle 8 and Unit 2 Cycle 7. Analysis of modern pressurized water reactor (PWR) fuels has demonstrated that the clad collapse time is significantly longer than its expected useful life. Therefore, cycle-specific clad collapse time is not calculated.

Each fuel rod assembly includes a unique serial number. The unique serial number ensures traceability of the fabrication history of each fuel rod. The fuel cladding is cold worked and stress-relief annealed Zircaloy-4 or ZIRLO seamless tubing. The actual tube forming process consists of a series of cold working and annealing operations.

The UO_2 pellets are dished and chamfered on both ends in order to better accommodate thermal expansion and fuel swelling. The pellet length to diameter ratio and the use of chamfered pellets decrease the interaction between the pellet and the clad. However, because the pellet dishes and chamfers constitute about 3% of the pellet, stack height density is reduced. The stack height density and pellet dimensions are given in Tables 3.3-1 and 3.3-2.

The compression spring, located at the top of the fuel pellet column, maintains the column in its proper position during handling and shipping. The alumina spacer disc at the lower end of the fuel rods with magnetic force welds is to protect the weld from radial strain induced by pellet swelling, while the upper spacer disc prevents UO_2 chips, if present, from entering the plenum region. Beginning with Unit 1 Cycle 12 and Unit 2 Cycle 11, the upper alumina (Al_2O_3) spacer disc was removed. Starting with the Unit 1 Cycle 16 rods built in Columbia, the lower alumina spacer was eliminated. The plenum spring is a low volume plenum spring. This provides greater margin between the EOL internal pin pressure and the rods mechanical design limit than earlier designs. The fuel rod plenum, initially pressurized with helium, provides space for axial thermal expansion of the fuel column and accommodates the gaseous fission products. The greater portion of the fission gas remains in the pellet lattice and does not contribute to the rod internal pressure.

Beginning in Unit 2 Cycle 19 and Unit 1 Cycle 21, the fuel is provided by AREVA/ Framatome and the general design is similar. The cladding is a zirconium alloy, M5®. The fuel column is sintered UO_2 pellets, 136.7" long (nominally) with a plenum spring at the top of the rod column. Each rod is pressurized with helium and sealed with caps welded at each end. The fuel column continues to have low enriched axial blanket pellets at both ends. The fuel rod is shown in Figures 3.3-3 and 3.3-16.

3.3.2.2 Burnable Poison Rod Mechanical Design

Fixed burnable poison (neutron absorbing) rods are included in selected fuel assemblies to reduce the BOL MTC. They replace fuel rods at selected locations. The various sheets of Figure 3.3-4 show assembly configurations for various fuel bundles. The poison rods are mechanically similar to fuel rods, but contain a column of burnable poison pellets instead of fuel pellets. The poison material consists of alumina with uniformly dispersed boron carbide particles. Mechanical design parameters are listed in Table 3.3-3.

The balance of the column contains Zircaloy-4 pellets. The BPR plenum spring produces a smaller preload on the pellet column than that in a fuel rod because of the lighter material in the poison pellets.

Each BPR includes a unique serial number and a batch identification mark. The serial number is used to record fabrication information for each component in the rod assembly. It ensures traceability of the fabrication history of each rod. The batch identification mark provides a visual check on the pellet boron concentration during fuel assembly fabrication.

For Unit 1 Cycle 10, four lead test assemblies containing Gadolinia as a burnable absorber were introduced. Twelve of the 176 fuel bearing rods in each of the test

assemblies contain a mixture of 10 wt% Gd_2O_3 and natural (not enriched in U-235) UO_2 pellets stacked over an active length of 122.7" within the rod. The top and bottom 7" of the column contain natural UO_2 pellets without Gadolinia. The test assembly poison rod pellets are otherwise mechanically identical to fuel pins.

For Unit 2 Cycle 9, four demonstration assemblies containing Erbium as a burnable absorber were introduced. Each assembly consists of 80 standard pins at 4.3 wt% U-235, 52 standard pins at 3.4 wt% U-235, and 44 Erbium bearing pins. The fuel stack in each Erbium bearing fuel pin consists of a central 115.7" region containing 3.4 wt% U-235, 0.9 wt% Er_2O_3, UO_2/Er_2O_3 pellets and two 10.5" cutback regions, one at each end of the stack containing standard 3.4 wt% U-235 pellets.

For Unit 2 Cycle 10, Batch 2M burnable absorber pins consist of a 115.7" central region containing the burnable material B_4C with two 10.5" cutback regions containing Al_2O_3, one at each end of the stack. This change is being made to enhance thermal margin by lowering the axial peak at BOC.

Beginning with Unit 1 Cycle 12 and Unit 2 Cycle 11, selected fuel pins contain erbia (Er_2O_3) as the integral burnable absorber (in lieu of B_4C). The erbium fuel pins consist of a central region containing the burnable absorber mixed with UO_2 at the batch enrichment and a cutback region at the upper and lower ends of the fuel rods. The cutback region consists of UO_2 at the batch enrichment, and enhances the thermal margin by lowering the core average axial peak.

Beginning with Unit 2 Cycle 16 and Unit 1 Cycle 18, selected fuel pins contain ZrB_2 as the integral burnable absorber (in lieu of erbia). The ZrB_2 fuel pins consist of a central region containing the burnable absorber. The ZrB_2 is applied as a very thin coating on the outside surface of select UO_2 fuel pellets. The ZrB_2 rods have a poison cutback region at the upper and lower ends of the fuel rods.

Beginning in Unit 2 Cycle 19 and Unit 1 Cycle 21, the fuel uses Gadolinia, dispersed in the UO_2 fuel as a burnable poison.

3.3.2.3 Fuel Assembly Mechanical Design

The fuel assembly (Figure 3.3-5) consists of 176 fuel rods and poison rods, 5 guide tubes, 5 guide tube sleeves (except as noted by Section 3.7), 8 fuel rod spacer grids, upper and lower end fittings (LEFs), and a hold-down device (Figure 3.3-6). The guide tubes, spacer grids, and end fittings form the structural frame of the assembly. The four outer guide tubes are mechanically attached to the end fittings and the spacer grids are welded to all five guide tubes.

The fuel rod spacer grids for the Westinghouse fuel (Figures 3.3-7, 3.3-7A, 3.3-7B, and 3.3-16) maintain the fuel rod pitch over the length of the rod. The grid provides positive lateral restraint to the fuel rod but only frictional restraint axially. The grids are fabricated from preformed Zircaloy, interlocked in an egg crate fashion, and welded together. The grid supports each fuel rod by two cantilever tab springs or two I-springs and four arches. The springs press the rod against the arches to restrict relative motion between the grids and the fuel rods. The spring and arch positions are reversed from grid to grid to provide additional movement restrictions. The perimeter strips contain features designed to prevent hang up of grids during a refueling operation. The eight Zircaloy-4 spacer grids are welded to each Zircaloy-4 guide tube at eight locations, four on the upper face of the grid and four on the lower face of the grid, where the spacer strips contact the guide tube surface.

The Westinghouse fuel assembly upper end fitting consists of a 304 SS flow plate, a SS hold-down plate, five machined posts, and five Inconel X-750 compression springs. The upper end fitting attaches to the guide tubes to serve as an aligning and lifting device for each fuel assembly. The flow plate is attached to the top ends of the guide tubes and is designed to prevent excessive axial motion of the fuel rods. Inconel X-750 is selected for the compression springs because of its previous use for coil springs and good resistance to relaxation during operation. The hold-down plate, together with the compression springs, comprise the hold-down device. The hold-down plate is axially movable. It is loaded by the compression springs and held down by the fuel alignment plate. The spring load combines with the fuel assembly weight to counteract upward hydraulic forces. The determination of upward hydraulic forces includes factors accounting for flow maldistribution, fuel assembly component tolerances, oxide buildup, drag coefficient, and bypass flow. The springs are sized and the spring preload selected such that a net downward force of at least 150 pounds will be maintained for all normal and anticipated transient flow and temperature conditions. The design criteria limit the maximum stress under the most adverse tolerance conditions to below yield strength of the spring material. The maximum stress occurs during cold conditions and decreases as the reactor heats up. The reduction in stress is due to a decrease in spring deflection resulting from differential thermal expansion between the Zircaloy fuel bundles and the SS internals.

The Westinghouse fuel LEF consists of an Inconel grid welded to a cast SS plate which has flow holes and four support legs. The support legs also serve as alignment posts. Precision-drilled holes in the support legs mate with four core support plate alignment pins, thereby properly locating the lower end of the fuel assembly.

Beginning with Batch 1D and 2D fuel and continuing with subsequent assemblies the bottom spacer grid is used in lieu of a mechanical retention grid to laterally locate the bottom of the fuel rods. The grid allows for removal and replacement of rods. The four outer guide tubes have a widened region at the upper end which contains an internal thread.

Beginning with Batch 1K and 2J fuel and continuing with subsequent assemblies, the height of the LEF was shortened by shortening the support legs. The overall lengths of the guide tubes were increased to compensate for the shorter LEF. The elevations of the Inconel grid and the uppermost Zircaloy grid were changed to maintain their same relative elevations with respect to previous assemblies.

In Batch 2L, a debris-resistant LEF design was used in which a 3x3 array of small flow holes replaces each of the large flow holes of the previous design. Also, wherever possible, additional small holes are added to minimize the increase in the pressure drop of the small hole LEF design, relative to the previous design.

Beginning with Batch 1N and 2M, the fuel incorporates the GUARDIAN™ fuel assembly design to entrap debris. The GUARDIAN™ design employs a redesigned Inconel spacer grid and redesigned rods that have longer, solid Zircaloy-4 lower end caps. Changes incorporated into the GUARDIAN™ fuel assembly include an increase in length of the lower end caps, an increase in the length of the fuel and burnable absorber rods, and a decrease in the length of the plenum regions. The length of the guide tubes is increased to maintain the shoulder gap, and the height of the upper end fitting is reduced to maintain the overall length of the fuel bundle. The change in height of the upper end fitting is accomplished by decreasing the compression region for the hold-down spring without a change in dimension of the

spring. The height of the LEF is reduced and "T" stanchions are added to aid fuel handling.

Beginning with Batch 1N and Batch 2M, Zircaloy spacer grids are redesigned to allow fuel rods located along the periphery of the fuel bundle to receive more coolant flow. This is performed through an increase in the outer pin cell size by enlargement of the outside envelope of the spacer grid assembly.

The externally-threaded end of each guide post passes through a hole in the flow plate and is torqued into the internally-threaded guide tube. When assembled, the flow plate is secured between flanges on the guide tubes and on the guide post. The connection with the upper end fitting is locked with a mechanical crimp. Each outer guide tube has, at its lower end, a welded Zircaloy-4 fitting. Either a threaded portion of this fitting passes through a hole in the fuel assembly LEF and is secured by a Zircaloy-4 nut and a SS locking ring, or a fitting with an internal thread engages with a hole in the LEF and is secured by a SS bolt and locking ring. The locking ring is tack welded to the LEF in four places.

The central guide tube inserts into sockets in the upper and lower end fittings and is thus retained laterally by the relatively small clearance at these locations. The upper end fitting socket is created by the center post which is threaded into the lower cast flow plate and tack welded in two places. The LEF socket is machined out of the LEF casting. There is no positive axial connection between the central guide tube and the end fittings.

A SS guide tube sleeve (except as noted by Section 3.7), located in the upper region of the guide tube/post, prevents guide tube wear. Fretting wear was caused by coolant turbulence inducing vibratory motion in the CEAs which rubbed against the guide tube wall. Significant wear has been found to be limited to the relative soft Zircaloy-4 guide tube because the Inconel-625 cladding on the CEAs provides a relatively hard wear surface. Beginning with Unit 1 Cycle 3, (Unit 2 Cycle 2) and continuing in subsequent cycles, SS sleeves were installed in fuel assembly guide tubes with significant wear, and in fuel assembly guide tubes under most CEAs. In addition to the installation of sleeves in guide tubes to prevent wear, some assemblies were fabricated for Unit 2 Cycle 2, Unit 1 Cycle 4, and Unit 1 Cycle 5 with reduced flow guide tubes to reduce CEA vibration.

The sleeve is of slightly cold worked 304 SS, chrome plated on the inside surface. The chrome plating provides resistance to wear without the risk of promoting wear in the CEA Inconel cladding. The nominal wall thickness is adequate for free movement of the CEA and does not significantly increase the maximum CEA drop time. To secure the sleeves in the guide tube, the lower ends of the sleeves are expanded radially so that the guide tubes are permanently expanded. The lower third of the sleeve is also expanded outward so that the outside of the sleeve contacts the guide tube.

Beginning with Batch 1K and 2J fuel assemblies a modified short-sleeve design is used. This allows for reconstitution of the assemblies without having to remove and reinstall the guide tube sleeves. All new fuel assemblies are sleeved with the short-sleeve design (Reference 3).

The five guide tubes have the effect of ensuring that bowing or excessive swelling of the adjacent fuel rods or poison rods cannot result in obstruction of the CEA pathway. This is so because:

a. There is sufficient clearance between the fuel rods and the guide tube surface to allow an adjacent fuel rod to reach rupture strain without contacting the guide tube surface.
b. The guide tube, having considerably greater diameter and wall thickness (and at a lower temperature) than the fuel rod, is considerably stiffer than the fuel rods and would, therefore, remain straight, rather than be deflected by contact with the surface of an adjacent fuel rod.

Therefore, the bowing or swelling of fuel rods would not result in obstruction of the control element channels such as could hinder CEA movement.

The fuel assembly design enables reconstitution (i.e., removal and replacement of fuel rods or poison rods) of an irradiated fuel assembly. The fuel rod and poison rod lower end caps are conically shaped to ensure proper insertion within the fuel assembly grid cage structure. The upper end caps are designed to enable remote grappling of the fuel rod or poison rod for purposes of removal and handling. The five posts may be untorqued and removed from the guide tubes, allowing the removal of the upper end fitting assembly as one unit (a hold-down plate, a flow plate, five posts and five springs) with a single tool. This removal provides access to the fuel rods and poison rods for replacement or servicing. Before loading into the core, the threaded joints which mechanically attach the upper end fitting to the guide tubes are properly torqued and locked.

A unique serial number on each fuel assembly upper end fitting enables verification of fuel enrichment and orientation of the fuel assembly. Indication is also provided on the LEF to ensure preservation of fuel assembly orientation in the event of upper end fitting removal.

The lower end of each rod has a serial number to provide a means of identifying the pellet enrichment, pellet lot, and fuel stack weight. In addition, a quality control program specification requires that measures be established for the identification and control of materials, components, and partially fabricated subassemblies. These means provide assurance that only acceptable items are used and also provides a method of relating an item or assembly from initial receipt through fabrication, installation, repair, or modification to an applicable drawing, specification, or other pertinent technical document.

For the AREVA/Framatome design, the spacer grids are the Zircaloy-4 HTP™ spacers at all elevations except the bottom spacer. The bottom spacer is an Alloy 718 high mechanical performance (HMP™) spacer. The upper end fitting is the standard reconstitutable design that has been used at other CE14 units. The lower end fitting is the FUELGUARD™ design used to provide resistance against debris entering the fuel assembly. Features such as the capability to reconstruct fuel assemblies, individual rod and bundle identification are maintained. The springs are sized and the spring preload selected such that a net downward force will be maintained for all normal and anticipated transient flow and temperature conditions. The fuel assembly is shown in Figure 3.3-16.

3.3.2.4 Control Element Assembly Mechanical Design

The CEA (Figures 3.3-8, 3.3-9A, and 3.3-9B and Table 3.3-4) consists of five Inconel 625 tubes (fingers) loaded with a stack of cylindrical neutron absorber pellets. The absorber material is boron carbide (B_4C), with the exception of the lower portion of the four corner fingers (original design) and some center fingers (new design) which contain silver indium cadmium (Ag-In-Cd). The silver indium cadmium material reduces clad strain which radiation-induced swelling of boron carbide might cause.

The AREVA/Framatome full strength CEA rod has a slightly different configuration in the lower portion of the rod. The full strength CEA rod design contains a stack support that resides within the annulus of the silver indium cadmium (Ag-In-Cd) stack. This stack support is comprised of a support column that passes through the Ag-In-Cd annulus and a support platform, upon which the B_4C column rests. The stack support prevents the weight of the B_4C column and plenum spring preload from compressing the Ag-In-Cd stack which is susceptible to deformation through creep during operation; a significant contributor to clad strain. The stack support reduces the creep mechanism of the lower absorber and thereby reduces cladding strain.

Above the poison pellet column is a plenum which provides expansion volume to limit the internal pressure from the gases released from the boron carbide such that the primary stress does not exceed the yield strength of the cladding material at operating conditions. The plenum contains a hold-down spring which restrains the absorber material against longitudinal movement while allowing for differential expansion between the absorber and the clad. The spring also maintains the position of the absorber material during shipping and handling.

Each finger is sealed by one Inconel 625 nose cap welded at the bottom and one Inconel 625 end fitting at the top. The end fittings are attached to a spider hub structure in a square array with one finger centrally located. The spider provides rigid support for the control elements. The spider provides a point of attachment for coupling the CEA to the CEA extension shaft. A unique serial number is on each hub to provide identification.

During normal operation all of the CEAs are normally in the fully withdrawn position. Mechanical reactivity control is achieved by vertically maneuvering the positions of the CEA groups by the magnetic jack CEDMs. Each CEDM is positioned on the reactor vessel closure head and is coupled to the CEA by the CEA extension shaft.

There are 37 single CEAs and 20 dual CEAs. Each dual CEA consists of two single CEAs connected to a single extension shaft and carried by a single CEDM. Considering the 20 dual CEAs as 40 single CEAs gives an overall equivalent of 77 single CEAs in the core (Figures 3.3-10 and 3.3-11). The center CEA in group 5 is weakened in absorption capability.

In the withdrawn position the CEA resides in the Upper Guide Structure (UGS), enclosed in CEA shrouds. The shrouds provide guidance and protect the CEA and the extension shaft from coolant cross flow. Within the core, each CEA finger travels in a Zircaloy guide tube. The guide tubes are part of the fuel assembly structure and ensure proper orientation of the CEAs with respect to the fuel rods.

When the extension shaft is released by the CEDM, gravity causes the CEA to insert into the full length of the fuel assembly. The four outer guide tubes of each assembly have a reduced diameter lower section which allows for hydraulic buffering action to

slow down the CEAs near the end of their travel. The CEA velocity is decreased to minimize impact. There is a small bleed hole on the side of the buffer section of the guide tube which prevents pressure buildup and allows some coolant flow. This hydraulic damping action is augmented by a spring arrangement attached between the central CEA post and the hub. When fully inserted, the CEAs rest on the central post of the fuel assembly upper end fitting.

A prototype CEA was installed in Unit 2 at the BOC 3. The changes from standard design included a change in cladding material (from Inconel to SS), reconstitutable fingers, and a change in material for the tips of the poison fingers from Ag/In/Cd to B_4C. The size of the B_4C pellets used in the tips was decreased from the pellet size used for the remainder of the rod length. A metal liner was added to prevent any B_4C fragments from collecting in the high flux tip. This CEA was discharged at the End of Cycle (EOC) 8.

In Unit 1, nine CEAs were replaced for Cycle 8 and the rest were replaced for Cycle 9. Eight CEAs (FLCEA2, FLCEA5) were replaced in Unit 2 Cycle 7. The replacement CEAs have essentially the same design as the original components with the exceptions that replacement CEAs have reconstitutable corner fingers, and have Ag-In-Cd tips in all fingers (with the exception of the weakened center CEA in Group 5).

For Unit 2 Cycle 8 and Unit 1 Cycle 10, the first 24-month cycles, the weakened CEA in the center CEA position was replaced with a less weak CEA (FLCEA5) with all reconstitutable fingers.

For Unit 2 Cycle 9, the 69 remaining full-strength, old-style CEAs (with B_4C to the bottom of the center finger) were replaced. The replacements (FLCEA1) were non-reconstitutable and have Ag-In-Cd tips in all fingers. In addition, the weakened center CEA was replaced (Unit 2 Cycle 9 and Unit 1 Cycle 11) with a weakened CEA containing SS in the bottom of each of the four weak fingers (FLCEA6) instead of a Zircaloy slug. The Zircaloy slug was found to be subject to hydriding, in this application.

For Unit 2 Cycle 14, the reduced strength re-constitutable CEA (FLCEA6) was replaced with an equivalent reduced strength non-reconstitutable CEA (FLCEA7).

For Unit 1 Cycle 16, the reduced strength re-constitutable CEA (FLCEA6) was replaced with an equivalent reduced strength non-re-constitutable CEA (FLCEA7). Additionally, eight full strength re-constitutable CEAs with 8'' Ag-In-Cd poison stacks (FLCEA2) were replaced with eight full strength non-reconstitutable CEAs with 12'' Ag-In-Cd poison stacks (FLCEA8).

For Unit 2 Cycle 15, 12 full length CEAs (10 of the standard design and 2 with reconstitutable corner fingers) were replaced with full strength, non-reconstitutable CEAs with 12” Ag-In-Cd poison stacks (FLCEA8).

For Unit 1 Cycle 17, 68 full-length full-strength re-constitutable CEAs with 8” Ag-In-Cd poison stacks (FLCEA2) were replaced with full-length full-strength non-reconstitutable CEAs with 12” Ag-In-Cd poison stacks (FLCEA8). All of the Unit 1 full-length full-strength CEAs are of the 12” Ag-In-Cd poison stack design.

For Unit 2 Cycle 16, 64 full-length full-strength CEAs with 8” Ag-In-Cd poison stacks were replaced with full-length full-strength CEAs with 12” Ag-In-Cd poison stacks.

All of the Unit 2 full-length full-strength CEAs are of the 12” Ag-In-Cd poison stack design.

For Unit 2 Cycle 18, 2 full-length full-strength CEAs with 12” Ag-In-Cd poison stacks were replaced with full-length full-strength CEAs with 8” Ag-In-Cd poison stacks.

For Unit 1 Cycle 20, 2-full length full-strength CEAs with 12” Ag-In-Cd poison stacks were replaced with full-length full-strength CEAs with 8” Ag-In-Cd poison stacks.

For Unit 2 Cycle 19, all of the full-length full-strength CEAs are of the 12” Ag-In-Cd poison stack design.

For Unit 1 Cycle 21, the center CEA is a full-length part-strength CEA of the 8” Ag-In-Cd poison stack design, and the remaining 76 CEAs are of the full-length full-strength 12” Ag-In-Cd poison stack design.

For Unit 2 Cycle 20, the center CEA is a full-length part-strength CEA of the 8” Ag-In-Cd poison stack design, and one CEA is of the full-length full-strength 8” Ag-In-Cd poison stack design. The remaining 75 CEAs are of the full-length full-strength 12” Ag-In-Cd poison stack design.

There are two approved for use CEA designs, full-length part-strength and full-length full-strength. The center CEA is a full-length part-strength CEA of the 12.5" Ag-In-Cd poison stack design. The remaining 76 CEAs are of the full-length full-strength 12.5" Ag-In-Cd poison stack design.

3.3.2.5 Neutron Source Design

A discrete neutron source was required for a quick, safe startup of the original core. Two plutonium-238/antimony-beryllium (Pu/Sb-Be) neutron sources were located in guide tubes of peripheral fuel assemblies. The discrete neutron sources are not necessary for restart, and were removed from the reactor for Unit 1 Cycle 9 and Unit 2 Cycle 8.

3.3.2.6 Guide Tube Flux Suppressor Design

For Unit 1 Cycle 11 and Cycle 12, GTFSs were installed into selected peripheral assemblies. The basic design of the GTFSs is identical to that of the CEA fingers with regard to the B_4C pellets, Al_2O_3 spacer pellets, and the Inconel 625 cladding (Table 3.3-4). The active core region consists of 116.2" of B_4C with 10.25" of Al_2O_3 spacers at each end.

3.3.2.7 Test Capsule Assembly Design

The Test Capsule Assembly Program is being conducted to evaluate the effects of irradiation at reactor temperatures on materials being considered for advanced spacer grid spring designs. TCA-1, TCA-2, and TCA-3 (inserted beginning with Unit 1 Cycle 12) consist of, from top to bottom, a holddown assembly, an upper extension tube, 7 capsules connected axially by 6 connecting tubes, and a lower extension tube with an endplug. TCA-4 and TCA-5 (inserted beginning with Unit 1 Cycle 13) consist of, from top to bottom, a holddown assembly, an upper extension tube, containing an unused test capsule, 6 test capsules connected axially by 6 connecting tubes, and a lower extension tube with a bottom endplug that contains a test capsule that is used. The SS holddown assembly, located entirely above the core, is similar to the holddown assembly for a flux suppressor and, like a flux suppressor, is designed to preload the capsule assembly against the bottom of the

guide tube in which it resides. The capsules, extension tubes, and connecting tubes are fabricated from Inconel CEA tubing and bar stock material. All tubular sections have holes which allow the free ingress and egress of reactor coolant. The upper extension tube is sized to position the used capsules in the middle 80% of the core. The lower extension tube is designed to extend into the buffer region of the outer guide tube in order to center the capsule assembly and to prevent lateral movement. The purpose of the connecting tubes is to facilitate separation of the capsules from one another using a shearing tool in the spent fuel pool.

In Unit 1 Cycle 12, three test capsules were placed in the outer guide tubes of three separate once-burned fuel assemblies.

Four test capsules were placed in the outer guide tubes of four separate fresh fuel assemblies in Unit 1 Cycle 13. Two of these capsules were from Unit 1 Cycle 12 and two are new capsules.

Two test capsules were placed in the outer guide tubes of two separate fuel assemblies in Unit 1 Cycle 14. Both of these capsules were reinserted from Unit 1 Cycle 13. The 2 test capsules (TCA-3 and TCA-5) were discharged at the end of Unit 1 Cycle 14.

3.3.2.8 ZIRLO Cladding (Westinghouse Fuel)

In the late 1990s, Calvert Cliffs identified clad spallation phenomena on its 2nd cycle high duty fuel. That fuel used the CE standard OPTIN cladding material. OPTIN is an Optimized Process Low Tin cladding that falls within the overall Zircaloy-4 material specification. In order to eliminate the spallation phenomena, Calvert Cliffs elected to switch to an alternate clad material that has better water-side corrosion properties. The alternate cladding material selected is the Westinghouse standard ZIRLO clad material. ZIRLO is a Westinghouse proprietary modification of Zircaloy-4 material achieved by reducing the tin and iron content, eliminating the chromium content, and adding niobium. Calvert Cliffs began to phase in the use of ZIRLO cladding starting with some of the rods for Unit 1 Cycle 16 (Batch 1V).

Westinghouse submitted a topical report (Reference 4) to the NRC. On September 12, 2001, the NRC issued a safety evaluation report to approve the use of ZIRLO cladding material in CE reactors. The NRC authorized full batch implementation of ZIRLO cladding without lead test fuel assemblies, but placed the following restrictions on the use of ZIRLO:

a. The corrosion limit, as predicted by the best-estimate model, will remain below 100 microns for all locations of the fuel.
b. All the conditions listed in the safety evaluations for all the CENPD methodologies used for ZIRLO fuel analysis will continue to be met, except that the use of ZIRLO cladding in addition to Zircaloy-4 cladding is now approved.
c. All CENP methodologies will be used only within the range for which ZIRLO data was acceptable and for which the verifications discussed in Reference 4 and responses to requests for additional information were performed.
d. Until data is available demonstrating the performance or ZIRLO cladding in CE designed plants, the fuel duty will be limited for each CE designed plant with some provision for adequate margin to account for variations in core design (e.g., cycle length, plant operating conditions, etc.). Details of this condition will be addressed on a plant specific basis during the approval to use ZIRLO in a specific plant.

e. The burnup limit for this approval is 60 GWD/MTU.

3.3.2.9 M5 Cladding (AREVA/Framatome Fuel)

Beginning with Unit 2 Cycle 19 and Unit 1 Cycle 21, new fuel uses M5® cladding. AREVA submitted a topical report (Reference 5) to the NRC. The NRC issued a safety evaluation report to approve the use of M5® cladding material in CE reactors with the following restrictions:

a. The corrosion limit, as predicted by the best-estimate model, will remain below 100 microns for all locations of the fuel.
b. All the conditions listed in the safety evaluations for all the FANP methodologies used for M5® fuel analysis will continue to be met, except that the use of M5® cladding in addition to Zircaloy-4 cladding is now approved.
c. All FANP methodologies will be used only within the range for which M5® data was acceptable and for which the verifications discussed in References 5 or 6 was performed.
d. The burnup limit for this approval is 62 GWD/MTU.

3.3.2.10 Axial Blankets

Beginning with Unit 2 Cycle 16 and Unit 1 Cycle 18, the top and bottom 6 inches of pellets in all new fuel pins contain low enriched (2.6 w/o) fuel. This feature reduces axial neutron leakage and increases fuel economics.

All Zirc diboride fuel pins contain axial blankets with annular holes that remove approximately 25% of the volume of the pellet. The annular holes provide additional volume for gas production as a result of the boron coating being converted into helium gas.

Beginning with Unit 2 Cycle 19 and Unit 1 Cycle 21, the fuel uses 6” of low enriched (≤2.0 w/o) axial blankets on the top and bottom of non-gadolina-bearing fuel rods. Twelve inches of low enriched (≤2.0 w/o) axial blankets are used on the top and bottom of gadolina-bearing fuel rods.

3.3.2.11 Radial Enrichment Zoning

Unit 2 Cycle 16 and Unit 1 Cycle 18 saw the introduction of radial enrichment zoning. In these cycles, eight pins adjacent to each CEA guide tube (40 in all) and three pins at each assembly corner (12 in all) contained a lower enrichment than the other fuel pins. Beginning in Unit 2 Cycle 17, some of the subbatches are as described above, and in others, three enrichments are used. The three enrichment patterns are intended primarily to reduce calculated steaming rates.

Beginning with Unit 2 Cycle 19 and Unit 1 Cycle 21, the fuel uses two-enrichment radial zoning with the eight pins adjacent to each CEA guide tube (40 in all) and three pins at each assembly corner (12 in all) containing a lower enrichment than the other fuel non-Gadolinia pins.

3.3.3 REACTOR INTERNAL STRUCTURES

The reactor internals are designed to support and orient the reactor core fuel assemblies and CEAs, absorb the CEA dynamic loads and transmit these and other loads to the reactor vessel flange, provide a passageway for the reactor coolant, and guide incore instrumentation.

The internals are designed to safely perform their functions during all steady state conditions and during DBEs. The internals are designed to safely withstand the forces due to deadweight, handling, system pressure, flow impingement, temperature differential, vibration and seismic acceleration. All reactor components are considered Category I for seismic design. The reactor internals design provides limits of deflection where functionally required. The structural components satisfy stress values given in the ASME B&PV Code, Section III. Certain components have been subjected to a fatigue analysis. Where appropriate, the effect of neutron irradiation on the materials concerned is included in the design evaluation.

The components of the reactor internals are divided into three major parts:

a. The core support barrel,
b. The lower core support structure (including the core shroud), and
c. The UGS (including the CEA shrouds and the ICI guide tubes).

The flow skirt, although functioning as an integral part of the coolant flow path, is separate from the internals and is affixed to the bottom head of the pressure vessel (Figure 3.1-1).

3.3.3.1 Core Support Assembly

The major support member of the reactor internals is the core support assembly. This assembled structure consists of the core support barrel, the lower support structure, and the core shroud. The major material for the assembly is Type 304 SS. The core support barrel supports the core support assembly.

The upper flange of the core support barrel rests on a ledge in the reactor vessel flange. The lower flange of the core support barrel supports and positions the lower support structure. The core support plate transmits the weight of the core to the core support barrel by means of vertical columns, an annular skirt, and beam structure. The core support plate provides support and orientation for the fuel assemblies. The core shroud, which provides lateral support for the peripheral fuel assemblies, is also supported by the core support plate. The lower end of the core support barrel is restrained radially by six snubbers.

3.3.3.2 Core Support Barrel

The core support barrel approximates a right circular cylinder with a nominal inside diameter of 148" and a minimum wall thickness of 1-3/4". It is suspended by a 4" thick flange from a ledge on the pressure vessel. The core support barrel supports the lower support structure upon which the fuel assemblies rest. Press fitted into the flange of the core support barrel are four alignment keys located 90° apart. The reactor vessel, the closure head, and the UGS assembly flanges are slotted in locations corresponding to the alignment key locations to provide proper alignment and to prevent excess motion between these components in the vessel flange region.

Since the core support barrel is about 27' long and is supported only at its upper end, it is possible that coolant flow could induce vibrations in the structure. Therefore, amplitude limiting devices, or snubbers (Figure 3.3-12), are installed on the outside of the core support barrel near the bottom end. The snubbers consist of six equally spaced double lugs around the circumference and are the grooves of a "tongue-and-groove" assembly; the pressure vessel lugs are the tongues. Minimizing the clearance between the two mating pieces limits the amplitude of any vibration. The pressure vessel tongues have bolted, lock welded Inconel X shims and the core support barrel grooves are hard faced with Stellite to minimize wear.

With this design, the internals may be viewed as a beam with supports at the furthest extremities. Radial and axial expansion of the core support barrel are accommodated, but lateral movement of the core support barrel is restricted by this design.

3.3.3.3 Core Support Plate and Support Column

The core support plate aligns the fuel assemblies and directs coolant flow through them. It is a 147" diameter, 2" thick, Type 304 SS plate with the necessary machined flow distributor holes for the fuel assemblies. Fuel assembly locating pins (four for each assembly) are shrink-fitted into the support plate. An annular skirt, columns, and support beams are located between the support plate and the bottom of the core support barrel. They provide a support for this plate and transmit the core load to the bottom flange of the core support barrel.

3.3.3.4 Core Shroud

The core shroud (Figure 3.3-13) provides an envelope for the core and limits the amount of coolant bypass flow. The shroud is 152-1/2" tall and 147-5/16" in diameter. The shroud consists of two Type 304 SS ring sections, aligned by means of radial shear pins and attached to the core support plate by eight Type 348 SS tie rods for Unit 2 and seven Type 348 SS tie rods for Unit 1. A gap is maintained between the core shroud outer perimeter and the core support barrel in order to provide some coolant flow upward between the core shroud and core support barrel. This minimizes thermal stresses in the core shroud and eliminates stagnant pockets.

The gap between the outside of the peripheral fuel assemblies and the shroud is maintained by eight tiers of stiffening plates attached to the shroud. In locations where mechanical connections are used, bolts and pins are lock welded. All bolts are designed to be captured in the event of fracture. The bolt heads are trapped by lock bars or lock welds and the bolt bodies are trapped by incomplete tapping of holes. Holes are provided in the core support structure to allow coolant to flow upward between the core shroud and the core support barrel, thereby minimizing thermal stresses in the shroud and eliminating stagnant pockets.

The reactor internals have been evaluated and only four (4) or more tie rods are required to be functional, see References 7 and 8.

3.3.3.5 Flow Skirt

The Inconel flow skirt is a 3,500 pound right circular cylinder, perforated with 2-11/16 in. diameter holes, and reinforced at the top and bottom with stiffening rings. The flow skirt is used to reduce inequalities in core inlet flow distributions and to prevent formation of large vortices in the lower plenum. The skirt provides a nearly equalized pressure distribution across the bottom of the core support barrel. The skirt is supported by nine equally spaced machined sections which are welded to the bottom head of the pressure vessel.

3.3.3.6 Upper Guide Structure Assembly

The UGS assembly (Figure 3.3-14) consists of:

a. The upper support structure;
b. Sixty-five CEA shrouds;
c. A fuel assembly alignment plate; and,
d. An expansion compensating ring.

The UGS assembly aligns and laterally supports the upper end of the fuel assemblies, maintains the CEA spacing, prevents fuel assemblies from being lifted

out of position during a severe accident condition, and protects the CEAs from the effect of coolant cross flow in the upper plenum. The UGS is handled as one unit during installation and is removed for refueling.

The upper end of the UGS assembly is a support plate welded to a grid array of 24" deep beams and a 24" deep cylinder which encloses, and is welded to the ends of the beams. The periphery of the plate contains four accurately machined and located alignment keyways, equally spaced at 90° intervals, which engage the core barrel alignment keys. The reactor vessel closure head flange is slotted to engage the upper ends of the alignment keys in the core barrel. This system of keys and slots provides an accurate means of aligning the core with the closure head. The grid structure aligns and supports the upper end of the CEA shrouds.

The CEA shrouds extend from the fuel assembly alignment plate to an Elevation about 3' above the support plate. There are 45 single-type shrouds. These consist of cylindrical upper sections welded to integral bottom sections, which are shaped to provide flow passages for the coolant passing through the alignment plate while shrouding the CEAs from cross flow. Also, there are 20 dual-type shrouds which, in configuration, consist of two single-type shrouds connected by a rectangular section shaped to accommodate the dual CEAs. The bottoms of the shrouds are bolted to the fuel assembly alignment plate. At the UGS support plate, the single shrouds are connected to the plate by spanner nuts which permit axial adjustment. The spanner nuts are tightened to the proper torque and lock-welded. The dual shrouds are welded to the upper plate.

The fuel assembly alignment plate is designed to align the upper ends of the fuel assemblies and the lower ends of the CEA shrouds, as well as support the CEA shrouds. Precision machined and located holes in the fuel assembly alignment plate align the fuel assemblies (Figure 3.3-6). The fuel assembly alignment plate also has four equally spaced slots on its outer edge which engage with Stellite hard-faced pins protruding from the core shroud to limit lateral motion of the UGS assembly during operation. The alignment plate load and the weight of a fuel assembly produce a net downward force to counteract upward hydraulic forces for normal operating conditions and all DBEs. The fuel assembly alignment plate would capture the core and limit upward movement in the event of an accident.

A holddown ring acts as a shim between the reactor vessel flange and the UGS. It resists axial upward movement of the UGS assembly. This arrangement accommodates axial differential thermal expansion between the core barrel flange, UGS flange, the reactor vessel flange mating surface and head flange recess. The UGS also supports the incore instrumentation guide tubes. The tubes are conduits which protect the incore instrumentation and guide them during removal and insertion operations.

3.3.4 CONTROL ELEMENT DRIVE MECHANISM

3.3.4.1 Design

The CEDM is of the magnetic jack-type drive. Each CEDM is capable of withdrawing, inserting, holding, or tripping the CEA from any point within its 137" stroke (Figure 3.3-15). The design of the CEDM is identical to that for Maine Yankee (Reference 2).

The CEDM drives the CEA within the reactor core and indicates the position of the CEA with respect to the core. The speed at which the CEA is inserted or withdrawn from the core is consistent with the reactivity change requirements during reactor

operation. For conditions that require a rapid shutdown of the reactor, the CEDM coils are deenergized, allowing the CEA and the extension shaft to drop into the core by gravity. The reactivity is reduced during such a drop at a rate sufficient to control the core under any operating transient or accident condition.

The CEA is decelerated at the end of the drop by the buffer section of the CEA guide tubes.

Originally, 65 CEDMs (61 CEDMs on the replacement reactor vessel closure head) were mounted on flanged nozzles on top of the reactor vessel closure head. Eight CEDMs were nonscrammable and were connected to the PLCEAs which have been removed (4 spare CEDMs are installed in the replacement reactor vessel closure head). Each CEDM extension shaft is connected to a CEA by a locked coupling. The weight of the CEAs and CEDMs is carried by the vessel head.

The CEDM is designed to handle dual or single CEAs. The total stroke of the drive is 137". The maximum withdrawing speed of CEDMs is 30" per minute for single CEAs and 20" per minute for dual CEAs. The maximum allowed time from receiving a trip signal to the essentially fully inserted position of the CEA is specified in the Technical Specifications.

a. CEDM Pressure Housing

   Each CEDM housing is attached to the reactor vessel head nozzle by means of a threaded joint and seal welded. It need not be removed since all servicing of the CEDM is performed from the top of the CEDM housing. This opening is closed by means of a threaded cap and omega seal weld.

   The CEDM upper housing design and fabrication conforms to the requirements of the ASME B&PV Code, Section III, for Class 1 appurtenances for the replacement reactor vessel closure head). The housing is designed for steady state conditions as well as all anticipated pressure and thermal transients.

b. Magnetic Jack Assembly

   The magnetic jack motor assembly fits into the CEDM housing through an opening in the top of the housing. This integral unit carries the motor tube, lift and hold pawls, and magnets. Electrical coils positioned around the CEDM housing supply the drive power. The CEDMs are cooled by forced air which maintains CEDM coil temperature below 350°F. Loss of cooling air will not prevent the CEDM from releasing the CEAs when a reactor trip is initiated. A description of the air circulation system is presented in Chapter 9.

   The upper housing cap is threaded into the CEDM housing and seal welded after the CEDM motor assembly is inserted. This cap supports the position indication housing which encloses the CEDM extension shaft.

   The lifting operation consists of a series of magnetically-operated step movements. Two sets of mechanical latches engage a notched drive shaft. To prevent excessive latch wear, a means has been provided to unload the latches during the engaging and disengaging operations.

   The magnetic force is obtained from large DC magnet coils mounted on the outside of the motor tube. Power for the electromagnets is obtained from

two separate supplies. A control programmer actuates the stepping cycle and positions the CEA by a forward or reverse stepping sequence. The CEA is held stationary by energizing one coil at a reduced current while all other coils are deenergized. The CEAs are tripped upon interruption of electrical power to all coils.

c. Position Indication

Three separate means are provided for transmitting CEA position indication.

The first method utilizes the electrical pulses from the magnetic coil power programmer. The second method utilizes reed switches and a voltage divider network mounted on the CEDM to provide an output voltage proportional to CEA position. The third method utilizes three pairs of reed switches spaced at discrete locations within a position transmitter assembly. A permanent magnet built into the drive shaft actuates the reed switches one at a time as it passes by them. CEA position instrumentation is discussed in detail in Chapter 7.

d. Control Element Assembly Disconnect

The CEA connects to the drive shaft extension with an internal collet-type coupling at its lower end. Coupling is performed before the vessel head is installed. In order to disengage the CEA from the drive shaft extension, a tool is attached to the top end of the drive shaft when the reactor vessel head (along with all the CEDMs) has been removed.

By pulling up on the spring-loaded operating rod in the center of the drive shaft, a tapered plunger is withdrawn from the center of the collet-type gripper causing it to collapse due to axial pressure from the CEA, thus permitting removal of the coupler from the CEA. Releasing the operating rod plunger after the coupler has been withdrawn from the CEA expands the coupler to a diameter that prevents recoupling to the CEA. At this point, the drive shaft buffer is resting on the positive stop in the CEA shroud. The drive shafts, uncoupled from the CEAs, are removed along with the UGS (when the UGS is removed from the vessel).

3.3.5 REFERENCES

1. Deleted
2. Maine Yankee Final Safety Report, Docket No. 50-309
3. Letter from A.E. Scherer (CE) to C.O. Thomas (NRC), "CEA Guide Tube Wear Sleeve Modification," LD-84-043, August 3, 1984
4. CENPD-404-P-A, “Implementation of ZIRLO Cladding Material in CE Nuclear Power Fuel Assembly Designs,” November 2001
5. BAW-10240P-A, Revision 0, “Incorporation of M5 Properties in Framatome ANP Approved Methods,” May 2004
6. BAW-10227P-A, Revision 01, “Evaluation of Advanced Cladding and Structural Material (M5) in PWR Reactor Fuel,” June 2003
7. CA10415, Revision 0, "A summary of the Method and Results for Qualification of the Core Shroud Tie Rods at Calvert Cliffs Units 1 and 2"
8. ECP-18-000534, Revision 0, "Design Analysis for Continued Operation of Units 1 and 2, Beyond One Cycle due to Failed Core Shroud Tie Rods'

TABLE 3.3-1

UNIT 1 BATCH-RELATED DATA

BATCH DESIGNATION	INITIAL ASSEMBLY AVERAGE ENRICHMENT wt% U-235	NUMBER OF B_4C SHIMS PER ASSEMBLY	INITIAL SHIM LOADING wt% B_4C	AVERAGE WEIGHT OF URANIUM PER ASSEMBLY Kg U	FUEL RODS PER ASSEMBLY
1A	2.05	0	---	395	176
1B	2.45	12	2.9	368	164
1C	2.99	0	---	395	176
1C+	2.99	12	1.1	369	164
1C.	2.99	12	.68	368	164
1D	3.03	0	---	388	176
1D/	2.73	0	---	388	176
1E	3.03	0	---	388	176
1E/	2.73	0	---	387	176
1F	3.03	0	---	389	176
1F/	2.73	0	---	389	176
1G	3.65	0	---	388	176
1G/	3.03	8	3.03	371	168
1H	4.00	0	---	389	176
1H/	3.55	8	3.03	372	168
1J	4.05	0	---	389	176
1J*	3.40	0	---	389	176
1K	4.05	0	---	389	176
1K*	3.40	0	---	388	176
1L	4.05	0	---	388	176
1L*	3.40	0	---	388	176
1M	4.08	0	---	393	176
1M*	4.08	12	4.09	365	164
1MX	3.85	0	---	377	176
1N	4.20	0	---	393	176
1NX	4.20	4	4.04	383	172
1N/	4.20	8	4.04	373	168

Batch 1MX is Advanced Nuclear Fuel (ANF) demonstration fuel with 12 Gd_2O_3 (10 wt%) fuel bearing (natural uranium) poison rods per assembly.

TABLE 3.3-1

UNIT 1 BATCH-RELATED DATA

BATCH DESIGNATION	INITIAL ASSEMBLY AVERAGE ENRICHMENT wt% U-235	NUMBER OF ERBIUM SHIMS PER ASSEMBLY	INITIAL SHIM LOADING wt% Er_2O_3	AVERAGE WEIGHT OF URANIUM PER ASSEMBLY Kg U	FUEL RODS PER ASSEMBLY
1P0	4.30	0	0.0	392	176
1P1	4.30	20	2.0	392	176
1P2	4.30	44	2.0	391	176
1P3	4.30	60	2.0	390	176
1R0	4.48	20	2.00	391	176
1R1	4.48	44	2.00	391	176
1R2	4.48	68	2.00	390	176
1RT	4.00 (VAP)	44	1.75	408	176
1S0	4.30	0	0.0	393	176
1S1	4.30	20	2.0	393	176
1S2	4.30	44	2.0	392	176
1S3	4.30	68	2.0	391	176
1T0	4.28 (VAP)	0	0.0	408	176
1T1	4.28 (VAP)	20	1.75	408	176
1T2	4.28 (VAP)	44	1.75	407	176
1V0	4.25 (VAP)	0	0.0	410	176
1V1	4.25 (VAP)	44	1.75	408	176
1V2	4.25 (VAP)	60	1.75	407	176
1W0	4.25 (VAP)	0	0.00	409	176
1W1	4.25 (VAP)	20	2.00	409	176
1W2	4.25 (VAP)	44	2.00	407	176
1W3	4.25 (VAP)	60	2.00	406	176
1W4	4.25 (VAP)	60	2.00	406	176

TABLE 3.3-1

UNIT 1 BATCH-RELATED DATA

BATCH DESIGNATION	INITIAL ENRICHMENTS wt% U-235	NUMBER OF ZrB_2 SHIMS PER ASSEMBLY	INITIAL SHIM LOADING (mg-B-10/ inch)	AVERAGE WEIGHT OF URANIUM PER ASSEMBLY Kg U	FUEL RODS PER ASSEMBLY
1X1	2.6/4.0/4.5 (VAP)	44	3.29	407	176
1X2	2.6/4.0/4.5 (VAP)	52	3.29	407	176
1X3	2.6/4.0/4.5 (VAP)	64	3.29	406	176
1X4	2.6/4.0/4.5 (VAP)	76	3.29	406	176
1X5	2.6/4.0/4.5 (VAP)	96	3.29	405	176
1X7	2.0 (VAP)	0	0	409	176
1Z1	4.95/4.65/2.60 (VAP)	0	0	409	176
1Z2	4.95/4.65/2.60 (VAP)	28	3.29	408	176
1Z3	4.95/4.65/2.60 (VAP)	44	3.29	407	176
1Z4	4.95/4.65/4.00/2.60 (VAP)	64	3.29	406	176
1Z5	4.95/4.65/4.00/2.60 (VAP)	76	3.29	406	176
1Z6	4.95/4.65/4.00/2.60 (VAP)	96	3.29	405	176
AA1	4.95/4.00/2.60 (VAP)	28	3.29	407	176
AA2	4.95/4.00/2.60 (VAP)	52	3.29	406	176
AA3	4.95/4.55/4.00/2.60 (VAP)	64	3.29	406	176
AA4	4.95/4.55/4.00/2.60 (VAP)	76	3.29	405	176
AA5	4.95/4.55/4.00/2.60 (VAP)	96	3.29	404	176
2X7	2.00 (VAP)	0	0	409	176

VAP Value Added Pellet

Batch 2X7 assemblies were purchased as spare assemblies for Unit 2 Cycle 18. They were not used for U2C18; hence they are being employed for U1C20.

TABLE 3.3-1

UNIT 1 BATCH-RELATED DATA

BATCH DESIGNATION	INITIAL ENRICHMENTS wt% U-235	NUMBER OF Gd_2O_3 RODS PER ASSEMBLY	INITIAL Gd_2O_3 LOADING wt%	AVERAGE WEIGHT OF URANIUM PER ASSEMBLY Kg U	FUEL RODS PER ASSEMBLY
AB1	4.60/4.00/2.00 (3.60/2.60)	4/12	4/8	407	176
AB2	4.60/4.00/2.00 (3.60/3.20)	4/12	4/6	408	176
AB3	4.60/4.00/2.00 (3.60)	12	4	409	176

BATCH DESIGNATION	INITIAL ENRICHMENTS wt% U-235	NUMBER OF Gd_2O_3 RODS PER ASSEMBLY	INITIAL Gd_2O_3 LOADING wt%	AVERAGE WEIGHT OF URANIUM PER ASSEMBLY Kg U	FUEL RODS PER ASSEMBLY
AC1	4.87/4.20/2.00 (3.60/2.80)	4/12	4/8	407	176
AC2	4.87/4.20/2.00 (3.20)	12	6	408	176
AC3	4.87/4.20/2.00 (3.60)	8	4	409	176

BATCH DESIGNATION	INITIAL ENRICHMENTS wt% U-235	NUMBER OF Gd_2O_3 RODS PER ASSEMBLY	INITIAL Gd_2O_3 LOADING wt%	AVERAGE WEIGHT OF URANIUM PER ASSEMBLY Kg U	FUEL RODS PER ASSEMBLY
AD1	4.90/4.30/2.00 (3.60/2.50)	4/12	4/8	407	176
AD2	4.90/4.30/2.00 (3.60/3.20)	4/12	4/6	408	176
AD3	4.90/4.30/2.00 (3.60)	12	4	409	176
AD4	4.90/4.30/2.00 (3.60/3.20)	4/4	4/6	409	176

TABLE 3.3-1

UNIT 1 BATCH-RELATED DATA

BATCH DESIGNATION	INITIAL ENRICHMENTS wt% U-235	NUMBER OF Gd_2O_3 RODS PER ASSEMBLY	INITIAL Gd_2O_3 LOADING wt%	AVERAGE WEIGHT OF URANIUM PER ASSEMBLY Kg U	FUEL RODS PER ASSEMBLY
AE1	4.85/4.25/1.60 (4.25/3.40)	8/12	2/6	408	176
AE2	4.85/4.25/1.60 (3.60/3.40)	8/8	4/6	408	176
AE3	4.85/4.25/1.60 (3.60)	12	4	409	176
AE4	4.85/4.25/1.60 (3.40)	8	6	409	176
AE5	4.85/4.25/1.60 (3.60)	8	4	409	176

TABLE 3.3-1

UNIT 1 BATCH-RELATED DATA

UNIT 1 CYCLE 1

ASSEMBLY BATCH	NUMBER OF ASSEMBLIES	TOTAL SHIMS	TOTAL FUEL RODS
1A	69	0	12,144
1B	80	960	13,108
1C	40	0	7,040
1C+	16	192	2,624
1C.	12	144	1,968
TOTALS	217	1,296	36,896

In Cycle 1, Batch B included three test assemblies. Each contains four SS rods as well as twelve poison rods.

UNIT 1 CYCLE 2

ASSEMBLY BATCH	NUMBER OF ASSEMBLIES	TOTAL SHIMS	TOTAL FUEL RODS
1B	77	924	12,620
1C	40	0	7,040
1C+	16	192	2,624
1C.	12	144	1,968
1D	48	0	8,448
1D/	24	0	4,224
TOTALS	217	1,260	36,924

In Cycle 2, Batch B included two test assemblies. Each contains four SS rods as well as twelve poison rods.

UNIT 1 CYCLE 3

ASSEMBLY BATCH	NUMBER OF ASSEMBLIES	TOTAL SHIMS	TOTAL FUEL RODS
1A	40	0	7,040
1B	1	12	160
1C	32	0	5,632
1D	48	0	8,448
1D/	24	0	4,224
1E	48	0	8,448
1E/	24	0	4,224
TOTALS	217	12	38,176

In Cycle 3, Batch B is a test assembly. In addition to the twelve poison rods, it contains four SS rods.

TABLE 3.3-1

UNIT 1 BATCH-RELATED DATA

UNIT 1 CYCLE 4

ASSEMBLY BATCH	NUMBER OF ASSEMBLIES	TOTAL SHIMS	TOTAL FUEL RODS
1B*	1	12	160
1D	48	0	8,488
1D/	24	0	4,224
1E	48	0	8,448
1E/	24	0	4,224
1F	48	0	8,448
1F/	24	0	4,224
TOTALS	217	12	38,176

* This is the test assembly. In addition to the twelve poison rods, it contains four SS rods, one in each corner.

UNIT 1 CYCLE 5

ASSEMBLY BATCH	NUMBER OF ASSEMBLIES	TOTAL SHIMS	TOTAL FUEL RODS
1D	1	0	175
1E	48	0	8,448
1E/	4	0	704
1F	48	0	8,448
1F/	24	0	4,224
1G	40	0	7,040
1G/	52	416	8,736
TOTALS	217	416	37,775

In Cycle 5, the Batch 1D fuel assembly contains one SS rod.

UNIT 1 CYCLE 6

ASSEMBLY BATCH	NUMBER OF ASSEMBLIES	TOTAL SHIMS	TOTAL FUEL RODS
1D	1	0	176
2D	8	0	1,408
1F	44	0	7,743
1G	40	0	7,040
1G/	52	416	8,736
1H	40	0	7,040
1H/	32	256	5,376
TOTALS	217	672	37,519

Batch F includes one test assembly (SCOUT) that contains an SS rod.

TABLE 3.3-1

UNIT 1 BATCH-RELATED DATA

UNIT 1 CYCLE 7

ASSEMBLY BATCH	NUMBER OF ASSEMBLIES	TOTAL SHIMS	TOTAL FUEL RODS
2B	12	144	1,968
2D/	12	0	2,112
1E/	12	0	2,112
1F	5	0	877
1G	40	0	7,038
1H	40	0	7,040
1H/	32	256	5,376
1J	48	0	8,448
1J*	16	0	2,816
TOTALS	217	400	37,787

Batch F includes one test assembly (SCOUT) that contains three SS rods.

Batch G includes four test assemblies (PROTOTYPE) that contains two stainless steel rods.

UNIT 1 CYCLE 8

ASSEMBLY BATCH	NUMBER OF ASSEMBLIES	NON-FUEL RODS	TOTAL FUEL RODS
2E	4	0	704
1F	1	3	173
1G	4	3	701
1H/	32	256	5,376
1H	40	0	7,040
1J*	16	0	2,816
1J	48	0	8,448
1K*	24	0	4,224
1K	48	0	8,448
TOTALS	217	262	37,930

The Batch F assembly is a test assembly (SCOUT) that contains three stainless steel rods.

The four Batch G test assemblies (PROTOTYPE) contain three SS rods.

TABLE 3.3-1

UNIT 1 BATCH-RELATED DATA

UNIT 1 CYCLE 9

ASSEMBLY BATCH	NUMBER OF ASSEMBLIES	NON-FUEL RODS	TOTAL FUEL RODS
2E	24	0	4,224
1G	4	2	702
1H	1	0	176
1J*	16	0	2,816
1J	48	2	8,446
1K*	24	2	4,222
1K	48	2	8,446
1L*	12	0	2,112
1L	40	0	7,040
TOTALS	217	8	38,184

All non-fuel rods in Cycle 9 contain SS.

In Batch 1G, one test assembly (PROTOTYPE) contains two SS rods. Prior to Cycle 9, one SS rod was replaced with a test rod from SCOUT.

Batch 1J includes one assembly with two stainless rods.

Batch 1K includes two assemblies with a total of two stainless rods.

Batch 1K* includes two assemblies with a total of two stainless rods.

UNIT 1 CYCLE 10

ASSEMBLY BATCH	NUMBER OF ASSEMBLIES	NON-FUEL RODS	TOTAL FUEL RODS
1K	48	2	8,446
1K*	21	2	3,694
1L	40	2	7,038
1L*	12	2	2,110
1M	16	0	2,816
1M*	76	912	12,464
1MX	4	0	704
TOTALS	217	920	37,272

Batch 1L includes one assembly with two SS rods.

Batch 1L* includes two assemblies with a total of two SS rods.

Batch 1MX is ANF demonstration fuel with 12 Gd_2O_3 (10 wt%) fuel bearing (natural uranium) poison rods per assembly.

Batches 1K and 1K* have four assemblies with one SS rod in each.

TABLE 3.3-1

UNIT 1 BATCH-RELATED DATA

UNIT 1 CYCLE 11

ASSEMBLY BATCH	NUMBER OF ASSEMBLIES	NON-FUEL RODS	TOTAL FUEL RODS
1K*	1	0	176
1L	36	3	6,333
1M	16	2	2,814
1M*	76	923	12,453
1MX	4	0	704
1N	12	0	2,112
1NX	20	80	3,440
1N/	52	416	8,736
TOTALS	217	1,424	36,768

Batch 1L includes two assemblies with a total of three SS rods.

Batch 1M includes one assembly with a total of two SS rods.

Batch 1M* includes five assemblies with a total of eleven SS rods.

Batch 1MX is ANF demonstration fuel with 12 Gd_2O_3 (10 wt%) fuel bearing (natural uranium) poison rods per assembly.

UNIT 1 CYCLE 12

ASSEMBLY BATCH	NUMBER OF ASSEMBLIES	NON-FUEL RODS	TOTAL FUEL RODS
1K*	1	0	176
1L	4	1	703
1M	16	2	2,814
1M*	20	245	3,275
1MX	4	0	704
1N	12	0	2,112
1NX	20	80	3,440
1N/	52	416	8,736
1P0	16	0	2,816
1P1	12	0	2,112
1P2	8	0	1,408
1P3	52	0	9,152
TOTALS	217	744	37,448

Batch 1L includes one assembly with a total of one SS rod.

Batch 1M includes one assembly with a total of two SS rods.

Batch 1M* includes one assembly with a total of five SS rods.

Batch 1MX is ANF demonstration fuel with 12 Gd_2O_3 (10 wt%) fuel bearing (natural uranium) poison rods per assembly.

TABLE 3.3-1

UNIT 1 BATCH-RELATED DATA

UNIT 1 CYCLE 13

ASSEMBLY BATCH	NUMBER OF ASSEMBLIES	NON-FUEL RODS	TOTAL FUEL RODS
2J*	1	0	176
1N	8	0	1,408
1NX	16	64	2,752
1N/	16	128	2,688
1P0	16	0	2,816
1P1	12	0	2,112
1P2	8	0	1,408
1P3	52	0	9,152
1R0	24	0	4,224
1R1	28	0	4,928
1R2	32	0	5,632
1RT	4	0	704
TOTALS	217	192	38,000

UNIT 1 CYCLE 14

ASSEMBLY BATCH	NUMBER OF ASSEMBLIES	NON-FUEL RODS	TOTAL FUEL RODS
2J*	5	0	880
1M*	4	48	656
1P0	16	0	2,816
1P1	12	0	2,112
1P2	8	0	1,408
1R0	24	0	4,224
1R1	28	0	4,928
1R2	32	0	5,632
1RT	4	0	704
1S0	24	0	4,224
1S1	4	0	704
1S2	40	0	7,040
1S3	16	0	2,816
TOTALS	217	48	38,144

TABLE 3.3-1

UNIT 1 BATCH-RELATED DATA

UNIT 1 CYCLE 15

ASSEMBLY BATCH	NUMBER OF ASSEMBLIES	NON-FUEL RODS	TOTAL FUEL RODS
1L*	4	0	704
1NX	4	16	688
1RT	2	2	350
1R2	6	1	1,055
1R0	24	0	4,224
1S3	16	0	2,816
1S2	40	0	7,040
1S1	4	0	704
1S0	24	0	4,224
1T2	60	0	10,560
1T1	4	0	704
1T0	28	0	4,928
2J*	1	0	176
TOTALS	217	19	38,173

Assembly 1RT1 has 2 stainless steel rods.

Assembly 1R222 has 1 stainless steel rod.

UNIT 1 CYCLE 16

ASSEMBLY BATCH	NUMBER OF ASSEMBLIES	NON-FUEL RODS	TOTAL FUEL RODS
1V0	24	0	4,224
1V1	48	0	8,448
1V2	24	0	4,224
1T0	28	0	4,928
1T1	4	0	704
1T2	60	0	10,560
1S0	20	0	3,520
1S1	4	0	704
1S2	4	0	704
2J*	1	0	176
TOTALS	217	0	38,192

TABLE 3.3-1

UNIT 1 BATCH-RELATED DATA

UNIT 1 CYCLE 17

ASSEMBLY BATCH	NUMBER OF ASSEMBLIES	NON-FUEL RODS	TOTAL FUEL RODS
1W0	20	0	3,520
1W1	12	0	2,112
1W2	36	0	6,336
1W3	16	0	2,816
1W4	4	0	704
1V0	24	0	4,224
1V1	48	0	8,448
1V2	24	0	4,224
1T0	20	0	3,520
1T1	4	0	704
1T2	8	0	1,408
1L*	1	0	176
TOTALS	217	0	38,192

UNIT 1 CYCLE 18

ASSEMBLY BATCH	NUMBER OF ASSEMBLIES	NON-FUEL RODS	TOTAL FUEL RODS
X1	32	0	5,632
X2	8	0	1,408
X3	12	0	2,112
X4	24	0	4,224
X5	20	0	3,520
X7	1	0	176
W0	20	0	3,520
W1	12	0	2,112
W2	36	4	6,332
W3	16	0	2,816
W4	4	0	704
V0	16	0	2,816
V1	16	0	2,816
TOTALS	217	4	38,188

Batch W2 includes three assemblies with a total of four stainless rods.

TABLE 3.3-1

UNIT 1 BATCH-RELATED DATA

UNIT 1 CYCLE 19

ASSEMBLY BATCH	NUMBER OF ASSEMBLIES	NON-FUEL RODS	TOTAL FUEL RODS
1Z1	4	0	704
1Z2	8	0	1,408
1Z3	12	0	2,112
1Z4	24	0	4,224
1Z5	40	0	7,040
1Z6	8	0	1,408
1X1	32	1	5,631
1X2	8	0	1,408
1X3	12	0	2,112
1X4	20	0	3,520
1X5	20	0	3,520
1W0	8	0	1,408
1W1	8	0	1,408
1W2	8	0	1,408
2V4	1	0	176
2TF	2	0	352
2TW	2	0	352
TOTALS	217	1	38,191

UNIT 1 CYCLE 20

ASSEMBLY BATCH	NUMBER OF ASSEMBLIES	NON-FUEL RODS	TOTAL FUEL RODS
AA1	12	0	2,112
AA2	8	0	1,408
AA3	12	0	2,112
AA4	36	0	6,336
AA5	20	0	3,520
2X7	4	0	704
1Z1	4	0	704
1Z2	8	0	1,408
1Z3	12	0	2,112
1Z4	24	0	4,224
1Z5	40	0	7,040
1Z6	8	0	1,408
1X1	24	0	4,224
1W0	4	0	704
2V4	1	0	176
TOTALS	217	0	38,192

TABLE 3.3-1

UNIT 1 BATCH-RELATED DATA

UNIT 1 CYCLE 21

ASSEMBLY BATCH	NUMBER OF ASSEMBLIES	NON-FUEL RODS	TOTAL FUEL RODS
AB1	48	0	8,448
AB2	16	0	2,816
AB3	32	0	5,632
AA1	12	0	2,112
AA2	8	0	1,408
AA3	12	0	2,112
AA4	36	0	6,336
AA5	20	0	3,520
2X7	4	0	704
1Z1	4	0	704
1Z2	8	0	1,408
1Z3	4	0	704
1Z4	4	0	704
1X4	1	0	176
1W1	4	0	704
1W2	4	0	704
TOTALS	217	0	38,192

UNIT 1 CYCLE 22

ASSEMBLY BATCH	NUMBER OF ASSEMBLIES	NON-FUEL RODS	TOTAL FUEL RODS
AC1	56	0	9,856
AC2	16	0	2,816
AC3	24	0	4,224
AB1	48	0	8,448
AB2	16	0	2,816
AB3	32	0	5,632
AA1	12	0	2,112
AA2	8	0	1,408
2X1	4	0	704
1X1	1	0	176
TOTALS	217	0	38,192

UNIT 1 CYCLE 23

ASSEMBLY BATCH	NUMBER OF ASSEMBLIES	NON-FUEL RODS	TOTAL FUEL RODS
AD1	36	0	6336
AD2	20	0	3520
AD3	16	0	2816
AD4	24	0	4224
AC1	56	0	9856
AC2	16	0	2816
AC3	24	0	4224
AB3	24	0	4224
BA5	1	0	176
TOTALS	**217**	**0**	38192

TABLE 3.3-1

UNIT 1 BATCH-RELATED DATA

	UNIT 1 CYCLE 24		
ASSEMBLY BATCH	**NUMBER OF ASSEMBLIES**	**NON-FUEL RODS**	**TOTAL FUEL RODS**
AE1	40	0	7040
AE2	16	0	2816
AE3	20	0	3520
AE4	8	0	1408
AE5	12	0	2112
AD1	36	0	6336
AD2	20	0	3520
AD3	16	0	2816
AD4	24	0	4224
AC3	24	0	4224
BA5	1	0	176
TOTALS	217	0	38,192

TABLE 3.3-1

UNIT 1 BATCH-RELATED DATA

PARAMETER	BATCHES						
	A	B	C	D	E	F	G
Active Length, inches	136.7	136.7	136.7	136.7	136.7	136.7	136.7
Pellet Diameter, inches	.3795	.3795	.3795	.3765	.3765	.3765	.3765
Pellet Length, inches	.650	.650	.650	.450	.450	.450	.450
Pellet Density, g/cc	10.193	10.193	10.193	10.385	10.385	10.385	10.385
Stack Height Density, g/cc	10.054	10.054	10.054	10.018	10.046	10.046	10.046
Clad ID, inches	.3880	.3880	.3880	.3840	.3840	.3840	.3840
Clad OD, inches	.440	.440	.440	.440	.440	.440	.440
Clad Thickness, inches	.026	.026	.026	.028	.028	.028	.028
Diametral Gap, inches	.0085	.0085	.0085	.0075	.0075	.0075	.0075

PARAMETER	BATCHES							
	H	J	K	L	M	MX[a]	N	P
Active Length, inches	136.7	136.7	136.7	136.7	136.7	136.7	136.7	136.7
Pellet Diameter, inches	.3765	.3765	.3765	.3765	.3765	.3700	.3765	.3765
Pellet Length, inches	.450	.450	.450	.450	.450	.425	.450	.450
Pellet Density, g/cc	10.385	10.385	10.385	10.385	10.385	10.302	10.439	10.439
Stack Height Density, g/cc	10.046	10.046	10.046	10.046	10.046	10.180[b]	10.100	10.100
Clad ID, inches	.3840	.3840	.3840	.3840	.3840	.378	.3840	.3840
Clad OD, inches	.440	.440	.4400	.440	.440	.440	.440	.440
Clad Thickness, inches	.028	.028	.0280	.028	.028	.031	.028	.028
Diametral Gap, inches	.0075	.0075	.0075	.0075	.0075	.008	.0075	.0075

TABLE 3.3-1

UNIT 1 BATCH-RELATED DATA

PARAMETER	BATCHES						
	R	RT	S	T	V	W	X
Active Length, inches	136.7	136.7	136.7	136.7	136.7	136.7	136.7
Pellet Diameter, inches	.3765	.3810	.3765	.3810	.3810	.3810	.3810
Pellet Length, inches	.450	.456	.450	.456	.456	.456	.456
Pellet Density, g/cc	10.439	10.467	10.439	10.467	10.467	10.467	10.467
Stack Height Density, g/cc	10.12	10.31	10.17	10.31	10.31	10.31	Regular 10.32 Annular 7.82
Clad ID, inches	.3840	.3880	.3840	.3880	.3880	.3880	.3880
Clad OD, inches	.440	.440	.440	.440	.440	.440	.440
Clad Thickness, inches	.028	.026	.028	.026	.026	.026	.026
Diametral Gap, inches	.0075	.0070	.0075	.0070	.0070	.0070	.0070

PARAMETER	BATCHES			
	Z	AA	AB	AC
Active Length, inches	136.7	136.7	136.7	136.7
Pellet Diameter, inches	.3810	.3810	0.3805	0.3805
Pellet Length, inches	.456	.456	0.476 (Central) 0.545 (Blanket)	0.476 (Central) 0.545 (Blanket)
Pellet Density, g/cc	10.467	10.467	10.5216	10.5216
Stack Height Density, g/cc	Regular 10.32 Annular 7.82	Regular 10.32 Annular 7.82	10.3743 (UO_2) 10.2277 (4 wt% Gd_2O_3) 10.1565 (6 wt% Gd_2O_3) 10.0867 (8 wt% Gd_2O_3) 10.3953 (Blanket)	10.3743 (UO_2) 10.2277 (4 wt% Gd_2O_3) 10.1565 (6 wt% Gd_2O_3) 10.0867 (8 wt% Gd_2O_3) 10.3953 (Blanket)
Clad ID, inches	.3880	.3880	0.387	0.387
Clad OD, inches	.440	.440	0.440	0.440
Clad Thickness, inches	.026	.026	0.0265	0.0265
Diametral Gap, inches	.0070	.0070	0.0065	0.0065

TABLE 3.3-1

UNIT 1 BATCH-RELATED DATA

PARAMETER	BATCHES	
	AD	AE
Active Length, inches	136.7	136.7
Pellet Diameter, inches	0.3805	0.3805
Pellet Length, inches	0.476 (Central) 0.545 (Blanket)	0.476 (Central) 0.545 (Blanket)
Pellet Density, g/cc	10.5216	10.5216
Stack Height Density, g/cc	10.3743 (UO_2) 10.2277 (4 wt% Gd_2O_3) 10.1565 (6 wt% Gd_2O_3) 10.0867 (8 wt% Gd_2O_3) 10.3953 (Blanket)	10.3743 (UO_2) 10.3003 (2 wt% Gd_2O_3) 10.2277 (4 wt% Gd_2O_3) 10.1565 (6 wt% Gd_2O_3) 10.3953 (Blanket)
Clad ID, inches	0.387	0.387
Clad OD, inches	0.440	0.440
Clad Thickness, inches	0.0265	0.0265
Diametral Gap, inches	0.0065	0.0065

(a) ANF Demonstration Assemblies.
(b) Pellet envelope includes both UO_2 and Gd_2O_3.

TABLE 3.3-2

UNIT 2 BATCH-RELATED DATA

BATCH DESIGNATION	INITIAL ASSEMBLY AVERAGE ENRICHMENT wt% U-235	NUMBER OF B_4C SHIMS PER ASSEMBLY	INITIAL SHIM LOADING wt% B_4C	AVERAGE WEIGHT OF URANIUM PER ASSEMBLY Kg U	FUEL RODS PER ASSEMBLY
2A	2.05	0	---	396	176
2B	2.45	12	2.9	370	164
2C	2.99	0	---	397	176
2C+	2.99	12	1.1	369	164
2C.	2.99	12	.7	369	164
2D	3.03	0	---	388	176
2D/	2.73	0	---	388	176
2E	3.03	0	---	389	176
2E/	2.73	0	---	389	176
2F	3.65	0	---	390	176
2F/	3.03	8	3.03	371	168
2G	4.00	0	---	389	176
2G/	3.55	8	3.03	372	168
2H	4.05	0	---	389	176
2H*	3.40	0	---	388	176
2J	4.05	0	---	390	176
2J*	3.40	0	---	390	176
2K	4.08	0	---	390	176
2K*	4.08	12	4.09	362	164
2K/	4.08	8	4.09	372	168
2L	4.30	0	---	389	176
2LX	4.30	4	4.09	380	172
2L/	4.30	8	4.09	371	168
2L*	4.30	12	4.09	363	164
2LE	3.81	0	---	389	176
2M	4.00	0	---	392	176
2M1	4.00	4	4.09	384	172
2M2	4.00	8	4.09	375	168
2M3	4.00	12	4.09	366	164

TABLE 3.3-2

UNIT 2 BATCH-RELATED DATA

BATCH DESIGNATION	INITIAL ASSEMBLY AVERAGE ENRICHMENT wt% U-235	NUMBER OF ERBIUM SHIMS PER ASSEMBLY	INITIAL SHIM LOADING wt% Er_2O_3	AVERAGE WEIGHT OF URANIUM PER ASSEMBLY Kg U	FUEL RODS PER ASSEMBLY
2N0	4.48	0	0	392	176
2N2	4.48	20	1.75	392	176
2N4	4.48	44	1.75	390	176
2N6	4.48	68	1.75	389	176
2NT	4.00	44	1.75	408	176
2P0	4.48	0	0	393	176
2P1	4.48	20	2.00	393	176
2P2	4.48	44	2.00	391	176
2R0	4.48	0	0	393	176
2R1	4.48	20	1.75	392	176
2R2	4.48	44	1.75	391	176
2R3	4.48	68	1.75	390	176
2S0	4.28 (VAP)	0	0	410	176
2S1	4.28 (VAP)	20	1.75	408	176
2S2	4.28 (VAP)	44	1.75	408	176
2S3	4.28 (VAP)	68	1.75	407	176
2T0	4.25 (VAP)	0	0	410	176
2TF	4.26 (FANP)	0	0	412	176
2TW	4.25 (VAP)	0	0	409	176
2T1	4.25 (VAP)	20	2.0	409	176
2T2	4.25 (VAP)	44	2.0	408	176
2T3	4.25 (VAP	68	2.0	407	176

FANP – Framatome Advanced Nuclear Power (AREVA)

BATCH DESIGNATION	INITIAL ENRICHMENTS wt% U-235	NUMBER OF ZrB_2 SHIMS PER ASSEMBLY	INITIAL SHIM LOADING (mg-B-10/ inch)	AVERAGE WEIGHT OF URANIUM PER ASSEMBLY Kg U	FUEL RODS PER ASSEMBLY
2V0	2.6/4.1/4.6 (VAP)	0	0	411	176
2V1	2.6/4.1/4.6 (VAP)	44	3.35	408	176
2V2	2.6/4.1/4.6 (VAP)	52	3.35	407	176
2V3	2.6/4.1/4.6 (VAP)	64	3.35	406	176
2V4	2.6/4.1/4.6 (VAP)	76	3.35	405	176
2V5	2.6/4.1/4.6 (VAP)	96	3.35	404	176

TABLE 3.3-2

UNIT 2 BATCH-RELATED DATA

BATCH DESIGNATION	INITIAL ENRICHMENTS wt% U-235	NUMBER OF ZrB_2 SHIMS PER ASSEMBLY	INITIAL SHIM LOADING (mg-B-10/ inch)	AVERAGE WEIGHT OF URANIUM PER ASSEMBLY Kg U	FUEL RODS PER ASSEMBLY
2W1	2.6/4.50/4.95 (VAP)	28	3.29	408	176
2W2	2.6/4.50/4.95 (VAP)	64	3.29	406	176
2W3	2.6/3.95/4.50/ 4.95 (VAP)	52	3.29	407	176
2W4	2.6/3.95/4.50/ 4.95 (VAP)	64	3.29	406	176
2W5	2.6/3.95/4.50/ 4.95 (VAP)	76	3.29	406	176
2W6	2.6/3.95/4.50/ 4.95 (VAP)	96	3.29	405	176
2X1	4.60/4.20/2.60 (VAP)	28	3.29	409	176
2X2	4.60/4.20/2.60 (VAP)	52	3.29	408	176
2X3	4.95/4.60/4.20/ 2.60 (VAP)	64	3.29	407	176
2X4	4.95/4.60/4.20/ 2.60 (VAP)	76	3.29	407	176
2X5	4.95/4.60/4.20/ 2.60 (VAP)	96	3.29	406	176
2X6	4.20/4.00/2.60 (VAP)	64	3.29	408	176

BATCH DESIGNATION	INITIAL ENRICHMENTS wt% U-235	NUMBER OF Gd_2O_3 RODS PER ASSEMBLY	INITIAL Gd_2O_3 LOADING wt%	AVERAGE WEIGHT OF URANIUM PER ASSEMBLY Kg U	FUEL RODS PER ASSEMBLY
2Z1	4.88/4.34/2.00	0	N/A	410	176
2Z2	4.88/4.34/2.00 (4.40)	4	2	410	176
2Z3	4.88/4.34/2.00 (4.40/3.42)	4/12	2/6	408	176
2Z4	4.88/4.34/2.00 (2.93)	16	8	407	176
2Z5	4.88/4.34/2.00 (2.93)	12	8	408	176

TABLE 3.3-2

UNIT 2 BATCH-RELATED DATA

BATCH DESIGNATION	INITIAL ENRICHMENTS wt% U-235	NUMBER OF Gd_2O_3 RODS PER ASSEMBLY	INITIAL Gd_2O_3 LOADING wt%	AVERAGE WEIGHT OF URANIUM PER ASSEMBLY Kg U	FUEL RODS PER ASSEMBLY
BA1	4.60/4.00/2.00	0	N/A	410	176
BA2	4.60/4.00/2.00 (3.60)	4	4	410	176
BA3	4.60/4.00/2.00 (4.00/3.60)	4/12	2/4	409	176
BA4	4.60/4.00/2.00 (3.60/3.20)	4/12	4/6	408	176
BA5	4.60/4.00/2.00 (4.00/3.20)	8/12	2/6	408	176
BA6	4.15/3.60/2.00 (3.20/2.40)	4/8	4/8	408	176
BA7	4.15/3.60/2.00 (3.20/2.60)	4/12	4/6	408	176

BATCH DESIGNATION	INITIAL ENRICHMENTS wt% U-235	NUMBER OF Gd_2O_3 RODS PER ASSEMBLY	INITIAL Gd_2O_3 LOADING wt%	AVERAGE WEIGHT OF URANIUM PER ASSEMBLY Kg U	FUEL RODS PER ASSEMBLY
BB1	4.92/4.32/2.00 (3.60)	8	4	409	176
BB2	4.92/4.32/2.00 (4.40/2.95)	4/4	2/6	409	176
BB3	4.92/4.32/2.00 (3.60/2.95)	4/8	4/6	408	176
BB4	4.92/4.32/2.00 (3.60/2.95)	4/12	4/8	407	176
BB5	4.92/4.32/2.00 (4.40/2.95)	8/12	2/8	407	176

TABLE 3.3-2

UNIT 2 BATCH-RELATED DATA

BATCH DESIGNATION	INITIAL ENRICHMENTS wt% U-235	NUMBER OF Gd_2O_3 RODS PER ASSEMBLY	INITIAL Gd_2O_3 LOADING wt%	AVERAGE WEIGHT OF URANIUM PER ASSEMBLY Kg U	FUEL RODS PER ASSEMBLY
BC1	4.90/4.30/1.60 (3.60)	8	4	409	176
BC2	4.90/4.30/1.60 (3.60/3.20)	4/4	4/6	409	176
BC3	4.90/4.30/1.60 (3.60/3.20)	4/8	4/6	408	176
BC4	4.90/4.30/1.60 (3.60/2.90)	4/12	4/8	407	176
BC5	4.90/4.30/1.60 (3.60/2.90)	4/12	6/8	407	176

BATCH DESIGNATION	INITIAL ENRICHMENTS wt% U-235	NUMBER OF Gd_2O_3 RODS PER ASSEMBLY	INITIAL Gd_2O_3 LOADING wt%	AVERAGE WEIGHT OF URANIUM PER ASSEMBLY Kg U	FUEL RODS PER ASSEMBLY
BD1	4.91/4.33/1.60 (3.60/2.95)	4/12	5.0/7.0	408	176
BD2	4.91/4.30/1.60 (4.33/2.95)	8/12	2.0/6.0	408	176
BD3	4.91/4.33/1.60 (3.60)	12	4.0	409	176
BD4	4.91/4.33/1.60 (3.60)	8	5.0	409	176
BD5	2.95/1.60 (2.95)	4	7.0	409	176

TABLE 3.3-2

UNIT 2 BATCH-RELATED DATA

UNIT 2 CYCLE 1

ASSEMBLY BATCH	NUMBER OF ASSEMBLIES	TOTAL SHIMS	TOTAL FUEL RODS
2A	69	0	12,144
2B	80	960	13,120
2C	40	0	7,040
2C+	16	192	2,624
2C.	12	144	1,968
TOTALS	217	1,296	36,896

UNIT 2 CYCLE 2

ASSEMBLY BATCH	NUMBER OF ASSEMBLIES	TOTAL SHIMS	TOTAL FUEL RODS
2B	65	780	10,660
2C	40	0	7,040
2C+	16	192	2,624
2C.	12	144	1,968
2D	48	0	8,448
2D/	36	0	6,336
TOTALS	217	1,116	37,076

UNIT 2 CYCLE 3

ASSEMBLY BATCH	NUMBER OF ASSEMBLIES	TOTAL SHIMS	TOTAL FUEL RODS
2B	1	12	164
2C	40	0	7,040
2C+	16	192	2,624
2C.	12	144	1,968
2D	48	0	8,448
2D/	36	0	6,336
2E	48	0	8,448
2E/	16	0	2,816
TOTALS	217	348	37,844

UNIT 2 CYCLE 4

ASSEMBLY BATCH	NUMBER OF ASSEMBLIES	TOTAL SHIMS	TOTAL FUEL RODS
2D	25	0	4,400
2E	48	0	8,448
2E/	16	0	2,816
2F	40	0	7,040
2F/	88	704	14,784
TOTALS	217	704	37,488

TABLE 3.3-2

UNIT 2 BATCH-RELATED DATA

UNIT 2 CYCLE 5

ASSEMBLY BATCH	NUMBER OF ASSEMBLIES	TOTAL SHIMS	TOTAL FUEL RODS
2D	13	0	2,288
2F	40	0	7,040
2F/	88	704	14,784
2G	48	0	8,448
2G/	28	224	4,704
TOTALS	217	928	37,264

UNIT 2 CYCLE 6

ASSEMBLY BATCH	NUMBER OF ASSEMBLIES	TOTAL SHIMS	TOTAL FUEL RODS
1E/	8	0	1,408
2D/	20	0	3,520
2D	1	0	176
2F	40	0	7,040
2G	48	0	8,448
2G/	28	224	4,704
2H	48	0	8,448
2H*	24	0	4,224
TOTALS	217	224	37,968

UNIT 2 CYCLE 7

ASSEMBLY BATCH	NUMBER OF ASSEMBLIES	TOTAL SHIMS	TOTAL FUEL RODS
2D	1	0	176
2E	8	0	1,408
2G	48	0	8,448
2G/	28	224	4,704
2H	48	0	8,448
2H*	24	0	4,224
2J	40	0	7,040
2J*	20	0	3,520
TOTALS	217	224	37,968

TABLE 3.3-2

UNIT 2 BATCH-RELATED DATA

UNIT 2 CYCLE 8

ASSEMBLY BATCH	NUMBER OF ASSEMBLIES	NON-FUEL RODS	TOTAL FUEL RODS
2H*	21	1	3,695
2H	48	7	8,441
2J*	20	0	3,520
2J	40	1	7,039
2K/	44	352	7,392
2K*	28	336	4,592
2K	16	0	2,816
TOTALS	217	697	37,495

Batch 2H* includes one assembly with one SS rod.

Batch 2H includes three assemblies with a total of seven SS rods.

Batch 2J includes one assembly with one SS rod.

UNIT 2 CYCLE 9

ASSEMBLY BATCH	NUMBER OF ASSEMBLIES	NON-FUEL RODS	TOTAL FUEL RODS
2L	16	0	2,816
2LX	20	80	3,440
2L/	24	192	4,032
2L*	28	336	4,592
2LE	4	0	704
2K	16	0	2,816
2K/	44	355	7,389
2K*	28	339	4,589
2J	36	1	6,335
2H*	1	0	176
TOTALS	217	1,303	36,889

Batch 2K/ includes two assemblies with a total of three SS rods.

Batch 2K* includes one assembly with three SS rods.

Batch 2J includes one assembly with one SS rod.

TABLE 3.3-2

UNIT 2 BATCH-RELATED DATA

UNIT 2 CYCLE 10

ASSEMBLY BATCH	NUMBER OF ASSEMBLIES	NON-FUEL RODS	TOTAL FUEL RODS
2M	12	0	2,112
2M1	16	64	2,752
2M2	20	160	3,360
2M3	40	480	6,560
2L[a]	16	0	2,816
2LX[a]	20	80	3,440
2L/[a]	24	192	4,032
2L*[a]	28	336	4,592
2LE[a,b]	4	0	704
2K[a]	16	0	2,808[f]
2K/[a]	16	128	2,688
2J*[c]	4	0	704
2H*[d]	1	0	174[e]
TOTALS	217	1,440	36,742

[a] Carried over from Unit 2, Cycle 9.

[b] Erbium demonstration assembly.

[c] Reinserted, discharged at End of Unit 2, Cycle 8.

[d] Reinserted, discharged at End of Unit 2, Cycle 7.

[e] The center assembly contains two SS replacement rods.

[f] Eight fuel rods were replaced by SS replacement rods in Batch 2K during the Cycle 9 to Cycle 10 refueling outage.

TABLE 3.3-2

UNIT 2 BATCH-RELATED DATA

UNIT 2 CYCLE 11

ASSEMBLY BATCH	NUMBER OF ASSEMBLIES	NON-FUEL RODS	TOTAL FUEL RODS
N0	12	0	2,112
N2	8	0	1,408
N4	16	0	2,816
N6	48	0	8,448
NT	4	0	704
M	12	0	2,112
M1	16	64	2,752
M2	20	160	3,360
M3	40	480	6,560
L	16	0	2,816
LX	12	48	2,064
LT	4	0	704
J	4	0	704
L	4	0	704
J*[a]	1	2	174
TOTALS	217	754	37,438

[a] Batch J* includes one assembly with a total of two SS rods.

UNIT 2 CYCLE 12

ASSEMBLY BATCH	NUMBER OF ASSEMBLIES	NON-FUEL RODS	TOTAL FUEL RODS
P0	24	0	4,224
P1	8	0	1,408
P2	60	0	10,560
N0	12	0	2,112
N2	8	0	1,408
N4	16	0	2,186
N6	48	0	8,448
NT	4	0	704
M	12	0	2,112
M1	16	64	2,752
N	4	0	704
M*	4	48	656
K1	1	0	176
TOTALS	217	112	38,080

TABLE 3.3-2

UNIT 2 BATCH-RELATED DATA

UNIT 2 CYCLE 13

ASSEMBLY BATCH	NUMBER OF ASSEMBLIES	NON-FUEL RODS	TOTAL FUEL RODS
R0	8	0	1,408
R1	12	0	2,112
R2	32	0	5,632
R3	40	0	7,040
P0	24	0	4,224
P1	8	0	1,408
P2	60	0	10,560
N0	12	0	2,112
N2	8	0	1,408
N4	4	0	704
K*	4	48	656
J*	5	0	880
TOTALS	217	48	38,144

UNIT 2 CYCLE 14

ASSEMBLY BATCH	NUMBER OF ASSEMBLIES	NON-FUEL RODS	TOTAL FUEL RODS
2S0	8	0	1,408
2S1	24	0	4,224
2S2	24	0	4,224
2S3	36	0	6,336
2R0	8	0	1,408
2R1	12	0	2,113
2R2	32	0	5,632
2R3	40	0	7,040
2P0	23	0	4,048
2P1	8	0	1,408
1L*	1	0	176
1RT	1	0	176
TOTALS	217	0	38,192

TABLE 3.3-2

UNIT 2 BATCH-RELATED DATA

UNIT 2 CYCLE 15

ASSEMBLY BATCH	NUMBER OF ASSEMBLIES	NON-FUEL RODS	TOTAL FUEL RODS
T0	20	0	3,520
T1	4	0	704
T2	40	0	7,040
T3	20	0	3,520
TF	4	0	704
TW	4	0	704
S0	8	0	1,408
S1	24	0	4,224
S2	24	0	4,224
S3	36	0	6,336
R0	8	0	1,408
R1	12	0	2,112
R2	12	0	2,112
J*	1	0	176
TOTALS	217	0	38,192

UNIT 2 CYCLE 16

ASSEMBLY BATCH	NUMBER OF ASSEMBLIES	NON-FUEL RODS	TOTAL FUEL RODS
2V0	12	0	2,112
2V1	28	0	4,928
2V2	4	0	704
2V3	16	0	2,816
2V4	12	0	2,112
2V5	20	0	3,520
2T0	20	0	3,520
2T1	4	0	704
2T2	40	0	7,040
2T3	20	0	3,520
2TF	4	0	704
2TW	4	0	704
2S0	8	0	1,408
2S1	24	0	4,224
1L*	1	0	176
TOTALS	217	0	38,192

TABLE 3.3-2

UNIT 2 BATCH-RELATED DATA

UNIT 2 CYCLE 17

ASSEMBLY BATCH	NUMBER OF ASSEMBLIES	NON-FUEL RODS	TOTAL FUEL RODS
W1	20	0	3,520
W2	4	0	704
W3	8	0	1,408
W4	12	0	2,112
W5	36	0	6,336
W6	16	0	2,816
V0	12	0	2,112
V1	28	0	4,928
V2	4	0	704
V3	16	0	2,816
V4	9	0	1,584
V5	20	0	3,520
1V0	2	0	352
1V1	2	0	352
T0	12	0	2,112
T2	8	0	1,408
T3	6	0	1,056
TW	2	0	352
TOTALS	217	0	38,192

UNIT 2 CYCLE 18

ASSEMBLY BATCH	NUMBER OF ASSEMBLIES	NON-FUEL RODS	TOTAL FUEL RODS
2X1	12	0	2,112
2X2	12	0	2,112
2X3	28	0	4,928
2X4	8	0	1,408
2X5	32	0	5,632
2X6	4	0	704
2W1	20	0	3,520
2W2	4	0	704
2W3	8	0	1,408
2W4	12	0	2,112
2W5	35	0	6,160
2W6	16	0	2,816
2V0	11	0	1,936
2V1	13	0	2,288
1X4	1	0	176
1X7	1	0	176
TOTALS	217	0	38,192

TABLE 3.3-2

UNIT 2 BATCH-RELATED DATA

UNIT 2 CYCLE 19

ASSEMBLY BATCH	NUMBER OF ASSEMBLIES	NON-FUEL RODS	TOTAL FUEL RODS
2Z1	8	0	1,408
2Z2	12	0	2,112
2Z3	28	0	4,928
2Z4	44	0	7,744
2Z5	4	0	704
		0	
2X1	12		2,112
2X2	12	0	2,112
2X3	28	0	4,928
2X4	8	0	1,408
2X5	32	0	5,632
2X6	4	0	704
2W1	12	0	2,112
2W2	4	0	704
2W4	7	0	1,232
2V1	1	0	176
2V4	1	0	176
TOTALS	217	0	38,192

UNIT 2 CYCLE 20

ASSEMBLY BATCH	NUMBER OF ASSEMBLIES	NON-FUEL RODS	TOTAL FUEL RODS
BA1	12	0	2,112
BA2	8	0	1,408
BA3	32	0	5,632
BA4	12	0	2,112
BA5	20	0	3,520
BA6	4	0	704
BA7	12	0	2,112
2Z1	8	0	1,408
2Z2	12	0	2,112
2Z3	24	0	4,224
2Z4	44	0	7,744
2Z5	4	0	704
2X1	8	0	1,408
2X2	8	0	1,408
2X3	8	0	1,408
1X1	1	0	176
TOTALS	217	0	38,192

TABLE 3.3-2

UNIT 2 BATCH-RELATED DATA

UNIT 2 CYCLE 21

ASSEMBLY BATCH	NUMBER OF ASSEMBLIES	NON-FUEL RODS	TOTAL FUEL RODS
BB1	12	0	2,112
BB2	8	0	1,408
BB3	20	0	3,520
BB4	28	0	4,928
BB5	28	0	4,928
BA1	12	0	2,112
BA2	8	0	1,408
BA3	32	0	5,632
BA4	12	0	2,112
BA5	17	0	2,992
BA6	4	0	704
BA7	12	0	2,112
2Z1	8	0	1,408
2Z2	8	0	1,408
2Z3	8	0	1,408
TOTALS	217	0	38,192

UNIT 2 CYCLE 22

ASSEMBLY BATCH	NUMBER OF ASSEMBLIES	NON-FUEL RODS	TOTAL FUEL RODS
BC1	12	0	2,112
BC2	8	0	1,408
BC3	20	0	3,520
BC4	20	0	3,520
BC5	36	0	6,336
BB1	12	0	2,112
BB2	8	0	1,408
BB3	20	0	3,520
BB4	28	0	4,928
BB5	24	0	4,224
BA1	12	0	2,112
BA2	8	0	1,408
BA3	4	0	704
BA5	1	0	176
2Z3	4	0	704
TOTALS	217	0	38,192

UNIT 2 CYCLE 23

ASSEMBLY BATCH	NUMBER OF ASSEMBLIES	NON-FUEL RODS	TOTAL FUEL RODS
BD1	28	0	4928
BD2	28	0	4928
BD3	20	0	3520
BD4	20	0	3520
BD5	1	0	176
BC1	12	0	2112
BC2	8	0	1408
BC3	20	0	3520
BC4	20	0	3520
BC5	36	0	6336
BB1	4	0	704
BA4	4	0	704
BA7	2	0	352
ZZ4	14	0	2464
TOTALS	217	0	38,192

TABLE 3.3-2

UNIT 2 BATCH-RELATED DATA

PARAMETER	BATCHES							
	A	**B**	**C**	**D**	**E**	**F**	**G**	**H**
Active Length, inches	136.7	136.7	136.7	136.7	136.7	136.7	136.7	136.7
Pellet Diameter, inches	.3805	.3805	.3805	.3765	.3765	.3765	.3765	.3765
Pellet Length, inches	.450	.450	.450	.450	.450	.450	.450	.450
Pellet Density, g/cc	10.412	10.412	10.412	10.385	10.385	10.385	10.385	10.385
Stack Height Density, g/cc	10.039	10.043	10.039	10.046	10.046	10.046	10.046	10.046
Clad ID, inches	.3880	.3880	.3880	.3840	.3840	.3840	.3840	.3840
Clad OD, inches	.440	.440	.440	.440	.440	.440	.440	.440
Clad Thickness, inches	.026	.026	.026	.028	.028	.028	.028	.028
Diametral Gap, inches	.0075	.0075	.0075	.0075	.0075	.0075	.0075	.0075

PARAMETER	BATCHES							
	J	**K**	**L**	**M**	**N**	**NT**	**P**	**R**
Active Length, inches	136.7	136.7	136.7	136.7	136.7	136.7	136.7	136.7
Pellet Diameter, inches	.3765	.3765	.3765	.3765	.3765	.3810	.3765	.3765
Pellet Length, inches	.450	.450	.450	.450	.450	.456	.450	.450
Pellet Density, g/cc	10.385	10.385	10.385	10.439	10.439	10.467	10.439	10.439
Stack Height Density, g/cc	10.046	10.046	10.046	10.100	10.12	10.31	10.12	10.12
Clad ID, inches	.3840	.3840	.3840	.3840	.384	.388	.384	.384
Clad OD, inches	.440	.440	.440	.440	.440	.440	.440	.440
Clad Thickness, inches	.028	.028	.028	.028	.028	.026	.028	.028
Diametral Gap, inches	.0075	.0075	.0075	.0075	.0075	.0070	.0075	.0075

TABLE 3.3-2

UNIT 2 BATCH-RELATED DATA

PARAMETER	BATCHES				
	S	T(Westinghouse)	T(FANP)	V	W
Active Length, inches	136.7	136.7	136.7	136.7	136.7
Pellet Diameter, inches	.3810	.3810	.3805	.3810	.3810
Pellet Length, inches	.456	.456	.435	.456	.456
Pellet Density, g/cc	10.467	10.467	10.522	10.467	10.467
Stack Height Density, g/cc	10.31	10.31	10.39	Regular 10.32 Annular 7.82	Regular 10.32 Annular 7.82
Clad ID, inches	.3880	.3880	.3870	.3880	.3880
Clad OD, inches	.440	.440	.440	.440	.440
Clad Thickness, inches	.026	.026	.0265	.026	.026
Diametral Gap, inches	.0070	.0070	.0065	.0070	.0070

PARAMETER	BATCHES			
	X	Z	BA	BB
Active Length, inches	136.7	136.7	136.7	136.7
Pellet Diameter, inches	.3810	0.3805	0.3805	0.3805
Pellet Length, inches	.456	0.476 (Central) 0.545 (Blanket)	0.476 (Central) 0.545 (Blanket)	0.476 (Central) 0.545 (Blanket)
Pellet Density, g/cc	10.467	10.5216	10.5216	10.5216
Stack Height Density, g/cc	Regular 10.32 Annular 7.82	10.3743 (UO_2) 10.3003 (2 wt% Gd_2O_3) 10.1565 (6 wt% Gd_2O_3) 10.0867 (8 wt% Gd_2O_3) 10.3953 (Blanket)	10.3743 (UO_2) 10.3003 (2 wt% Gd_2O_3) 10.2277 (4 wt% Gd_2O_3) 10.1565 (6 wt% Gd_2O_3) 10.0867 (8 wt% Gd_2O_3)	10.3743 (UO_2) 10.3003 (2 wt% Gd_2O_3) 10.2277 (4 wt% Gd_2O_3) 10.1565 (6 wt% Gd_2O_3) 10.0867 (8 wt% Gd_2O_3)

TABLE 3.3-2

UNIT 2 BATCH-RELATED DATA

				10.3953 (Blanket)	10.3953 (Blanket)
Clad ID, inches	.3880	0.3870		0.3870	0.3870
Clad OD, inches	.440	0.440		0.440	0.440
Clad Thickness, inches	.026	0.0265		0.0265	0.0265
Diametral Gap, inches	.0070	0.0065		0.0065	0.0065

PARAMETER	**BATCHES**	
	BC	**BD**
Active Length, inches	136.7	136.7
Pellet Diameter, inches	0.3805	0.3805
Pellet Length, inches	0.476 (Central) 0.545 (Blanket)	0.476 (Central) 0.545 (Blanket)
Pellet Density, g/cc	10.5216	10.5216
Stack Height Density, g/cc	10.3743 (UO_2) 10.2277 (4 wt% Gd_2O_3) 10.1565 (6 wt% Gd_2O_3) 10.0867 (8 wt% Gd_2O_3) 10.3953 (Blanket)	10.3743 (UO_2) 10.3003 (2% Gd_2O_3) 10.2277 (4% Gd_2O_3) 10.1920 (5% Gd_2O_3) 10.1565 (6% Gd_2O_3) 10.1215 (7% Gd_2O_3) 10.3953 (Blanket)
Clad ID, inches	0.387	0.387
Clad OD, inches	0.440	0.440
Clad Thickness, inches	0.0265	0.0265
Diametral Gap, inches	0.0065	0.0065

TABLE 3.3-3

BURNABLE POISON ROD DATA

UNITS 1 AND 2

BATCH	B,C+,C.	1G/,1H/ 2F/,2G/	2K/,2K*,1NX, 1N/,1M*,2L*, 2L/,2LX	1MX	2LE	2M	1P	2N	2NT	2P
Active Length	122.7	122.7	122.7	122.7	115.7	115.7	108.7	112.7	112.7	112.2
Pellet Diameter	.376	.362	.362	.370	.3765	.362	.3765	.3765	.3810	.3765
Clad ID	.388	.384	.384	.378	.384	.384	.384	.384	.388	.384
Clad OD	.440	.440	.440	.440	.440	.440	.440	.440	.440	.440
Clad Thickness, inches	.026	.028	.028	.031	.028	.028	.028	.028	.026	.028
Diametral Gap, inches	.012	.022	.022	.008	.0075	.022	.0075	.0075	.0070	.0075

BATCH	1R	1RT	2R	1S	1T	2S	1V	2T	1W	2V
Active Length	114.2	114.2	112.7	114.2	112.2	112.7	112.2	112.2	114.2	114.7
Pellet Diameter	.3765	.3810	.3765	.3765	.3810	.3810	.3810	.3810	.3810	.3810
Clad ID	.384	.388	.384	.384	.388	.388	.388	.388	.3880	.388
Clad OD	.440	.440	.440	.440	.440	.440	.440	.440	.440	.440
Clad Thickness, inches	.028	.026	.028	.028	.026	.026	.026	.026	.026	.026
Diametral Gap, inches	.0075	.0070	.0075	.0075	.0070	.007	.007	.007	.0070	.0070

BATCH	1X	2W	1Z	2X	AA	2Z	AB	BA	AC
Active Length	116.7	116.7	116.7	116.7	116.7	112.7	112.7	112.7	112.7
Pellet Diameter	.3810	.3810	.3810	.3810	.3810	0.3805	0.3805	0.3805	0.3805
Clad ID	.388	.388	.388	.388	.388	0.3870	0.387	0.387	0.387
Clad OD	.440	.440	.440	.440	.440	0.440	0.440	0.440	0.440
Clad Thickness, inches	.026	.026	.026	.026	.026	0.0265	0.0265	0.0265	0.0265
Diametral Gap, inches	.0070	.0070	.0070	.0070	.0070	0.0065	0.0065	0.0065	0.0065

TABLE 3.3-3

BURNABLE POISON ROD DATA

UNITS 1 AND 2

BATCH	BB	AD	BC	AE	BD
Active Length, inches	112.7	112.7	112.7	112.7	112.7
Pellet Diameter, inches	0.3805	0.3805	0.3805	0.3805	0.3805
Clad ID, inches	0.387	0.387	0.387	0.387	0.387
Clad OD, inches	0.440	0.440	0.440	0.440	0.440
Clad Thickness, inches	0.0265	0.0265	0.0265	0.0265	0.0265
Diametral Gap, inches	0.0065	0.0065	0.0065	0.0065	0.0065

All dimensions in inches.

Batch 1 MX is ANF demonstration fuel with 12 Gd_2O_3 (10 wt%) fuel bearing (natural uranium) poison rods per assembly.

Batch 2LE is Erbium bearing demonstration fuel with 44 Er_2O_3 (0.9 wt%) fuel bearing (3.40 wt% U-235) rods per assembly.

TABLE 3.3-4

CONTROL ELEMENT ASSEMBLY DATA

UNITS 1 AND 2

All Dimensions are Nominal and are in inches

CEA TYPE	**FLCEA8 Non-reconstitutable**	**FLCEA7 Non-reconstitutable**	**FLCEA10 Non-reconstitutable**	**FLCEA9 Non-reconstitutable**
Number	76(1)	1(2)	76(1)	1(2)
Clad Thickness	0.040	0.040	0.040	0.040
Clad OD	0.948	0.948	0.948	0.948
Diametral Gap B4C/UAIC/LAIC/USS/LSS	.008(3)	.008(3)	.008/.012/.017/NA/NA	.008/.012/.017/.118/.012
Corner Element Pitch	4.64	4.64	4.64	4.64
Pellet Type	B4C/AIC	AL2O3/SS/B4C/AIC	B4C/UAIC/LAIC	B4C/UAIC/LAIC/USS/LSS
Pellet Diameter	0.86/0.86	0.85/0.86/0.86/0.86	0.86/0.856/0.851	0.86/0.856/0.851/0.75/0.856

Note (1) up to 76 FLCEA1, FLCEA2, FLCEA8 or FLCEA10
Note (2) up to 1 of FLCEA7 or FLCEA9
Note (3) diametral gap is .008 regardless of pellet type
AIC: Ag-In-Cd (Silver-Indium-Cadmium)
UAIC: Upper AIC
LAIC: Lower AIC
SS: Stainless Steel
USS: Upper SS
LSS: Lower SS

TABLE 3.3-4

CONTROL ELEMENT ASSEMBLY DATA

UNITS 1 AND 2

GUIDE TUBE FLUX SUPPRESSOR DATA

UNIT 1 (CYCLES 11 AND 12)

PARAMETER	**GTFS**
Number	24(U1)
Clad Thickness	.040
Clad OD	.948
Diametral Gap	.008
Pellet Type	Al_2O_3/B_4C
Pellet Diameter	.85/.86

NOTE: All dimensions in inches except where noted.

TABLE 3.3-5

CORE RELATED DATA

UNIT 1 AND UNIT 2

CORE ARRANGEMENT

Number of Fuel Assemblies in Core, Total	217
Number of CEAs	77
Total Number of Fuel Rods and Non-Fuel Rods	38,192
CEA Pitch, min, inches	11.57
Spacing Between Fuel Assemblies, Fuel Rod Surface to Surface, inches	.20
Spacing, Outer Fuel Rod Surface to Core Shroud, inches	.204
Hydraulic Diameter, Nominal Channel, feet	.044
Total Flow Area (Excluding Guide Tubes), ft^2	53.5
Total Core Cross-section Area, ft^2	101.1
Core Equivalent Diameter, inches	136
Core Circumscribed Diameter, inches	143.3
Core Volume, ft^3	1151

3.4 NUCLEAR DESIGN AND EVALUATION

3.4.1 SUMMARY

This section summarizes the nuclear characteristics of the core and discusses the important design parameters which are of significance to the performance of the core during transient and steady state operation. A discussion of the nuclear design methods employed and comparisons with experiments which support the use of these methods is included. Summaries of nuclear parameters are presented in Table 3.4-1. Design limits for shutdown margin, reactivity coefficients, reactivity insertion rates, and power distribution are discussed in the appropriate sections.

Fuel enrichment and BPR distributions are shown in Table 3.3-1, Table 3.3-2, and Figure 3.3-4.

Physical features of the lattice, fuel assemblies, and CEAs are described in Section 3.3.2. The soluble boron insertion rates are sufficient to compensate for the maximum reactivity addition due to xenon burnout and normal plant cooldown.

3.4.2 REACTIVITY AND CONTROL REQUIREMENTS

At the beginning of each cycle, the core is loaded with sufficient fuel to generate essentially full power for the cycle length. This results in built-in excess reactivity (the reactivity present in the reactor with all control material withdrawn from the core) which must be sufficient to compensate for the reactivity lost during the cycle due to:

a. Fuel burnup;
b. Fission product buildup; and,
c. Negative reactivity feedbacks.

The excess reactivity must be stable and controlled through the cycle to permit power operations while maintaining the ability to rapidly shut down the reactor if necessary (Table 3.4-2).

Excess reactivity is controlled during the cycle by adjusting both the position of the CEAs and the concentration of boric acid dissolved in the RCS. The CEAs permit rapid changes in reactivity, as required for reactor trip, and may be used to compensate for changes in moderator temperature, fuel temperature, and moderator density associated with changes in power level.

Adjustment of the boric acid concentration is used to control the relatively slow reactivity changes associated with plant heatup and cooldown, fuel burnup, certain xenon variations, and slow power level changes. The use of boric acid dissolved in the reactor coolant makes it possible to maintain the CEAs in an essentially fully-withdrawn position during full power operation, thus minimizing distortions in power distribution. Although the boric acid system reduces reactivity relatively slowly, the rate of reduction is more than sufficient to maintain the shutdown margin against the effects of normal cooldown and xenon decay. Table 3.4-1 lists the predicted concentrations of natural boron required to maintain the first cycle critical under various conditions, assuming all CEAs to be fully withdrawn. The hot full power, equilibrium xenon, BOC boron concentration predictions for the present cycles are also given in Table 3.4-1.

Design criteria require reactivity control and stability. In a stable reactor, a reactivity perturbation during steady state operation leads to another steady state. This desirable, self-limiting characteristic is due to negative feedback of reactivity. The parameters used to quantify feedback are the reactivity coefficients which relate changes in core reactivity to variations in fuel and/or moderator conditions. Verifications of predicted nuclear

parameters are conducted at the beginning of each cycle during startup testing (Chapter 13). Results of these tests verify prediction of the Moderator Temperature Coefficient. For each DBE in the Safety Analysis (Chapter 14), suitably conservative reactivity coefficient values are used. Values assumed in the transient analyses are listed in Chapter 14.

3.4.2.1 Fuel Temperature Coefficient

The FTC reflects the change of core reactivity per degree change in average fuel temperature. A change in fuel temperature affects the density of the fuel pellet and the nuclear density of the uranium in the pellet, thus changing the probability of interaction with a neutron. A fuel temperature change also modifies the reaction rates in uranium in both the thermal and epithermal neutron energy regimes.

The Doppler effect is the principal contributor to the change in reaction rate with fuel temperature in the epithermal range. This effect results from the increased (non-fissioning) neutron absorption in U-238 with increasing fuel temperature. This increase in neutron absorption rate with fuel temperature causes a negative FTC since the temperature increase decreases the fission rate. In the thermal energy regime, a change in reaction rate with fuel temperature arises from the effect of temperature dependent scattering properties of the fuel matrix on the thermal neutron spectrum. In typical PWR fuels containing strong resonance absorbers such as U-238 and Pu-240, the component of the FTC arising from the Doppler effect is more than a factor of ten larger than the thermal energy component.

The variation of FTC with temperature predicted for the first cycle is shown in Figure 3.4-1. The predicted first cycle hot, full power FTC was -1.06×10^{-5} $\Delta\rho/°F$ which is approximately equivalent to -1.49×10^{-3} $\Delta\rho/(kW/ft)$.

3.4.2.2 Moderator Temperature Coefficient

The MTC relates changes in reactivity to changes in the moderator average temperature and includes the effects of temperature on the moderator density.

Typically, an increase in the moderator temperature causes a decrease in moderator density and therefore less neutron thermalization which reduces core reactivity. When an increase in moderator temperature causes a decrease in reactivity, the core has a negative temperature coefficient. This adds to the stability since a temperature increase will reduce reactor power and vice versa.

When sufficient boron is present in the moderator, a reduction in moderator density also causes a reduction in the boron density in the core, thus producing a positive contribution to the MTC. One core design objective is to limit the MTC to values near zero, if positive, or to slightly negative values (the MTC positive limits are listed in the Technical Specifications). In order to limit the dissolved boron concentration and its positive contribution to the MTC, BPRs (shims) may be provided in the cycle design (Tables 3.3-1 and 3.3-2). The reactivity control provided by the shims makes possible a reduction in the dissolved boron concentration and therefore a reduction in the MTC.

Moderator Temperature Coefficient values for various core conditions during the first cycle and for the current cycle are given in Table 3.4-1. As shown in the table, the least negative value at full power conditions occurs in the unrodded core when the dissolved boron content is at its maximum. The MTC becomes more negative at the EOC due mainly to the reduction in the dissolved boron content with burnup.

CEA insertion provides a negative contribution to the coefficient since a corresponding reduction in the dissolved boron content is required to maintain the reactor critical.

The effects of plutonium and fission products on the MTC are small when compared to the effects of dissolved boron changes. The buildup of fission product xenon supplies a positive contribution to the MTC for a constant boron concentration. However, when the dissolved boron concentration is reduced by the reactivity equivalent of the xenon, MTC becomes more negative.

The change in MTC as a function of boron concentration is almost linear and was about $+0.16 \times 10^{-4}$ $\Delta\rho$/F per 100 ppm soluble boron for the first cycle.

3.4.2.3 Moderator Pressure Coefficient

The Moderator Pressure Coefficient is the change in reactivity per unit change in RCS pressure. Since an increase in pressure increases the water density, the pressure coefficient is opposite in sign to the temperature coefficient. The reactivity effect of increasing the pressure is reduced in the presence of dissolved boron because an increase in coolant density also increases the boron density. The Moderator Pressure Coefficient decreases as the RCS boron concentration increases. The calculated pressure coefficients for the beginning and end of the first cycle at full power were $+0.3 \times 10^{-6}$ $\Delta\rho$/psi and $+2.6 \times 10^{-6}$ $\Delta\rho$/psi, respectively. The Moderator Pressure Coefficient was measured to be $-.5 \times 10^{-6}$ $\Delta\rho$/psi at the beginning of Unit 1 Cycle 1 with a nominal RCS temperature of 450°F by changing pressure in the 1100 psia to 2250 psia range. The pressure coefficient of reactivity is relatively insignificant and is several orders of magnitude smaller than the MTC.

3.4.2.4 Moderator Void Coefficient

The occurrence of small amounts of local subcooled boiling in the reactor during full power operation may result in small steam bubbles (voids). These are called voids because they contain almost no moderating nuclei. The average void fraction is the fraction by volume of the moderator that is in void form and it is substantially less than 1% at normal operating conditions. The change in reactivity associated with these voids in the moderator is the Void Coefficient of Reactivity. An increase in voids reduces the moderator density and decreases core reactivity. The presence of soluble boron tends to add a positive contribution to the void coefficient because an increase in voids results in a reduction in boron density in the core. The calculated values at the beginning and at the end of the first cycle were -0.1×10^{-3} $\Delta\rho$/% void and -1.3×10^{-3} $\Delta\rho$/% void, respectively.

3.4.2.5 Power Coefficient

The Power Coefficient is the change in core reactivity per percent change incore power level. Although all of the previously mentioned coefficients (FTC, MTC, Moderator Pressure Coefficient and the Moderator Void Coefficient) contribute to the Power Coefficient, only the MTC and the FTC are significant. To determine the change in reactivity with power, it is necessary to know the change in the average moderator temperature and effective fuel temperature with power.

The average moderator temperature is a linear function of power. The effective fuel temperature is dependent on both power level and burnup. Due to fuel pellet cracking and fission gas release with irradiation, this functional relationship changes during the cycle.

The Power Coefficient can be obtained from the following equation:

$$\frac{dRho}{dP} = \left(\frac{dRho}{dT_f}\ x\ \frac{dT_f}{dP}\right) + \left(\frac{dRho}{dT_m}\ x\ \frac{dT_m}{dP}\right)$$

The first term of the equation provides the fuel temperature contribution to the Power Coefficient. The first term is the product of FTC of reactivity and the effective change of fuel temperature with respect to power. The second term in the equation provides the moderator contribution to the Power Coefficient. The first factor is the MTC and the second factor is a constant since the moderator temperature is a linear function of power.

Since the factors $dRho/dT_f$ and $dRho/dT_m$ are functions of one or more independent variables (e.g., burnup, temperature, soluble boron content, xenon worth, and CEA insertion), the total Power Coefficient, dRho/dP, also depends on these variables.

Plots of the calculated FTC and a plot of the predicted Power Coefficient for the beginning of the first cycle are shown in Figures 3.4-1 and 3.4-2, respectively. The full power value of the Power Coefficient for the unrodded first cycle is -1.49×10^{-3} $\Delta\rho$/(kW/ft). The Power Coefficient becomes more negative with burnup due to the increasing negative FTC and MTC.

3.4.3 SHUTDOWN REACTIVITY CONTROL

The reactivity worth requirement of all the CEAs is determined by:

a. Shutdown reactivity margin;
b. Power defect (including moderator voids); and,
c. CEA bite.

The total worth of all CEAs provides adequate shutdown at full power even if the CEA with the most worth is stuck in the fully withdrawn position. Table 3.4-2 compares available CEA reactivity with the various required reactivity components at BOC and EOC for the first cycle. The table also lists the current cycle's most limiting values of reactivity worths and allowances. Individual components are discussed below.

3.4.3.1 Shutdown Reactivity Margin

The shutdown margin requirement is based on the reactivity requirements for the most limiting postulated accident. This requirement varies throughout core life as a function of fuel depletion, boron concentration, and RCS temperature.

Sufficient CEA worth must be available for rapid insertion to ensure that:

a. The reactor can be made subcritical from all operating conditions.
b. Reactivity transients associated with postulated accident conditions are controllable.

A steam line break or excess load event (Chapter 14) at EOC requires the maximum CEA shutdown margin due to the large, rapid cooldown and the large, negative MTC. These accidents provide the basis for the shutdown margin Technical Specification with RCS temperature above 200°F.

Allowances of 2.0% and 2.4% $\Delta\rho$ at the beginning of first cycle and at the end of first cycle, respectively, were made for the predicted shutdown margin and safety

feature allowances at hot, zero power conditions. The current cycle values of CEA worths and allowances for the limiting event are listed in Table 3.4-2.

3.4.3.2 Power Defect

The power defect is the reactivity change in the core from hot zero power to a higher power. During a reactor trip, this increase in reactivity must be compensated for by the CEAs.

The power defect increases as the power level is increased and results from the following changes:

a. Fuel Temperature Variation
b. Moderator Temperature Variation
c. Moderator Voids Variation

These three reactivity variations are described below.

a. Fuel Temperature Variation

The reactivity increase that occurs when the fuel temperature decreases from its full (or other) power value to its zero power value is primarily due to changes in epithermal absorption resonance's (the Doppler effect) in U-238. As exposure accumulates, concentrations of plutonium increase making the FTC more negative. However, pellet swelling and clad creepdown associated with increasing exposure improves the heat transfer which decreases the fuel temperature. The competing effects of a more negative FTC and decreasing fuel temperature tends to minimize the burnup dependence of the fuel temperature defect. The Unit 1 Cycle 1 reactivity increase associated with a fuel temperature decrease from full power to zero power was 1.7% $\Delta\rho$ at BOC and 1.8% $\Delta\rho$ at EOC.

b. Moderator Temperature Variation

The average reactor coolant temperature increases with increasing power. This decreases the moderator density and causes a reactivity change which is usually negative (except at very high boron concentrations). The moderator temperature variation allowance is large enough to compensate for any reactivity increase that may occur when the moderator temperature decreases from full power to zero power. This reactivity increase, which is primarily due to the negative MTC, is largest at the EOC when the soluble boron concentration is near zero and the moderator coefficient is strongly negative. At BOC, when the MTC is less negative, the reactivity change associated with the moderator temperature change is smaller.

c. Moderator Voids Variation

Increasing the power level causes a decrease in reactivity resulting from formation of small steam bubbles (voids) due to local boiling. The average void content in the core is very small and is estimated to be less than 1% at full power. As with the moderator temperature effect, the maximum increase in reactivity from full to zero power occurs at EOC when the least amount of dissolved boron is present. At BOC the void coefficient is essentially zero.

3.4.3.3 Control Element Assembly Bite and Power Dependent Insertion Limits

Control element assembly bite is the CEA reactivity worth permitted to be inserted in the core when critical for power shaping and to compensate for minor variations

in moderator temperature, boron concentration, xenon concentration, and power level.

The substantially smaller power defects for shutdown initiated at lower power levels allow a reduction in the CEA worth required to be available for shutdown. The corresponding increase in allowed CEA insertion is reflected by the transient Power Dependent Insertion Limits (PDILs) of the Technical Specifications. The transient PDIL restricts the amount of CEA insertion into the core while at power. The amount of CEA insertion permitted by PDIL provides sufficient reactivity for control while ensuring the minimum shutdown requirement is maintained in the withdrawn CEAs.

The allowance for first cycle CEA bite was 0.1% $\Delta\rho$. In addition, 0.1% $\Delta\rho$ was allowed for the first cycle for compensating fuel depletion effects between adjustments of the dissolved boron concentration. The current allowances for CEA bite are reflected in the Technical Specification transient PDIL curves.

3.4.3.4 Shutdown Conditions

Boric acid is used to provide a large margin for shutdown and refueling. After a normal shutdown or reactor trip, boric acid is injected into the RCS to compensate for reactivity increases caused by normal cooldown and xenon decay. Although the boric acid system reduces reactivity slowly, compared to CEAs, the rate of reduction is more than sufficient to maintain the shutdown margin against the effects of cooldown and xenon decay. The boron concentration established for refueling is listed in the Technical Specifications. This boron concentration provides more than adequate negative reactivity to maintain the shutdown condition.

3.4.4 CONTROL ELEMENT ASSEMBLY PATTERN, OPERATIONS, AND WORTHS

The CEA is described in Section 3.3.2.4 and shown in Figures 3.3-8, 3.3-9A and 3.3-9B. The CEAs are designated as Regulating CEAs or Shutdown CEAs. The Regulating CEAs are divided into five groups (1 through 5). The Shutdown CEAs are divided into three groups (A, B, and C). The locations of all the CEAs in one of four symmetrical core quadrants are shown on Figure 3.3-10.

All CEAs within a particular group are designated to be withdrawn or inserted nearly simultaneously. For startups the Shutdown CEA groups are withdrawn without overlap; then the Regulating groups are withdrawn with overlap.

The PDILs specify the maximum permitted CEA insertion as discussed in Section 3.4.3.3. The PDIL curve for the current cycle of each Unit is in the Technical Specifications. The PDIL curve illustrates the Regulating CEA Groups insertion order (5-4-3-2-1) with overlap between successive groups. The typical CEA withdrawal procedure is as follows:

a. With the reactor subcritical, Shutdown Group A is fully withdrawn, followed by Shutdown Group B and then Shutdown Group C.
b. Withdrawal of regulating CEAs commences starting with Regulating Group No. 1. CEA withdrawal continues with the prescribed overlap of Regulating Groups 2 through 5.

All CEAs are inserted for cold shutdown conditions and are essentially fully withdrawn during full power steady state operation. Reactivity insertion rates are discussed in Section 3.4.5. The allowable CEA misalignment within any CEA group is specified in Technical Specifications and intentional misalignment of CEAs within a group for the purpose of power shaping is not allowed.

The accidents involving CEAs are analyzed with conservative assumptions as discussed in Chapter 14. The CEA withdrawal accident is analyzed with the maximum calculated differential reactivity insertion rate resulting from a sequential CEA bank withdrawal with overlap. The CEA drop accident is analyzed by selecting the dropped CEA that maximizes the increase in the radial peaking factor. The typical reactivity insertion during a reactor scram is presented in Chapter 14. This reactivity insertion is computed by static or space time axial models and is used for all accidents which are terminated by a scram.

3.4.5 REACTIVITY INSERTION RATES

Normal operating practices require reactivity changes to accommodate power level changes, fuel depletion, temperature control, etc. The principal reactivity control mechanisms are CEA Regulating Groups and boration/dilution. The analysis of CEA withdrawal events (Chapter 14) shows that maximum CEDM speed results in a differential reactivity per inch and consequence which will not exceed the Specified Acceptable Fuel Design Limits (SAFDLs). The analysis of the boron dilution event (Chapter 14) for the worst case of initial refueling in the drained-down mode shows that adequate time exists to take corrective measures.

Reactivity addition rates due to control rods vary with the CEA group, CEA group position, RCS temperature, dissolved boron concentration, fuel depletion, power level, and power distribution. Reactivity addition rates due to changes in dissolved boron vary with CEA insertion, temperature, fuel depletion, and power level due primarily to their effect on the dissolved boron concentration. Both spectral and spatial self-shielding effects are involved.

3.4.6 POWER DISTRIBUTION

3.4.6.1 General

The core is designed and the reactor is operated to maintain a relatively uniform power distribution. Significant deviations from the expected power distribution are restricted by the Limiting Safety System Settings (LSSSs) [e.g., Axial Shape Index (ASI)] and the Limiting Conditions for Operation (LCOs) [e.g., F_r^T, Peak Linear Heat Rate (PLHR) and T_q]. These operating limits are bounded by sufficient thermal margin to prevent DNB and fuel/clad melting during Anticipated Operational Occurrences (AOOs).

3.4.6.2 Objective

A stable uniform power distribution increases thermal margin by minimizing peak heat flux and enthalpy rise. The relative power distribution is approximately the ratio of the maximum local power to the core average power. The power peaking factors (F_r^T, ASI, and T_q) are minimized by design to allow operational flexibility to deviate from the nominal core power distribution without encroaching upon the LSSSs and LCOs.

3.4.6.3 Fuel Management and Operations

The peaking factors are most strongly influenced by the core loading which is therefore designed to reduce the inherent power peaking. To accomplish this goal in reload core designs, the arrangement of fresh and depleted assemblies together increases the power sharing. Reload batches may have multiple enrichments. Fuel assemblies located in a low neutron leakage or high power density region may have BPRs. Figures 3.4-3 through 3.4-5 show the assembly location for the first and current cycles. The expected power distributions at selected burnups and CEA insertions for the first and current cycles are shown in Figures 3.4-6 through

3.4-22. Figures 3.4-23 through 3.4-26 show the effect of CEA insertion on power peaking and distribution for the first cycle.

The radial power distribution and fuel depletion are almost insensitive to reactor operations due to the high order of radial symmetry maintained and the negative radial and azimuthal stability factor. The APD, however, is subject to nonuniform axial temperatures, burnups, control rods, and xenon oscillations. Prudent use of CEAs will control undesirable axial power oscillations and the PDILs (first cycle shown in Figure 3.4-27) on CEA position prevent the expected burnup distribution from being negated by excessive CEA use.

3.4.6.4 Power Peaking Limits

Specified Acceptable Fuel Design Limits require that the core power distribution does not result in either fuel/clad melt or a DNB. Assurance that SAFDLs are not exceeded is obtained through the RPS and the Technical Specifications which enforce LCO. Limiting Conditions for Operation are established such that the initial conditions assumed in the analysis of AOOs and postulated accidents are conservative with respect to allowed reactor conditions. However, during certain AOOs the margin to fuel design limits deteriorates either in a manner that is undetected by the RPS or in such a manner that the RPS would not act before some margin loss has occurred. Therefore, the reactor must be operated such that losses in margin do not result in exceeding SAFDLs before the RPS restores the reactor to a safe condition. Limiting Conditions for Operation assure that sufficient initial margin to overcome margin losses exists.

3.4.6.5 Power Distribution Monitoring Capability

Neutron flux detectors are provided both within the active core (incore) and outside (excore) the reactor vessel. The RPS continuously monitors the excore detectors and reactor coolant variables to determine whether the plant is being operated within the LSSSs. Indicators are provided to solicit operator action prior to reaching an LSSS. In the event that conditions reach an LSSS, the RPS will automatically initiate a reactor trip.

Incore detectors provide the detailed power distributions necessary for Technical Specification surveillance of power peaks and core data trends.

The 35 incore self-powered rhodium detector strings are placed in the center CEA guide tube of selected assemblies. Each detector string has four, 40 cm long, rhodium detectors located at approximately 20, 40, 60, and 80% core height.

3.4.7 REACTOR STABILITY

3.4.7.1 General

Pressurized water reactors with negative overall power coefficients are inherently stable with respect to power oscillations. Therefore, this discussion will be limited to xenon-induced power distribution oscillations.

Xenon-induced oscillations occur as a result of rapid perturbations to the power distribution which cause the xenon and iodine fission product distributions to be out of phase with the perturbed power distribution. This results in a shift in the iodine and xenon distribution that causes the power distribution to change in an opposite direction from the initial perturbation and, thus, initiate oscillations. The magnitude of the power distribution oscillation can either increase or decrease with time. Thus, the core can be considered to be either unstable or stable with respect to these oscillations. Xenon stability analyses on previous Calvert Cliffs cores

indicate that any radial and azimuthal xenon oscillations induced in the core would be damped. Axial xenon oscillations, however, could exhibit instabilities during later portions of the cycle in the absence of appropriate control action. Before discussing the methods of analysis and control, it is appropriate to reiterate several important aspects of the xenon oscillation phenomenon.

a. The time scale for the oscillations is long and any induced oscillation typically exhibits a period of about one day.
b. Xenon oscillations are readily detectable as discussed below.
c. As long as the initial power peak associated with the perturbation initiating the oscillation is acceptable, the operator has time, in the order of from hours to days, to take appropriate remedial action before the allowable peaking factors are exceeded.

3.4.7.2 Method of Analysis

A xenon oscillation may be described by the following equation:

$$\phi(\bar{r},t) = \phi_o(\bar{r}) + delta\ \phi_o(\bar{r}) e^{bt} \sin(\omega t + \sigma)$$

where:

$\phi(\bar{r},t)$	is the space-time solution of the neutron flux
$\phi_o(\bar{r})$	is the initial fundamental flux
delta $\phi_o(\bar{r})$	is the perturbed flux mode
b	is the stability index
ω	is the frequency of the oscillation
σ	is a phase shift

The stability of a reactor can be characterized by a stability index or a damping factor which is defined as the natural exponent which describes the growing or decaying amplitude of the oscillation.

A positive stability index (b) indicates an unstable core. A zero or a negative value indicates stability for the oscillatory mode being investigated. The stability index is generally expressed in units of inverse hours, so that a value of -0.01/hr would mean that the amplitude of each subsequent oscillation cycle decreases by about 25% for a period of about 30 hours for each cycle. Xenon oscillation modes can be classified into three general types: radial, azimuthal, and axial.

3.4.7.3 Radial Stability

A radial xenon oscillation consists of a power shift inward and outward from the center of the core to the periphery. This oscillatory mode is generally more stable than an azimuthal mode.

To confirm that the radial mode is extremely stable, for the first cycle a space-time calculation was run for a reflected, zoned core 11' in diameter without including the damping effects of the negative power coefficient. The initial perturbation was a poison worth of 0.4% in reactivity placed in the central 20% of the core for 1 hr. Following removal of the perturbation, the resulting oscillation was followed in 4-hr time steps for a period of 80 hours. The resulting oscillation died out very rapidly with a damping factor of about -0.06/hr. If this damping coefficient is corrected for a finite time mesh, it would become even more strongly convergent. On this basis, it is concluded that radial oscillations are highly unlikely.

This conclusion is of particular significance because it means that there is no type of oscillation where the inner portions of the core act independently of the peripheral portions of the core, whose behavior is more closely followed by the excore detectors. Primary reliance is placed on these detectors for the detection of any xenon oscillations.

3.4.7.4 Azimuthal Stability

An azimuthal oscillation consists of an X-Y power shift from one side of the reactor core to the other. Azimuthally-symmetric operation and design practices and a negative stability index ensure proper azimuthal power distribution.

3.4.7.5 Axial Stability

Axial xenon oscillations consist of a power shift between the top and bottom of the reactor core. This type of oscillation may be unstable toward the EOC.

3.4.7.6 Detection and Control of Oscillations

Primary reliance for the detection of any xenon oscillations is placed on the excore flux monitoring instrumentation. As indicated earlier, oscillations in modes such as radial, which would allow the center of the core to behave independently from the peripheral portions of the core, are highly unlikely and this lends support to reliance on the excore detectors for this purpose.

Although the primary response of these detectors will be to the power in the peripheral fuel assemblies, the lower modes of any induced oscillations will affect the power shapes in these peripheral assemblies. Therefore, azimuthal or axial flux tilts can be observed and identified with the use of incore or excore instrumentation and appropriate remedial action can be taken.

In addition, the incore flux monitoring instrumentation is used to verify the correlation between indications from the excore detectors and the space-dependent flux distribution within the core.

The reactor is operated in such a manner as to avoid inducing sizable spatial perturbations. As was discussed previously, radial and azimuthal xenon oscillations are expected to be damped in the Calvert Cliffs cores. Axial oscillations, however, may be undamped in the latter stages of core life. These unstable xenon oscillations require control action to prevent them from building in magnitude; however, they are very slow acting and thus leave time for appropriate control strategies to be determined. The part-length CEAs initially installed to control axial oscillations were removed since full-length CEAs have proved to be effective in controlling all xenon oscillations.

3.4.8 NEUTRON FLUX AT PRESSURE VESSEL

The original design of the reactor vessel considers the fast neutron fluence (neutron energy greater than 1 MeV) to the inner wall of the vessel. The fluence was determined by combining the results of the computer code P3MG1 (Reference 7) and SHADRAC (Reference 2). A detailed neutron transport analysis using the discrete ordinate computer code DOT-4 (Reference 10) is periodically performed to determine the fast neutron fluence on the vessel. The analysis considers the neutron flux from previous fuel cycles, and projected low fluence core design. The method is verified by examination of surveillance capsules. Beginning with Unit 1 Cycle 11 and Unit 2 Cycle 10, low fluence fuel management is used to reduce the fluence at the vessels' beltline region welds.

3.4.9 ANALYTICAL METHODS

3.4.9.1 General

Calvert Cliffs reactor cores are designed using a series of calculations to determine the energy and spatial dependent neutron flux, the integral or differential core reactivity, and the power distribution. The computer code DIT (Reference 4) calculates the energy dependent flux, the spatial dependent flux, and the flux weighted assembly-wide cross-sections necessary to perform core-wide calculations. Originally, the computer code PDQ (Reference 3) was used to calculate a few group pin power distribution. Starting with Unit 2 Cycle 8 and Unit 1 Cycle 10 the fine-mesh code MC (Reference 4) replaced PDQ. The computer code ROCS (Reference 4) was used to calculate a coarse-mesh two- or three-dimensional power distribution and the core averaged reactivity coefficients.

Starting with Unit 2 Cycle 16 and Unit 1 Cycle 18, the PARAGON and ANC computer codes are used for nuclear design analysis. PARAGON (Reference 11) calculates the energy dependent flux, the spatial dependent flux, and the flux weighted assembly-wide cross-sections, and the pin peak reconstruction factors necessary to perform core-wide calculations. The computer code ANC (References 12, 13, and 14) calculates a coarse and fine mesh two- or three-dimensional power distribution and the core averaged reactivity coefficients. Previously the computer codes DIT and ROCS (Reference 4) were used for these purposes. Both PARAGON and ANC have been extensively benchmarked to a wide variety of measurements including those taken on several past cycles of the Calvert Cliffs units.

Starting with Unit 2 Cycle 19 and Unit 1 Cycle 21, the MICBURN-3/CASMO-3G and PRISM computer codes are used for nuclear design analysis. MICBURN-3/CASMO-3G (Reference 15) calculates the cross-sections, discontinuity factors, and heterogeneous form functions for the core simulator code, PRISM. The computer code PRISM (Reference 15) calculates the core-wide power distribution in three dimensions. MICBURN-3/CASMO-3G and PRISM have been extensively benchmarked to a wide variety of measurements including those taken on several past cycles of the Calvert Cliffs units.

MICBURN-3 is a multigroup one-dimensional transmission probability code which calculates the microscopic burnup in Gadolinium-loaded fuel containing initially homogeneously distributed poison. These cross-sections, as a function of absorber number density, are input to CASMO-3.

CASMO-3G is a multi-group, two-dimensional transport theory code for burnup calculations on assemblies. CASMO-3G is capable of modeling the geometry of the Calvert Cliffs cores including non-symmetric fuel bundles. The microscopic depletion is calculated in each fuel rod and burnable absorber rod. The output consists of cross-sections, discontinuity factors, and heterogeneous form functions for the core simulator code, PRISM.

The PRISM code performs core-wide two-group calculations. It uses pin power reconstruction to establish the individual rod histories and reactivities. The reactor core for Calvert Cliffs is modeled as 4 radial nodes and 32 axial nodes per assembly. With this reactor model, axial effects, including predicted values of LHR, F_r^T, and F_z can be studied. Thermal hydraulic feedback and axial exposure distribution effects on power shapes, rod worths, and cycle lifetime are explicitly included in the PRISM analysis.

The computer code INCA (Reference 5) was used to perform the on-line incore calculations. In Unit 2 Cycle 9 and Unit 1 Cycle 11, INCA is replaced by CECOR 3.3 for power distribution surveillance. Starting with Unit 2 Cycle 19 and Unit 1 Cycle 21, CECOR is replaced by POWERTRAX for power distribution surveillance. Satisfactory comparisons between these measured data and the predictions validate the design procedures.

3.4.9.2 Coarse-Mesh Diffusion Calculations - Westinghouse only

Coarse-mesh calculations are performed by ANC. This code contains a nodal solution to the diffusion equation to obtain a high degree of accuracy with a low number of spatial mesh points. The reactor core is typically modelled in ANC as four radial nodes and 20 to 30 axial nodes per fuel assembly. The axial and radial reflector regions are explicitly represented as additional nodes that are attached to the core boundary. ANC also contains equilibrium thermal models required to correctly determine the neutronic impact of changes in the spatial distributions of fuel temperatures and moderator density.

3.4.9.3 Power Distribution Monitoring

During normal operating conditions, signals proportional to the rhodium activation rates are obtained from the incore detectors. These signals are related to local power by use of calculated signal-to-power conversion factors for the appropriate core conditions. The measured signals are corrected for background, calibration, and depletion.

The POWERTRAX system replaces CECOR starting with Unit 2 Cycle 19 and Unit 1 Cycle 21. POWERTRAX provides a method of synthesizing detailed three dimensional assembly and peak-pin power distributions. This method is described below.

a. Calculated 3-D Nodal Power and Signal Distributions

The calculated nodal power and detector signals are provided by the POWERTRAX system nodal simulator.

b. Measured Powers at Operable Detector Locations

Measured powers at the operable detector locations are generated by multiplying the calculated nodal power by the corresponding ratio of the measured to calculate detector signals. The calculation is performed at all axial detector levels.

c. Measured Powers at other Locations

Other locations include those detector axial levels in un-instrumented assembly locations and those locations with failed detectors. The measured nodal powers at other locations are computed using the relation between the calculated nodal powers at these locations and at the locations with operable detectors.

d. Radial Power Distributions

A radial power distribution is a combination of the measured powers at operable detector locations and measured power at other locations.

e. Axial Power Profile

The axial power profiles are derived from the axial profiles from the 3-D nodal simulator calculation and adjusted by the differences in the measured and

calculated radial power distribution described above. These adjustments are made by modulating the calculated nodal power distribution with the ratio of inferred segment powers to the calculated nodal powers.

f. Final Normalization

The resulting 3-D power distribution is then re-normalized to the core thermal power to produce the final inferred 3-D nodal power distribution.

g. Peak Pin Power Distributions

Using the calculated nodal power distribution provided in step a, F_r (F_r-total is the maximum average pin power integrated over the entire core height; F_r-unrodded is the maximum average pin power integrated over the unrodded portion of the core) and pin-to box factor (PF-total is calculated for each assembly as the F_r-total value divided by the measured assembly average power; PF-unrodded is calculated for each assembly as the F_r-unrodded value divided by the average of the measured nodal powers averaged over the unrodded planes) can be obtained.

h. Azimuthal Power Tilt

The azimuthal power tilt is computed by determining the maximum values and locations of the maximum values from quadrant power tilt calculations for the upper and lower halves of the reactor core at each degree of rotation angle for 360° rotationally.

3.4.10 REFERENCES

1. Deleted
2. SHADRAC, "Shield Heating and Dose Rate Attenuation Calculation," G30-1365, March 25, 1966
3. W.R. Cadwell, "PDQ-7 Reference Manual," WAPD-TM-678, January 1968
4. CENPD-266-P-A, "The ROCS and DIT Computer Codes for Nuclear Design," April 1983
5. CENPD-153-P, Rev. 1-P-A, "Evaluation of Uncertainties in the Nuclear Power Peaking Measured by the Self-Powered Fixed In-core Detector System," May 1980
6. Deleted
7. CENPD 302, "Fast Attenuation by the P3MG, C-17 Shielding Method," July 1967
8. Deleted
9. Deleted
10. ORNL-5851, "An Updated Version of the DOT-4 One- and Two-Dimensional Neutron/Photon Transport Code," W.A. Rhoades, R.L. Childs, Oak Ridge National Laboratory, Oak Ridge, TN, July 1982
11. WCAP-16045-P-A, “Qualification of the Two Dimensional Transport Code PARAGON,” August 2004
12. WCAP-10965-P-A, “ANC: A Westinghouse Advanced Nodal Computer Code,” September 1986
13. WCAP-10965-P-A Addendum 1, “ANC: A Westinghouse Advanced Nodal Computer Code: Enhancements to ANC Rod Power Recovery,” April 1989

14. WCAP-11596-P-A, “Qualification of the PHEONIX-P/ANC Nuclear Design System for Pressurized Water Reactor Cores,” June 1988

15. EMF-96-029(P)(A), Volumes 1 and 2, “Reactor Analysis System for PWRs Volume 1 - Methodology Description, Volume 2 - Benchmarking Results,” Siemens Power Corporation, January 1997

TABLE 3.4-1

NUCLEAR PARAMETERS

I. FIRST CYCLE NUCLEAR PARAMETERS	
Control Characteristics	
k_{eff}, BOL, No Control Element Assemblies or Dissolved Boron with BPRs in	
Cold (68°F)	1.194
Hot (532°F), Zero Power	1.152
Hot (572°F), Full Power	1.128
Hot, Equilibrium Xe, Full Power	1.094
Total CEA Worth, %	
BOL	
Hot (572°F)	9.8
Cold (68°F)	5.7
EOC	
Hot (572°F)	9.7
Cold (68°F)	5.6
Dissolved Boron	
Dissolved Boron Content for Criticality, ppm, (CEAs withdrawn, BOL)	
Cold (68°F)	1120
Hot (532°F), Zero Power, Clean	1095
Hot (572°F), Full Power	960
Hot (572°F), Equilibrium Xe, Full Power	725
Dissolved Boron Content for Refueling, ppm	1720
Boron Worth, ppm/%	
Hot (572°F)	86
Cold (68°F)	69
Reactivity Coefficients (CEAs Withdrawn Unless Otherwise Indicated)	
MTC, $\Delta\rho$/°F	
Hot (572°F)	
BOC, 960 ppmb	-0.20×10^{-4}
BOC, 847 ppmb (1% CEAs In)	-0.49×10^{-4}
EOC, Zero ppmb	-1.96×10^{-4}
EOC, Zero ppmb (1% CEAs In)	-2.20×10^{-4}
Cold (68°F) Zero Power	
BOC, 1120 ppmb	-0.06×10^{-4}
FTC, $\Delta\rho$/°F	
Hot, Zero Power	-1.46×10^{-5}
Full Power	-1.06×10^{-5}
Moderator Void Coefficient, $\Delta\rho$/% Void	
Hot, Operating, BOL	-0.1×10^{-3}
EOC	-1.3×10^{-3}
Moderator Pressure Coefficient, $\Delta\rho$/psi	
Hot, Operating, BOL	$+0.3\times10^{-6}$
EOC	$+2.6\times10^{-6}$

TABLE 3.4-1

NUCLEAR PARAMETERS

II. CURRENT CYCLE NOMINAL NUCLEAR CHARACTERISTICS

	UNIT 1 CYCLE 24	UNIT 2 CYCLE 23
Dissolved Boron, ppm		
Dissolved Boron Content for Criticality, CEAs Withdrawn, Hot Full Power, Equilibrium Xenon, BOC	1341	1378
Boron Worth, ppm/% $\Delta\rho$		
Hot Full Power, BOC	146	147
Hot Full Power, EOC	106	106
Moderator Temperature Coefficient (CEAs Withdrawn), 10^{-4} $\Delta\rho$/°F Hot Full Power, Equilibrium Xenon		
BOC	-0.46	-0.43
EOC	-2.85	-2.85

TABLE 3.4-2

CEA REACTIVITY WORTH AND ALLOWANCES, (% $\Delta\rho$)

I. UNIT 1 FIRST CYCLE VALUES

	BOC	EOC
Fuel Temperature Variation	1.7	1.8
Moderator Temperature Variation	0.7	1.4
Moderator Voids	0.0	0.1
CEA Bite and Boron Deadband	0.2	0.2
Shutdown Margin and Safety Features Allowance	2.0	2.4
Total Reactivity Allowances	4.6	5.9
Stuck CEA Allowance	1.9	2.2
Calculated CEA Worth at 572°F (77 Full-Length CEAs)	9.8	9.7
Uncertainty Allowance and Margin	3.3	1.6

II. CURRENT CYCLE LIMITING VALUES FOR EXCESS SHUTDOWN MARGIN

Limiting Condition	**UNIT 1 CYCLE 24** EOC HFP	**UNIT 2 CYCLE 23** EOC HFP
Control Rod Worth		
ARI (All rods inserted)	8.471	8.383
MRR (Most reactive rod)	1.563	1.538
PDIL	0.180	0.177
(ARI-MRR-PDIL)*0.9	6.055	6.002
Positive Reactivity Insertion		
Power Defect	2.204	2.203
Axial Flux Redistribution	0.216	0.180
Coolant Void Effects	0.050	0.050
Total Positive Reactivity Insertion	2.470	2.433
Shutdown Margin		
(ARI-MRR-PDIL)*0.9 - Total Positive Reactivity Insertion	3.586	3.569
Required Shutdown Margin	3.500	3.500
Excess Shutdown Margin	0.086	0.069

3.5 THERMAL AND HYDRAULIC DESIGN AND EVALUATION

3.5.1 GENERAL

This section presents the thermal and hydraulic characteristic data and design methodology. The objective of the thermal and hydraulic design of the reactor is to ensure that the core can meet steady state and transient performance requirements without violating the design bases. The principal thermal and hydraulic design bases are related to DNB, fuel/clad melting, and hydraulic loading. Instrument and control uncertainties, delays between parameter changes, RPS trip signals, and initiation of CEA movement are involved in the transient calculations. The RPS monitors and trips the reactor upon sensing an adverse condition. The Engineered Safety Feature Actuation Signal (ESFAS) provides automatic corrective action when operating parameters exceed their setpoints. The Safety Analysis determines the setpoints such that the design bases will not be exceeded during AOOs and most postulated accidents. The Safety Analysis (Chapter 14) discusses each of the DBEs in detail. A summary of the key thermal and hydraulic parameters is presented in Table 3.5-1.

3.5.1.1 Cycle Summaries

The following cycle summaries provide a brief synopsis of major changes associated with each cycle.

a. Unit 1

1. Cycle 2

   The core power level was increased from 2560 MWt to 2700 MWt.

   Several design changes to the type D fuel improved the thermal performance and were included in the performance analysis. The parameters that affected the gap conductance, such as decreased pellet/cladding gap and the increased pellet density that decreased the effects of densification, were responsible for the improved thermal performance of the type D fuel.

2. Cycle 3

   Excessive CEA guide tube wear was identified. In order to reduce the wear on the guide tubes and CEA fingers, SS sleeves were inserted into the top end of some of the guide tubes. The sleeves protect the guide tubes against wear by CEA fingers.

   Part-length CEAs were also removed to reduce guide tube wear and dummy CEA plugs were inserted to minimize the increase in bypass flow.

   Minimum Departure from Nucleate Boiling Ratio was calculated using TORC/CE-1. TORC was used to generate the LCO in the Technical Specifications and was also used for all AOOs and postulated accidents. The TORC thermal hydraulics code replaces COSMO-INTHERMIC.

   TORC uses the CE-1 DNBR correlation, whereas previous cycles used COSMO-INTHERMIC, which uses the W-3 DNBR correlation (References 2, 3, 4, and 5).

   The detailed version of TORC (Reference 2) is a benchmarking code. The simplified version (Reference 3) runs considerably faster but is set

to be more conservative when benchmarked against the detailed version.

Mechanical design and power distribution uncertainty factors used in the calculation of thermal margin were previously combined multiplicatively. In Cycle 3, these factors:

F_q^e = Engineering Factor,

F_q^n = Nuclear Factor,

F_q^f = Fuel Rod Bowing Factor and,

F_q^p = Poison Rod Factor

were combined using a root-sum-square (RSS) technique. The RSS technique is appropriate for combining random uncertainties. The multiplicative technique is appropriate for combining systematic/dependent uncertainties.

Augmentation factors were calculated using the FATES (Reference 1) fuel rod model.

3. Cycle 4

   The guide tubes of reload fuel assemblies were either sleeved or their flow holes were changed. The sleeves protect the guide tubes against wear. The flow hole modification reduced coolant flow and thereby reduced the CEA vibration which caused the guide tubes to wear. Irradiated fuel assemblies previously resident in CEA locations, but not having sleeves, were sleeved in order to regain structural margin.

   Fuel assemblies exceeding the 24,000 MWD/MTU rod bow penalty threshold were placed in core locations where their power density was sufficiently low to offset rod bow penalties on the MDNBR limit.

4. Cycle 5

   The RPS was modified to include an asymmetric steam generator transient protection trip function. The trip function originates from the thermal margin/low pressure (TM/LP) logic and trips the reactor for those AOOs associated with secondary system malfunctions which would result in asymmetric primary loop temperatures. The limiting event is the loss of load to one steam generator caused by the closure of a single main steam isolation valve.

5. Cycle 6

   The TORC/CE-1 thermal design code has been replaced by the CETOP/CE-1 code (Reference 12). The treatment of core system parameter uncertainties on the DNBR SAFDL has been changed from the deterministic approach to statistical combination of uncertainties (SCU) (References 13, 14, and 15). The calculational factors (engineering heat flux factor, engineering factor on hot channel heat input, rod pitch and clad diameter factor) have been combined statistically with other uncertainty factors to define a new design limit on CE-1 MDNBR at the 95/95 confidence/probability level.

The performance of the fuel has been analyzed using FATES-3 (Reference 17), a fuel performance code.

The analysis with these methodology changes resulted in a MDNBR limit of 1.23.

6. Cycle 7

   The effects of fuel rod bowing on DNBR margin were evaluated using the methods described in Reference 11.

7. Cycle 8

   The PLCEA plugs were removed for Cycle 8 to facilitate the installation of the Reactor Vessel Level Monitoring System and to expedite refueling outage operations. An assessment concluded that the removal of the CEA plugs from all eight partial length rod locations has insignificant effect on the thermal and hydraulic design.

   The axial fuel densification factor is reduced from 1.01 to 1.002. A negative bias of 15% is added to the FTC data used in the safety analysis to establish consistency with the bias in the ROCS/DIT topical. This bias is used conservatively by selective application.

8. Cycle 9

   The fuel thermal performance calculations used FATES3B (Reference 18) which is an updated version of the FATES3 (Reference 17) fuel evaluation model. The statistically derived DNBR limit was reduced from 1.23 to 1.21. This reduction resulted from Nuclear Regulatory Commission (NRC) approval of a reduced CE-1 DNBR limit for CE's 14x14 fuel.

9. Cycle 10

   The DNBR SAFDL calculational factors (engineering heat flux factor, engineering factor on hot channel heat input, rod pitch and clad diameter factor) have been combined statistically with other uncertainty factors using the extended statistical combination of uncertainties (ESCU) methodology of Reference 19. This combination is used to derive an overall uncertainty allowance which, when used with the CE-1 critical heat flux (CHF) correlation DNBR design limit of 1.15 for 14x14 fuel, provides a 95/95 probability/confidence level of assurance against DNB occurring during steady state operation and AOOs. The statistically derived ESCU uncertainty allowance includes a 0.006 DNBR rod bow penalty which accounts for the adverse effects of rod bowing on CHF for 14x14 fuel with burnup not exceeding 45 GWD/T.

10. Cycle 11

    The fresh assemblies (Batch N) in Cycle 11 employ the GUARDIAN™ debris-resistant fuel design and large envelope Zircaloy grids. This fuel design results in a greater hydraulic resistance than the debris-resistant LEF design of the Batch 2L fuel used in Unit 2 Cycle 9. This increase in hydraulic resistance results in a slight decrease in the inlet flow for the Batch N fuel. The TORC and CETOP models used in the DNB analysis account for this flow reduction.

11. Cycle 12

    The fresh assemblies (Batch P) in Cycle 12 employ the GUARDIAN™ design with an improved top grid design. The top laser-welded grid introduces a backup arch in each grid cell in addition to the existing backup arches in the peripheral cell locations. This results in a greater hydraulic resistance in the Batch P assemblies. The TORC and CETOP models used in the DNB analysis account for the hydraulic resistance of each assembly type.

12. Cycle 13

    The standard fresh assemblies (Batch 1R) in Unit 1 Cycle 13 employ the laser welded, straight strip GUARDIAN™ grid design. The Batch 1R fuel also utilizes laser welded wavy strip intermediate Zircaloy spacer grids. The Unit 1 Cycle 13 DNB analysis explicitly accounted for the resistance of each assembly type in the Unit 1 Cycle 13 core.

13. Cycle 14

    The standard fresh assemblies (Batch 1S) in Unit 1 Cycle 14 employ the laser welded, straight strip GUARDIAN™ grid design. The Batch 1S fuel also utilizes laser welded wavy strip intermediate Zircaloy spacer grids. The Unit 1 Cycle 14 DNB analysis explicitly accounted for the resistance of each assembly type in the Unit 1 Cycle 14 core.

14. Cycle 15

    The standard fresh assemblies (Batch 1T) in Unit 1 Cycle 15 employ the laser welded, straight strip GUARDIAN™ grid design. The Batch 1T fuel also utilizes laser welded wavy strip intermediate Zircaloy spacer grids. The Unit 1 Cycle 15 DNB analysis explicitly accounted for the resistance of each assembly type in the Unit 1 Cycle 15 core.

    Mid-cycle the ABB-NV CHF correlation was approved. Therefore, both the CE-1 and ABB-NV correlations are applicable for DNB analysis for Unit 1 starting in Cycle 15. Calculations done with the new correlation were implemented mid-cycle.

15. Cycle 16

    The 96 fresh Turbo assemblies (Batch 1V) both with ZIRLO and OPTIN cladding in Unit 1 Cycle 16 employ the same straight strip GUARDIAN™ grid design as earlier Batches S and T. Batch 1V Turbo fuel also utilizes two bottom and one top straight strip advanced no-vane Zircaloy spacer grids and five intermediate advanced Zircaloy spacer grids with mixing vanes. The Unit 1 Cycle 16 DNB analysis explicitly accounts for the resistance of each assembly type in Unit 1 Cycle 16 mixed core.

    ABB-NV and ABB-TV CHF correlations have been developed applicable to Westinghouse standard and Turbo types of fuel assemblies, respectively, in Reference 20. The ABB-TV correlation has a better CHF performance compared to the ABB-NV correlation due to the presence of mixing vane grids in Turbo type fuel assemblies.

    Because of the higher hydraulic resistance of the Turbo fuel assemblies compared to the standard fuel assemblies, Turbo assemblies lose flow to standard fuel assemblies along the height of the core. This loss of

flow from Turbo fuel assemblies to the surrounding standard fuel assemblies in mixed core configuration such as in Unit 1 Cycle 16 is explicitly accounted for in the TORC DNB analysis.

Dual bundle tests have shown that the TORC prediction of this diversion cross-flow from a Turbo fuel assembly to a standard fuel assembly is fairly close with the test results. However, in order to conservatively compensate for any minor adverse effect on DNB margin assessment of Turbo type fuel assemblies due to small differences between the test results and TORC prediction of the diversion cross-flow from a Turbo fuel assembly to a standard fuel assembly, a margin neutral approach has been adopted for Unit 1 Cycle 16 DNB analysis. Based on this approach, Turbo fuel assemblies in Cycle 16 have been conservatively treated as standard fuel assemblies and the DNB margin assessment for Cycle 16 has been performed using ABB-NV CHF correlation documented in Reference 20. In other words, no margin credit has been taken for the ABB-TV CHF correlation that is applicable to Turbo fuel.

16. Cycle 17

    Eighty-eight fresh assemblies were installed for Unit 1 Cycle 17 (batch designation 1W).

    Batch 1W is the third batch of VAP for Unit 1. Erbia remains the burnable absorber, the Erbia fuel pins have cutback regions of 10.5 inches at the top of the rod and 12.0 inches at the bottom.

    Batch 1W is the second batch of the Turbo fuel assembly design for Unit 1. All but four assemblies utilized the same design and the same grid cage design as the U2C15 Westinghouse LFAs, see Section 3.7.3.13. The four different assemblies do not have the increased backup-arch length and have been given a unique sub-batch identifier. All of the fuel was manufactured by Westinghouse at their Columbia, SC facility. The cladding material for all fresh fuel is ZIRLO™.

    As Unit 1 contains approximately 85% of the Turbo fuel assembly design, transient analyses were updated to utilize the ABB-TV CHF correlation. Since the Turbo fuel has a non-mixing vane lower axial section and an upper section with mixing grids, both the ABB-NV and the ABB-TV CHF correlations are applied in the safety analysis.

17. Cycle 18

    The fresh assemblies (Batch 1X) for Unit 1 Cycle 18 employ the laser-welded, straight strip GUARDIAN grid design. Cycle 18 also employs the third full batch of the Turbo advanced grid design for Unit 1 and is the first Unit 1 core to contain all Turbo fuel assemblies.

18. Cycle 19

    Ninety-six fresh assemblies (Batch 1Z) were loaded for Unit 1 Cycle 19. All assemblies utilized in Cycle 19 employ the laser-welded, straight strip GUARDIAN grid design and the TURBO advanced grid design.

19. Cycle 20

    The rated thermal power was increased from 2700 MWt to 2737 MWt.

    Ninety-two fresh assemblies (eighty-eight Batch AA and four Batch 2X7) were loaded for Unit 1 Cycle 20. All assemblies utilized in Cycle 20 employ the laser-welded, straight strip GUARDIAN grid design and the TURBO advanced grid design.

20. Cycle 21

    Ninety-six fresh assemblies were loaded, which were manufactured by AREVA. These assemblies used the HTP correlation to determine DNBR. A thermal hydraulic compatibility analysis was performed to assess the impact on DNB performance of the core with addition of the AREVA fuel assemblies and the co-resident fuel assemblies.

    AREVA design uses HTP™/HMP™ spacer grids, FUELGUARD™ lower end fitting, reconstitutable upper end fitting, and M5® clad fuel rods.

21. Cycle 22

    Ninety-six fresh assemblies were loaded, which were manufactured by AREVA. These assemblies used the HTP correlation to determine DNBR. A thermal hydraulic compatibility analysis was performed to assess the impact on DNB performance of the core with addition of the AREVA fuel assemblies and the co-resident fuel assemblies.

    AREVA design uses HTP™/HMP™ spacer grids, FUELGUARD™ lower end fitting, reconstitutable upper end fitting, and M5® clad fuel rods.

22. Cycle 23

    Ninety-six fresh assemblies were loaded, which were manufactured by AREVA. These assemblies used the HTP correlation to determine DNBR. AREVA design uses HTP™/HMP™ spacer grids, FUELGUARD™ lower end fitting, reconstitutable upper end fitting, and M5® clad fuel rods.

23. Cycle 24

    Ninety-six fresh assemblies were loaded, which were manufactured by AREVA/Framatome. These assemblies used the HTP™ correlation to determine DNBR. AREVA/Framatome design uses HTP™/HMP™ spacer grids, FUELGUARD™ lower end fitting, reconstitutable upper end fitting, and M5® clad fuel rods.

b. Unit 2

1. Cycle 2

The core power level was increased from 2560 MWt to 2700 MWt.

The following modifications made to Unit 1 Cycles 3 and 4 were also made to the design for Unit 2 Cycle 2:

a) SS sleeves were installed in CEA guide tubes of selected reload fuel assemblies;
b) The size and number of CEA guide tube flow holes were modified on other selected fuel assemblies;
c) Part-length CEAs were removed and replaced by CEA plugs;
d) Minimum Departure from Nucleate Boiling Ratio was calculated using TORC/CE-1; and
e) Mechanical design and power distribution uncertainty factors, used in the calculation of thermal margin, which were previously combined multiplicatively were combined using an RSS technique.

2. Cycle 3

All fuel assemblies placed in CEA locations had SS sleeves installed in the guide tubes in order to prevent guide tube wear.

Augmentation factors were calculated using the FATES (Reference 1) fuel rod model.

Fuel assemblies exceeding the 24,000 MWD/MTU rod bow penalty threshold were placed in core locations where their power density was sufficiently low to offset rod bow penalties on the MDNBR limit.

3. Cycle 4

The RPS was modified to include the asymmetric steam generator transient protection trip function. The trip function originates from the TM/LP logic and trips the reactor for those AOOs associated with secondary system malfunctions which would result in asymmetric primary loop temperatures. The most limiting event is the loss of load to one steam generator caused by the closure of a single main steam isolation valve.

4. Cycle 5

The TORC/CE-1 thermal design code has been replaced by the CETOP/CE-1 Code (Reference 12). The treatment of core system parameter uncertainties has been changed from the deterministic approach to SCU (References 13, 14, and 15). The DNBR SAFDL calculational factors (engineering heat flux factor, engineering factor on hot channel heat input, rod pitch and clad diameter factor) have been combined statistically with other uncertainty factors to define a new design limit on CE-1 MDNBR at the 95/95 confidence/probability level.

The analysis with these methodology changes resulted in a MDNBR limit of 1.23.

5. Cycle 6

   The effects of fuel rod bowing on DNBR margin were evaluated using the methods described in Reference 11.

6. Cycle 7

   The statistically derived DNBR limit was reduced from the value of 1.23 to a value of 1.21. The reduction results from NRC approval of a reduced CE-1 DNBR limit for CE's 14x14 fuel. At the time the SCU analysis was approved for the Calvert Cliffs units, NRC review of the applicability of the CE-1 CHF correlation to rods with nonuniform APDs was incomplete. An interim CE-1 DNBR limit of 1.19 was thus used in the original SCU analysis. In the review of CE's nonuniform APD topical report, the NRC reduced the CE-1 DNBR limit from 1.19 to 1.15 for 14x14 fuel. The SCU DNBR limit was correspondingly reduced from 1.23 to 1.21. The 1.21 SCU DNBR limit includes the following penalties imposed by the NRC in their review of the SCU analysis.

   - Critical heat flux correlation cross validation penalty (5% increase in standard deviation of CHF correlation uncertainty distribution).
   - T-H code uncertainty penalty (5%, equal to two standard deviations).

   The 1.21 SCU DNBR limit also includes a 0.006 DNBR rod bow penalty which accounts for the adverse effects of rod bowing on CHF for 14x14 fuel with burnup not exceeding 45 GWD/T.

   The axial fuel densification factor was reduced from 1.01 to 1.002 to make it consistent with existing calculations.

   The PLCEA plugs were removed for Cycle 7 to facilitate the installation of the Reactor Vessel Level Monitoring System and to expedite refueling outage operations.

7. Cycle 8

   The thermal performance of the fuel was evaluated using the FATES3B (Reference 18) fuel evaluation model.

8. Cycle 9

   The fresh assemblies (Batch L) in Cycle 9 have small flow hole LEF plates, which result in greater hydraulic resistance than the LEF plates of the irradiated fuel. This increase in hydraulic resistance will result in a slight decrease in the inlet flow for these Batch L assemblies. The cycle specific TORC and CETOP models used in the Cycle 9 DNB analyses accounted for this flow reduction.

   The calculational factors (engineering heat flux factor, engineering factor on hot channel heat input, rod pitch and clad diameter factor) have been combined statistically with other uncertainty factors using the ESCU methods (Reference 19). This combination is used to derive an overall uncertainty allowance which, when used with the CE-1 CHF correlation design limit of 1.15 for 14x14 fuel, provides a 95/95

probability/confidence level of assurance against DNB occurring during steady state operation or AOOs.

9. Cycle 10

   The fresh assemblies (Batch 2M) in Cycle 10 employ the GUARDIAN™ debris resistant fuel design. This fuel design results in a greater hydraulic resistance than the Batch 2L fuel which trapped debris by employing small flow holes in the lower end fitting.

10. Cycle 11

    The standard fresh assemblies (Batch 2N) in Unit 2 Cycle 11 are the second Unit 2 batch to employ the GUARDIAN™ design. For Batch 2N, a straight strip GUARDIAN™ grid design was introduced, replacing the previously employed wavy GUARDIAN™ grid design. The new straight strip GUARDIAN™ grid design has lower hydraulic resistance than the Batch 2M wavy strip GUARDIAN™ grid design.

    Laser welded wavy strip intermediate Zircaloy spacer grids were also introduced for the Batch 2N fuel, replacing the previously employed TIG welded wavy strip intermediate Zircaloy spacer grids. The laser welded intermediate grids have a slightly lower hydraulic resistance than the TIG welded grids. The Cycle 11 DNB analysis explicitly accounted for the resistance of each assembly type in the Unit 2 Cycle 11 core.

11. Cycle 12

    The standard fresh assemblies (Batch 2P) in Unit 2 Cycle 12 employ the laser welded, straight strip GUARDIAN™ grid design. The Batch 2P fuel also utilizes laser welded wavy strip intermediate Zircaloy spacer grids. The perimeter strips have small guide holes to match pins on the grid assembly weld fixture. This is to ensure more consistent alignment of the grid strips within the fixture during welding. The Unit 2 Cycle 12 DNB analysis explicitly accounted for the resistance of each assembly type in the Unit 2 Cycle 12 core.

12. Cycle 13

    The standard fresh assemblies (Batch 2R) in Unit 2 Cycle 13 employ the laser welded, straight strip GUARDIAN™ grid design. The Batch 2R fuel also utilizes laser welded wavy strip intermediate Zircaloy spacer grids. The DNB analysis for Unit 2 Cycle 13 explicity accounted for the resistance of each assembly type.

13. Cycle 14

    The fresh assemblies (Batch 2S) in Unit 2 Cycle 14 employ the laser-welded, straight-strip GUARDIAN™ grid design. The Batch 2S fuel also utilizes laser-welded wavy-strip intermediate Zircaloy spacer grids. The DNB analysis for Unit 2 Cycle 14 explicitly accounted for the resistance of each assembly type. The ABB-NV DNB correlation was used instead of the CE-1 correlation.

14. Cycle 15

The fresh assemblies (Batch 2T) manufactured by Westinghouse in Unit 2 Cycle 15 employ the laser-welded, straight strip GUARDIAN™ grid design. Unit 2 Cycle 15 also contains the first full batch of the Turbo advanced grid design for Unit 2. Unit 1 received the first full batch of the Turbo advanced grid design at Calvert Cliffs in Unit 1 Cycle 16. The Turbo grid features include mixing vanes (at five of the eight spacer grid locations) and new rod retention device known as I-springs (at all eight spacer grid locations). The Unit 2 Cycle 15 DNB analysis explicitly accounts for the resistance of each assembly type in the Unit 2 Cycle 15 mixed core.

ABB-NV and ABB-TV CHF correlations have been developed applicable to Westinghouse standard and Turbo types of fuel assemblies, respectively, in Reference 20. The ABB-TV correlation has a better CHF performance compared to the ABB-NV correlation due to the presence of mixing vane grids in Turbo type fuel assemblies.

Because of the higher hydraulic resistance of the Turbo fuel assemblies compared to the standard fuel assemblies, Turbo assemblies lose flow to standard fuel assemblies along the height of the core. This loss of flow from Turbo fuel assemblies to the surrounding standard fuel assemblies in mixed core configuration such as in Unit 2 Cycle 15 is explicitly accounted for in the TORC DNB analysis.

Dual bundle tests have shown that the TORC prediction of this diversion cross-flow from a Turbo fuel assembly to a standard fuel assembly is fairly close with the test results. However, in order to conservatively compensate for any minor adverse effect on DNB margin assessment of Turbo type fuel assemblies due to small differences between the test results and TORC prediction of the diversion cross-flow from a Turbo fuel assembly to a standard fuel assembly, a margin neutral approach has been adopted for Unit 2 Cycle 15 DNB analysis. Based on this approach, Turbo fuel assemblies in Cycle 15 have been conservatively treated as standard fuel assemblies and the DNB margin assessment for Cycle 15 has been performed using ABB-NV CHF correlation documented in Reference 20. In other words, no margin credit has been taken for the ABB-TV CHF correlation that is applicable to Turbo fuel.

Batch 2T also contains LFAs from Westinghouse and FANP/AREVA. See Section 3.7.3.13 for detailed discussion on the Unit 2 Cycle 15 LFA.

In order to accommodate growth of the guide tube thimbles, the center guide tube recess hole in the lower end fitting of the fuel assembly was made approximately 1-7/8 inches deeper. This was accomplished via a process known as electric discharge machining and was performed or the fresh fuel after delivery.

15. Cycle 16

The fresh fuel assemblies (Batch 2V) for Unit 2 Cycle 16 employ the laser-welded, straight strip GUARDIAN grid design. Cycle 16 also contains the second full batch of the Turbo advanced grid design for Unit 2. The TORC DNB analysis explicitly accounts for the difference in the hydraulic resistance between the Turbo and standard fuel

assemblies. This is the second cycle for the Westinghouse and AREVA LFAs.

16. Cycle 17

    The fresh assemblies (Batch 2W) for Unit 2 Cycle 17 employ the laser-welded, straight strip GUARDIAN grid design. Cycle 17 also employs the third full batch of the Turbo advanced grid design for Unit 2 and is the first Unit 2 core to contain all Turbo fuel assemblies.

17. Cycle 18

    The rated thermal power was increased from 2700 MWt to 2737 MWt.

    Ninety-six fresh assemblies (Batch 2X) were loaded for Unit 2 Cycle 18. All assemblies utilized in Cycle 18 employ the laser-welded, straight strip GUARDIAN grid design and the TURBO advanced grid design.

18. Cycle 19

    Ninety-six fresh assemblies were loaded, which were manufactured by AREVA. These assemblies used the HTP correlation to determine DNBR. A thermal-hydraulic compatibility analysis was performed to assess the impact on DNB performance of the core with the addition of the AREVA fuel assemblies and the co-resident fuel assemblies.

    AREVA design uses HTP™/HMP™ spacer grids, FUELGUARD™ lower end fitting, reconstitutable upper end fitting, and M5® clad fuel rods.

19. Cycle 20

    One-hundred fresh assemblies were loaded, which were manufactured by AREVA. These assemblies used the HTP correlation to determine DNBR. A thermal-hydraulic compatibility analysis was performed to assess the impact on DNB performance of the core with the addition of the AREVA fuel assemblies and the co-resident fuel assemblies.

    AREVA design uses HTP™/HMP™ spacer grids, FUELGUARD™ lower end fitting, reconstitutable upper end fitting, and M5® clad fuel rods.

20. Cycle 21

    Ninety-six fresh assemblies were loaded, which were manufactured by AREVA. These assemblies used the HTP correlation to determine DNBR.

    AREVA design uses HTP™/HMP™ spacer grids, FUELGUARD™ lower end fitting, reconstitutable upper end fitting, and M5® clad fuel rods.

21. Cycle 22

    Ninety-six fresh assemblies were loaded, which were manufactured by AREVA. These assemblies used the HTP correlation to determine DNBR. AREVA design uses HTP™/HMP™ spacer grids, FUELGUARD™ lower end fitting, reconstitutable upper end fitting, and M5® clad fuel rods.

22. Cycle 23

Ninety-seven fresh assemblies were loaded, which were manufactured by Framatome. These assemblies used the HTP™ correlation to determine DNBR.

The Framatome design uses HTP™/HMP™ spacer grids, FUELGUARD™ lower end fitting, reconstitutable upper end fitting, and MS® clad fuel rods"

3.5.2 THERMAL AND HYDRAULIC DESIGN BASES

Avoidance of thermally- or hydraulically-induced fuel damage during normal steady state operation and during AOOs is the principal thermal and hydraulic design basis. In order to satisfy the design basis for reactor operation, the following design limits are established, but exceeding these limits will not necessarily result in fuel damage. The RPS provides for automatic reactor trip and the ESFAS provides other corrective action before these design limits are violated for AOOs. However, there is a small probability of limited fuel damage for certain other DBEs discussed in Chapter 14.

3.5.2.1 Minimum Departure from Nucleate Boiling Ratio

The minimum allowed DNBR provides at least a 95% probability with a 95% confidence that DNB does not occur on a fuel rod having the calculated MDNBR during steady state operation and AOOs. The ABB-NV correlation coupled with the CETOP code provides at least this probability and confidence. The DNBR limit may be modified to account for the possibility of fuel rod bow at burnups in excess of 45,000 MWD/MTU (Table 3.5-1). Starting with Unit 1 Cycle 17, the ABB-TV correlation was used in conjunction with the ABB-NV correlation to make DNB determinations.

Starting with Unit 2 Cycle 19 and Unit 1 Cycle 21, the HTP™ correlation was used to determine DNBR for the AREVA/Framatome fuel assemblies. The burnup limit for fuel rod bow impact on DNBR is greater than fuel assembly burnups for all anticipated core designs. Therefore, it is not necessary to modify the HTP™ correlation limit due to the effects of fuel rod bow.

3.5.2.2 Fuel Design Basis

a. Fuel Melt

The UO_2 melting point will not be reached during steady state operation and AOOs. For Westinghouse fuel assemblies, the UO_2 melting point is 5080°F unirradiated, and reduced by 58°F per 10,000 MWD/MTU burnup and reduced by 10.4°F for each weight percent of erbia of the maximum core erbia loading. For AREVA/Framatome fuel assemblies, a bounding value of 4595°F was used for the UO_2 melting point. This value bounds all anticipated limiting fuel burnup distributions and Gadolinia concentrations. The thermal and hydraulic parameters which influence the fuel centerline temperature include maximum linear heat rate (LHR), coolant velocity, pressure, temperature, clad temperature, fuel-to-gap conductance, fuel burnup, and UO_2 temperature.

b. Fuel Cladding Integrity

The fuel design bases for fuel clad integrity and fuel assembly integrity are given in Section 3.2.3.5. Thermal and hydraulic parameters that influence the fuel integrity include maximum LHR, core coolant velocity, coolant

temperature, clad temperature, fuel-to-clad gap conductance, fuel burnup, and UO_2 temperature.

The cladding minimizes deformation from external hydraulic pressure or internal gas/pellet pressure. Excessive contraction of the clad may lead to power spiking and excessive expansion may significantly decrease the flow channel area.

Conformance with the design limits and conformance with the design bases are sufficient to ensure fuel clad integrity, fuel assembly integrity, and the avoidance of thermally- or hydraulically-induced fuel damage for steady-state operation and AOOs.

3.5.2.3 Hydraulic Stability

Reactor internal flow passages and fuel coolant channels are designed to prevent hydraulic instabilities. Permissible flow maldistributions are limited by design to be compatible with the specified thermal design criteria.

3.5.3 STATISTICAL COMBINATION OF UNCERTAINTIES

The input data required for a detailed thermal-hydraulic analysis can be defined by type: (1) system parameters which describe the physical system and are not monitored during reactor operation; and (2) state parameters, which describe the operational state of the reactor and are monitored during operation. There is a degree of uncertainty in the value used for each of the input parameters used in the design safety analyses. This uncertainty has been handled in the past by assuming that each variable affecting DNB is at the extreme most adverse limit of its uncertainty range. The assumption that all factors are simultaneously at their most adverse values leads to conservative restrictions in reactor operation.

Beginning with Unit 1 Cycle 6, a new methodology was applied to statistically combine uncertainties in the calculation of new limits for Calvert Cliffs. These limits will ensure that neither the DNB nor fuel centerline melt design bases will be violated. The methodology is presented in three parts (References 13, 14, and 15). Part 1 (Reference 13) describes the application of the SCU to the development of the local power density (LPD) and TM/LP LSSSs. These are used in the analog RPS to protect against fuel centerline melt and DNB, respectively. Part 2 (Reference 14) uses SCU methods to develop a new DNBR limit which accommodates system parameter uncertainties. Part 3 (Reference 15) uses SCU methods to define LCOs.

For Unit 1 Cycle 10, an improved method was used for statistically combining uncertainties for the CE calculated TM/LP LSSS and DNB LCO. The extended combination of uncertainties (ESCU) methodology (Reference 19) is a modification of the SCU methodology (References 13, 14, and 15).

With the introduction of AREVA fuel assemblies for Unit 2 Cycle 19 and Unit 1 Cycle 21, a new method for the statistical combination of uncertainties was used to verify the TM/LP LSSS, the LPD LSSS, the DNB LCO, and LPD LCO. This methodology is described in Section 14.1.4.1 and Reference 23.

3.5.4 REACTOR HYDRAULICS

3.5.4.1 Coolant Flow

The minimum coolant flow at full power is shown in Table 3.5-1. Coolant enters the four inlet nozzles and flows down through the annular plenum between the reactor vessel and the core support barrel. Coolant continues through the flow skirt to the

plenum below the core lower support structure. Pressure losses in the skirt and lower support structure help to even out the inlet flow distribution to the core. The coolant passes through the openings in the lower core plate and flows axially through the fuel assemblies. After passing through the core, the coolant flows past the fuel alignment plate and into the region outside the CEA shrouds. From this region the coolant flows across the CEA shrouds and passes out through the outlet sleeves on the core barrel to the two outlet nozzles.

The principal core bypass routes (coolant flow paths other than through the fuel assemblies and next to the fuel rods) are direct inlet-to-outlet coolant flow at the joint between the core support barrel sleeve and the outlet nozzle and the flow in the radial reflector region between the core shroud and core support barrel. A small portion flows into the guide tubes in the fuel assemblies. The flow through the guide tubes has been modified by a reduction in size of the flow holes in the bottom of the guide tubes in other fuel assemblies. The coolant required to cool the CEAs flows in the annulus between the CEA and the guide tube and into the region outside the CEA shrouds. A similar but smaller leakage will occur around the restriction to flow at the upper end of those guide tubes without CEAs. The design limits the total guide tube flow and core bypass flow to a maximum of 3.9% of total reactor vessel flow as compared to the calculated bypass flow shown in Table 3.5-2.

3.5.4.2 Pressure Losses

The irrecoverable pressure losses from the inlet to outlet nozzles are calculated using standard loss coefficient methods and information from flow model tests. The nominal design pressure losses are listed in Table 3.5-3.

3.5.4.3 Partial Flow Operation

The plant operates with all four Reactor Coolant Pumps functioning. Partial pump operation will only occur during transients prior to trip and is discussed in Chapter 14. The most limiting partial pump operation is during a Seized Rotor Event which is more limiting than a four-pump Loss of Coolant Flow Event.

Partial pump operation creates an unbalanced inlet and outlet nozzle flow rate and a core inlet flow maldistribution. Furthermore, unbalanced steam generator flow rates create a greater possibility of temperature nonuniformities at the core inlet due to incomplete mixing of the incoming coolant.

3.5.5 MAXIMUM CORE TEMPERATURE

The maximum core temperature occurs at the center of the hottest pellet. The temperature drops radially across the pellet, gap, clad and coolant film. Heat transfer correlations relate the physical properties, heat flux, and temperature drops. The different physical geometry and properties necessitate separate correlations. The Jens-Lottes/Dittus-Boelter equation, clad conductivity, gap conductance, and pellet conductance relate the temperature drops across the coolant film, cladding, gap, and pellet, respectively.

For AREVA/Framatome fuel, the maximum fuel centerline temperature reached during the event is explicitly calculated using heat structure in the S-RELAP5 model which represents the hot node in the core for either a UO_2 rod or Gadolinia rod, whichever is limiting for the fuel centerline melt.

3.5.6 DEPARTURE FROM NUCLEATE BOILING

3.5.6.1 Design Approach to Departure from Nucleate Boiling

The margin to DNB at any point in the core is expressed in terms of the DNBR. The DNBR is defined as the ratio of the heat flux predicted to produce DNB at specific local conditions to the calculated local heat flux at the same local conditions. At some point in the core the DNBR is a minimum and, at this point, the margin to DNB for the core is evaluated. The following items are important in determining the core margin to DNB:

a. the coolant inlet conditions (e.g., pressure, temperature, and velocity distribution),
b. the geometry,
c. the power level,
d. the nuclear power distribution,
e. the analytical methods used to predict local coolant conditions, and
f. the correlation used to predict DNB heat flux.

Correlations of DNB are derived from experimental data and reduced to key parameters. Correlations for DNB are intended only to predict actual DNB and, therefore, the concept of DNB ratio can be misleading if one attempts to associate a physical meaning rather than a statistical meaning. Because of the uncertainties associated with predicting DNB there is a finite probability that if a channel is operated at a specified DNB ratio greater than unity based on a particular correlation, it will be at or above its DNB heat flux. Therefore, the proper interpretation of DNB ratio is that it is a measure of the probability that DNB would occur in the particular design situation to which the DNB correlation is applied. This interpretation assumes that all operating parameters are known precisely and that the probability being evaluated is only that associated with the correlation. The approach used in design is to select core operating conditions and analytical methods in such a way that there is a very small probability that the actual hot subchannel coolant conditions are more severe than the calculated conditions used as input to the DNB correlation. Starting with Unit 1 Cycle 17, the ABB-TV correlation was used in conjunction with the ABB-NV correlation to make DNB determinations.

Starting with Unit 2 Cycle 19 and Unit 1 Cycle 21, the HTP correlation (Reference 24) was used to determine DNBR for the AREVA/Framatome fuel assemblies. The DNBR limit accounts for state and system parameter uncertainties.

3.5.6.2 Evaluation of Margin to DNB

DNBR analysis is performed over a wide range of coolant parameters to determine the envelope in which the DNBR is at least greater than the SAFDL (Table 3.5-1). The inlet coolant flow distribution used was empirically developed from scale models.

Starting with Unit 2 Cycle 19 and Unit 1 Cycle 21, the XCOBRA-IIIC code was used to calculate the core thermal-hydraulic conditions for the AREVA/Framatome assemblies. These conditions are then used with the HTP correlation to determine DNBR for the AREVA/Framatomre assemblies.

3.5.7 VAPOR FRACTION

At steady state the reactor is operated at a negative coolant quality (subcooled temperature). Therefore, vapor formation is minimized and, for the most adverse steady

state conditions core vapor fraction is less than 0.1%. To avoid the possibility of DNB resulting from local flow oscillations, a conservative vapor fraction limit prevents flow instabilities. The limits to assure stable flow are based on avoiding flow regime changes in the hot channel that could affect the flow pressure drop characteristics and cause an instability. A thermal margin trip will occur before the flow instability limit is reached; thus DNB resulting from flow oscillations is prevented.

AREVA/Framatome fuel was added to the core starting from Unit 2 Cycle 19 and Unit 1 Cycle 21. Flow instability is not part of the AREVA evaluation and no changes to the flow stability occurred with the transition to AREVA/Framatome fuel.

3.5.8 THERMAL AND HYDRAULIC EVALUATION

The margin to CHF or DNB is expressed in terms of DNBR.

3.5.8.1 Statistical Analysis of Hot Channel Factors

Random variations from nominal values in enrichment, pellet density, pellet diameter and clad diameter, will affect the engineering heat flux factor on heat flux. Similar random variations in heat flux, as well as rod diameter, pitch, and bow contribute to the enthalpy rise factor. The calculation of these factors uses randomly-collected inspection data on "as-manufactured" fuel assemblies. Statistically random and independent constituent uncertainties are combined statistically.

3.5.8.2 Fuel Temperature Conditions

An assessment of the fuel centerline temperature has been made. The results demonstrate that a significant margin to centerline fuel melting will exist over the normal range of plant operation.

3.5.8.3 Flow Stability

Flow oscillations of significant amplitude may be sustained in some channels when heat is added to two-phase flow in parallel channels. This possibility is mitigated by the low vapor fraction during steady state and AOOs.

The two-phase flow regimes may be classed as separated or homogeneous. Separated flow is annular or slug. Homogeneous flow is bubbly or froth flow. For homogeneous flow, the channel pressure drop continuously increases with increasing flow rate or increasing vapor fraction. A change in the flow regime to separated flow results in a change in the flow characteristics and flow oscillations in the parallel channels are then possible. Cross flow tends to damp the oscillations and tends to make the open channel array stable when parallel closed channels would not be stable.

3.5.8.4 AREVA/Framatome Fuel Assemblies

Starting with Unit 2 Cycle 19 and Unit 1 Cycle 21, the HTP correlation was used to determine DNBR for the AREVA/Framatome fuel assemblies. The HTP correlation is described in Reference 24 and is applicable to the following operating conditions and nominal range of fuel design parameters:

Parameter	Minimum Value	Maximum Value
Pressure, psia	1385	2425
Local Mass Flux, mlb/hr/ft^2	0.498	3.573
Inlet Enthalpy (Btu/lb)	382.3	649.9
Local Quality	---	0.515

Parameter	Minimum Value	Maximum Value
Fuel Rod Diameter (in)	0.360	0.440
Fuel Rod Pitch (in)	0.496	0.580
Axial Spacer Span (in)	10.5	26.2
Hydraulic Diameter (in)	0.4571	0.5334
Heated Length (ft)	8.0	14.0

Based on the overall core conditions calculated at selected times during a transient evaluation, the XCOBRA-IIIC fuel assembly thermal-hydraulic code is used to calculate the flow and enthalpy distributions for the entire core and the DNB performance for the DNB-limiting assembly. The XCOBRA-IIIC model consists of a thermal-hydraulic model of the core (representing each assembly by a single "channel") linked to a detailed thermal-hydraulic model of the limiting assembly (representing each subchannel by a single "channel"). The limiting assembly DNBR calculations are performed using an approved DNB correlation.

The use of XCOBRA-IIIC is limited to the "snapshot" mode when used for transients and is restricted from use in LOCAs and other calculations with flow reversal and recirculation as per the NRC licensing restrictions (Reference 25). This mode is based on a series of steady-state calculations for input over a series of time steps.

3.5.9 REFERENCES

1. CENPD-139-P-A and CENPD-139, Supplement 1, Rev. 1, "CE Fuel Evaluation Model Topical Report," July 1974
2. CENPD-161-P-A, "TORC Code: A Computer Code for Determining the Thermal Margin of a Reactor Core," April 1986
3. CENPD-206-P-A, "TORC Code Verification and Simplified Modeling Methods," June 1981
4. CENPD-162-P-A, "Critical Heat Flux Correlation for C-E Fuel Assemblies with Standard Spacer Grids, Part 1, Uniform Axial Power Distribution," September 1976
5. CENPD-207-P-A, "Critical Heat Flux Correlation for C-E Fuel Assemblies with Standard Spacer Grids, Part 2, Nonuniform Axial Power Distributions," December 1984
6. Deleted
7. Deleted
8. Deleted
9. Deleted
10. Deleted
11. CENPD-225-P-A, "Fuel and Poison Rod Bowing," June 1983
12. CEN-191(B)-P, CETOP-D Code Structure and Modeling Methods for Calvert Cliffs Units 1 and 2," December 1981
13. CEN-124(B)-P, "Statistical Combination of Uncertainties, Part 1, December 1981
14. CEN-124(B)-P, "Statistical Combination of Uncertainties, Part 2, January 1980
15. CEN-124(B)-P, "Statistical Combination of Uncertainties, Part 3," March 1980
16. Deleted
17. CEN-161(B)-P, "Improvements to Fuel Evaluation Model (FATES 3)," July 1981

18. CEN-161(B)-P, Supplement 1-P, "Improvements to Fuel Evaluation Model (FATES 3B)," April 1986

19. CEN-348(B)-P, "Extended Statistical Combination of Uncertainties," January 1987

20. CENPD-387-P-A, “ABB Critical Heat Flux Correlations for PWR Fuel,” May 2000

21. Deleted

22. Deleted

23. EMF-1961(P)(A), Revision 0, “Statistical Setpoint/Transient Methodology for Combustion Engineering Type Reactors,” Siemens Power Corporation, July 2000

24. EMF-92-153(P)(A), Revision 1, “HTP: Departure from Nucleate Boiling Correlation for High Thermal Performance Fuel,” Siemens Power Corporation, March 2005

25. Letter from Mr. D. V. Pickett (NRC) to Mr. G. H. Gellrich (CCNPP), dated February 18, 2011, Calvert Cliffs Nuclear Power Plant, Unit Nos. 1 and 2 - Amendment Re: Transition from Westinghouse Nuclear Fuel to AREVA Nuclear Fuel (TAC Nos. ME2831 and ME2832)

TABLE 3.5-2

REACTOR COOLANT FLOWS IN BYPASS CHANNELS

BYPASS ROUTE	UNIT 1 PERCENT OF TOTAL REACTOR FLOW	UNIT 2 PERCENT OF TOTAL REACTOR FLOW
Outlet nozzle clearances	0.75	0.75
Alignment keyways	0.10	0.10
Core shroud annulus	0.64	0.61
Guide tubes	2.04	2.04
Total bypass	3.54	3.51

NOTE: The Unit 1 and Unit 2 bypass flows are based on a full core consisting of Turbo fuel assemblies that are conservative for mixed core configurations. Units 1 and 2 bypass flow accounts for 35 ICI thimbles. The total design bypass flow rate used for safety analysis is typically 3.9% which accounts for uncertainties and the increase in hydraulic resistance due to postulated crud buildup.

Starting with Unit 2 Cycle 19 and Unit 1 Cycle 21, the guide tube bypass flow will decrease from 2.04% to 2.02% as the core transitions from a full core of Westinghouse Turbo fuel to a full core of AREVA fuel.

TABLE 3.5-3

DESIGN REACTOR PRESSURE LOSSES

	VELOCITY, ft/sec	UNIT 1[(a)] PRESSURE LOSS, psid	UNIT 2[(a)] PRESSURE LOSS, psid
Inlet Nozzle and 90° Turn	42.0	5.7	5.7
Lower Plenum	7.5	9.6	9.6
Core	15.5	16.2	16.2
Core Outlet to Outlet Nozzle	46.8	6.7	6.7
TOTAL		38.2	38.2

(a) The values presented are valid for 2737 MWt, 2250 psia, 396,125 gpm, 548°F inlet temperature, and a full core of AREVA HTP™ fuel. Bounding analyses are also performed for the limiting conditions on power, pressure, flow, and temperature with mixed cores using both HTP™ and Turbo fuel.

3.6 ORIGINAL FUEL DESIGN EVALUATION

3.6.1 FUEL DESIGN AND ANALYSIS

The fuel rod cladding is designed to satisfy the design bases given in Section 3.2.3.5. The effects of irradiation on UO_2 and cladding materials are considered in the design calculations. The predicted effects of anticipated transients are also considered in the design process.

As stated in Section 3.2.3.5, the fuel rod cladding is designed to the following bases:

Basis 1

Maximum primary stress during steady state operation, expected transients, and depressurization is limited to two-thirds of the minimum yield strength of the material at operating temperature.

Basis 2

Predicted permanent hoop strain of the cladding at the end of fuel life is less than 1.0%.

These bases are conservative and the calculations used to demonstrate their satisfaction were conducted for limiting cases using limiting assumptions. This is considered advisable in the prediction of long-term fuel behavior under irradiation.

Maximum tensile stress in the fuel cladding occurs during a depressurization transient near EOL when internal gas pressure is highest. Clad thickness is such that under the anticipated transient conditions, this stress does not exceed two-thirds of the unirradiated value of yield stress of the clad material at its operating temperature. An unirradiated value is used for conservatism.

The satisfaction of Basis 2, the long-term total strain limit, was demonstrated as follows:

a. Clad stress-strain behavior was based on a stress analysis which includes the effect of creep. The loads considered were those due to fuel thermal and fission growth, fission gas pressure and external coolant pressure.

b. The fuel thermal and fission growth was calculated considering the fuel as a solid rod with unrestrained thermal expansion and a volumetric growth rate of 0.16% for 10^{20} fissions/cm^3 (Reference 1), and a LHR of 17.5 kW/ft. The fission gas pressure was calculated for a 31% fission gas release (which was based on the derivation of Lewis (Reference 2) considering the change in plenum volume due to the thermal expansion and growth of the rod).

c. The analysis was based upon an incremental approach, which divided the three-year fuel life span into discrete time intervals and evaluated the clad stress and strain, including the effect of creep, during these intervals. The relation between the incremental creep and the actual stress state is expressed by the Prandtl-Reuss formulae. The basis for creep is given by the von Mises criterion and the relation between creep rate and generalized stress is that given by Holmes (Reference 3). The rapidly convergent iterative technique was employed to solve the resulting non-linear equations.

d. For the nominal fuel-to-clad gap, at about 775 hours after BOL, the fuel has expanded to completely fill the fuel-to-clad gap and to restore the clad to a circular shape after its initial collapse onto the fuel. The fuel was subsequently assumed to swell unrestrained with the clad following. Based upon this conservative assumption, the final strain after three years service was 0.5%. That is, for

average fuel-to-clad gap at peak power density, Basis 2 was satisfied without credit for fuel strain under load.

e. For the most adverse initial condition, i.e., minimum clad ID, maximum pellet OD coincident with the point of maximum power density which was assumed to be sustained over lifetime, application of the unrestrained fuel growth model resulted in a computed strain at the end of the third cycle (EOC3) of 0.8%. However, as is well known (References 4, 5, and 6), the effect of restraint from the exterior, cooler regions of the fuel pellet, the clad, and the external pressure result in a significant limitation on radial swelling with corresponding flow of pellet material into the dish provided.

These analyses were conducted throughout with design BOL power density, although it was known that for fuel in its third burnup cycle, LPD would be substantially below these values. Thus, the LPD increase which might be associated with overpower transients near end of fuel life was conservatively considered. Further consideration of EOL power density is provided in subsequent paragraphs together with a summary of data justifying the maximum linear heat ratings and peak burnups. Table 3.6-1 contains typical maximum linear heat ratings as a function of burnup. The maximum linear heat rating for the first core was 17.5 kW/ft at BOL. The maximum heat rating near EOC3 was 14.9 kW/ft, resulting in a BOL/EOC3 ratio of 1.18. This was greater than the value of 1.12 for the ratio of maximum transient to steady state heat ratings. Thus, use of BOL power densities in these calculations for EOC3 transients provided considerable margin.

Studies by Notely, et al (References 5 and 6) in which 27 fuel elements were irradiated without failure, reported measured clad strains up to 3.33%.

In a series of experimental element irradiations, Westinghouse (Reference 4) reported strain values at failure for Zr-4 clad fuel elements of 0.78 to 2.6% depending on the fuel properties assumed. Also, Lustman (Reference 7) noted that failures in pile have occurred at strain values between 0.5 to 1.0%. However, these results are based on relatively low Zr-4 cladding temperatures as compared to contemporary, large, commercial PWRs. It is known (Reference 8) that permissible strain values for Zircaloy increase above 650°F. In the zone of interest, the average Zr-4 cladding temperature is about 720°F; this should result in increased ductility and thus a higher strain limit to failure.

For the AREVA/Framatome design, compliance was demonstrated using the NRC-approved methodology using the RODEX2 code.

3.6.2 ANALYSIS OF BURNUP AND LINEAR HEAT RATINGS

Prior to a discussion of the experimental bases for justifying the initial maximum linear heat ratings and burnups, it is necessary to relate these parameters so that they may be viewed in the proper perspective. The maximum linear heat rating was reached but not exceeded only during approximately the first 28,000 MWD/MTU of peak burnup. The maximum linear heat rating decreased with additional burnup beyond this value.

Typical values at the time of initial design are shown in Table 3.6-1, which contains an analysis of burnup, total nuclear peaking factors, and the corresponding maximum linear heat rating (including consideration of the combination of total nuclear and mechanical peaking factors), for the most adverse equilibrium core.

Table 3.6-2 contains a comparison of maximum heat ratings for a number of plants of that period. Peak linear heat ratings for this plant were consistent with current practice and were considered as slightly conservative with respect to a number of the designs.

Although it was believed that fuel rods could operate satisfactorily with a small amount of fuel melting, the initial design did not permit fuel melting even under conditions imposed by anticipated transients. Cycle 1 design offered considerable margin with respect to the core linear heat rating of 24 kW/ft for melting (BOL value; typical EOC3 value was about 23 kW/ft), even when expected transients (112%) were considered.

3.6.3 SUMMARY OF PERTINENT FUELS IRRADIATION INFORMATION

The LHRs specified in this section are as they appeared in the referenced literature and represent total core heat rates.

3.6.3.1 High Linear Heat Rating Irradiations

The determination of the effect of linear heat rating and fuel-cladding gap on the performance of Zircaloy-clad UO_2 fuel rods was the object of two experimental capsule irradiation programs conducted in the Westinghouse Test Reactor (WTR) (Reference 9). In the first program, 18 rods containing 94% TD UO_2 pellets were irradiated at 11, 16, 18 and 24 kW/ft with cold diametral gaps of 0.006", 0.012" and 0.025". The wall thickness to diameter ratio (t/OD) of the Zircaloy-cladding was 0.064 which is slightly higher than the value of 0.059 of Cycle 1. Although these irradiations were short duration (about 40 hours), significant results applicable to Cycle 1 design were obtained. No significant dimensional changes were found in any of the fuel rods. Only one rod, which operated at 24 kW/ft with an initial diametral gap of 0.025", experienced center melting. Rods which operated at 24 kW/ft with cold gaps of 0.006" and 0.012" did not exhibit center melting on these bases. The initial gap of 0.0085" and the maximum linear heat ratings for this design (Table 3.6-1) provided adequate margin against center melting even when 12% overpower conditions were considered. These results also indicated that an initial diametral gap of 0.0085" was adequate to accommodate radial thermal expansion without inducing cladding dimensional changes, even at 24 kW/ft. This margin with respect to thermal expansion, decreased with increasing burnup at a rate of 0.16% ΔV per 10^{20} fissions/cm^3. However, the linear heat rating also diminished with burnup (Table 3.6-1). Since the diametral thermal expansion (assuming BOL maximum heat ratings) is almost twice as great as the swelling diametral growth (on the EOC3 burnup), these data added considerable weight to the conservative treatment of the influence of transients on fuel element integrity.

Further substantiation of the capability of operation at maximum linear heat ratings in excess of those in the first cycle design was obtained from later irradiation tests in WTR (Reference 9). Thirty-eight-inch long and 6" long fuel rods were irradiated at linear heat ratings of 19 kW/ft and 22.2 kW/ft to burnups of 3450 and 6250 MWD/MTU. The cold diametral gaps in these Zircaloy-clad rods containing 94% dense UO_2 were 0.002", 0.006" and 0.012". The cladding t/OD was 0.064. No measurable diameter changes were noted for the 0.006" or 0.012" diametral gap. Only small changes were observed for the rods with a 0.002" diametral gap.

Additional successful radiations had been performed with SS cladding in Saxton at 23 kW/ft and in Plum Point at 22 to 25 kW/ft.

3.6.3.2 Shippingport Blanket Irradiations

Zircaloy-clad fuel rods operated successfully (three defects had been observed which were a result of fabrication defects) in the Shippingport blanket with burnups of about 37,000 MWD/MTU and maximum linear power ratings of about 13 kW/ft (References 9, 10, and 11). Although higher linear heat ratings at lower burnups would be experienced, swelling (primarily burnup-dependent) and thermal

expansion (linear heat rating dependent) provide the primary forces for fuel cladding strain at the damage limit. Thus, Shippingport irradiations demonstrated that Zircaloy-clad rods with a cladding t/OD comparable to that for this plant (0.059) should successfully contain the swelling associated with 37,000 MWD/MTU burnup, while at the same time containing the radial thermal expansion associated with heat ratings of the time. Irradiation test programs in support of Shippingport in in-reactor loads demonstrated successful operation of burnups of 40,000 MWD/MTU and linear heat ratings of about 11 kW/ft with cladding t/OD ratios as low as 0.053 (compared with 0.059 for this plant) (Reference 12).

3.6.3.3 NRX Irradiations (AECL - Canada)

Eleven Zircaloy-clad, large diameter fuel elements (approximately .750" OD) with clad thicknesses of .016", .024", and 0.037" (t/OD = .021, .031, and .047 corresponding to TD percentages of 94.3, 94.3 and 93.7, respectively) were irradiated in the NRX pressurized loop facility of AECL, Canada (Reference 13) at loop pressures of 2000 to 3000 psi. The cold diametral gaps for the test elements were .0035" and .0040", and the fuel was UO_2 sintered pellets (0.700" diameter) loaded in an argon atmosphere.

The elements were operated for 535 full power days to an average burnup of 10,280 MWD/MTU at a maximum linear power output of 14.8 kW/ft. These elements experienced 308 power cycles. No failures were reported for these elements, and the final dimensions of the rods were reported to be virtually unchanged from pre-irradiation values.

The successful operation of these elements with considerable lower clad-to-diameter ratios than those for Cycle 1 demonstrated the capability of safe operation of Zircaloy-clad elements with thin cladding for many power cycles.

Additional tests on similar elements were then in progress at NRX involving test elements with UO_2 and (U, Pu) O_2 (PuO_2 = 2.4 wt%) at average linear heat ratings of 11.4 and 17.2 kW/ft. Those elements had accumulated burnups of 6,400 and 28,700 MWD/MTU without failure.

3.6.3.4 Saxton Irradiations

UO_2-PuO_2 fuel rods containing pellets of 94% TD and clad with Zircaloy-4 had been successfully irradiated in Saxton to burnups approaching 25,000 MWD/MTU at 16 kW/ft under USAEC Contract AT(30-1)-3385 (Reference 14). The t/OD of the cladding was 0.059 which is equivalent to the Cycle 1 design. The amount of PuO_2, 6.6%, was considered as insignificant with respect to providing any differences in performance when compared with that for UO_2. In fact, the higher thermal expansion coefficient for this PuO_2-UO_2 composition than that for UO_2 would induce greater cladding strain under equivalent irradiation conditions. Subsequent tests on two of the above rods (18,600 MWD/MTU at 10.5 kW/ft) successfully demonstrated the capability of these rods to undergo power transients from 16.8 kW/ft to 18.7 kW/ft.

3.6.3.5 Vallecitos Boiling Water Reactor - Dresden

The combined Vallecitos Boiling Water Reactor (VBWR) - Dresden irradiation of Zircaloy-clad oxide pellets (Reference 15 and 16) provided additional confidence with respect to the design conditions for the fuel rods for Cycle 1 core. Ninety-eight rods irradiated in VBWR to an average burnup of about 10,700 MWD/MTU were assembled in fuel assemblies and irradiated in Dresden to a peak burnup

greater than 48,000 MWD/MTU. The reported maximum heat ratings for these rods was 17.3 kW/ft, which occurred in VBWR. The t/OD cladding ratio of 0.052, pellet TD of 95%, and the external pressure of about 100 psi are conditions which are all in the direction of less conservatism with respect to fuel rod integrity when compared with the design values of 0.059 cladding t/OD ratio and an external pressure of 2250 psi. Ten of these VBWR - Dresden rods representing maximum combinations of burnup, heat rating and pellet density had been selected for detailed destructive examinations as part of an AEC program. The remaining 88 rods were returned to Dresden and successfully irradiated to the termination of the program.

3.6.3.6 Large Seed Blanket Reactor Rods

Two rods operated in the B-4 loop at the Materials Testing Reactor provided a very interesting simulation for contemporary PWR designs (Reference 4, 17, and 18). Both rods were comprised of 95% TD pellets with dished ends clad in Zircaloy. The first of these, No. 79-2, was operated successfully to a burnup of 12.41×10^{20} f/cc (approximately 48,000 MWD/MTU) through several power cycles which included linear power from 5.6 to 13.6 kW/ft. The second fuel pin, No. 79-25, operated successfully to 15.26×10^{20} f/cc (approximately 60,000 MWD/MTU). The basic difference in this rod was the 0.028" wall thickness, as compared to 0.016" (t/OD 0.058) in the first rod. All other parameters were essentially identical. The linear heat rating ranged from 7.1 to 16.0 kW/ft. After the seventh interim examination, the rod operated at a peak linear power of 12.9 kW/ft at a time when the peak burnup was 49,500 MWD/MTU. These high burnups were achieved with fuel elements which were assembled by shrinking the cladding onto the fuel. This indicated that a comparable irradiation of the fuel elements for this reactor would allow a considerable increase in swelling life at a given clad strain.

One additional rod irradiated in Materials Testing Reactor as part of the Large Seed Blanket Reactor (LSBR) series (rod 79-18) demonstrated the effect of clad restraint on the swelling behavior of a UO_2-Zircaloy-clad rod (Reference 19). A starting fuel density of 81.4% of theoretical was used in conjunction with a zero cold gap and a 0.060 cladding t/OD ratio. The rod was irradiated to 49,000 MWD/MTU with no measurable change in rod diameter.

3.6.3.7 Central Melting in Big Rock

As part of a Joint U.S. - Euratom Research and Development Program, Zircaloy-clad UO_2 pellet rods with 95% of TD had been irradiated under conditions designed to induce central melting in the Consumers Big Rock Point Reactor (Reference 20). The test included 0.7" diameter fuel rods (cladding t/OD = 0.061, fuel-to-clad gap of about 0.011") at maximum linear heat ratings of about 27 kW/ft and 22 kW/ft with peak burnups up to 20,000 MWD/MTU. Results of these irradiations provided a basis for incorporating linear heat ratings well in excess of those calculated for this reactor (Reference 21). These results showed that the presence of localized regions of fuel melting were not catastrophic to the fuel assembly.

3.6.3.8 Peach Bottom 2

General Electric (GE) had successfully irradiated fuel pins of the Peach Bottom 2 design to burnups in excess of 42,000 MWD/MTU at peak linear heat ratings of 23 kW/ft. An interim examination at 32,500 MWD/MTU indicated a satisfactory condition (Reference 22).

3.6.4 EVALUATION

It was concluded from the above information that heat ratings as high as 23 to 24 kW/ft could be achieved in the fuel elements without fuel centerline melting. Linear heat ratings in the Cycle 1 core design fell significantly below this limit even at the 112% overpower condition.

Heating ratings and burnups for this design were well demonstrated by the existing technology. Nevertheless, it was felt fruitful to consider the question of what constitutes a fuel element failure. For one, the cladding must be violated. On the subject of the influence of expected transients, a conservative analysis had been presented of the factors which influence cladding performance during such transients. The fuel rod cladding was designed on a conservative basis and the calculations considered limiting cases and limiting assumptions. Consideration of peaking factor reductions shown in Table 3.6-1 increased the conservatism of these analyses.

The analyses had been conducted throughout with design BOL power density, although it was known that for fuel in its third burnup cycle, LPD would be substantially below these values. Thus, the LPD increase which might be associated with overpower transients near end of fuel life had been conservatively considered. Cladding integrity had been demonstrated even under these adverse conditions. Consideration of peaking factor decreases noted in Table 3.6-1 made this analysis even more conservative.

Present heat rating limits are based on LOCA/Emergency Core Cooling System stored energy considerations and are included in Section 14.17.

3.6.5 REFERENCES

1. M.L. Bleiberg, R.M. Berman, and B. Lustman, "Effects of High Burnup on Oxide Ceramic Fuel," WAPD-T-1455, March 1962
2. B. Lewis, "Engineering for the Fission Gas in UO_2 Fuel," Nuclear Applications, Vol. 2, No. 2, April 1966
3. J.J. Holmes, J.A. Williams, D.H. Nyman, and J.C. Tobin, "In-Reactor Creep of Cold Worked Zircaloy Z," Flow and Fracture of Metals and Alloys in Nuclear Environments, ASTM-STP-380, 1965
4. E. Duncombe, J.E. Meyer, and W.A. Coffman, "Comparison with Experiment of Calculated Dimensional Changes and Failure Analysis of Irradiated Bulk Oxide Fuel Test Rods Using the CYGRO-I Computer Program," WAPD-TM-583, September 1966
5. Notely, Bain, and Robertson, "The Longitudinal and Diametral Expansion of UO_2 Fuel Elements," AECL-2143, November 1964
6. M.J.F. Notely and J.R. MacEwan, "The Effect of UO_2 Density on Fission Product Gas Release and Sheath Expansion," AECL-2230, March 1965
7. B. Lustman, "Fuel Clad Design Basis for Thermal Reactors," Bettis Atomic Power Laboratory, May 1966
8. P.J. Pankaskie, "Creep Properties of Zircaloy-2 for Design Application," HW-75267, October 1962
9. Indian Point Nuclear Generating Unit No. 2, Preliminary Safety Analysis Report, Appendix A
10. J.T. Stiefel, H. Feinroth, and G.M. Oldham, "Shippingport Atomic Power Station Operating Experience, Developments and Future Plans," WAPD-TM-390, April 1963

11. Question V.B.2, Prairie Island Nuclear Generating Plant, Preliminary Safety Analysis Report, (Docket No. 50-306)

12. T.D. Anderson, "Effects of High Burnup on Bulk UO_2 Fuel Elements," Nuclear Safety, Vol. 6, No. 2 Winter 1964-1965, p. 164-169

13. R.D. MacDonald, et al, "Zircaloy-2 Clad Fuel Elements Irradiated to a Burnup of 10,000 MWd/MTU," AECL-1952, 1964

14. R.S. Miller, et al, "Operating Experience with the Saxton Reactor Partial Plutonium Core-II" paper presented at AEC Plutonium Meeting in Phoenix, August 1967

15. C.J. Baroch, J.P. Hoffmann, H.E. Williamson, and T.J. Pashos, "Comparative Performance of Zircaloy and Stainless Steel Clad Fuel Rods Operated to 10,000 Mwd/T in the VBWR," GEAP-4849, April 1966

16. F.H. Megerth, "Zircaloy-Clad UO_2 Fuel Rod Evaluation Program, Quarterly Progress Report No. 2, February 1968 - April 1968," GEAP-5624 (May 1968)

17. R.M. Berman, H.B. Meieran, and P. Patterson, "Irradiation Behavior of Zircaloy-Clad Fuel Rods Containing Dished-End UO_2 Pellets," (LWBR-LSBR Development Program), WAPD-TM-629, July 1967

18. J.T. Engel, et al, "Performance of Fuel Rods Having 97 Percent Theoretical Density UO_2 Pellets Sheathed in Zircaloy-4 and Irradiated at Low Thermal Ratings," (LSBR/LWBR Development Program), WAPD-TM-631, July 1968

19. J.E. McCauley, et al, "Evaluation of the Irradiation Behavior of a Zircaloy-4 Clad Fuel Rod Containing for Density UO_2 Fuel Pellets," LWBR-LSBR Development Program, WAPD-TM-596, January 1968

20. J.P. Blakely, "Action on Reactor and Other Projects Undergoing Regulatory Review of Consideration" Nuclear Safety, Vol. 9, No. 4, p. 326 (July-August 1968)

21. S.Y. Ogawa, Final Report, "Power Reactor High Performance UO_2 Program," Joint US-Euratom Research and Development Report, GEAP-10042, June 1969

22. Summary description of Peach Bottom Atomic Power Station Units No. 2 and No. 3 and Review of Considerations Important to Safety, Docket No. 50-277 and 50-278

TABLE 3.6-1

TYPICAL PEAK BURNUP - MAXIMUM HEAT RELATIONSHIP

MAXIMUM LOCAL EXPOSURE MWD/MTU	TOTAL NUCLEAR PEAKING Factor	MAXIMUM HEAT RATING kW/ft
24,200	2.86	17.5
24,200 - 36,000	2.86	17.5
36,000 - 48,500	2.42	14.9

TABLE 3.6-2

COMPARISON OF MAXIMUM HEAT RATINGS

REACTOR	kW/ft
Maine Yankee	16.7
Fort Calhoun	17.1
Calvert Cliffs, Unit 1	17.5
Calvert Cliffs, Unit 2	17.5
Hutchinson Island, Unit 1	17.8
Millstone Unit 2	17.8
Turkey Point	17.3
Surrey	17.5
Prairie Island	17.4
Three Mile Island	17.5
Oconee	17.5
Indian Point, Unit 2	18.5
Diablo Canyon	18.9
Browns Ferry	18.5
Sequoyah	18.8
San Onofre, Units 2 and 3	18.5

3.7 SUPPLEMENTARY FUEL DESIGN AND EVALUATION

3.7.1 FUEL ROD DESIGN EVALUATION

3.7.1.1 Mechanical Design Evaluation

a. Clad Creepdown/Creep-Collapse

Historical Perspective

Clad creepdown is the phenomenon caused by inward stresses on the cladding (caused by the difference in external and internal pressure) in combination with effects from temperature and neutron fluence. If the clad slowly ingresses toward the pellet stack, it would reduce gap size and increase gap conductance. Densification of fuel pellets leads to the formation of axial gaps in the fuel stacks and a loss of support for the cladding in these locations. Creepdown and subsequent collapse into axial gaps induced by fuel densification is called creep-collapse.

The minimum time to collapse for CE Zircaloy-clad fuel was calculated by the CEPAN computer code (Reference 13). The experimental database used for modeling creep collapse consists of measurements made on fuel rods irradiated in a CE reactor. The analytical creep correlation used in the model was fit to this data. That correlation leads to the time to collapse predictions given by CEPAN.

Beginning with Unit 1 Cycle 6, improvements were made in the modeling technique. These improvements (Reference 26) revised the method for establishing uncertainties in cladding geometrical parameters (diameters, thicknesses, etc.) used in the collapse analysis, and provided new criterion for the occurrence of collapse.

Present Analysis

Analysis of the phenomena of interpellet gap formation and clad collapse in modern PWR fuel rods (i.e., nondensifying fuel in prepressurized tubes), demonstrates that the collapse time for modern fuel is significantly larger than its expected useful life. This conclusion is discussed in an EPRI-sponsored report (Reference 28) and is based upon both empirical data covering several vendors' fuel and an analytical evaluation of the propensity for clad collapse into a postulated gap of finite length. Based upon the conclusion and recommendation of this report, cycle-specific clad collapse analyses are not necessary for modern CE manufactured fuel. A cycle-specific calculation was not prepared beginning with Unit 1 Cycle 8, and Unit 2 Cycle 7.

Beginning with Unit 2 Cycle 19 and Unit 1 Cycle 21, the RODEX2 fuel rod analysis code is used to evaluate the cladding creepdown and creep collapse for AREVA/Framatome fuel. Creep collapse and the subsequent potential for fuel failure are avoided in the fuel system design by eliminating the formation of axial gaps in the fuel column. The licensing criterion for preventing cladding collapse is to maintain a radial gap large enough to prevent pellet hang up and, therefore, axial gap formation. The maximum cladding circumferential creep and ovalization, up to the time of maximum densification, are computed to demonstrate that a radial gap between pellet and cladding is maintained. The evaluation is performed using the approved RODEX2 code (References 33 and 34) and the COLAPX code on a cycle specific basis beginning with Unit 2 Cycle 19 and Unit 1 Cycle 21. The RODEX2 code is used to provide initial in-reactor fuel rod

conditions to COLAPX. The COLAPX code calculates the cladding ovality changes (flattening) and creep deformation of the cladding as a function of time. M5® properties were incorporated, as appropriate, into these codes in Reference 36.

b. Fuel Rod Bowing

Fuel rod bowing is the phenomenon whereby a curvature of the rod is experienced, changing the thermal-hydraulic and neutronics characteristics of the region, and potentially affecting the mechanical performance of the fuel. It is primarily caused by a combination of rod axial growth and spacer grid restraint. Rod axial growth is largely the result of normal Zircaloy/ZIRLO growth, although some enhancement due to stresses caused by Pellet-clad Interaction (PCI) is possible. Fuel design changes to decrease the effects of PCI (chamfering, reduced length/diameter, etc.) tend to reduce PCI contributions to rod axial growth, and to bowing of the rod.

Fuel rod bowing leads to variations in the flow characteristics and neutronics of the affected region. Neutronic changes due to enhanced/decreased moderation (depending on the direction of bow) and, in the case of bowed BPRs, enhanced/decreased thermal neutron absorption, lead to changes in local LHRs. Flow changes due to opening/closing of channels can lead to changes in the margin to DNB. Both of these effects are analyzed in Reference 14, and are shown to be within existing margins.

Mechanical performance of the fuel itself can be affected by rod bowing. Rods bowed toward each other may come into contact. Restriction of flow in this region can enhance clad corrosion. Flow induced vibration of the rods may cause fretting wear. Present fuel designs are such that bowing to this extent is not experienced. Only a small reduction in channel size is seen, as compared to the channel closure necessary for mechanical degradation.

The effects of fuel rod bowing on DNBR are discussed in Section 3.5.3.2.b.8.

Starting with Unit 2 Cycle 19 and Unit 1 Cycle 21, the methodology described in Reference 35 was used to evaluate fuel rod bowing for the AREVA/ Framatome assemblies.

c. Shoulder Gap Closure

The fuel assembly shoulder gap is defined as the axial gap between the top of a fuel rod and the bottom surface of the upper end fitting. During irradiation, the gap becomes smaller due to differences in irradiation-induced growth and thermal expansion of fuel rods and guide tubes (fuel rod growth has an interactive component related to pellet-clad interaction). Complete closure of the gap would result in additional stresses on the fuel, enhancing rod bowing. Therefore, it is important to ensure that the BOL gap is large enough to preclude gap closure by the EOL of the fuel. The model for Zircaloy growth is presented in Reference 15. Reference 32 discusses the impact of ZIRLO clad. Shoulder gap is reviewed using SIGREEP (Reference 31).

AREVA/Framatome fresh fuel reloads use M5® clad fuel rods with Zircaloy-4 guide tubes. The growth of the fuel rods is assessed using M5® cladding growth correlations. The upper bound fuel rod growth is considered in conjunction with the lower bound assembly growth along with the

manufacturing tolerances that would result in the minimum fabricated clearance.

3.7.1.2 Fuel Thermal Design Evaluation

a. Introduction

The Combustion Engineering fuel rod thermal Analysis code, FATES (Reference 17), is used in the fuel evaluation model to predict fuel rod temperature distributions, fuel-clad gap conductance, rod internal pressures, and fuel rod stored energy. The effects of fuel densification and the subsequent formation of axial gaps are taken into account to calculate augmentation factors used to modify linear heat generation rate values. The densification process itself is modeled. Fission gas production is predicted by FATES and, using the internally-modeled temperatures, fission gas release is predicted as well.

Reference 17 compares FATES results with experimental data from in-reactor and out-of-reactor tests to show the conservatism in the model as well as to show the validity of the modeling techniques used.

Beginning with Unit 1 Cycle 6, an improved version of FATES, entitled FATES3 (Reference 27) was used for fuel thermal design evaluation. While a great number of the models remained unchanged, revisions included the models for 1) fission gas release, 2) fuel swelling, 3) closed gap conductance, 4) fuel relocation, 5) cladding axial growth [a calculation previously performed via Reference 15], and 6) plenum gas temperature. Additionally, the code was modified to include an annular fuel pellet geometry. This modeling modification required changes to the models for fuel pellet temperature distribution, fuel pellet thermal expansion, and rod internal void volume calculations.

Beginning with Unit 1 Cycle 9, an improved model, FATES3B (Reference 29), is used for fuel thermal design evaluation. FATES3B incorporates changes to the fission gas release model, specifically related to burnup dependence, kinetics of grain growth, and fission gas release calculation.

Reference 32 documents a modification to FATES3B for implementation of ZIRLO clad material.

Beginning with Unit 2 Cycle 19 and Unit 1 Cycle 21, the approved fuel rod thermal analysis code, RODEX2 (References 33 and 34), is used to evaluate AREVA/Framatome fuel. The RODEX2 code incorporates models to describe the gas generation and release, swelling, densification, and cracking in the pellet, gap conductance, radial thermal conduction, free volume, gas pressure internal to the fuel rod, fuel and cladding temperatures and deformations, and cladding corrosion. The calculations are performed on a time incremental basis with conditions being updated at each calculated increment.

b. Fuel Densification and Swelling

1. Fuel Densification

The FATES model includes correlations to account for burnup-dependent fuel densification. This phenomenon is different from fuel densification caused by high temperatures and thermal gradients experienced by the fuel (Reference 18). The rate and extent of burnup-dependent densification varies with original fuel density and microstructure. Original Calvert Cliffs fuel was of a relatively unstable, densifying type. Subsequent design changes have resulted in a more stable, non-densifying fuel.

The primary concerns regarding fuel densification were:

a) Decrease in pellet diameter (increased gap size) which lowers gap conductivity and increases fuel temperatures and stored energy.

b) Decrease in pellet length, which increases the Linear Heat Generation Rate along the fuel rod.

c) Decrease in pellet length coupled with pellet cocking, which leads to axial gaps in the fuel pellet stack. Augmentation factors for LHGR were based on the formation of these axial gaps.

Burnup-dependent densification is a factor only at BOL of fuel. The terminal density is predicted to be achieved at a burnup of 4000 MWD/MTU. The terminal density is determined in one of two ways, depending on the type of fuel (densifying/non-densifying) (Reference 17).

The effects of densification on the Safety Analyses are presented in Reference 19. As the fuel will begin to swell after 4,000 MWD/MTU, some of the effects of densification (axial and radial shrinkage) will be reversed by the swelling process.

The RODEX2 fuel rod analysis code contains both time and burnup dependent fuel densification correlations which are applied in the densification model for Uranium and Gadolinia fuel. The densification of the fuel is a phenomenon that is only observed at BOL, this is reflected in both the burnup and time dependent densification correlations. The densification model calculates the change in volume per unit volume or dilatation of the fuel material along with radial displacement, axial fuel stack length change, and change in the void fraction.

2. Fuel Swelling

Fuel swelling refers to the change in pellet volume which occurs as a result of the buildup of porosity and accumulation of fission products with increasing burnup. During the first 4,000 MWD/MTU of exposure, the densification mechanism prevails, but after the point where the fuel reaches its terminal density, the fuel begins to expand. Fuel swelling is said to be unrestrained until the time of pellet-clad contact, after which it is said to be restrained. The FATES model (Reference 17) contains a correlation for the rates of diametral and axial swelling while swelling is unrestrained. A new, restrained swelling rate is assumed after contact.

The FATES3 model (Reference 27), used beginning with Unit 1 Cycle 6, incorporated a lower swelling rate than that incorporated into the original FATES model. This new rate is based on results of recently published data and post-irradiation measurements made on Calvert Cliffs Unit 1 fuel.

The RODEX2 fuel rod analysis code has models that account for the phenomenological swelling processes (solid swelling and gaseous swelling). The swelling of the fuel material contributes to the radial deformations, axial fuel column length changes, filling of dish volumes, and is related to the fabricated porosity and available crack volume; the models incorporated into RODEX2 take into account such design variables. The swelling models in RODEX2 also take into account restraint of the fuel (due to pellet-to-clad contact) as well as an incubation period in which nondensified porosity is utilized by swelling.

3. Fuel Pellet Relocation

During irradiation, the fuel pellet cracks radially (and reheals in a distorted shape) and the pellet pieces approach the clad, decreasing gap size and enhancing gap conductivity. This improved heat transfer due to relocation reduces centerline temperature and stored energy.

The FATES3 model incorporates a modeling change with regard to fuel relocation after the pellet-clad gap has closed.

Additionally, the FATES3 model explicitly treats the pellet-clad interface, allowing for calculation of pellet-clad interfacial pressure and gap conductance after contact occurs. The previous FATES model used preassigned maximum values for these parameters after pellet-clad contact occurred.

Beginning with Unit 2 Cycle 19 and Unit 1 Cycle 21, the RODEX2 fuel rod analysis code is used for fuel thermal design evaluations. The RODEX2 code contains models that account for fuel relocation prior to and after contact between pellet and cladding. The radial displacements caused by pellet cracking are factored into calculations of the effective width of the open gap, which in turn is used to establish the gap conductance.

c. Linear Heat Generation Rate Augmentation Factor

Historical Perspective

One former concern regarding fuel densification was the decrease in pellet length. This allegedly decreases the overall pellet stack length, increasing the LHR. Presumably the pellets will tend to settle at the bottom of the rod, but interference from clad creepdown and pellet cocking and lockup may lead to the formation of axial gaps in the fuel column. It was assumed that these gaps could cause local power peaking in that axial region in surrounding rods, because the loss of neutron absorption in the gap outweighs the loss of fission. If the clad collapses completely into the gap (less likely in pre-pressurized fuel), local peaking is enhanced further due to the replacement of the gap void with moderator.

Present Analysis

The local power peaking is dependent on the number of gaps as well as the size of gaps, both of which are modeled in FATES. A peaking factor was determined, called the augmentation factor, which is defined as the ratio of peak augmented power to peak unaugmented power. The peak augmented power was determined statistically so that there is a 95% certainty that no more than one rod will be at a higher power.

Analysis of the phenomenon of interpellet gap formation in modern PWR fuel (Reference 28) demonstrates that the increased power peaking associated with the small interpellet gaps found in modern, i.e., pre-pressurized and non-densifying, fuel is insignificant compared to the uncertainties in the safety analyses and Technical Specifications. Consequently, augmentation factors used for interpellet gap formation were eliminated from the analysis beginning with Unit 1 Cycle 8 and Unit 2 Cycle 7.

The RODEX2 fuel rod analyses, performed for AREVA/Framatome fuel, use a conservative engineering heat flux augmentation factor to perform the fuel thermal design evaluations (Reference 35). The factor is based on a 95/95 statement including pellet and pellet lot variations in enrichment, as-sintered pellet density, and pellet diameter. The factor includes conservative allowances for in-reactor densification.

d. Fission Gas Release

1. Fission Gas Generation

Products that remain within the fuel matrix after fissioning of U-235 include primarily unstable isotopes with mass numbers ranging from 72 to 160. Each of these will experience an average of three stages of radioactive decay before being converted into a stable nucleus. This results in over 200 isotopes of 30 or more different elements present as fission products within the fuel pellets. Xenon and krypton, two of the stable gaseous elements liberated from the fuel matrix, are assumed to comprise the fission gas. FATES models the amount of fission gas generated in the fuel. The fuel rod is divided into axial nodes, and the gas generated in that node is calculated as a function of local burnup.

The RODEX2 fuel rod analysis code is used for fuel thermal design evaluations of AREVA/Framatome fuel. The RODEX2 code uses a bounding, power dependent fission gas generation rate per unit of energy produced that is applied to each axial region of the fuel column.

2. Fission Gas Release

While gas generation is strictly a function of burnup, the release of the fission gas from the fuel matrix is dependent on temperature and on temperature gradient. At low temperatures, recoil and knockout are the primary release mechanisms, as the relatively low energy of the gas precludes diffusion-type movement in the matrix. Recoil release is the direct release from the matrix to the free space directly as an energetic fission fragment, and knockout release is release resulting from the impact of another energetic fission fragment. At higher temperatures, the diffusion of gases within the grains is significant, and by diffusing to grain boundaries, gases can escape to cracks or to porosity already

present in the fuel matrix. At high temperatures, gas bubbles are driven along the thermal gradient and released to the free space.

Grain growth also plays an important part in fission gas release, and is itself strongly temperature dependent. At fairly high temperatures the pores initially present in the fuel begin migrating along the thermal gradient toward the center of the pellet. These pores leave a trail of small gas bubbles which form the boundary of a columnar grain extending radially from the pellet center. As the pores move inward they collect fission gas from the fuel matrix and grain boundaries, and eventually deposit it in the center of the pellet, forming, with other pores, the central void. Migration of these pores leave behind a crystal structure which is more dense than the original microstructure. The growth rate and extent of growth of columnar grains plays an important part in the fission gas release mechanism.

FATES modeled fission gas release in the following manner. The columnar grain growth boundary temperature T_g was determined by the equation:

$\int_{400°C}^{T_g} k_{95} dT$ = 42W / cm (Reference 17)

where: k_{95} is the thermal conductivity of 95% td UO_2

The FATES model combined the work of Notley and MacEwan with that of Lewis.

The original Lewis model is of the form:

$$\%Release = \frac{a\int_{T_s}^{1000} k_{dt} + b\int_{1000}^{1300} k_{dt} + c\int_{1300}^{1000} k_{dt} + d\int_{1000}^{T_c} k_{dt}}{\int_{T_s}^{T_c} k_{dt}}$$

where k is a function of temperature.

Notley and MacEwan showed the effect of columnar grain growth on release. The temperature bands in the Lewis model were retained in the FATES model, but the limits of the bands were changed to incorporate the temperature bands defined for the growth of columnar grains. A burnup-dependent correction factor was applied to the first three integrals of the FATES model to account for the gas diffusion mechanism which prevails in regions operating below the columnar grain growth boundary temperature.

The release function was calculated for each axial node. To obtain the accumulated fission gas release, the axial fractional releases were summed. No allowances were made in FATES for re-absorption of fission gas or any re-entry into the fuel matrix once the gas has been released.

A comparison of FATES predictions with experimental data is presented in Reference 17. Overall results are shown to be conservative.

Beginning with Unit 1 Cycle 6, the FATES 3 (Reference 27) model for fission gas release was used. The burnup and fuel microstructural (grain size) effects on fission gas release were more implicitly modeled in FATES 3. A restriction was placed on the effective grain size of the

fuel for FATES 3 analyses. This restriction was burnup-dependent, and had no effect on the model at low burnups. At higher burnups, the restriction acted by incorporating a smaller grain size into the gas release model yielding higher predicted releases, which was conservative.

Beginning with Unit 1 Cycle 9, the FATES3B (Reference 29) model for fission gas release is used. The imposed grain size restriction is removed based on recent high burnup, high temperature fission gas release data. The new model increases the burnup dependence of fission gas release, i.e., it predicts higher releases at high burnup while not significantly affecting lower burnup release predictions. The grain growth model is modified in FATES3B, as is the calculated gas release following grain growth.

The RODEX2 fuel rod analysis code, used for AREVA/Framatome fuel, contains a physically based fission gas release model. The model is based on several physical mechanisms, described in References 33 and 34, that are active in producing the release of the fission gas in the fuel. The importance of each mechanism is dependent upon the operational history of the fuel, the fuel design and the structure of the fuel material. The release model involves a two-stage release process of gas being released from the grains and accumulating in the grain boundary region and then this gas being released to the free volumes in the fuel rod as the gas concentration in the boundary increases. The phenomena incorporated into the gas release evaluation model are:

1. Release to the open porosity by a direct recoil mechanism
2. Release to the grain boundary by grain boundary sweeping due to grain growth
3. Release to the free volume due to columnar grain formation
4. Diffusion to the grain boundary controlled by a re-solution barrier
5. Release from the grain boundaries to the interconnected free gas volume when the boundary concentration barrier is exceeded

3.7.1.3 License Conditions with RODEX2 Methodology

Use of the RODEX2 methodology is restricted by the following NRC imposed license conditions from Reference 37. These license conditions are required to compensate for the RODEX2 methodology which does not explicitly model degraded fuel thermal conductivity nor adequately account for modeling uncertainties.

a) A reduction of the rod internal pressure limit is required to compensate for the RODEX2 methodology. Cycles which rely on the RODEX2 methodology must ensure that predicted maximum rod internal pressure in fuel remains below the steady-state system pressure.

b) A reduction of the LHGR fuel centerline melt safety limit is required to compensate for the RODEX2 methodology. The linear heat generation rate fuel centerline melting safety limit shall remain below 21.0 kW/ft.

3.7.2 DESIGN EVALUATION OF OTHER FUEL ASSEMBLY COMPONENTS

3.7.2.1 Burnable Poison Rod Design Evaluation

a. Introduction

Fixed BPRs (neutron absorbing) are included in selected fuel assemblies to reduce the BOL MTC. They replace fuel rods at selected locations. The poison rods are mechanically similar to fuel rods, but contain a column of burnable poison pellets instead of fuel pellets. The poison pellets consist of alumina with uniformly dispersed boron carbide particles.

b. BPR Hydriding and Bowing

At the end of Unit 1 Cycle 1, it was noticed that a BPR end cap had become detached from its rod in one assembly. A subsequent detailed inspection revealed extensive hydriding of several BPRs, with subsequent failure of some cladding. A significant amount of rod bowing/Zircaloy growth was also seen. Analysis of rods examined showed that they were acceptable for reinsertion for Cycle 2 use as scheduled.

1. Hydriding

Hydride-induced failure occurs primarily due to initial moisture in the pellets. At high temperatures, the water dissociates and hydrogen gas accumulates in the gap. This hydrogen interacts with the Zircaloy-clad, forming hydride blisters, embrittling the clad and allowing subsequent perforation of the clad walls. An analysis of the neutronic and thermal hydraulic effects of hydride blisters, perforation of the clad, and loss of some exposed poison material by erosion, as well as a discussion of the possibility of fuel rod fretting caused by material dispersed in the coolant, is given in Reference 3.

2. Bowing

Bowing in BPRs is largely a result of grid restraint, rod axial growth, and pellets becoming cocked and lodged against the clad wall resulting in localized stresses. The rod axial growth is, in part, the irradiation-induced growth of Zircaloy, but is enhanced by outward pressure on the clad inner surface by poison pellet swelling. Clad creepdown, caused by the inward pressure on the clad due to coolant pressure, limits pellet movement resulting in pellet cocking and lockup. These stresses, together with those resulting from spacer grid restraint, when coupled with axial elongation of the rod itself, result in rod bow.

c. Burnable Poison Rod Improvements

Improved designs were used in manufacturing BPRs subsequent to Unit 1 Cycle 1. Pellet moisture content was maintained at a lower level during manufacturing to prevent hydriding and pellet/clad design was modified (chamfered pellet, smaller pellet, thicker clad wall, larger gap) to decrease PCI which can induce bowing and rod elongation.

3.7.2.2 CEA Guide Tube Evaluation

The CEA guide tubes form part of the structural frame of the fuel assembly and provide channels which guide the CEAs over their entire length of travel. The center guide tube houses the incore instrumentation assemblies and irradiation samples/surveillance capsules in selected assemblies. One of the corner guide tubes housed the neutron source assemblies in each of two peripheral assemblies.

The neutron sources were removed beginning with Unit 1 Cycle 9 and Unit 2 Cycle 8. For Unit 1 Cycle 11 and Cycle 12, GTFSs were inserted into the guide tubes of selected peripheral assemblies.

The guide tubes are constructed of Zircaloy-4 and are integrated into the assembly as described in Section 3.3.2.3. The Zircaloy-4 is softer than the Inconel 625 cladding on the CEA, which can result in significant wear of the guide tube as a result of CEA vibration caused by turbulent coolant flow. As a result, SS sleeves have been installed in fuel assembly guide tubes that show wear or which house CEAs. In Unit 1 Cycle 8 and Unit 2 Cycle 7, a short-sleeve design was implemented which is considered the permanent fix to CEA guide tube wear (Reference 30). All new fuel assemblies will contain the short-sleeve.

The sleeves are constructed of Type 304 SS and extend 15.375" into the guide tubes. They are chrome-plated on the wear surface to provide resistance to wear without promoting wear on the CEA cladding (Reference 5). The sleeving program was initiated with Unit 1 Cycle 3, Unit 2 Cycle 2 and has been maintained since.

Several additional measures have been taken to mitigate guide tube wear. As described in Section 3.3.2.6, PLCEAs were replaced with CEA plugs which retain the dynamic operating characteristics of the region (flow rate, pressure drops), but prevent vibration wear. The fingers of the plugs extend only 5" into the top of the fuel assembly and are positioned by a leaf spring to prevent vibration. The CEA plugs were installed beginning in Unit 1 Cycle 3, Unit 2 Cycle 2 and removed at the end of Unit 1 Cycle 7, Unit 2 Cycle 6.

In Unit 2 Cycle 2, Unit 1 Cycle 4, and Unit 1 Cycle 5, some assemblies were fabricated with small flow hole guide tubes to reduce flow induced CEA vibration (Reference 6). This design has since been discontinued.

AREVA/Framatome fuel was added to the core starting in Unit 2 Cycle 19 and Unit 1 Cycle 21. The guide tubes are similar to the Westinghouse design described here. The guide tubes are constructed of Zircaloy-4 with 22” wear sleeves constructed of Type 304 stainless steel.

3.7.3 DEMONSTRATION PROGRAMS

3.7.3.1 Introduction

In an effort to provide data on fuel design and performance, several experimental programs have been established. These programs include the SCOUT and PROTOTYPE assemblies, a prototype CEA design, surveillance capsules, a joint CE/EPRI fuel performance evaluation program, a separate CE program involving the irradiation of test fuel rods, and the ANF demonstration assemblies.

3.7.3.2 CE/EPRI Fuel Performance Evaluation

Three Batch B fuel assemblies in the initial core of Unit 1 were modified to provide fuel performance data in a variety of areas. A major modification was the reconstitutability feature to facilitate pin removal for inspection.

One assembly was intended for one cycle of irradiation, while the other two were intended for two and three cycles of irradiation, respectively. Each assembly contained fueled and non-fueled test rods. The non-fueled rods were included to obtain information concerning Zircaloy-clad creep. Steel mandrels took the place of fuel pellets to act as support for the clad, prohibiting complete collapse. The fueled rods were of varying enrichment, pellet geometry, fill pressure, and pellet

microstructure. Pellet density was varied using different pore-formers to determine the effect of pellet microstructure on the densification characteristics of the fuel. Fill pressures were varied from 150 psig to 450 psig to learn the effects of fuel pressure on clad creepdown. Higher enriched fuel rods were included to gain information concerning clad creepdown at higher clad temperatures and the performance of fuel rods operating at higher LHR.

At the end of Unit 1 Cycle 1, all three assemblies were inspected and BT01 and BT02 were disassembled. Pins from each were examined for growth, visual appearances, etc. (Reference 20). BT01 was discharged as planned and BT02 was reassembled and reinserted along with BT03 for Cycle 2. At the EOC 2, BT02 and BT03 were inspected and disassembled and pins from each inspected (Reference 20). BT02 was discharged as planned and BT03 was reassembled and reinserted for Cycle 3. After Cycle 3, BT03 was inspected and disassembled and pins were removed for inspection (Reference 21). Six pins from BT03 were sent for examination in a hot cell and were replaced with six two-cycle rods from BT02. BT03 was then reinserted for Cycle 4. At the EOC 4, BT03 was inspected, disassembled and pins were removed for inspection (Reference 22). BT03 was not returned to the core for Cycle 5, but 13 pins (5 of which were 3-cycle rods and 8 were 4-cycle rods) along with one 2-cycle non-fueled rod from BT02 were inserted into a bundle from another test program (Section 3.7.3.3) for a fifth cycle. Results from analysis concerning densification and swelling, as well as fission gas release, performed on the pins sent to the hot cell, are documented (References 23, 24, and 25).

3.7.3.3 CE Irradiation of Test Fuel Rods

Three Unit 1 Batch D assemblies (D042, D047, D048) used initially in Unit 1 Cycle 2 contained graphite coated rods. Other than graphite coating on the cladding inner surface, there was no difference between the design of the test fuel and that of standard Batch D fuel. Fuel assembly D042 contained only graphite rods, while the other two assemblies each had one-fourth of their rods graphite coated. All three assemblies were irradiated for three cycles, and D047 was reinserted into Unit 1 Cycle 5 for a fourth cycle. It served as a carrier for the 14 test pins from BT03/BT02 (Section 3.7.3.2). D047 was removed at the EOC 5, and D042 was reinserted into Cycle 6 for its fourth cycle of irradiation. D042 was removed at the EOC 6 after its fourth cycle of irradiation.

3.7.3.4 SCOUT Program

One Unit 1 Batch F Assembly (F048) was designated as SCOUT. It was designed as a high burnup demonstration assembly. It contained 15 rods of various non-standard designs (Reference 8), and 5 well-characterized standard design rods for comparison. It was discharged at the EOC 8 after five cycles of irradiation.

3.7.3.5 PROTOTYPE Program

Four Unit 1 Batch G assemblies (G003, G004, G006, G008) were designated as PROTOTYPE assemblies and were initially inserted in Cycle 5. They were designed to obtain data concerning fuel performance on significant numbers of rods of standard and non-standard design in conjunction with the extended burnup program. There are several factors to consider in looking at the ability of fuel to withstand prolonged exposure, such as fission gas release and clad stresses. These factors were the bases of the experimental fuel designs used in PROTOTYPE (Reference 10) as well as in SCOUT. Before returning the PROTOTYPE assemblies to the core for their third cycle of irradiation in Cycle 7, two segmented test rods were removed from one of the assemblies and replaced with two SS rods.

The PROTOTYPE assemblies remained in the core for Cycle 9, their fifth cycle of irradiation. The PROTOTYPE assemblies were removed at the EOC 9.

3.7.3.6 Materials Surveillance Specimens

Three surveillance capsules were inserted in the Unit 1 Cycle 5 core in order to obtain data on the material properties of irradiated Inconel 625. These specimens resided in the center guide tubes of assemblies in high flux areas. One capsule was removed at the EOC 5, another at the EOC 6, and the last one at the EOC 7.

In the initial Unit 1 core, each of the three test assemblies (Section 3.7.3.2) contained a surveillance capsule in the center guide tube. These capsules contained Zircaloy and Zr-Mo-Si alloy specimens. One capsule was removed after one cycle, and another after two cycles. The third and final capsule was removed at the EOC 6.

3.7.3.7 Prototype CEA

A prototype CEA was installed in Unit 2 at the BOC 3. The changes from standard design included a change in cladding material (from Inconel to SS), reconstitutable fingers, and a change in material for the tips of the poison rods from Ag/In/Cd to B_4C. The size of the B_4C pellets used in the tips was decreased from the pellet size used for the remainder of the rod length. A metal liner was added to prevent any B_4C fragments from collecting in the high flux tip.

3.7.3.8 ANF Demonstration Assemblies

Four new demonstration assemblies, designated as Batch 1MX, were loaded into Unit 1 Cycle 10. These assemblies were manufactured by ANF and contain gadolinium as the burnable poison material. Each assembly consists of 164, 4.08 wt% U-235 enriched fuel pins and 12 fuel-bearing gadolinium poison pins. The poison pins contain natural uranium and 10 wt% Gd_2O_3. The mechanical configuration of the MX assemblies is essentially the same as the other Batch 1M assemblies. The purpose of installing the ANF assemblies in the Unit 1 core for Cycle 10 is to qualify an alternate source of supply for 24-month fuel assemblies. The ANF assemblies were reinserted into Unit 1 Cycle 11 for their second cycle of irradiation.

3.7.3.9 Erbium Demonstration Assemblies

For Unit 2 Cycle 9, four demonstration assemblies containing Erbium as a burnable absorber were introduced. Each assembly consists of 80 standard pins at 4.3 wt% U-235, 52 standard pins at 3.4 wt% U-235, and 44 Erbium bearing pins. The fuel stack in each erbium bearing fuel pin consists of a central 115.7" region containing 3.4 wt% of U-235, 0.9 wt% Er_2O_3, UO_2/Er_2O_3 pellets and two 10.5" cutback regions, one at each end of the stack containing standard 3.4 wt% U-235 pellets. The major incentives of erbium as a burnable absorber is an increase in core thermal margin and lower local peaking through the decrease in nonfuel bearing discrete burnable absorbers. The erbium assemblies were reinserted into Unit 2 Cycle 10 for their second cycle of irradiation.

3.7.3.10 Test Capsule Assemblies

The Test Capsule Assembly Program is being conducted to evaluate the effects of irradiation at reactor temperatures on materials being considered for advanced spacer grid spring designs.

In Unit 1 Cycle 12, three test capsules were placed in the outer guide tubes of three separate once-burned fuel assemblies.

Four test capsules were placed in the outer guide tubes of four separate fresh fuel assemblies in Unit 1 Cycle 13. Two of these capsules were from Unit 1 Cycle 12 and two are new capsules.

Two test capsules were placed in the outer guide tubes of two separate fuel assemblies in Unit 1 Cycle 14. Both of these capsules were from Unit 1 Cycle 13. Test capsules TCA-3 and TCA-5 were discharged at the end of Unit 1 Cycle 14.

3.7.3.11 Lead Fuel Assemblies for Unit 2 Cycle 11

Four Lead Fuel Assemblies were loaded in Unit 2 Cycle 11. The Lead Fuel Assemblies, designated Batch 2NT, have larger pellet diameter, larger pellet length, slightly reduced clad thickness, greater stack height density and shorter rod length. Zircaloy-2P is used for 216 fuel rods. The remaining rods are standard Zircaloy-4 clad. The Batch 2NT LFAs were re-inserted for a second cycle of operation in Unit 2 Cycle 12 and were discharged to the spent fuel pool after completion of that cycle.

3.7.3.12 Batch 1RT Lead Fuel Assemblies

Four Lead Fuel Assemblies (LFAs) designated as Batch 1RT were loaded into Unit 1 Cycle 13. These assemblies all have a larger pellet diameter, larger pellet length, slightly reduced clad thickness, greater stack height density and shorter rod length.

Five cladding variants were used in 176 rods in two of the Batch 1RT Lead Fuel Assemblies (12 rods of Zircaloy-2P, 20 rods of Zircaloy-4F, 60 rods of Zirconium Alloy E, 24 rods of Zirconium Alloy C, and 60 rods of Anikuloy™).

Two of the Batch 1RT LFAs utilize an advanced assembly design. From the bottom to the top of the assembly, the advanced assembly design contains the laser welded straight strip GUARDIAN™ grid, two laser welded straight strip intermediate spacer grids, four laser welded straight strip mixing grids, and a laser welded straight strip end grid. The advanced assembly design also contains an advanced spring design and a locking guide tube to upper flow plate design.

In Unit 1 Cycle 14, the Batch 1RT LFAs were carried over for their second cycle of irradiation. The LFA set was split up and asymmetrically loaded into the Unit 1 Cycle 14 core. The asymmetric loading (2 LFAs on the core periphery, and 2 LFAs in the core interior) was performed to gather data about Batch 1RT LFA performance on the core periphery.

In Unit 1 Cycle 15, Batch 1RT LFAs (1RT1 and 1RT3) were located on the core periphery for a second cycle in a row to gather data about Turbo test grids performance. Batch 1RT LFAs (1RT2 and 1RT4) were discharged to the spent fuel pool following Unit 1 Cycle 14.

In Unit 2 Cycle 14, the reconstituted LFA 1RT4 was located on the core periphery to gather data about Turbo test grids and advanced cladding material performance. The original LFA 1RT4 was reconstituted with fuel rods from LFA 1RT2, after Unit 1 Cycle 14. The original LFA 1RT4 assembly was reconstituted because the corrosion performance of Anikuloy, Zircaloy-2P, and Zirconium Alloy C claddings were not better than the standard OPTIN cladding. During the reconstitution, 1RT4 fuel rods with Anikuloy, Zircaloy-1P, and Zirconium Alloy C claddings were replaced with LFA 1RT2 fuel rods with OPTIN and Zirconium Alloy E claddings. The reconstituted LFA 1RT4 contains fuel rods with OPTIN, Zirconium Alloy E, and Zircaloy-4F claddings.

3.7.3.13 Framatome and Westinghouse Lead Fuel Assemblies for Unit 2 Cycle 15

Eight LFAs were loaded into Unit 2 Cycle 15. Four assemblies were manufactured by Westinghouse, and they were designated as 2TW, and four assemblies were manufactured by FANP, and they were designated as 2TF. The purpose of the LFAs is to test fuel cladding variants, and in the case of FANP, to evaluate an alternate fuel supplier.

In the Westinghouse LFAs, the standard ZIRLO cladding is present along with three test claddings. In the FANP LFAs, their standard M5® cladding is present. The test claddings (e.g., low tin ZIRLO and M5®) in the LFA do not meet the NRC definition of Zircaloy-4 or ZIRLO. An explicit submittal for each set of LFAs was made. The NRC reviewed each LFA submittal and approved the use of the LFAs for peak rod burnups up to 60,000 MWD/MTU. Neither LFAs contain any burnable absorbers.

The Westinghouse LFAs utilize the standard Turbo grid cage design, with one minor design change where the back-up arch on the perimeter Turbo grid strip is slightly longer. This change further improves the grid to rod fretting performance and does not impact the flow, structural, or mechanical characteristics of the grid.

The FANP LFAs for the Calvert Cliffs Unit 2 reactor will be the CE 14x14 design. The bundle uses nine Zircaloy-4 grid spacers of the high thermal performance design. The lower tie plate is the FUELGUARD™ design, and the upper tie plate is the standard, reconstitutable FANP design for CE 14x14 fuel. The high thermal performance spacer was generically reviewed and accepted by the NRC and has been used for reload designs for CE, Westinghouse, and Kraft-werke Union reactors since 1991. The FUELGUARD™ lower tie plate has also been used in reload designs for CE, Westinghouse, and boiling water reactor designs. The reconstitutable upper tie plate design has been in use for reloads for CE plants since the early 1980s. Except for the changes to the fuel rod described in the following paragraphs, the LFA fuel bundle design has been used in reloads for other CE 14x14 plants. An illustration of this design is shown in Figure 3.7-1.

Each fuel bundle contains four corner guide tubes, one center guide tube/instrument tube, and 176 fuel rods. The corner guide tubes in the LFAs have the same nominal inside diameter/outside diameter (ID/OD) and dashpot design as used for the standard CE 14x14 reload fuel supplied by FANP. The elevations of the features (e.g., weep holes, upper sleeve attachment, etc.), except for the total length, are the same as has been used on other CE 14x14 reload designs. Similarly, the center guide tube has the same nominal ID/OD as has been used on other CE 14x14 designs and as the co-resident fuel. The height and elevations are established to be compatible with the Calvert Cliffs core plate separation distance, the co-resident fuel and the FANP manufacturing processes.

The fuel rod design for Calvert Cliffs uses a 136.7 inch fuel column of uranium dioxide pellets. The rod consists of cladding, an upper end cap, a lower end cap,

fuel pellets, and a plenum spring. The differences between the Calvert Cliffs lead assemblies and the standard FANP reload design for CE designed 14x14 plants are changes to the fuel rod design.

Specifically, the rod changes are:

* the cladding material used for the fuel rod is M5® instead of Zircaloy-4;
* the cladding inner diameter is increased by 0.003 inches to 0.387 inches;
* the pellet diameter is increased by 0.0035 inches to 0.3805 inches;
* the pellet density is 96% TD instead of 95.35% TD;
* the initial rod internal pressure will be increased from 315 psig to 375 psig; and
* the cladding length is increased by about 0.2 inches.

The increased cladding length provides more plenum volume, but requires the plenum spring to be modified to accommodate the longer plenum. The cladding OD is unchanged and is the same as the standard CE 14x14 reload fuel supplied by FANP and the same as the co-resident fuel. The lengths of the end caps will be the same as used for the standard CE 14x14 reload design.

All eight LFAs resided in symmetric core locations for both Unit 2 Cycle 15 and Unit 2 Cycle 16. For Unit 2 Cycle 17, only two Westinghouse LFAs (2TW02 and 2TW03) were inserted along the core periphery to gather additional data on grid-to-rod fretting resistance. The remaining LFAs (four FANP and two Westinghouse were discharged to the spent fuel pool).

For Unit 1 Cycle 19, two Westinghouse LFAs and two FANP LFAs were loaded in symmetric locations to evaluate the cladding at high pin burnups (up to 70 GWD/MTU).

3.7.4 CHRONOLOGY OF FUEL EXPERIENCE

The following summaries provide a brief synopsis of major fuel performance-related changes and experiments associated with each cycle.

3.7.4.1 Unit 1

a. Cycle 1

Three assemblies of Batch B fuel designated as experimental assemblies were inserted for the purpose of providing fuel design and performance data, and were the only assemblies inserted in Cycle 1 which were designed to be reconstitutable. One was scheduled to be irradiated for one cycle (BT01), one for two cycles (BT02), and one for three cycles (BT03). Experimental designs for fuel pellets, BPRs, and plenum springs were incorporated, as well as test samples of zirconium alloys and non-fueled rods to test cladding design/materials. The test assemblies are described in Section 3.7.3.2; Reference 1 gives a detailed survey of the fabrication and characterization of the test assemblies.

b. Cycle 2

The design of Batch D fuel was modified from the original design used in Batches A, B, and C. Some design changes were made to allow for the reconstitution of all assemblies in order to permit replacement of failed rods

or to provide for removal of rods for post irradiation examination. Design changes were also made to improve fuel performance. These changes included:

1. Changes in pellet shape [chamfering and reduced length/diameter (L/D) ratio];
2. Increased pellet density;
3. Increased clad thickness;
4. Decrease in helium fill gas pressure; and,
5. Decrease in pellet-clad gap size.

The density was increased to increase the stability of the fuel to densification, thereby improving gap conductance. The gap conductance was also enhanced by the reduction in gap size. The increased clad thickness and changes in pellet shape were made in order to reduce the susceptibility of fuel to failure by PCI/Corrosion cracking. The fill pressure could be reduced due to improved collapse resistance caused by thicker clad and a more stable fuel pellet design. The design changes are listed in Tables 3.3-1 and 3.3-2. The fuel assembly modifications were made, as stated above, to allow reconstitution, as well as to accommodate flow forces. Changes made to permit reconstitution were to the upper-end-fitting-to-guide-tube joint, anti-rotation device, and fuel rod upper and lower end caps. In addition, an Inconel bottom spacer grid replaced the mechanical retention grid.

Three test assemblies of a new design were incorporated into Unit 1 Cycle 2. The design of these three Batch D assemblies (D042, D047, D048), as well as an analysis of their impact on operations under normal and transient conditions, is contained in Reference 2. In addition to these three test assemblies, the two-and three-cycle Batch B test assemblies remained in the core for Cycle 2.

A detailed inspection program was undertaken to determine the extent and effect of bowing and hydriding of BPRs, which were present in Batch B fuel and 28 Batch C assemblies. This inspection was the result of: 1) the finding of a BPR end cap which had become detached from its BPR, and 2) the finding of several BPRs whose cladding had failed due to hydriding (Reference 3).

c. Cycle 3

The design of Batch E fuel was identical to standard Batch D design used in Cycle 2 with the exception of a 40 psi fill gas pressure reduction, and a pellet dish depth reduction of .002", increasing stack density to 10.046 g/cc. The increased density served to enhance fuel stability. The reduction in fill gas pressure reduced fuel temperature by accelerating clad creepdown and improving heat transfer. The resulting reduced fuel internal gas pressures remained conservative relative to predicted time for clad collapse.

Only one assembly containing BPRs (Batch B test assembly) remained in the core for Cycle 3. All three Batch D test assemblies remained in the core for their second cycle of irradiation.

A problem with CEA guide tube wear was noted prior to Cycle 3. This wear was the product of CEA vibration in the guide tubes (Reference 4). For Cycle 3 it was determined that no assemblies which had been under a CEA in a previous cycle would be inserted in a CEA location for Cycle 3 with the

exception of BT03 in the core center location. In addition, all assemblies which were to be placed in CEA locations would have sleeved guide tubes (Reference 4). The core reload pattern was modified in order to ensure that CEAs were in previously unworn guide tubes. This resulted in eight Batch C assemblies being discharged and replaced with eight Batch A assemblies.

All part length control rods were replaced (for preservation of pressure drops, flow rates, etc.) with CEA plugs (Reference 5).

d. Cycle 4

There were no design changes to the fuel pellets used in Batch F fuel. Batch F fuel assemblies were modified from previous design in that the holddown plate in the upper end fitting was thickened slightly, and the cross bracing that connects the lower end fitting posts was thickened and raised slightly from the lowermost surface of the fuel assembly.

As part of the continuing effort to mitigate guide tube wear, all previously burned fuel assemblies scheduled to be placed in CEA locations were sleeved (Reference 4). The only exception to this was test bundle BT03, which was in the center of the core for Cycles 3 and 4. This location is typically a low-wear location, and the degree of wear found during inspection after Cycle 3 was acceptable for placement under the center CEA for Cycle 4. Of the 72 new Batch F assemblies, 24 were placed under CEAs and were sleeved. Of the 48 F assemblies not under CEAs, 16 assemblies (unsleeved) had modified guide tubes (Reference 7) and 32 assemblies (unsleeved) had standard guide tubes.

At the EOC 3, test bundle BT03 was discharged, disassembled, and inspected. Six pins were removed to go to hot cell for examination and pins from the BT02 two-cycle assembly were inserted in their place. BT03 was then placed back in the center of the core. The three D test assemblies were retained in the core for a third cycle.

In addition to these, a new test fuel assembly was introduced into the Cycle 4 core. The Batch F SCOUT bundle was designed as a high burnup demonstration to provide information for the extended cycle/high burnup program (Reference 8).

e. Cycle 5

Batch G assemblies introduced into the Unit 1 core were composed of higher enriched fuel (40 assemblies at 3.65 wt% and 52 assemblies at 3.03 wt%) for extended cycle length/extended burnup. The 52 assemblies of lower enriched fuel contained 8 BPRs per assembly. These poison rods were of an improved design to eliminate the hydriding induced failure found in the earlier design, as well as to mitigate poison rod growth and bowing. The BPR changes included reduced pellet moisture limit and improved manufacturing to lessen moisture ingress. To reduce the likelihood of PCI which leads to axial growth/rod wall perforation, several other BPR design modifications were made, including: 1) increased pellet/clad gap, 2) chamfered pellets, 3) increased rod pressurization, and 4) reduced plenum spring preload.

Besides the addition of BPRs and the higher enrichment, no design changes were initiated with standard Batch G fuel.

As in previous cycles, assemblies placed in CEA locations had modified guide tubes to mitigate wear (with the exception of test bundle D047 in the core center location). Thirty-two of those assemblies were of the modified design while the rest were sleeved. Sixteen of the modified assemblies were Batch F assemblies placed in single CEA locations. The remaining 16 were Batch G assemblies placed in dual CEA locations.

In an effort to expand the database on material properties of irradiated Inconel 625 CEA cladding, three empty CEA tubes were placed in the center guide tubes of assemblies placed in high flux areas (Reference 9). Test bundle D047, placed in the center of the core, was left in the core for its fourth cycle of irradiation. It served as a carrier for 14 test pins; 13 pins from test bundle BT03, of which 8 were 4-cycle rods and 5 were 3-cycle rods, and 1 2-cycle non-fueled rod taken from BT02.

The Batch F SCOUT assembly remained in the core for its second cycle of irradiation. Introduced into the core for the first time in Cycle 5 were four lead assemblies called PROTOTYPE. They contained rods similar in design to SCOUT but greater in number in order to provide a sound statistical database for proper evaluation of fuel performance (Reference 10).

f. Cycle 6

Batch H assemblies introduced into Unit 1 core were composed of higher enriched fuel (40 assemblies at 4.00 wt% and 32 assemblies at 3.55 wt%) for extended cycle length/extended burnup. The 32 low enriched Batch H assemblies contained 8 BPRs per assembly. These BPRs were of similar design to those utilized in the low enriched Unit 1 Batch G fuel.

An additional design change introduced with Batch H fuel was a decrease in the overall length of the fuel rods of .200". This decrease yields additional shoulder gap clearance allowing for increased rod growth expected as the fuel is taken to higher burnups.

As in previous cycles, assemblies placed in CEA locations had modified guide tubes or were sleeved to mitigate wear. Four assemblies in CEA locations for Cycle 6 had modified guide tubes, while the remainder were sleeved.

Test assembly 1D042, which had been irradiated in Cycles 2, 3, and 4, was returned to the core for a fourth and final cycle of irradiation in Cycle 6. The Batch F SCOUT assembly remained in the core for its third cycle of irradiation. The four Batch G PROTOTYPE assemblies remained in the core for their second cycle of irradiation.

g. Cycle 7

Sixty-four new Batch J fuel assemblies were introduced into the Unit 1 core for Cycle 7. Of those, 48 were high enriched (4.05 wt%) and 16 were low enriched (3.40 wt%). None of the Batch J fuel contained BPRs. The mechanical design of Unit 1 Batch J fuel was identical to that of the Batch H fuel introduced in Cycle 6.

The SCOUT assembly remained in the core for its fourth cycle of irradiation during Cycle 7. At the EOC 6, two fuel rods were removed and replaced with SS rods.

The four PROTOTYPE assemblies remained in the core for their third cycle of irradiation during Cycle 7. At the EOC 6, two fuel rods were removed from one PROTOTYPE assembly, and replaced with SS rods.

Several Batch 1G and 1F fuel assemblies (remaining in the core for a third cycle of irradiation) were modified to allow for fuel rod growth. The modification involved the installation of a spacer shim which effectively raised the flow plate by .285". Modified upper end fitting corner posts were then installed to ensure compatibility between the upper end fitting and guide tubes. This modification is required when spacer shims are added.

Three inconel test specimens were placed in the core for irradiation during Unit 1 Cycle 5. Two of these remained in the core during Cycle 6. One specimen was then removed, leaving one specimen in the core for a third and final cycle of irradiation during Cycle 7.

h. Cycle 8

Seventy-two new Batch K fuel assemblies were introduced into the Unit 1 core for Cycle 8. Of those, 48 were high enriched (4.05 wt%) and 24 were low enriched (3.40 wt%). None of the Batch K fuel contained BPRs.

The mechanical design of the Batch K reload fuel was identical to that of Batch J, with the exception of the design features noted below:

1. The height of the lower end fitting is shorter. This reduction is achieved by shortening the legs of the lower end fitting assembly.
2. The overall lengths of the guide tubes are increased to compensate for the shorter lower end fitting described in 1. This increase is achieved by increasing the length of the buffer region, i.e., tapered region. The combination of this shorter lower end fitting and the longer guide tubes maintains the same overall assembly length as that of the Batch J fuel.
3. The elevations of the Inconel grid and the uppermost Zircaloy grid are changed to maintain their same relative elevations with respect to fuel rods as those of the reference cycle fuel design.

The changes described above were analyzed and found to have no significant adverse effect on the performance of the Batch K fuel relative to that of the Batch J fuel. These changes will result in improved fuel performance by increasing the shoulder gap from 1.400" to 1.775".

The SCOUT demonstration assembly remained in the core for its fifth cycle of irradiation in Cycle 8. The four PROTOTYPE assemblies remained in the Unit 1 core for their fourth cycle of irradiation.

As described in Section 3.3.2.4, nine CEAs were replaced and the configuration of two CEA banks were changed for Cycle 8 to increase net available scram worth.

CEA plugs were removed for Cycle 8 to facilitate the installation of the Reactor Vessel Level Monitoring System and to expedite refueling operation.

The phenomena of interpellet gap formation and clad collapse in modern PWR fuel rods was reassessed. It was concluded that the minimum time to clad collapse is significantly greater than its expected life and the

augmentation factor associated with interpellet gaps is insignificant compared with the uncertainties in the safety analysis. Therefore, the cycle-specific clad collapse analysis is not necessary and the augmentation factor associated with interpellet gaps is removed from the Technical Specifications.

i. Cycle 9

Fifty-two new Batch L fuel assemblies were introduced into the Unit 1 Cycle 9 core. Of those, 40 were high enriched (4.05 wt%) and 12 were low enriched (3.40 wt%). None of the Batch L fuel contained BPRs. The mechanical design of Batch L fuel is identical to that of the Batch K fuel introduced in Cycle 8.

The four Batch G PROTOTYPE assemblies remained in the core for their fifth cycle of irradiation. One SS rod (inserted at EOC 6) was replaced with a test fuel rod from the SCOUT assembly (which was discharged at EOC 8).

One Batch H assembly was kept in the core for a fourth cycle of irradiation to obtain high burnup data. It resides in the center core location.

Six fuel rods (three failed, one damaged and two for future inspection) were replaced by SS rods prior to Cycle 9.

Sixty-eight CEAs (all CEAs not replaced at EOC 7) were replaced with new CEAs. These CEAs are similar in design to original CEAs with the following notable exceptions:

1. Ag-In-Cd slug in the tip of the center finger
2. Reconstitutable corner fingers.

j. Cycle 10

Ninety-six new Batch M assemblies were introduced into the Unit 1 core for Cycle 10, the first Unit 1 24-month fuel cycle. It is also the first Unit 1 cycle to use low-leakage fuel loading pattern. Ninety-two of the assemblies were supplied by CE with 4.08 wt% U-235 enrichment. Of these, 16 assemblies had no BPRs and 76 assemblies had 12 B_4C BPRs. The remaining four assemblies (Batch MX) are the ANF demonstration assemblies which have 3.85 wt% U-235 average assembly enrichment and contain 12 gadolinium, fuel bearing (natural uranium) BPRs.

The mechanical design of the CE supplied Batch M reload fuel is identical to that of the Batch L fuel except some Batch M assemblies contain BPRs. The design of these poison rods is the same as that of the poison rods in Batch 2K assemblies from Unit 2 Cycle 8. The only changes in BPR design concern the use of higher poison loadings and hollow spacers rather than solid spacers.

Four damaged fuel rods were replaced with SS dummy rods in three Batch L assemblies prior to Cycle 10.

To support 24-month cycle operation, the very weak center CEA (all Al_2O_3 fingers) installed as part of the CEA bank configuration prior to Cycle 8 were replaced with a weak CEA (center finger B_4C, other four Al_2O_3).

k. Cycle 11

Eighty-four new Batch N fuel assemblies were introduced into the Unit 1 Cycle 11 core. This includes 12 assemblies with no BPRs, 20 assemblies with 4 BPRs, and 52 assemblies with 8 BPRs. All Batch N assemblies were enriched with 4.20 wt% U-235. Guide Tube Flux Suppressors were placed in selected fuel assemblies near the periphery of the core to reduce the fluence at the critical vessel weld. The Batch N fuel employs the GUARDIAN™ debris-resistant fuel design. The GUARDIAN™ design includes a new grid and fuel pin design. The four Batch MX ANF fuel assemblies were returned to the Unit 1 Cycle 11 core for their second cycle of irradiation.

Changes incorporated by the GUARDIAN™ fuel design include the following: the length of the Zircaloy lower end cap was increased to provide a solid Zircaloy region in the area where debris is to be trapped. The overall length of the fuel and BPRs was increased, while the length of the plenum regions was reduced. This was done to compensate for the increase in the length of the lower end cap. The guide tube length was increased to maintain the same shoulder gap. The position of the active fuel region and burnable poison region was raised due to the increase in height of the lower end cap. The height of the lower end fitting was decreased to keep the overall length of the bundle unchanged. This was accomplished by decreasing the compression region for the hold-down spring without a change in dimension of the spring.

The Zircaloy spacer grids were redesigned by increasing the size of the outer pin cell through enlargement of the outside envelope of the spacer grid assembly. This allows fuel rods located along the periphery of the fuel bundle to receive more coolant flow when in contact with adjacent bundles.

Fourteen fuel rods were replaced with SS dummy rods during reconstitution, for a total of 16 SS rods reinserted into Unit 1 Cycle 11.

The weak center CEA (center finger B_4C, others Al_2O_3) was replaced with a similar CEA utilizing a SS slug in the bottom of each weak finger. This replaced the Zircaloy slug which was subject to hydriding.

l. Cycle 12

Eighty-eight new Batch P fuel assemblies with 4.3 wt% U-235 were introduced into the Unit 1 Cycle 12 core. This includes 16 assemblies with no burnable absorbers, 12 assemblies with 20 erbium pins, 8 assemblies with 44 erbium pins, and 52 assemblies with 60 erbium pins. Guide tube flux suppressors remained in select peripheral assemblies to reduce the fluence to the critical vessel weld. The four Batch MX ANF fuel assemblies were returned to the Unit 1 Cycle 12 core for their third cycle or irradiation.

The Batch 1P GUARDIAN™ fuel assembly employs a design change which involves the replacement of the top TIG-welded Zircaloy grid with a laser weld Zircaloy grid. This design change introduces a backup arch in each grid cell in addition to the existing design with backup arches placed only in peripheral cell locations.

Three test capsule assemblies were placed in the outer guide tubes of select once-burned assemblies for Cycle 12. The capsules contain test specimens of an advanced spacer grid spring design.

m. Cycle 13

There was a design change to the perimeter spring design in the GUARDIAN™ grid to reduce protrusion of the spring beyond the outer edge of the grid.

Four test capsule assemblies were placed in the outer guide tubes of four separate fresh fuel assemblies for Cycle 13. Two of the capsules are from Cycle 12, and two are new. The capsules contain test specimens of advanced spacer grid spring designs.

Batch 1R erbium rods have cutback regions of 10.5" at the top and 12.0" at the bottom.

n. Cycle 14

The Batch 1S erbium rods have cutback regions of 10.5" at the top and 12.0" at the bottom.

Two test capsules were placed in the outer guide tubes of two separate fuel assemblies in Unit 1 Cycle 14. Both of these capsules were from Unit 1 Cycle 13. The capsules contain test specimens of advanced spacer grid spring designs.

o. Cycle 15

The Batch 1T fresh fuel assemblies represent the first full batch implementation of the VAP fuel assembly design. The VAP feature has been tested at Calvert Cliffs in lead fuel assembly batches 1RT and 2NT. Value Added Pellets' diameter is 0.0045" larger than a standard pellet. The VAP clad wall thickness is 0.026" vs 0.028" for standard fuel. The Batch 1T erbium rods have cutback regions of 10.5" at the top of the fuel column and 14.0" at the bottom of the fuel column.

Unit 1 Cycle 15 is the first Calvert Cliffs reload designed with the ENDF/B-VI cross-section library in lieu of traditional ENDF/B-IV cross-sections.

Test capsules TCA-3 and TCA-5 were discharged to the spent fuel pool prior to the startup of Unit 1 Cycle 15.

Lead fuel assemblies 1RT1 and 1RT3 were returned to the core for a third cycle of irradiation. Lead fuel assemblies 1RT2 and 1RT4 were discharged to the spent fuel pool at the end of Unit 1 Cycle 14.

During the refueling outage, inspections were performed on the Batch 1R and 1RT fuel assemblies. Higher than expected grid-to-rod fretting was observed in certain fuel assemblies that had resided on the core periphery near the core shroud. Grid-to-rod fretting is an ongoing historical phenomena observed at Calvert Cliffs. To minimize grid to rod fretting during Unit 1 Cycle 15, several compensatory actions were implemented. First of all, the fuel management pattern was changed to rotate 1RT1 by 180° so that it would not have the same face against the core shroud for two consecutive cycles. Next, several fuel rods were rotated to present a fresh unworn surface to the rod support features. Finally, one heavily worn pin in 1R222 and two heavily worn pins in 1RT1 were replaced with stainless steel pins. These actions will minimize grid-to-rod fretting for Unit 1 Cycle 15. The grid-to-rod fretting wear that is expected to occur during Unit 1 Cycle 15 will

occur in low power peripheral fuel rods that will not contribute significant activity to the coolant if they were to fail. The number of grid-to-rod fretting failures likely to be experienced in Cycle 15 will not result in the RCS coolant activity approaching the Technical Specification limit. The impact of the population of fuel rods exhibiting significant wear such that integrity under transient and accident conditions could be challenged is small enough that the coolant activity impact is bounded by previously analyzed levels.

p. Cycle 16

Due to the merger of Westinghouse and CE, the CE fuel fabrication facility at Hermatite was permanently shut down. Before it was closed, all of the Batch 1V erbium rods were built at Hermatite. The remaining non-erbium rods were built at the Westinghouse Columbia manufacturing facility.

The integration of the basic CE fuel designs into the Columbia fabrication process necessitated numerous internal rod design changes including TIG welding of end caps, elimination of the lower alumina spacer, redesign of the plenum spring, etc.

The merger of Westinghouse and CE resulted in the Westinghouse standard cladding material (ZIRLO) becoming available to Calvert Cliffs. Since ZIRLO has better water side corrosion properties than the CE standard OPTIN cladding material, Calvert Cliffs elected to phase in ZIRLO cladding. ZIRLO was only available in time to support manufacturing of the non-erbium pins. The erbium pins for Unit 1 Cycle 16 still use the OPTIN cladding material.

Unit 1 Cycle 16 is the first full batch implementation of the advanced grid design known as Turbo. This grid design was tested in the Batch 1RT LFAs. The Turbo grid features include mixing vanes (at five of the eight spacer grid locations) and a new rod retention device known as I-springs (at all eight spacer grid locations).

Batch 1V will be the second full batch of VAP fuel assemblies for Unit 1.

Some of the Batch 1V fuel assemblies will use a 60 erbium pin lattice pattern. This is the first use of the 60-pin pattern with VAPs. The 60 pin pattern was previously used at Calvert Cliffs in Batch 1P with standard fuel pellets.

q. Cycle 17

Eighty-eight fresh assemblies were installed for Unit 1 Cycle 17 (batch designation 1W).

Batch 1W is the third batch of VAP for Unit 1. Erbia remains the burnable absorber, the Erbia fuel pins have cutback regions of 10.5 inches at the top of the rod and 12.0 inches at the bottom.

Batch 1W is the second batch of the Turbo fuel assembly design for Unit 1. All but four assemblies utilized the same design and the same grid cage design as the U2C15 Westinghouse LFAs, see Section 3.7.3.13. The four different assemblies do not have the increased backup-arch length and have been given a unique sub-batch identifier. All of the fuel was manufactured by Westinghouse at their Columbia, SC facility. The cladding material for all fresh fuel is ZIRLO™.

As Unit 1 contains approximately 85% of the Turbo fuel assembly design, transient analyses were updated to utilize the ABB-TV CHF Correlation. Since the Turbo fuel has a non-mixing vane lower axial section and an upper section with mixing grids, both the ABB-NV and the ABB-TV CHF correlations are applied in the safety analysis.

r. Cycle 18

Ninety-seven fresh assemblies were installed for Unit 1 Cycle 18 (batch designation 1X). This reload incorporated the “T” pattern and contains no fresh fuel on the core periphery.

Beginning with Cycle 18, ZrB_2 (IFBA) has replaced erbia as the burnable absorber. Batch 1X fuel assemblies, with the exception of single 1X7 assembly, also contain axial blankets, which consist of a lower-enrichment at the top and bottom 6” of the fuel. The axial blankets in the fuel rods that contain IFBA consist of annular pellets to provide extra plenum volume to accommodate increased helium gas production associated with the ZrB_2.

Also beginning with Cycle 18 is the addition of radial enrichment zoning. Batch 1X assemblies, with the exception of single 1X7 assembly, contain fuel rods of two different enrichments, with lower enriched rods placed on the assembly corners and next to guide tube locations.

Cycle 18 also contains a single assembly, sub-batch 1X7, which is a single-enrichment assembly at 2.0 wt% U-235 and does not contain either IFBA rods or axial blankets. The assembly has been placed in the center of the core in lieu of a twice burned assembly. This is the first reload in which a low-enriched fresh assembly is used in this location.

During the refueling outage prior to the startup of Cycle 18, inspections were performed on several reinsert Batch 1W assemblies due to indications of pin failures during their first duty cycle. In three assemblies, a total of four fuel pins were replaced with other fuel pins (from the parent assemblies) and a total of four stainless rods were inserted.

s. Cycle 19

Ninety-six fresh assemblies were loaded for Unit 1 Cycle 19 with a batch designation of 1Z. Cycle 19 included the “T” pattern and contains no fresh fuel on the core periphery.

Batch 1Z consists of sub-batches with two-enrichment and three-enrichment radial zoning. Batch 1Z retains the use of IFBA as a burnable

absorber and the use of axial blankets. Annular pellets are used in the blanket regions of rods that contain IFBA to provide extra plenum volume to accommodate increased helium gas production associated with the ZrB_2.

Two Westinghouse LFAs and two FANP LFAs were loaded in symmetric locations for a third cycle of irradiation of up to 70 GWD/MTU.

During the 2008 refueling outage prior to U1C19 startup, fuel inspections identified failed fuel pins in three once-burned (Batch 1X) assemblies slated for reinsertion into Cycle 19. Two of the failed assemblies were replaced with substitute assemblies and were not reinserted into the core. An inert stainless steel pin was inserted into the third failed assembly, allowing it to be used in Cycle 19.

t. Cycle 20

Ninety-two fresh assemblies were loaded for Unit 1 Cycle 20, eighty-eight with a batch designation of AA, and four with a batch designation of 2X7. Cycle 20 included the “T” pattern and contains no fresh fuel on the core periphery.

Batch AA consists of sub-batches with two-enrichment and three-enrichment radial zoning. Batch AA retains the use of IFBA as a burnable absorber and the use of axial blankets. Annular pellets are used in the blanket regions of rods and contain IFBA to provide extra plenum volume to accommodate increased helium gas production associated with the ZrB_2.

Batch 2X7 was originally purchased as spare fuel for Unit 2 Cycle 18. These assemblies were not used in U2C18 and are fresh for U1C20. Batch 2X7 consists of only one enrichment and does not contain any IFBA as a burnable absorber.

The rated thermal power was raised from 2700 MWt to 2737 MWt during this cycle and was based on flow measurement uncertainty capture.

u. Cycle 21

Ninety-six fresh AREVA Advanced CE HTP™ fuel assemblies were loaded for Unit 1 Cycle 21 with a batch designation of AB. The AREVA Advanced CE HTP™ fuel design employs the FUELGUARD™ lower tie plate, MONOBLOC™ guide tubes, and HTP™ spacer grids. Zr-4 was used for the guide tubes and spacer grids. M5® was used as the fuel cladding material. This is the first implementation of AREVA fuel in Calvert Cliffs Unit 1. Cycle 21 included the “T” pattern and contains no fresh fuel on the core periphery.

Batch AB consists of sub-batches with two-enrichment radial zoning. Batch AB uses Gd_2O_3 as a burnable absorber. Six inch low-enriched blankets are used on the top and bottom of non-gadolina-bearing fuel rods. Twelve inch low enriched axial blankets are used on the top and bottom of gadolina-bearing fuel rods.

Unit 1 Cycle 21 was designed using the AREVA physics code package (CASMO/PRISM).

v. Cycle 22

Ninety-six fresh AREVA Advanced CE HTP™ fuel assemblies were loaded for Unit 1 Cycle 22 with a batch designation of AC. The AREVA Advanced CE HTP™ fuel design employs the FUELGUARD™ lower tie plate, MONOBLOC™ guide tubes, and HTP™ spacer grids. Zr-4 was used for the guide tubes and spacer grids. M5® was used as the fuel cladding material. This is the second implementation of AREVA fuel in Calvert Cliffs Unit 1. Cycle 22 included the "T" pattern and contains no fresh fuel on the core periphery.

Batch AC consists of sub-batches with two-enrichment radial zoning. Batch AC uses Gd_2O_3 as a burnable absorber. Six inch low-enriched axial blankets are used on the top and bottom of non-gadolina-bearing fuel rods. Twelve inch low enriched axial blankets are used on the top and bottom of gadolina-bearing fuel rods.

Unit 1 Cycle 22 was designed using the AREVA physics code package (CASMO/PRISM). Unit 1 Cycle 22 is the second Calvert Cliffs reload to use the HTP critical heat flux correlation for AREVA fuel.

w. Cycle 23

Ninety-six fresh AREVA Advanced CE HTP™ fuel assemblies were loaded for Unit 1 Cycle 23 with a batch designation of AD. The AREVA Advanced CE HTP™ fuel design employs the FUELGUARD™ lower tie plate, MONOBLOC™ guide tubes, and HTP™ spacer grids. Zr-4 was used for the guide tubes and spacer grids. M5® was used as the fuel cladding material. This is the third implementation of AREVA fuel in Calvert Cliffs Unit 1. Cycle 23 included the "T" pattern and contains no fresh fuel on the core periphery.

Batch AD consists of sub-batches with two-enrichment radial zoning. Batch AD uses Gd_2O_3 as a burnable absorber. Six inch low-enriched axial blankets are used on the top and bottom of non-gadolina-bearing fuel rods. Twelve inch low enriched axial blankets are used on the top and bottom of gadolina-bearing fuel rods.

Unit 1 Cycle 23 was designed using the AREVA physics code package (CASMO/PRISM). Unit 1 Cycle 23 is the third Unit 1 reload to use the HTP critical heat flux correlation for AREVA fuel.

x. Cycle 24

Ninety-six fresh AREVA Advanced CE HTP™ fuel assemblies were loaded for Unit 1 Cycle 24 with a batch designation of AE. The AREVA Advanced CE HTP™ fuel design employs the FUELGUARD™ lower tie plate, MONOBLOC™ guide tubes, and HTP™ spacer grids. Zr-4 was used for the guide tubes and spacer grids. M5® was used as the fuel cladding material. This is the fourth implementation of AREVA/Framatome fuel in Calvert Cliffs Unit 1. Cycle 24 included the "T" pattern and contains no fresh fuel on the core periphery.

Batch AE consists of sub-batches with two-enrichment radial zoning. Batch AE uses Gd_2O_3 as a burnable absorber. Six inch, low-enriched, axial blankets are used on the top and bottom of non-gadolina-bearing fuel rods.

Twelve inch, low enriched, axial blankets are used on the top and bottom of gadolina-bearing fuel rods.

Unit 1 Cycle 24 was designed using the physics code package CASMO/PRISM. Unit 1 Cycle 24 is the fourth Unit 1 reload to use the HTP™ critical heat flux correlation.

3.7.4.2 Unit 2

a. Cycle 1

Except for differences noted earlier in this chapter, the design of Unit 2 Cycle 1 fuel was identical to that of Unit 1 Cycle 1 fuel. BPRs incorporated into Cycle 1 fuel were of the improved design.

b. Cycle 2

Batch D fuel was identical in design to Batch E fuel from Unit 1. Design differences from original core load fuel were:

1. A 40 psi reduction in fill gas pressure,
2. A reduction in pellet dish depth of .002", increasing stack density to 10.046 g/cc.

To mitigate guide tube wear, all assemblies to be placed under CEAs were modified. Sixteen Batch D low enrichment assemblies had modified guide tubes. Of the 16, 4 were put in non-CEA locations, 4 were placed under single CEAs and the remaining 8 were placed as 4 pairs under dual CEAs (Reference 4). The remainder of the assemblies to be placed under CEA locations were sleeved (Reference 4).

All PLCEAs were replaced with CEA plugs (Reference 11).

c. Cycle 3

The mechanical design of new Batch E reload fuel was identical to that of Batch D fuel for the Unit 1 Cycle 2 reload. All assemblies placed under CEAs were sleeved to mitigate guide tube wear and, in addition, all Batch E fuel assemblies were sleeved prior to insertion. None of the modified assemblies in Batch D were used in CEA locations for Cycle 3.

A prototype CEA (Reference 12) was introduced as part of CEA Group 5. The design of the prototype involved a change in cladding material from Inconel to SS, as well as a change to reconstitutable poison rods. The poison rods themselves were modified to replace the Ag/In/Cd tips with B_4C for economic as well as material availability reasons.

d. Cycle 4

The mechanical design of Batch F reload fuel was identical to that of Batch G fuel used in Unit 1 Cycle 5 reload. The enrichment was increased from the previous cycle to accommodate the extended cycle/extended burnup program. The lower enriched Batch F assemblies each contained eight BPRs of the improved design. All assemblies placed in CEA locations contained sleeves to mitigate guide tube wear.

e. Cycle 5

The mechanical design of Batch G reload fuel was identical to that of the Batch H fuel used in Unit 1 Cycle 6. The overall rod length was reduced by .200" from that of Unit 2 Batch F fuel. This decrease yields additional shoulder gap clearance allowing for increased rod growth expected as the fuel is taken to higher burnups. Fuel enrichments were increased over Unit 2 Batch F enrichments to accommodate higher burnup/extended cycles. Batch G was comprised of 48 high-enriched (4.0 wt% U-235) and 28 low-enriched (3.55 wt% U-235) assemblies. The lower enriched assemblies each contained eight BPRs. All assemblies placed in CEA locations contained sleeves to mitigate guide tube wear problems.

f. Cycle 6

Seventy-two new Batch H assemblies were introduced into the Unit 2 core for Cycle 6. Of those, 48 were high-enriched (4.05 wt%) and 24 were low-enriched (3.40 wt%). None of the Batch H fuel contained BPRs. The mechanical design of Unit 2 Batch H fuel was identical to that of the Batch J fuel introduced in Unit 1 Cycle 7 with the following exception. A 0.2" spacer shim was installed between the upper end of the guide tube and the upper end fitting to provide more space for rod growth. The upper end fitting design was then modified to make it compatible.

Several of the high-enriched Batch 2F assemblies (remaining in the core for a third cycle of irradiation) required field installation of .285" spacer shims to allow for rod growth during Cycle 6. Four failed fuel pins from Batch 2G fuel assemblies (once burned) were identified and replaced with SS dummy pins prior to Cycle 6.

The prototype CEA-X remained in the core center location for its fourth cycle of irradiation in Cycle 6.

g. Cycle 7

Sixty new Batch J assemblies were introduced into the Unit 2 core for Cycle 7. Of those, 40 were high-enriched (4.05 wt%) and 20 were low-enriched (3.40 wt%). None of the Batch J fuel contained BPRs.

The mechanical design of Batch J reload fuel was identical to that of Batch K fuel used in Unit 1 Cycle 8.

The reassessment of the phenomena of interpellet gap formation and clad collapse in modern PWR fuels led to the conclusion that the minimum time to clad collapse is significantly greater than its expected life, and the augmentation factor associated with interpellet gaps is insignificant. Therefore, the cycle-specific clad collapse analysis and the augmentation factor associated with interpellet gaps were eliminated.

As described in Section 3.3.2.4, the composition of eight CEAs and the configuration of two CEA banks were changed. The prototype CEA-X was moved to another core location as part of the CEA bank reconfiguration and remained in the core for its fifth cycle of irradiation.

The eight CEA plugs were removed to facilitate the installation of the Reactor Vessel Level Monitoring System and to expedite refueling operation.

h. Cycle 8

Eighty-eight new Batch K assemblies were introduced into the Unit 2 core for Cycle 8, the first 24-month cycle. It is also the first cycle to use low-leakage fuel loading pattern. All 88 were enriched to 4.08 wt%. Of these, 16 assemblies had no BPRs, 28 assemblies had 12 BPRs and 44 assemblies had 8 BPRs.

The mechanical design of Batch K reload fuel is identical to that of Batch J fuel except some Batch K fuel assemblies contain BPRs. The design of these poison rods is essentially the same as that of the poison rods in Batch 2G assemblies from Cycle 5. The only changes in BPR design concern the use of higher poison loadings and hollow spacers rather than solid spacers.

Nine fuel rods were replaced with SS dummy rods prior to Cycle 8.

The prototype CEA-X was discharged at the EOC 8 after its sixth cycle of irradiation.

To support 24-month cycle operation, the very weak center CEA (five Al_2O_3 fingers), installed as part of the CEA bank reconfiguration prior to Cycle 7, was replaced with a weak CEA (center finger B_4C, other Al_2O_3).

i. Cycle 9

Ninety-Two new Batch L assemblies were introduced into the Unit 2 Core for Cycle 9: 16 unshimmed Batch L assemblies, 20 4-shimmed (B_4C) Batch LX assemblies, 24 8-shimmed (B_4C) Batch L/assemblies, 28 12-shimmed (B_4C) Batch L* assemblies all at 4.30 wt% U-235 enrichment, and 4 Batch LE Erbium demonstration assemblies.

The Erbium demonstration assemblies are included in Cycle 9 in order to determine their incore characteristics during a 24-month cycle. These assemblies contain Erbium as the burnable poison material. Each assembly consists of 80 standard pins at 4.30 wt% U-235, 52 standard pins at 3.40 wt% U-235, and 44 Erbium bearing pins at 3.40 wt% U-235. This configuration results in an assembly average U-235 enrichment of 3.81 wt%.

The mechanical design for the Batch L reload fuel is essentially identical to that of the Batch K fuel except as noted below.

The lower end fitting of the Batch L fuel is essentially the same as that of the previous design except for the configuration of the flow holes. In the Batch L design, a 3x3 array of small flow holes has replaced each of the large flow holes. Also, wherever possible, additional small holes were added to the Batch L design to minimize the increase in the pressure drop of the small hole lower end fitting design, relative to the previous design. This design change was made to improve the debris resistance of the Batch L reload fuel.

The fuel rod plenum spring in the Batch L fuel has been redesigned to minimize the amount of rod internal void volume that it occupies.

The overall length of the Batch L poison rods was increased such that the poison rod length is now the same as the fuel rod length.

The size and quantity of the crimp holes in the upper end of the guide tubes were modified for the Batch L fuel. This change allows the upper end fitting posts to be re-used if an assembly must be reconstituted.

Seven fuel rods were replaced with SS dummy rods prior to Cycle 9.

The weak center CEA (center finger B_4C, other Al_2O_3), installed prior to Cycle 8, was replaced with a similar CEA utilizing a SS slug in the bottom of each weak finger. The slug was used instead of Zircaloy, which in this application was found to be subject to hydriding.

j. Cycle 10

Eighty-eight new Batch 2M fuel assemblies were introduced into the Unit 2 core for Cycle 10. One-hundred twenty-four Batch 2K and 2L assemblies were retained from Cycle 9. One reinserted Batch 2H* assembly which had been discharged from Unit 2 Cycle 7 and four reinserted Batch 2J* assemblies which had been discharged at the end of Unit 2 Cycle 8 make up the remainder of the core. Four erbium demonstration assemblies (2LE) are carried over from Unit 2 Cycle 9 from a second cycle of irradiation.

The Batch 2M fuel employs the debris resistant GUARDIAN™ design as described in Section 3.7.4.1.k.

Eight fuel rods were replaced by SS replacement rods in Batch 2K during the refueling outage prior to Cycle 10.

The Batch 2M burnable absorber pins consist of a 115.7" central region containing the burnable material B_4C with two 10.5" cutback regions containing Al_2O_3, one at each end of the stack. This change is being made to enhance thermal margin by lowering the axial peak at BOC.

k. Cycle 11

The following changes were made to the Unit 1 Batch P fuel bundle assembly design to create the Unit 2 Batch N standard fuel bundle assembly design:

The TIG welded wavy strip GUARDIAN™ Inconel bottom spacer grid assembly has been replaced by a laser welded straight strip GUARDIAN™ spacer grid assembly. In conjunction with this change, the fuel rod lower end cap was redesigned for compatibility with the new spacer grid and to facilitate manufacturing. The new lower end cap has one long taper, rather than a taper, a flat and then another taper at the bottom of the cap.

The TIG welded wavy strip intermediate Zircaloy spacer grid assemblies have been replaced by laser welded wavy strip intermediate Zircaloy spacer grid assemblies.

Batch 2N erbium rods have a 12” cutback in neutron absorbing material.

l. Cycle 12

The following changes were made to the Unit 1 Cycle 13 (Batch 1R) fuel assembly design to create the Unit 2 Cycle 12 (Batch 2P) standard fuel bundle assembly design.

The perimeter strips have small guide holes to match pins on the grid assembly weld fixture. This is to ensure more consistent alignment of the grid strips within the fixture during welding.

Batch 2P erbium rods have cutbacks in the neutron absorbing material of 14.0" at the bottom and 10.5" at the top.

m. Cycle 13

Ninety-two fresh Batch 2R fuel assemblies were introduced into the Unit 2 Cycle 13 core. The Batch 2R erbium rods have a symmetric cutback region of 12.0” at the top and bottom of the fuel column.

n. Cycle 14

Ninety-two fresh Batch 2S VAP fuel assemblies were introduced into the Unit 2 Cycle 14 core. The Batch 2S VAP fuel assemblies represent the first full batch of VAP assemblies in Unit 2. Value Added Pellets' diameter are 0.0045" larger than a standard pellet. The VAP clad wall thickness is 0.026" vs 0.028" for standard fuel. The Batch 2S erbium rods have a symmetric cutback region of 12.0" at the top and bottom of the fuel column.

Unit 2 Cycle 14 was designed with the ENDF/B-VI cross-section library in lieu of the traditional ENDF/B-IV cross-sections.

Reconstituted LFA 1RT4 was inserted into the Unit 2 Cycle 14 core. The original LFA 1RT4 was reconstituted with fuel rods from LFA 1RT2, after Unit 1 Cycle 14. The original LFA 1RT4 assembly was reconstituted because the corrosion performance of Anikuloy, Zircaloy-2P, and Zirconium Alloy C claddings were not better than the standard OPTIN cladding. During the reconstitution, 1RT4 fuel rods with Anikuloy, Zircaloy-2P, and Zirconium Alloy C Claddings were replaced with LFA 1RT2 fuel rods with OPTIN or Zirconium Alloy E claddings. The reconstituted LFA 1RT4 contains fuel rods with OPTIN, Zirconium Alloy E, and Zircaloy-4F claddings.

Unit 2 Cycle 14 is the first Calvert Cliffs reload designed with ABB-NV critical heat flux correlation in lieu of the traditional CE-1 correlation.

o. Cycle 15

Ninety-two fresh Batch 2T VAP fuel assemblies were introduced into the Unit 2 Cycle 15 core. The Batch 2T VAP fuel assemblies represent the second full batch of VAP for Unit 2. The Batch 2T erbium rods had an asymmetric cutback region of 10.5 inches at the top of the rod and 14.0 inches at the bottom. Included in the 92 fresh assemblies are 8 LFAs: 4 from Westinghouse and 4 from FANP. These LFAs are further described in Section 3.7.3.13.

Due to the merger of Westinghouse and CE, the CE fuel fabrication facility at Hermatite was permanently shut down. All of the Batch 2T rods were built at the Westinghouse Columbia manufacturing facility.

The integration of the basic CE fuel designs into the Columbia fabrication process necessitated numerous internal rod design changes, including TIG welding of end caps, elimination of the lower alumina spacer, redesign of the plenum spring, etc.

The merger of Westinghouse and CE resulted in the Westinghouse standard cladding material (ZIRLO) becoming available to Calvert Cliffs. Since ZIRLO has better water side corrosion properties than the CE standard OPTIN cladding material, Calvert Cliffs elected to utilize the ZIRLO cladding.

Unit 2 Cycle 15 is the second full batch implementation of the advanced grid design known as Turbo at Calvert Cliffs. The first full batch of Turbo was implemented on Unit 1 Cycle 16. This grid design was tested in the Batch 1RT LFAs. The Turbo grid features include mixing vanes (at five of the eight spacer grid locations) and a new rod retention device known as I-springs (at all eight spacer grid locations).

Batch 2T will be the second full batch of VAP fuel assemblies for Unit 2.

p. Cycle 16

Ninety-two fresh assemblies were installed for Unit 2 Cycle 16 (batch designation 2V). This reload incorporated the “T” pattern and contains no fresh fuel on the core periphery.

Beginning with Cycle 16, ZrB_2 (Integral Fuel Burnable Absorber or IFBA) has replaced erbia as the burnable absorber. Batch 2V fuel assemblies also contain axial blankets, which consist of a lower-enrichment at the top and bottom 6” of the fuel. The axial blankets in fuel rods that contain IFBA consist of annular pellets to provide extra plenum volume to accommodate increased helium gas production associated with the ZrB_2.

Also beginning with Cycle 16 is the addition of radial enrichment zoning. Batch 2V assemblies contain fuel rods of two different enrichments, with lower enriched rods placed on the assembly corners and next to guide tube locations.

Sixty-four CEAs were replaced for Cycle 16. All Unit 2 CEAs now have a 12” Ag-In-Cd slug to increase life expectancy.

q. Cycle 17

Ninety-six fresh assemblies were installed for Unit 2 Cycle 17 (batch designation 2W). This reload continues use of the “T” pattern and contains no fresh fuel on the core periphery.

As with Batch 2V, Batch 2W fuel assemblies also contain axial blankets, which consist of a lower-enrichment at the top and bottom 6” of the fuel. The axial blankets in the fuel rods that contain IFBA consist of annular pellets to provide extra plenum volume to accommodate increased helium gas production associated with the ZrB_2.

Some subbatches (W1 and W2) use, like Batch 2V, two radial enrichment zones. But, beginning with Cycle 17, other subbatches (W3 through W6) use three radial enrichment zones.

Two Westinghouse LFAs (2TW02 and 2TW03) were reinserted into Unit 2 Cycle 17 for a third cycle of irradiation. The other two Batch 2TW and four Batch 2TF LFAs were discharged to the spent fuel pool.

r. Cycle 18

Ninety-six fresh assemblies were loaded for Unit 2 Cycle 18 with a batch designation of 2X. Cycle 18 included the "T" pattern and contains no fresh fuel on the core periphery.

Batch 2X consists of sub-batches with two-enrichment and three-enrichment radial zoning. Batch 2X retains the use of IFBA as a burnable absorber and the use of axial blankets. Annular pellets are used in the blanket regions of rods that contain IFBA to provide extra plenum volume to accommodate increased helium gas production associated with the ZrB_2.

During the 2009 refueling outage prior to U2C18 startup, fuel inspections indicated failed fuel pins in assembly 2V109, which was replaced with 2V103. Additionally, assembly 2V011 was flagged as suspect (but later cleared) and was replaced with 2V101. Lastly, assembly 2W508 was found with an elevated CEA, and was replaced with 1X411 (a once-burned assembly from Unit 1).

s. Cycle 19

Ninety-six fresh AREVA Advanced CE HTP™ fuel assemblies were loaded for Unit 2 Cycle 19 with a batch designation of 2Z. The AREVA Advanced CE HTP™ fuel design employs the FUELGUARD™ lower tie plate, MONOBLOC™ guide tubes, and HTP™ spacer grids. Zr-4 was used for the guide tubes and spacer grids. M5® was used as the fuel cladding material. This is the first implementation of AREVA fuel in Calvert Cliffs Unit 2. Cycle 19 included the "T" pattern and contains no fresh fuel on the core periphery.

Batch 2Z consists of sub-batches with two-enrichment radial zoning. Batch 2Z uses Gd_2O_3 as a burnable absorber. Six inch low-enriched axial blankets are used on the top and bottom of non-gadolina-bearing fuel rods. Twelve inch low enriched axial blankets are used on the top and bottom of gadolina-bearing fuel rods.

Unit 2 Cycle 19 was designed using the AREVA physics code package (CASMO/PRISM). Unit 2 Cycle 19 is the first Calvert Cliffs reload to use the HTP critical heat flux correlation for AREVA fuel.

t. Cycle 20

One-hundred fresh AREVA Advanced CE HTP™ fuel assemblies were loaded for Unit 2 Cycle 20 with a batch designation of BA. Four assemblies from batch 2Z were discharged to the pool for contingency planning for failed fuel assemblies. The AREVA Advanced CE HTP™ fuel design employs the FUELGUARD™ lower tie plate, MONOBLOC™ guide tubes, and HTP™ spacer grids. Zr-4 was used for the guide tubes and spacer grids. M5® was used as the fuel cladding material. This is the second implementation of AREVA fuel in Calvert Cliffs Unit 2. Cycle 20 included the "T" pattern and contains no fresh fuel on the core periphery.

Batch BA consists of sub-batches with two-enrichment radial zoning. Batch BA uses Gd_2O_3 as a burnable absorber. Six inch low-enriched axial blankets are used on the top and bottom of non-gadolina-bearing fuel rods. Twelve inch low-enriched axial blankets are used on the top and bottom of gadolina-bearing fuel rods.

Unit 2 Cycle 20 was designed using the AREVA physics code package (CASMO/PRISM). Unit 2 Cycle 20 is the second Calvert Cliffs reload to use the HTP critical heat flux correlation for AREVA fuel.

u. Cycle 21

Ninety-six fresh AREVA Advanced CE HTP™ fuel assemblies were loaded for Unit 2 Cycle 21 with a batch designation of BB. The AREVA Advanced CE HTP™ fuel design employs the FUELGUARD™ lower tie plate, MONOBLOC™ guide tubes, and HTP™ spacer grids. Zr-4 was used for the guide tubes and spacer grids. M5® was used as the fuel cladding material. This is the third implementation of AREVA fuel in Calvert Cliffs Unit 2. Cycle 21 included the “T” pattern and contains no fresh fuel on the core periphery.

Batch BB consists of sub-batches with two-enrichment radial zoning. Batch BB uses Gd_2O_3 as a burnable absorber. Six inch low-enriched axial blankets are used on the top and bottom of non-gadolina-bearing fuel rods. Twelve inch low enriched axial blankets are used on the top and bottom of gadolina-bearing fuel rods.

Unit 2 Cycle 21 was designed using the AREVA physics code package (CASMO/PRISM). Unit 2 Cycle 21 is the third reload to use the HTP critical heat flux correlation for AREVA fuel.

w. Cycle 22

Ninety-six fresh AREVA Advanced CE HTP™ fuel assemblies were loaded for Unit 2 Cycle 22 with a batch designation of BC. The AREVA Advanced CE HTP™ fuel design employs the FUELGUARD™ lower tie plate, MONOBLOC™ guide tubes, and HTP™ spacer grids. Zr-4 was used for the guide tubes and spacer grids. M5® was used as the fuel cladding material. This is the fourth implementation of AREVA fuel in Calvert Cliffs Unit 2. Cycle 22 included the “T” pattern and contains no fresh fuel on the core periphery.

Batch BC consists of sub-batches with two-enrichment radial zoning. Batch BC uses Gd_2O_3 as a burnable absorber. Six inch low-enriched axial blankets are used on the top and bottom of non-gadolina-bearing fuel rods. Twelve inch, low enriched, axial blankets are used on the top and bottom of gadolina-bearing fuel rods.

Unit 2 Cycle 22 was designed using the AREVA physics code package (CASMO/PRISM). Unit 2 Cycle 22 is the fourth Unit 2 reload to use the HTP critical heat flux correlation for AREVA fuel.

x. Cycle 23

Ninety-seven fresh Framatome Advanced CE HTP fuel assemblies were loaded for Unit 2 Cycle 23 with a batch designation of BD. The Framatome Advanced CE HTP fuel design employs the FUELGUARD lower tie plate,

MONOBLOC guide tubes, and HTP spacer grids. Zr-4 was used for the guide tubes and spacer grids. M5 was used as the fuel cladding material. This is the fifth implementation of Framatome fuel in Calvert Cntfs Unit 2. Cycle 23 included the "T" pattern and contains no fresh fuel on the core periphery.

Batch BD consists of sub-batches with two-enrichment radial zoning. Batch BD uses Gd203 as a burnable absorber. Six inch, low-enriched, axial blankets are used on the top and bottom of non- gadolinia-bearing fuel rods. Twelve inch, low enriched, axial blankets are used on the top and bottom of gadolinia-bearing fuel rods.

Unit 2 Cycle 23 was designed using the Framatome physics code package (CASMO/PRISM). Unit 2 Cycle 23 is the fifth Unit 2 reload to use the HTP critical heat flux correlation for Framatome fuel.

3.7.5 REFERENCES

1. CENPD-232-P, "Fabrication and Characterization of BG&E-1 Test Fuel Assemblies," July 1976
2. CEN-36(B)-P, "Irradiation of Test Fuel Rods in Calvert Cliffs-1"
3. CEN-48(B)-P, "Calvert Cliffs Unit 1 Fuel Inspection Report," February 1977
4. CEN-83(B)-P and Amendment 1 to same, "Calvert Cliffs Unit 1 Reactor Operation with Modified CEA Guide Tubes," February 1978
5. A.E. Lundvall, Jr. to E.G. Case, letter, "Supplement to Cycle 3 Reload Application," March 17, 1978
6. CEN-101(B)-P, "Calvert Cliffs Unit 2 Cycle 2 Reload Submittal Amendment," August 28, 1978
7. CEN-107(B)-P, "Response to NRC Questions on the Calvert Cliffs Unit 1 Cycle 4 Reload Submittal Appendix," April 25, 1979
8. CE-NPSD-169-P, "A Summary of the Design, Fabrication and Characterization of the SCOUT High Burnup Demonstration Assembly," February 1982
9. Letter from A.E. Lundvall, Jr. to R.A. Clark, "Amendment to Operating License DPR-53, Fifth Cycle License Application," September 22, 1980
10. Letter from A.E. Lundvall, Jr. to R.A. Clark, "Responses to NRC Staff Questions," November 20, 1980
11. Letter from A.E. Lundvall, Jr. to R.W. Reid, "Application for Cycle 2 Reload for CCNPP-2," July 26, 1978
12. Letter from A.E. Lundvall, Jr. to R.W. Reid, "Supplement to Application for Cycle 4 Reload - B_4C Type CEA Design," March 5, 1979
13. CENPD-187-P-A, "Method of Analyzing Creep Collapse of Oval Cladding, CEPAN," March 1976
14. CENPD-225-P-A, "Fuel and Poison Rod Bowing," June 1983
15. CENPD-198-P, "Zircaloy Growth - In Reactor Dimensional Changes in Zircaloy-4 Fuel Assemblies," December 1975
16. Deleted
17. CENPD-139-P-A, "Fuel Evaluation Model, FATES," July 1974

18. Technical Report on Densification of Light Water Reactor Fuels, Regulatory Staff, U. S. Atomic Energy Commission, November 1972

19. CENPD-106, "Effect of Fuel Densification on the Calvert Cliffs Safety Analysis," September 1973

20. CE-NPSD-72, "Examination of Calvert Cliffs 1 Test Fuel Assemblies at EOCs 1 and 2," September 1978

21. CE-NPSD-87, "Examination of Calvert Cliffs 1 Test Fuel Assembly After Cycle 3," September 1979

22. CE-NPSD-146, "Examination of Calvert Cliffs 1 Test Fuel Assembly After Cycle 4," October 1981

23. CE-NPSD-75, "Gas Release and Microstructural Evaluation of One and Two Cycle Fuel Rods from Calvert Cliffs 1," March 1979

24. CE-NPSD-119, "Gas Release and Microstructural Evaluation of Three-Cycle Fuel Rods from Calvert Cliffs-1," December 1980

25. "Densification, Swelling and Microstructures of LWR Fuels Through Extended Burnup," ANS Topical Meeting on LWR Extended Burnup - Fuel Performance and Utilization, Vol. 1, pgs. 4-39, April 4-8, 1982

26. CEN-182(B), "Statistical Approach to Analyzing Creep Collapse of Oval Fuel Rod Cladding Using CEPAN," September 1981

27. CEN-161(B)-P, "Improvements to Fuel Evaluation Model (FATES3)," July 1981

28. Letter from A.E. Lundvall, Jr. (BGE) to J.R. Miller (NRC), Docket Nos. 50-317 & 50-318, "Request for Amendment (Clad/Collapse Augmentation Factors)," December 31, 1984

29. CEN-161(B)-P, Supplement 1-P, "Improvements to Fuel Evaluation Model," (FATES3B), April 1986

30. Letter from A.E. Scherer (C-E) to C.O. Thomas (NRC), "CEA Guide Tube Wear Sleeve Modification," LD-84-043, August 3, 1984

31. CENPD-269-P, Revision 1-P, "Extended Burnup Operation of Combustion Engineering PWR Fuel," July 1984

32. CENPD-404-P-A, Revision 0, “Implementation of ZIRLO‘ Cladding Material in CE Nuclear Power Fuel Assembly Designs,” November 2001

33. ANF-81-58(P)(A), Revision 2 and Supplements 3 and 4, “RODEX 2 Fuel Rod Thermal Mechanical Response Evaluation Model,” April 1990

34. XF-NF-81-58(P)(A), Revision 2 and Supplements 1 and 2, “RODEX 2 Fuel Rod Thermal-Mechanical Response Evaluation Model,” March 1984

35. XN-75-32(P)(A), Supplements 1, 2, 3, and 4, “Computational Procedure for Evaluating Fuel Rod Bowing,” Exxon Nuclear Company Inc., October 1983

36. BAW-10240(P)-A, Revision 0, “Incorporation of M5 Properties in Framatome ANP Approved Methods,” May 2004

37. Letter from Mr. D. V. Pickett (NRC) to Mr. G. H. Gellrich (CCNPP), dated February 18, 2011, Calvert Cliffs Nuclear Power Plant, Unit Nos. 1 and 2 - Amendment Re: Transition from Westinghouse Nuclear Fuel to AREVA Nuclear Fuel (TAC Nos. ME2831 and ME2832)

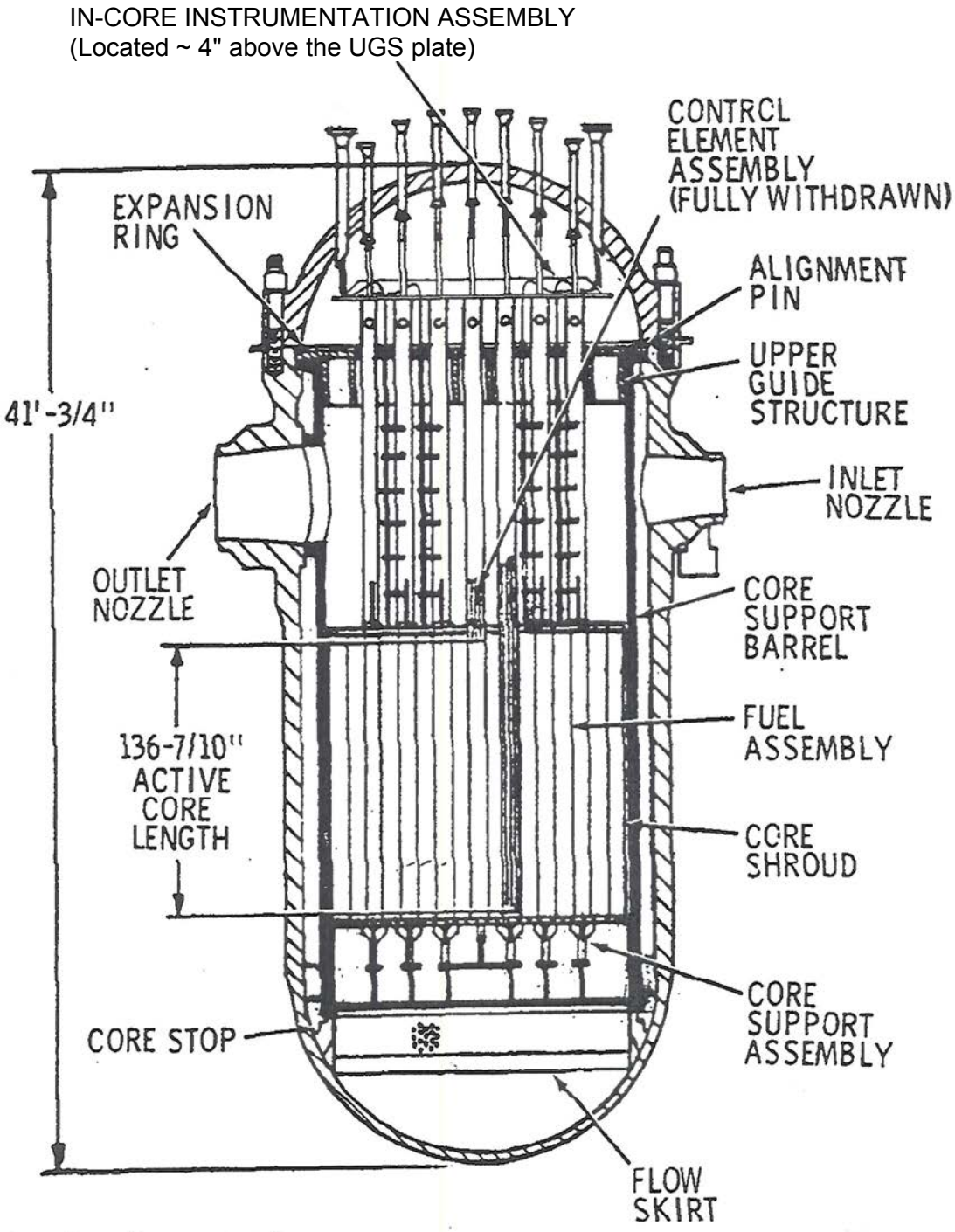

Calvert Cliffs Nuclear Power Plant	REACTOR VERTICAL ARRANGEMENT	Figure 3.1-1 Revision 39

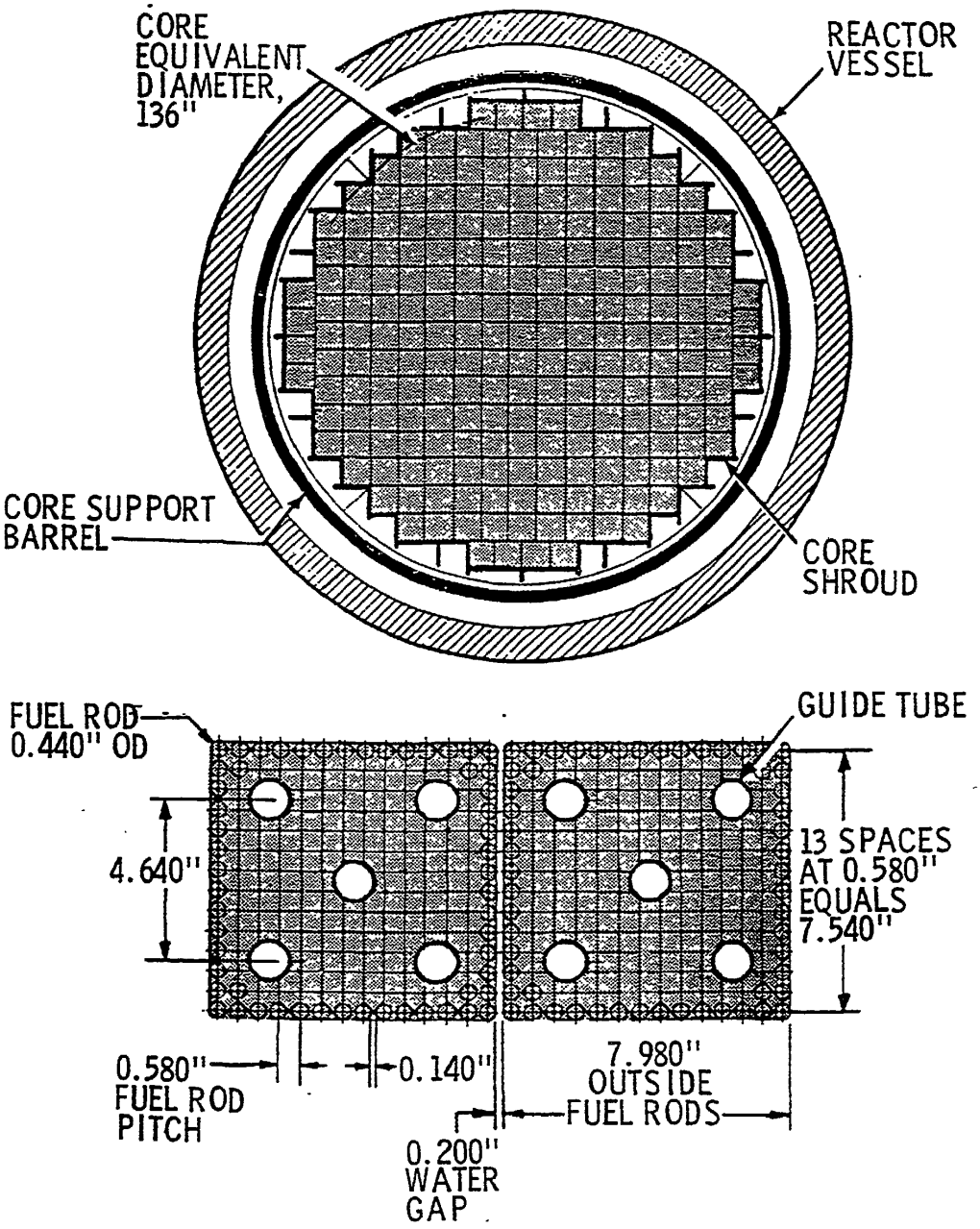

BALTIMORE GAS & ELECTRIC CO. Calvert Cliffs Nuclear Power Plant	Reactor Core Cross-Section	Figure 3.3-1

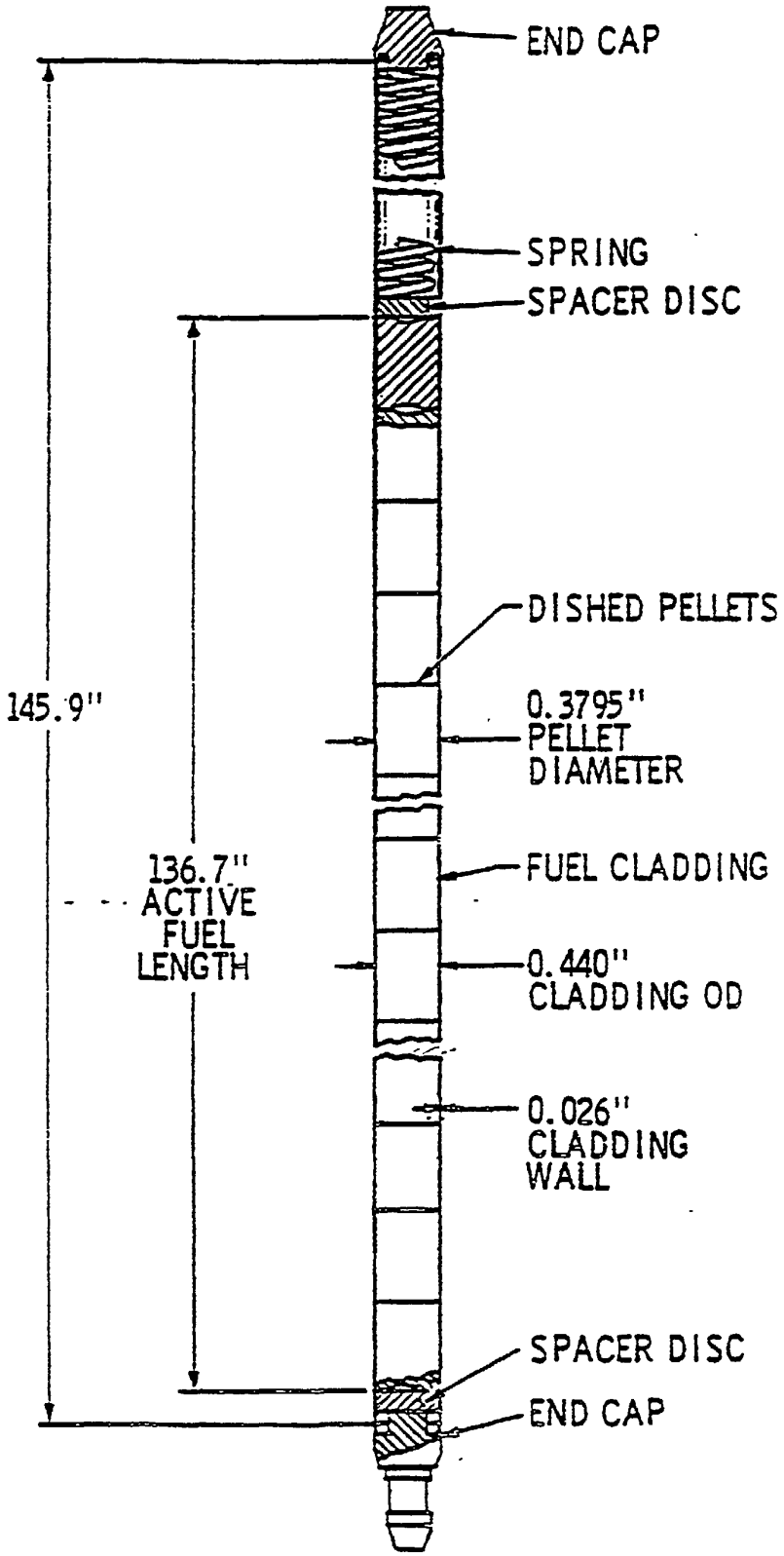

BALTIMORE GAS & ELECTRIC CO. Calvert Cliffs Nuclear Power Plant	FIRST CYCLE FUEL ROD	Figure 3.3-2

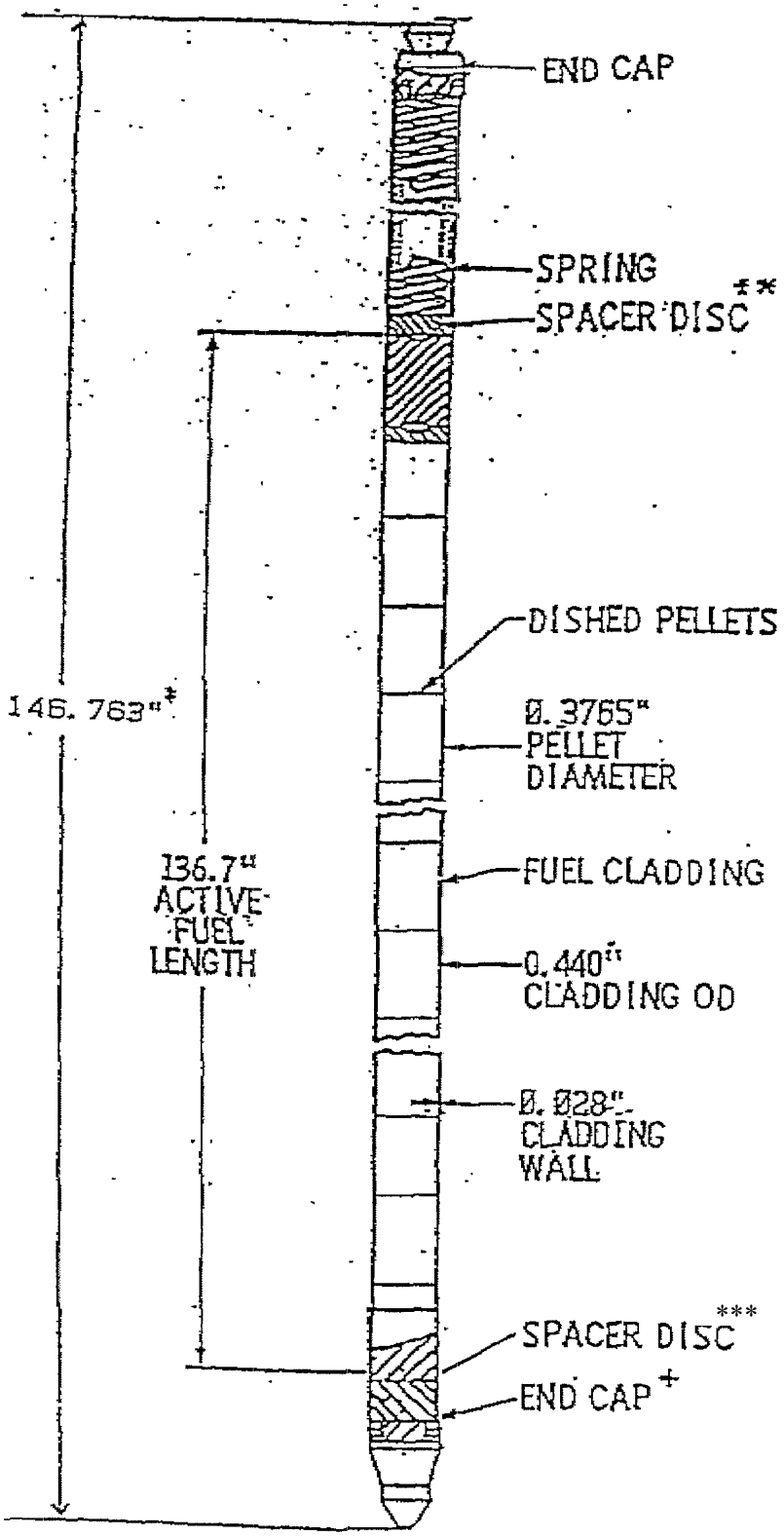

The HTP fuel assemblies use a 0.0265" cladding wall, a 0.3805" pellet diameter, and a rod length on 146.67"

Value Added Pellet fuel assemblies use a 0.026” cladding wall, a 0.3810” pellet diameter, and a rod length of 146.903” (Hematite) and 146.955” (Columbia)

Beginning with Unit 2 Cycle 11 and Unit 1 Cycle 13, the lower end cap was redesigned to one taper, rather than the taper – flat – taper design as shown.

* The GUARDIAN™ fuel design has a total length of 147.229"

** Upper spacer disc removed beginning with Unit 1 Cycle 12 and Unit 2 Cycle 11.

*** Lower spacer disc removed for rods manufactured at Columbia.

Calvert Cliffs Nuclear Power Plant	FUEL ROD	Figure 3.3-3 Revision 51

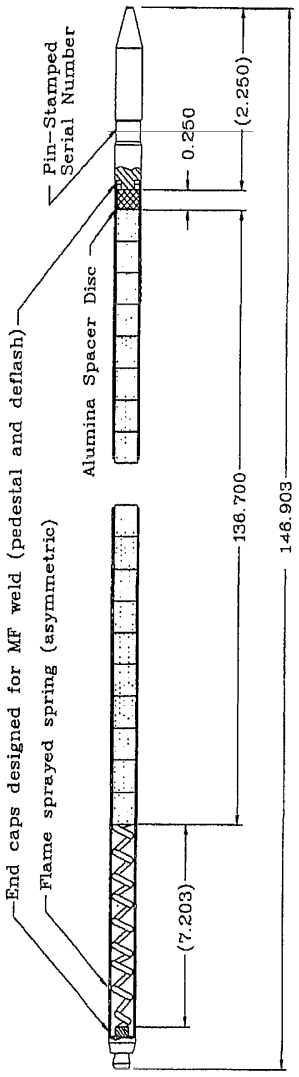

Typical Rod from Hematite(1)

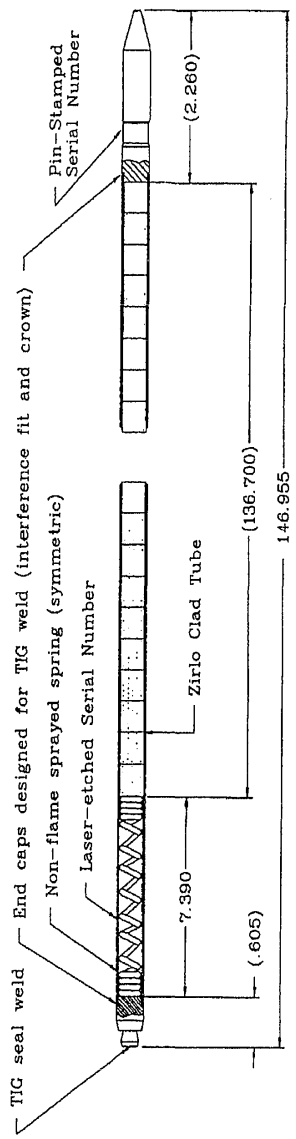

Typical Rod from Columbia(1)

(1) Rod dimensions are nominal values. Batch specific values may vary slightly due to manufacturing practices and tolerances. Significant details for lead fuel assemblies may vary and are described in Section 3.7.

Calvert Cliffs Nuclear Power Plant	FUEL ROD ASSEMBLY (Westinghouse)	Figure 3.3-3A Revision 43

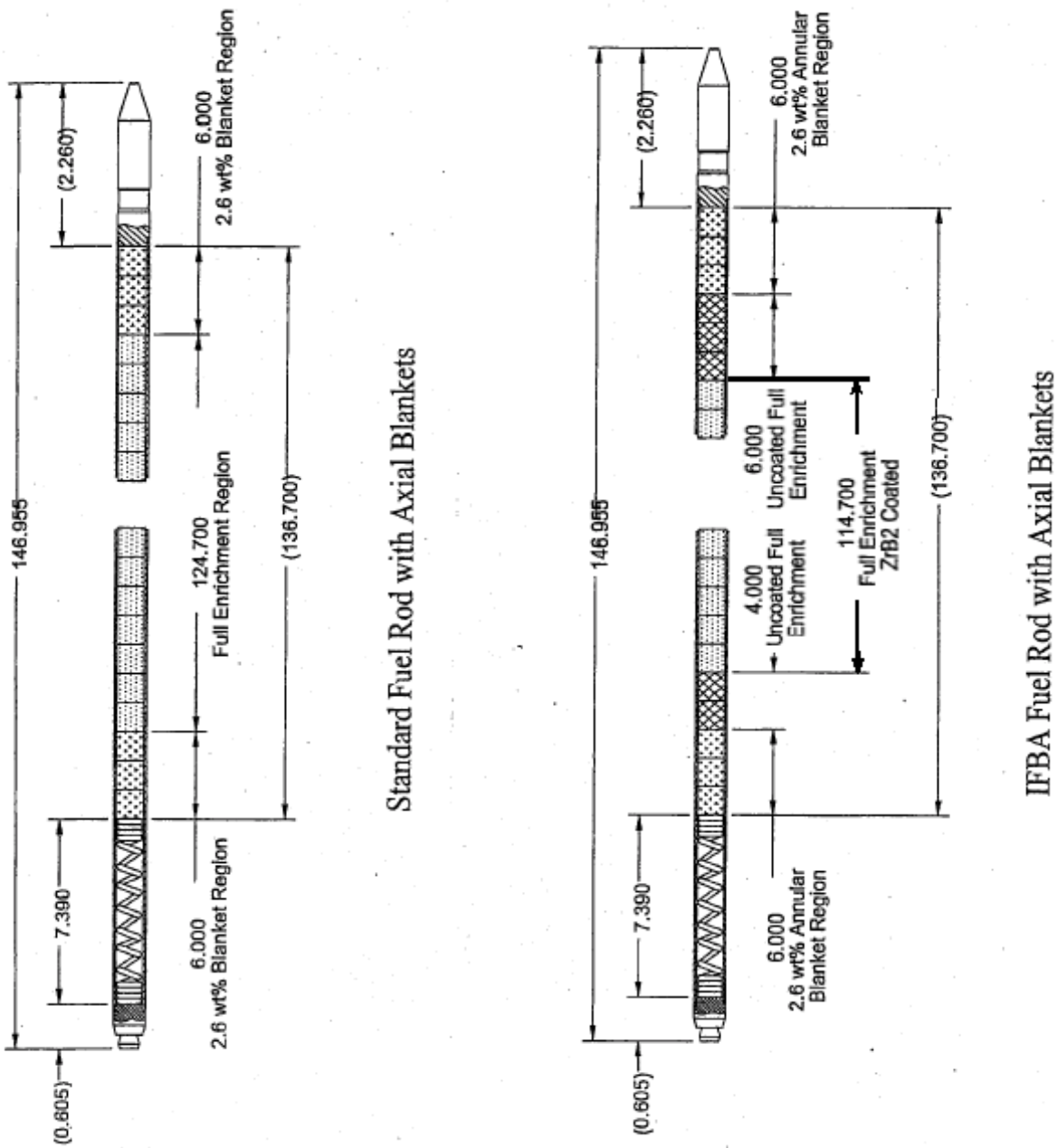

All dimensions are in inches.

Calvert Cliffs Nuclear Power Plant	FUEL ROD DESIGN (UNIT 2 CYCLE 16)	Figure 3.3-3B Revision 40

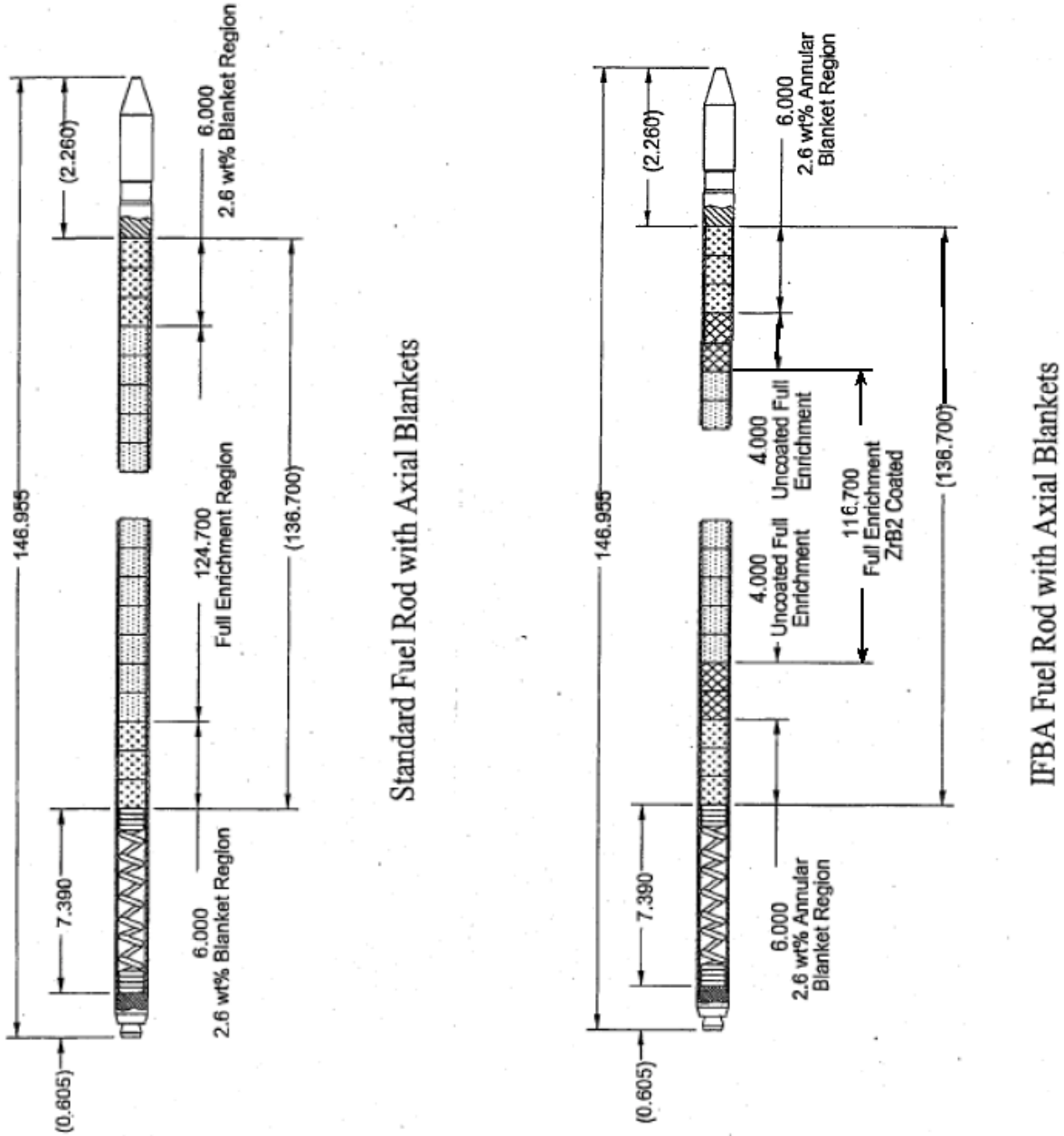

All dimensions are in inches.

Calvert Cliffs Nuclear Power Plant	FUEL ROD DESIGN (UNIT 1 CYCLES 18, 19, & 20 AND UNIT 2 CYCLES 17 & 18)	Figure 3.3-3C Revision 42

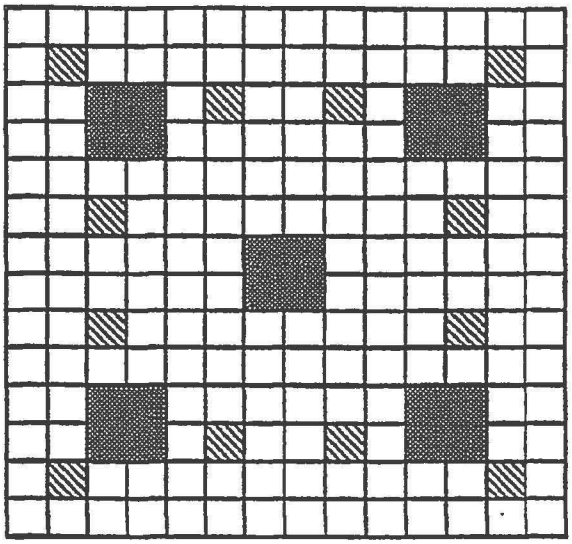

12 POISON ROD ASSEMBLY

BUNDLES	
2K*	1M*
2L*	1MX
2F*	
2M3	

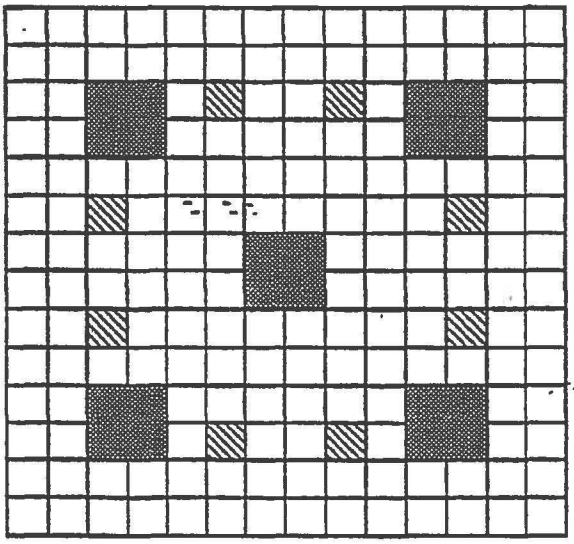

8 POISON ROD ASSEMBLY

BUNDLES
1G/
2F/

Fuel Rod Location

Poison Rod Location

Guide Tube Location

BALTIMORE GAS & ELECTRIC CO. Calvert Cliffs Nuclear Power Plant	BURNABLE POISON ROD LOCATION	Figure 3.3-4 Sheet 1 Rev. 15

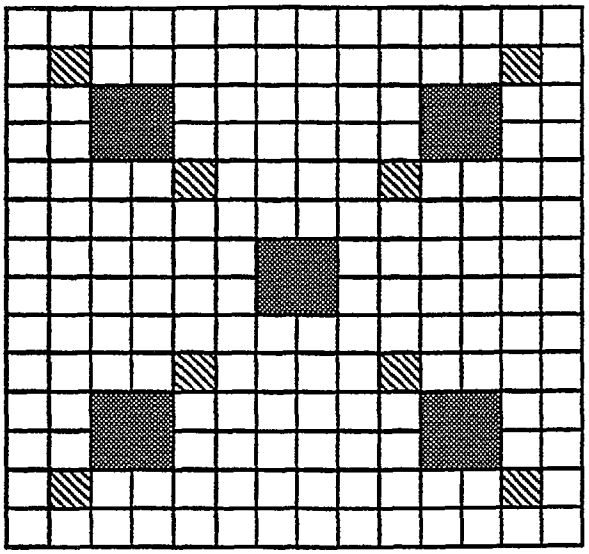

8 POISON ROD ASSEMBLY

BUNDLES	
1H/	2M2
2G/	
2K/	
2L/	
1N/	

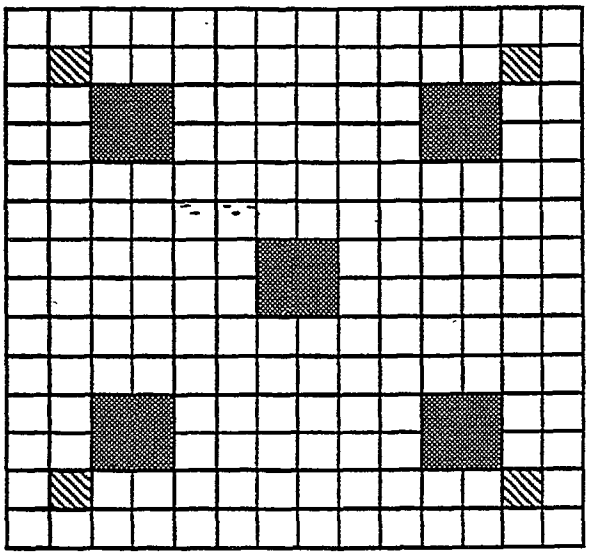

4 POISON ROD ASSEMBLY

BUNDLES
2LX
1NX
2M1

Fuel Rod Location

Poison Rod Location

Guide Tube Location

BALTIMORE GAS & ELECTRIC CO. Calvert Cliffs Nuclear Power Plant	BURNABLE POISON ROD LOCATION	Figure 3.3-4 Sheet 2 Rev. 15

ERBIUM DEMONSTRATION ASSEMBLY

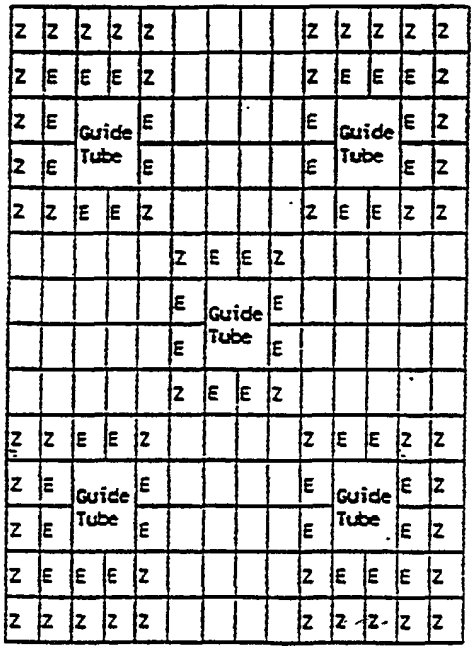

Z 3.40 w/o U235 fuel rod
E 3.40 w/o U235 w/ 0.90 w/o Er_2O_3 fuel rod

BALTIMORE GAS & ELECTRIC CO. Calvert Cliffs Nuclear Power Plant	BURNABLE POISON ROD LOCATION	Figure 3.3-4 Sheet 3 Rev. 18

20 Pin Erbium Assembly

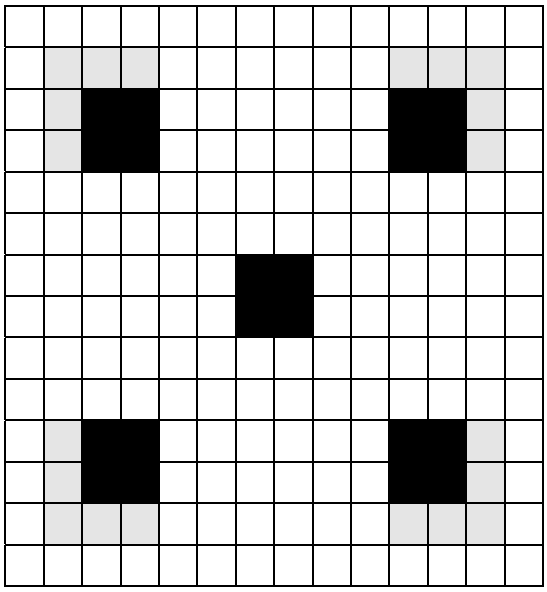

Bundles				
1P1	1R0	1S1		
2N2	2P1	2R1	1T1	2S1
2T1	1W1			

44 Pin Erbium Assembly

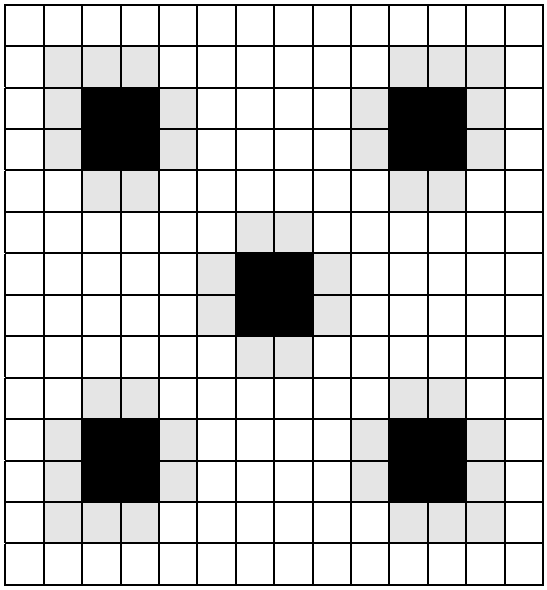

Bundles				
1P2	1R1	1RT	1S2	
2N4	2NT	2P2	1R2	1T2
2S2	1V1	2T2	1W2	

Fuel Rod Location

Erbium Rod Location

Guide Tube Location

Calvert Cliffs Nuclear Power Plant	BURNABLE POISON ROD LOCATION Sheet 4	Figure 3.3-4 Revision 35

60 Pin Erbium Assembly

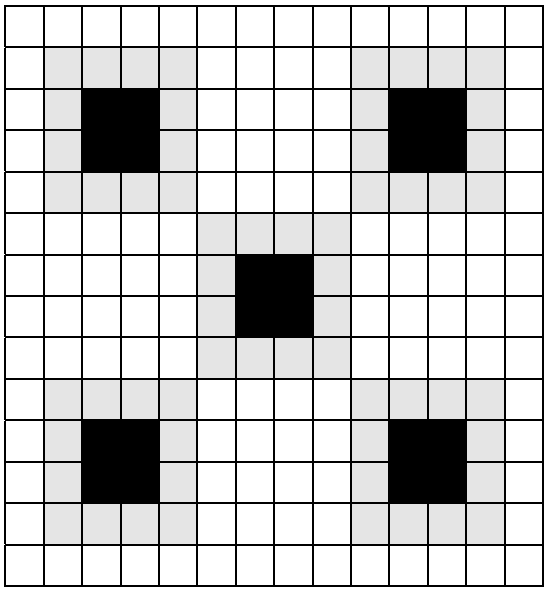

Bundles
1P3 1V2
1W3 1W4

68 Pin Erbium Assembly

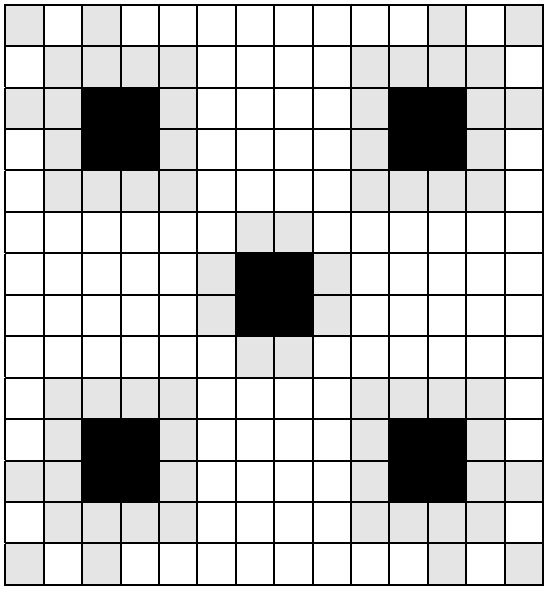

Bundles
1R2 1S3
2N6 2R3 2S3 2T3

Fuel Rod Location

Erbium Rod Location

Guide Tube Location

Calvert Cliffs Nuclear Power Plant	BURNABLE POISON ROD LOCATION Sheet 5	Figure 3.3-4 Revision 35

Radial Zoned Assembly with No IFBA Pins

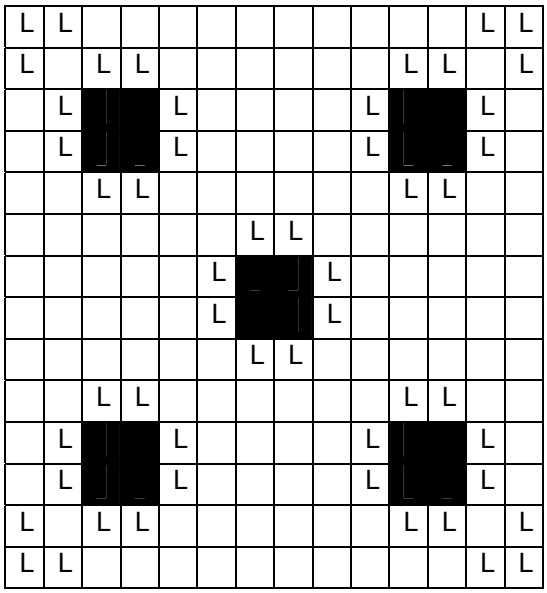

Bundles
2V0, 1Z1

44 IFBA Pin Radial Zoned Assembly

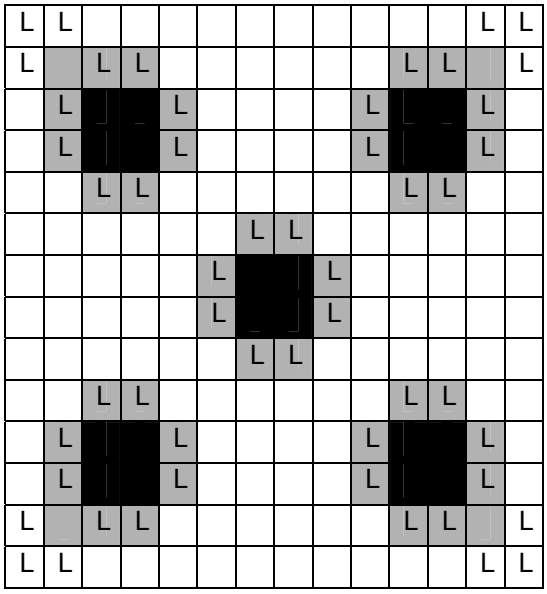

Bundles
2V1, 1X1, 1Z3

L Low Enriched Rod Location with No IFBA

High Enriched Rod Location with No IFBA

L IFBA Low Enriched Rod Location

IFBA High Enriched Rod Location

Calvert Cliffs Nuclear Power Plant	BURNABLE POISON ROD LOCATION Sheet 6	Figure 3.3-4 Revision 40

52 IFBA Pin Radial Zoned Assembly

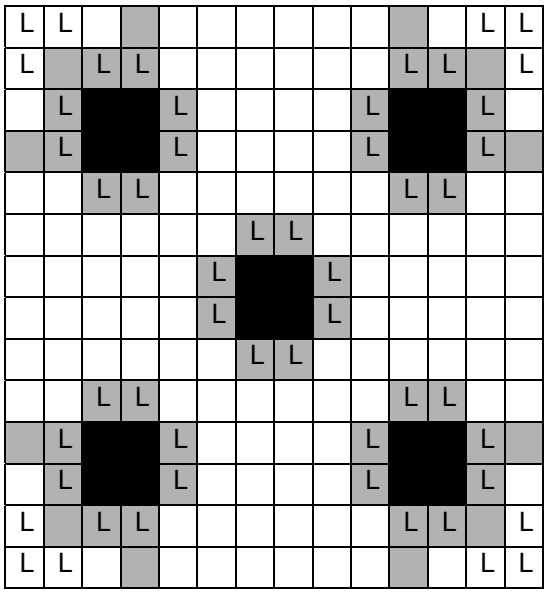

Bundles	
2V2	2X2
1X2	AA2

64 IFBA Pin Radial Zoned Assembly

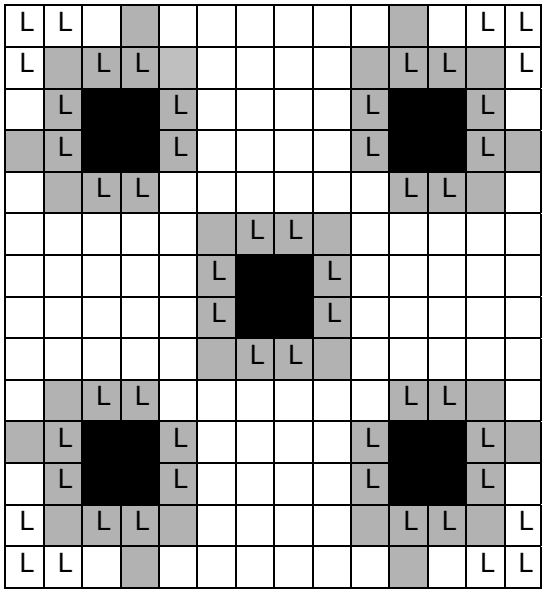

Bundles	
2V3	2W2
1X3	

L Low Enriched Rod Location with No IFBA

L IFBA Low Enriched Rod Location

High Enriched Rod Location with No IFBA

IFBA High Enriched Rod Location

Calvert Cliffs Nuclear Power Plant	BURNABLE POISON ROD LOCATION Sheet 7	Figure 3.3-4 Revision 42

76 IFBA Pin Radial Zoned Assembly

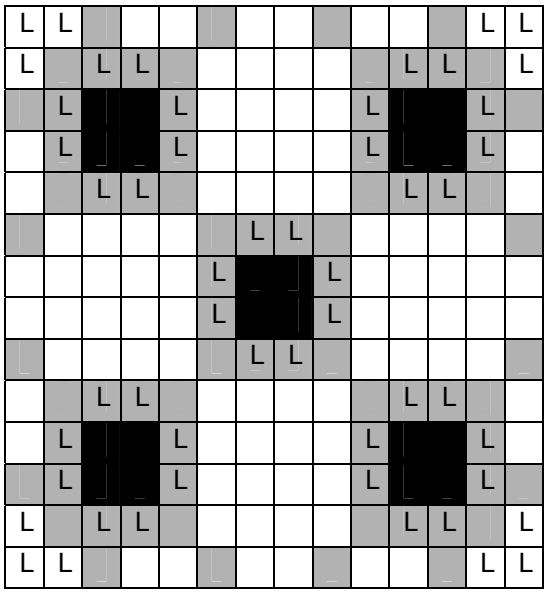

Bundles
2V4
1X4

96 IFBA Pin Radial Zoned Assembly

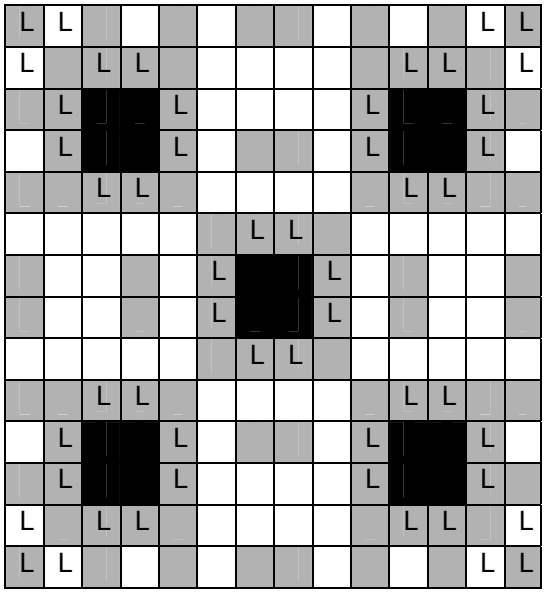

Bundles
2V5
1X5

L Low Enriched Rod Location with No IFBA

L IFBA Low Enriched Rod Location

High Enriched Rod Location with No IFBA

IFBA High Enriched Rod Location

Calvert Cliffs Nuclear Power Plant	BURNABLE POISON ROD LOCATION Sheet 8	Figure 3.3-4 Revision 38

28 IFBA Pin Radial Zoned Assembly

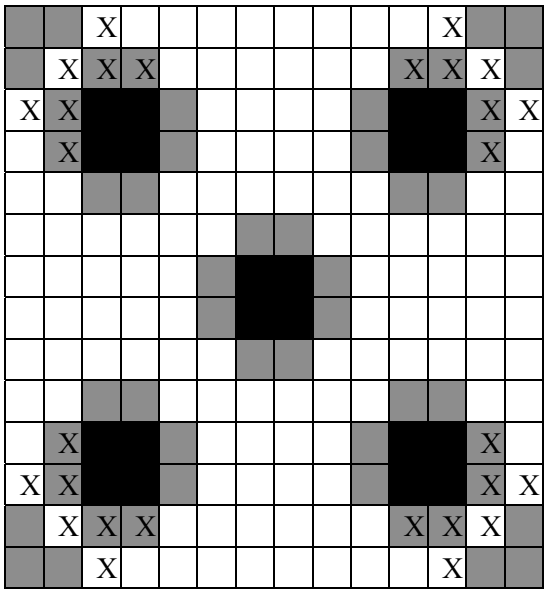

Bundles

2W1, 1Z2, 2X1, AA1

High Enriched Fuel Rod

X High Enriched ZrB_2 Rod

Low Enriched Fuel Rod

X Low Enriched ZrB_2 Rod

Calvert Cliffs Nuclear Power Plant	BURNABLE POISON ROD LOCATION Sheet 9	Figure 3.3-4 Revision 42

52 ZrB_2 Rods

3	3	2	5	2	2	1	1	2	2	5	2	3	3
3	5	6	6	2	1	1	1	1	2	6	6	5	3
2	6			6	1	1	1	1	6			6	2
5	6			6	2	1	1	2	6			6	5
2	2	6	6	2	2	2	2	2	2	6	6	2	2
2	1	1	2	2	2	6	6	2	2	2	1	1	2
1	1	1	1	2	6			6	2	1	1	1	1
1	1	1	1	2	6			6	2	1	1	1	1
2	1	1	2	2	2	6	6	2	2	2	1	1	2
2	2	6	6	2	2	2	2	2	2	6	6	2	2
5	6			6	2	1	1	2	6			6	5
2	6			6	1	1	1	1	6			6	2
3	5	6	6	2	1	1	1	1	2	6	6	5	3
3	3	2	5	2	2	1	1	2	2	5	2	3	3

Legend:

1. High Enriched Fuel
2. Medium Enriched Fuel
3. Low Enriched Fuel
4. High Enriched with ZrB_2
5. Medium Enriched with ZrB_2
6. Low Enriched with ZrB_2

Bundles

2W3

64 ZrB_2 Rods

3	3	2	5	2	2	1	1	2	2	5	2	3	3
3	5	6	6	5	1	1	1	1	5	6	6	5	3
2	6			6	1	1	1	1	6			6	2
5	6			6	2	1	1	2	6			6	5
2	5	6	6	2	2	2	2	2	2	6	6	5	2
2	1	1	2	2	5	6	6	5	2	2	1	1	2
1	1	1	1	2	6			6	2	1	1	1	1
1	1	1	1	2	6			6	2	1	1	1	1
2	1	1	2	2	5	6	6	5	2	2	1	1	2
2	5	6	6	2	2	2	2	2	2	6	6	5	2
5	6			6	2	1	1	2	6			6	5
2	6			6	1	1	1	1	6			6	2
3	5	6	6	5	1	1	1	1	5	6	6	5	3
3	3	2	5	2	2	1	1	2	2	5	2	3	3

Bundles

2W4, 1Z4, 2X3, 2X6, AA3

76 ZrB_2 Rods

3	3	5	2	2	5	1	1	5	2	2	5	3	3
3	5	6	6	5	1	1	1	1	5	6	6	5	3
5	6			6	1	1	1	1	6			6	5
2	6			6	2	1	1	2	6			6	2
2	5	6	6	5	2	2	2	2	5	6	6	5	2
5	1	1	2	2	5	6	6	5	2	2	1	1	5
1	1	1	1	2	6			6	2	1	1	1	1
1	1	1	1	2	6			6	2	1	1	1	1
5	1	1	2	2	5	6	6	5	2	2	1	1	5
2	5	6	6	5	2	2	2	2	5	6	6	5	2
2	6			6	2	1	1	2	6			6	2
5	6			6	1	1	1	1	6			6	5
3	5	6	6	5	1	1	1	1	5	6	6	5	3
3	3	5	2	2	5	1	1	5	2	2	5	3	3

Legend:

1. High Enriched Fuel
2. Medium Enriched Fuel
3. Low Enriched Fuel
4. High Enriched with ZrB_2
5. Medium Enriched with ZrB_2
6. Low Enriched with ZrB_2

Bundles

2W5, 1Z5, 2X4, AA4

96 ZrB_2 Rods

6	3	5	2	5	2	4	4	2	5	2	5	3	6
3	5	6	6	5	1	1	1	1	5	6	6	5	3
5	6			6	1	1	1	1	6			6	5
2	6			6	2	1	1	2	6			6	2
5	5	6	6	5	5	2	2	5	5	6	6	5	5
2	1	1	2	5	5	6	6	5	5	2	1	1	2
4	1	1	1	2	6			6	2	1	1	1	4
4	1	1	1	2	6			6	2	1	1	1	4
2	1	1	2	5	5	6	6	5	5	2	1	1	2
5	5	6	6	5	5	2	2	5	5	6	6	5	5
2	6			6	2	1	1	2	6			6	2
5	6			6	1	1	1	1	6			6	5
3	5	6	6	5	1	1	1	1	5	6	6	5	3
6	3	5	2	5	2	4	4	2	5	2	5	3	6

Bundles

2W6, 1Z6, 2X5, AA5

0 Gd_2O_3 Rods

L	L	H	H	H	H	H	H	H	H	H	H	L	L
L	H	L	L	H	H	H	H	H	H	L	L	H	L
H	L			L	H	H	H	H	L			L	H
H	L			L	H	H	H	H	L			L	H
H	H	L	L	H	H	H	H	H	H	L	L	H	H
H	H	H	H	H	H	L	L	H	H	H	H	H	H
H	H	H	H	H	L			L	H	H	H	H	H
H	H	H	H	H	L			L	H	H	H	H	H
H	H	H	H	H	H	L	L	H	H	H	H	H	H
H	H	L	L	H	H	H	H	H	H	L	L	H	H
H	L			L	H	H	H	H	L			L	H
H	L			L	H	H	H	H	L			L	H
L	H	L	L	H	H	H	H	H	H	L	L	H	L
L	L	H	H	H	H	H	H	H	H	H	H	L	L

Legend:
- H High Enriched Fuel
- L Low Enriched Fuel
- 2 2 w/o Gd_2O_3
- 6 6 w/o Gd_2O_3
- 8 8 w/o Gd_2O_3

Bundles

2Z1

4 Gd_2O_3 Rods

L	L	H	H	H	H	H	H	H	H	H	H	L	L
L	2	L	L	H	H	H	H	H	H	L	L	2	L
H	L			L	H	H	H	H	L			L	H
H	L			L	H	H	H	H	L			L	H
H	H	L	L	H	H	H	H	H	H	L	L	H	H
H	H	H	H	H	H	L	L	H	H	H	H	H	H
H	H	H	H	H	L			L	H	H	H	H	H
H	H	H	H	H	L			L	H	H	H	H	H
H	H	H	H	H	H	L	L	H	H	H	H	H	H
H	H	L	L	H	H	H	H	H	H	L	L	H	H
H	L			L	H	H	H	H	L			L	H
H	L			L	H	H	H	H	L			L	H
L	2	L	L	H	H	H	H	H	H	L	L	2	L
L	L	H	H	H	H	H	H	H	H	H	H	L	L

Bundles

2Z2

16 Gd_2O_3 Rods

L	L	H	H	H	H	H	H	H	H	H	H	L	L
L	2	L	L	H	H	H	H	H	H	L	L	2	L
H	L			L	6	H	H	6	L			L	H
H	L			L	H	H	H	H	L			L	H
H	H	L	L	6	H	H	H	H	6	L	L	H	H
H	H	6	H	H	H	L	L	H	H	H	6	H	H
H	H	H	H	H	L			L	H	H	H	H	H
H	H	H	H	H	L			L	H	H	H	H	H
H	H	6	H	H	H	L	L	H	H	H	6	H	H
H	H	L	L	6	H	H	H	H	6	L	L	H	H
H	L			L	H	H	H	H	L			L	H
H	L			L	6	H	H	6	L			L	H
L	2	L	L	H	H	H	H	H	H	L	L	2	L
L	L	H	H	H	H	H	H	H	H	H	H	L	L

Legend:

H	High Enriched Fuel
L	Low Enriched Fuel
2	2 w/o Gd_2O_3
6	6 w/o Gd_2O_3
8	8 w/o Gd_2O_3

Bundles

2Z3

16 Gd_2O_3 Rods

L	L	H	H	H	H	H	H	H	H	H	H	L	L
L	8	L	L	H	H	H	H	H	H	L	L	8	L
H	L			L	8	H	H	8	L			L	H
H	L			L	H	H	H	H	L			L	H
H	H	L	L	8	H	H	H	H	8	L	L	H	H
H	H	8	H	H	H	L	L	H	H	H	8	H	H
H	H	H	H	H	L			L	H	H	H	H	H
H	H	H	H	H	L			L	H	H	H	H	H
H	H	8	H	H	H	L	L	H	H	H	8	H	H
H	H	L	L	8	H	H	H	H	8	L	L	H	H
H	L			L	H	H	H	H	L			L	H
H	L			L	8	H	H	8	L			L	H
L	8	L	L	H	H	H	H	H	H	L	L	8	L
L	L	H	H	H	H	H	H	H	H	H	H	L	L

Bundles

2Z4

12 Gd_2O_3 Rods

L	L	H	H	H	H	H	H	H	H	H	H	L	L
L	8	L	L	H	H	H	H	H	H	L	L	8	L
H	L			L	H	H	H	H	L			L	H
H	L			L	8	H	H	8	L			L	H
H	H	L	L	H	H	H	H	H	H	L	L	H	H
H	H	H	8	H	H	L	L	H	H	8	H	H	H
H	H	H	H	H	L			L	H	H	H	H	H
H	H	H	H	H	L			L	H	H	H	H	H
H	H	H	8	H	H	L	L	H	H	8	H	H	H
H	H	L	L	H	H	H	H	H	H	L	L	H	H
H	L			L	8	H	H	8	L			L	H
H	L			L	H	H	H	H	L			L	H
L	8	L	L	H	H	H	H	H	H	L	L	8	L
L	L	H	H	H	H	H	H	H	H	H	H	L	L

Legend:

H	High Enriched Fuel
L	Low Enriched Fuel
2	2 w/o Gd_2O_3
6	6 w/o Gd_2O_3
8	8 w/o Gd_2O_3

Bundles

2Z5

Calvert Cliffs Nuclear Power Plant	BURNABLE POISON ROD LOCATION Sheet 14	Figure 3.3-4 Revision 43

16 Gd_2O_3 Rods

L	L	H	H	H	H	H	H	H	H	H	H	L	L
L	4	L	L	H	H	H	H	H	H	L	L	4	L
H	L			L	8	H	H	8	L			L	H
H	L			L	H	H	H	H	L			L	H
H	H	L	L	8	H	H	H	H	8	L	L	H	H
H	H	8	H	H	H	L	L	H	H	H	8	H	H
H	H	H	H	H	L			L	H	H	H	H	H
H	H	H	H	H	L			L	H	H	H	H	H
H	H	8	H	H	H	L	L	H	H	H	8	H	H
H	H	L	L	8	H	H	H	H	8	L	L	H	H
H	L			L	H	H	H	H	L			L	H
H	L			L	8	H	H	8	L			L	H
L	4	L	L	H	H	H	H	H	H	L	L	4	L
L	L	H	H	H	H	H	H	H	H	H	H	L	L

Legend:
- H High Enriched Fuel
- L Low Enriched Fuel
- 4 4 w/o Gd_2O_3
- 6 6 w/o Gd_2O_3
- 8 8 w/o Gd_2O_3

Bundles

AB1

16 Gd_2O_3 Rods

L	L	H	H	H	H	H	H	H	H	H	H	L	L
L	4	L	L	H	H	H	H	H	H	L	L	4	L
H	L			L	6	H	H	6	L			L	H
H	L			L	H	H	H	H	L			L	H
H	H	L	L	6	H	H	H	H	6	L	L	H	H
H	H	6	H	H	H	L	L	H	H	H	6	H	H
H	H	H	H	H	L			L	H	H	H	H	H
H	H	H	H	H	L			L	H	H	H	H	H
H	H	6	H	H	H	L	L	H	H	H	6	H	H
H	H	L	L	6	H	H	H	H	6	L	L	H	H
H	L			L	H	H	H	H	L			L	H
H	L			L	6	H	H	6	L			L	H
L	4	L	L	H	H	H	H	H	H	L	L	4	L
L	L	H	H	H	H	H	H	H	H	H	H	L	L

Bundles

AB2

12 Gd_2O_3 Rods

L	L	H	H	H	H	H	H	H	H	H	H	L	L
L	4	L	L	H	H	H	H	H	H	L	L	4	L
H	L			L	H	H	H	H	L			L	H
H	L			L	4	H	H	4	L			L	H
H	H	L	L	H	H	H	H	H	H	L	L	H	H
H	H	H	4	H	H	L	L	H	H	4	H	H	H
H	H	H	H	H	L			L	H	H	H	H	H
H	H	H	H	H	L			L	H	H	H	H	H
H	H	H	4	H	H	L	L	H	H	4	H	H	H
H	H	L	L	H	H	H	H	H	H	L	L	H	H
H	L			L	4	H	H	4	L			L	H
H	L			L	H	H	H	H	L			L	H
L	4	L	L	H	H	H	H	H	H	L	L	4	L
L	L	H	H	H	H	H	H	H	H	H	H	L	L

Legend:

H High Enriched Fuel

L Low Enriched Fuel

4 4 w/o Gd_2O_3

Bundles

AB3

Calvert Cliffs Nuclear Power Plant	BURNABLE POISON ROD LOCATION Sheet 16	Figure 3.3-4 Revision 45

No Gd_2O_3 Rods

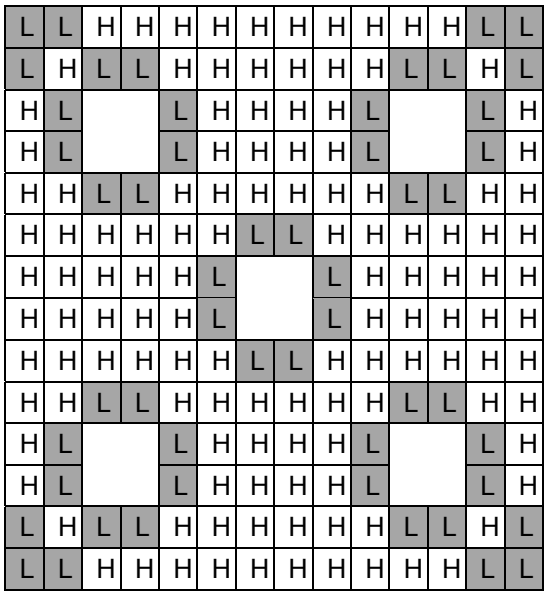

Legend:

H	High Enriched Fuel
L	Low Enriched Fuel
2	2 w/o Gd_2O_3
4	4 w/o Gd_2O_3
6	6 w/o Gd_2O_3
8	8 w/o Gd_2O_3

Bundles

BA1

4 Gd_2O_3 Rods

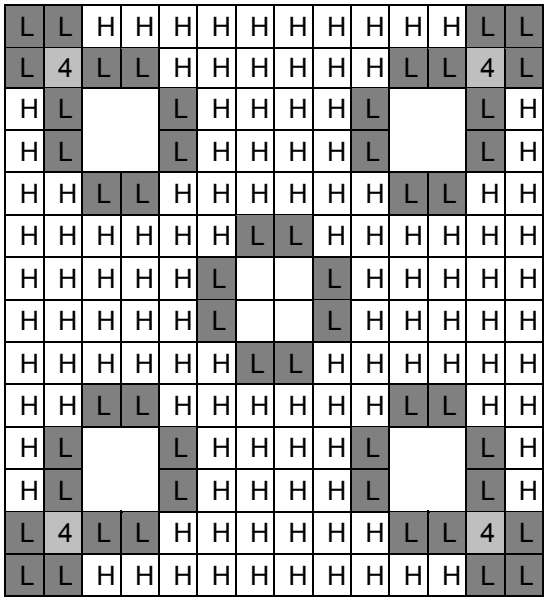

Bundles

BA2

Calvert Cliffs Nuclear Power Plant	BURNABLE POISON ROD LOCATION Sheet 17	Figure 3.3-4 Revision 46

16 Gd_2O_3 Rods

L	L	H	H	H	H	H	H	H	H	H	H	L	L
L	2	L	L	H	H	H	H	H	H	L	L	2	L
H	L			L	4	H	H	4	L			L	H
H	L			L	H	H	H	H	L			L	H
H	H	L	L	4	H	H	H	H	4	L	L	H	H
H	H	4	H	H	H	L	L	H	H	H	4	H	H
H	H	H	H	H	L			L	H	H	H	H	H
H	H	H	H	H	L			L	H	H	H	H	H
H	H	4	H	H	H	L	L	H	H	H	4	H	H
H	H	L	L	4	H	H	H	H	4	L	L	H	H
H	L			L	H	H	H	H	L			L	H
H	L			L	4	H	H	4	L			L	H
L	2	L	L	H	H	H	H	H	H	L	L	2	L
L	L	H	H	H	H	H	H	H	H	H	H	L	L

Legend:

H	High Enriched Fuel
L	Low Enriched Fuel
2	2 w/o Gd_2O_3
4	4 w/o Gd_2O_3
6	6 w/o Gd_2O_3
8	8 w/o Gd_2O_3

Bundles

BA3

16 Gd_2O_3 Rods

L	L	H	H	H	H	H	H	H	H	H	H	L	L
L	4	L	L	H	H	H	H	H	H	L	L	4	L
H	L			L	6	H	H	6	L			L	H
H	L			L	H	H	H	H	L			L	H
H	H	L	L	6	H	H	H	H	6	L	L	H	H
H	H	6	H	H	H	L	L	H	H	H	6	H	H
H	H	H	H	H	L			L	H	H	H	H	H
H	H	H	H	H	L			L	H	H	H	H	H
H	H	6	H	H	H	L	L	H	H	H	6	H	H
H	H	L	L	6	H	H	H	H	6	L	L	H	H
H	L			L	H	H	H	H	L			L	H
H	L			L	6	H	H	6	L			L	H
L	4	L	L	H	H	H	H	H	H	L	L	4	L
L	L	H	H	H	H	H	H	H	H	H	H	L	L

Bundles

BA4

20 Gd_2O_3 Rods

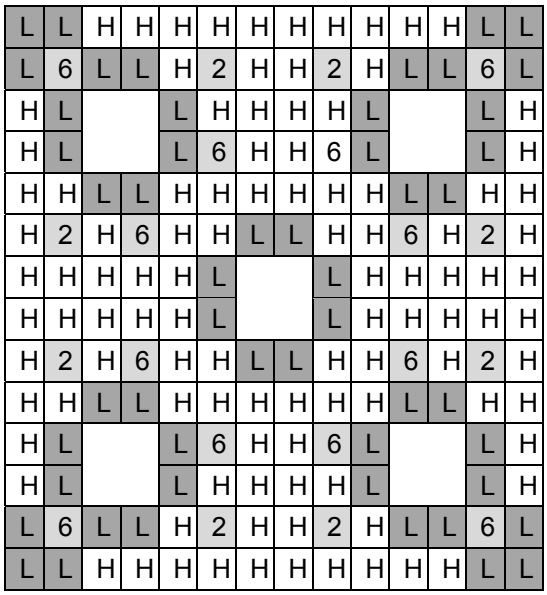

L	L	H	H	H	H	H	H	H	H	H	H	L	L
L	6	L	L	H	2	H	H	2	H	L	L	6	L
H	L			L	H	H	H	H	L			L	H
H	L			L	6	H	H	6	L			L	H
H	H	L	L	H	H	H	H	H	H	L	L	H	H
H	2	H	6	H	H	L	L	H	H	6	H	2	H
H	H	H	H	H	L			L	H	H	H	H	H
H	H	H	H	H	L			L	H	H	H	H	H
H	2	H	6	H	H	L	L	H	H	6	H	2	H
H	H	L	L	H	H	H	H	H	H	L	L	H	H
H	L			L	6	H	H	6	L			L	H
H	L			L	H	H	H	H	L			L	H
L	6	L	L	H	2	H	H	2	H	L	L	6	L
L	L	H	H	H	H	H	H	H	H	H	H	L	L

Legend:

- H High Enriched Fuel
- L Low Enriched Fuel
- 2 2 w/o Gd_2O_3
- 4 4 w/o Gd_2O_3
- 6 6 w/o Gd_2O_3
- 8 8 w/o Gd_2O_3

Bundles

BA5

12 Gd_2O_3 Rods

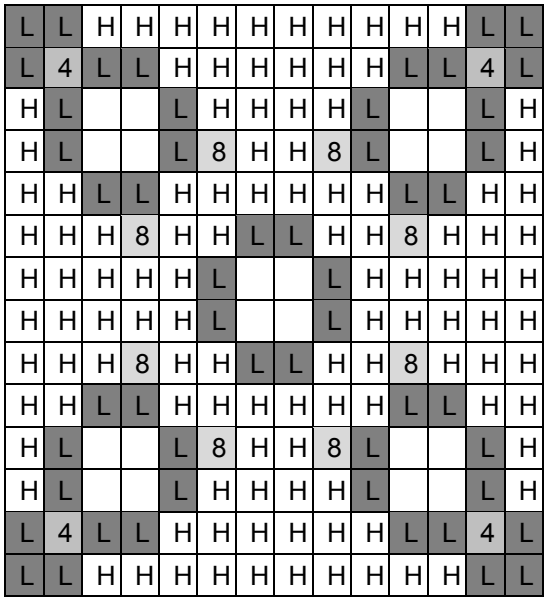

L	L	H	H	H	H	H	H	H	H	H	H	L	L
L	4	L	L	H	H	H	H	H	H	L	L	4	L
H	L			L	H	H	H	H	L			L	H
H	L			L	8	H	H	8	L			L	H
H	H	L	L	H	H	H	H	H	H	L	L	H	H
H	H	H	8	H	H	L	L	H	H	8	H	H	H
H	H	H	H	H	L			L	H	H	H	H	H
H	H	H	H	H	L			L	H	H	H	H	H
H	H	H	8	H	H	L	L	H	H	8	H	H	H
H	H	L	L	H	H	H	H	H	H	L	L	H	H
H	L			L	8	H	H	8	L			L	H
H	L			L	H	H	H	H	L			L	H
L	4	L	L	H	H	H	H	H	H	L	L	4	L
L	L	H	H	H	H	H	H	H	H	H	H	L	L

Bundles

BA6

16 Gd_2O_3 Rods

L	L	H	H	H	H	H	H	H	H	H	H	L	L
L	4	L	L	H	H	H	H	H	H	L	L	4	L
H	L			L	6	H	H	6	L			L	H
H	L			L	H	H	H	H	L			L	H
H	H	L	L	6	H	H	H	H	6	L	L	H	H
H	H	6	H	H	H	L	L	H	H	H	6	H	H
H	H	H	H	H	L			L	H	H	H	H	H
H	H	H	H	H	L			L	H	H	H	H	H
H	H	6	H	H	H	L	L	H	H	H	6	H	H
H	H	L	L	6	H	H	H	H	6	L	L	H	H
H	L			L	H	H	H	H	L			L	H
H	L			L	6	H	H	6	L			L	H
L	4	L	L	H	H	H	H	H	H	L	L	4	L
L	L	H	H	H	H	H	H	H	H	H	H	L	L

Legend:

H	High Enriched Fuel
L	Low Enriched Fuel
2	2 w/o Gd_2O_3
4	4 w/o Gd_2O_3
6	6 w/o Gd_2O_3
8	8 w/o Gd_2O_3

Bundles

BA7

Calvert Cliffs Nuclear Power Plant	BURNABLE POISON ROD LOCATION Sheet 20	Figure 3.3-4 Revision 46

16 Gd_2O_3 Rods

L	L	H	H	H	H	H	H	H	H	H	H	L	L
L	4	L	L	H	H	H	H	H	H	L	L	4	L
H	L			L	8	H	H	8	L			L	H
H	L			L	H	H	H	H	L			L	H
H	H	L	L	8	H	H	H	H	8	L	L	H	H
H	H	8	H	H	H	L	L	H	H	H	8	H	H
H	H	H	H	H	L			L	H	H	H	H	H
H	H	H	H	H	L			L	H	H	H	H	H
H	H	8	H	H	H	L	L	H	H	H	8	H	H
H	H	L	L	8	H	H	H	H	8	L	L	H	H
H	L			L	H	H	H	H	L			L	H
H	L			L	8	H	H	8	L			L	H
L	4	L	L	H	H	H	H	H	H	L	L	4	L
L	L	H	H	H	H	H	H	H	H	H	H	L	L

Legend:
- H High Enriched Fuel
- L Low Enriched Fuel
- 4 4 w/o Gd_2O_3
- 6 6 w/o Gd_2O_3
- 8 8 w/o Gd_2O_3

Bundles

AC1

12 Gd_2O_3 Rods

L	L	H	H	H	H	H	H	H	H	H	H	L	L
L	6	L	L	H	H	H	H	H	H	L	L	6	L
H	L			L	H	H	H	H	L			L	H
H	L			L	6	H	H	6	L			L	H
H	H	L	L	H	H	H	H	H	H	L	L	H	H
H	H	H	6	H	H	L	L	H	H	6	H	H	H
H	H	H	H	H	L			L	H	H	H	H	H
H	H	H	H	H	L			L	H	H	H	H	H
H	H	H	6	H	H	L	L	H	H	6	H	H	H
H	H	L	L	H	H	H	H	H	H	L	L	H	H
H	L			L	6	H	H	6	L			L	H
H	L			L	H	H	H	H	L			L	H
L	6	L	L	H	H	H	H	H	H	L	L	6	L
L	L	H	H	H	H	H	H	H	H	H	H	L	L

Bundles

AC2

16 Gd_2O_3 Rods

L	L	H	H	H	H	H	H	H	H	H	H	L	L
L	4	L	L	H	H	H	H	H	H	L	L	4	L
H	L			L	H	H	H	H	L			L	H
H	L			L	H	H	H	H	L			L	H
H	H	L	L	4	H	H	H	H	4	L	L	H	H
H	H	H	H	H	H	L	L	H	H	H	H	H	H
H	H	H	H	H	L			L	H	H	H	H	H
H	H	H	H	H	L			L	H	H	H	H	H
H	H	H	H	H	H	L	L	H	H	H	H	H	H
H	H	L	L	4	H	H	H	H	4	L	L	H	H
H	L			L	H	H	H	H	L			L	H
H	L			L	H	H	H	H	L			L	H
L	4	L	L	H	H	H	H	H	H	L	L	4	L
L	L	H	H	H	H	H	H	H	H	H	H	L	L

Legend:

H	High Enriched Fuel
L	Low Enriched Fuel
4	4 w/o Gd_2O_3
6	6 w/o Gd_2O_3
8	8 w/o Gd_2O_3

Bundles

AC3

Calvert Cliffs Nuclear Power Plant	BURNABLE POISON ROD LOCATION Sheet 22	Figure 3.3-4 Revision 47

Bundles: BB1

8 Gd_2O_3 Rods

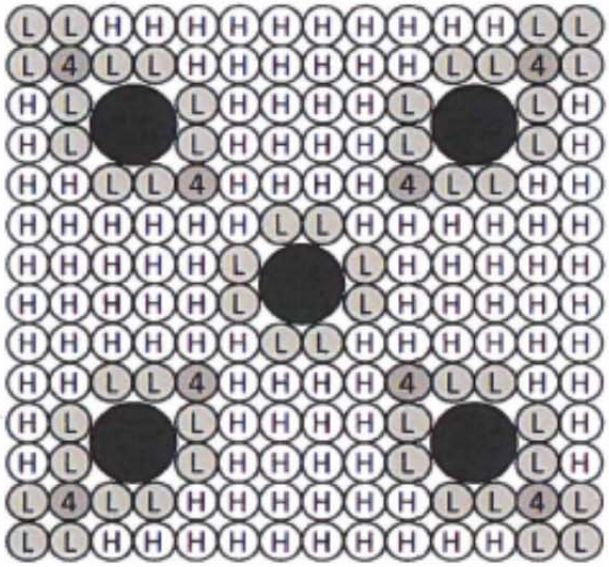

Legend:
- H High Enriched Fuel
- L Low Enriched Fuel
- 2 2 w/o Gd_2O_3
- 4 4 w/o Gd_2O_3
- 6 6 w/o Gd_2O_3
- 8 8 w/o Gd_2O_3

Bundles: BB2

8 Gd_2O_3 Rods

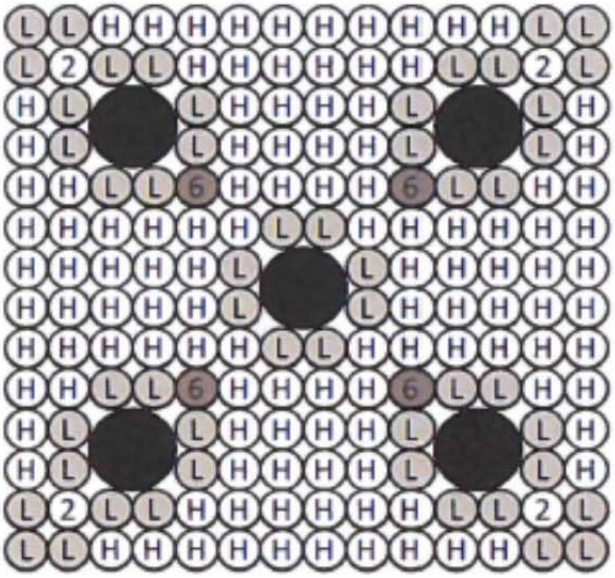

Legend:
- H High Enriched Fuel
- L Low Enriched Fuel
- 2 2 w/o Gd_2O_3
- 4 4 w/o Gd_2O_3
- 6 6 w/o Gd_2O_3
- 8 8 w/o Gd_2O_3

Calvert Cliffs Nuclear Power Plant	BURNABLE POISON ROD LOCATION Sheet 23	Figure 3.3-4 Revision 48

Bundles: BB3

12 Gd_2O_3 Rods

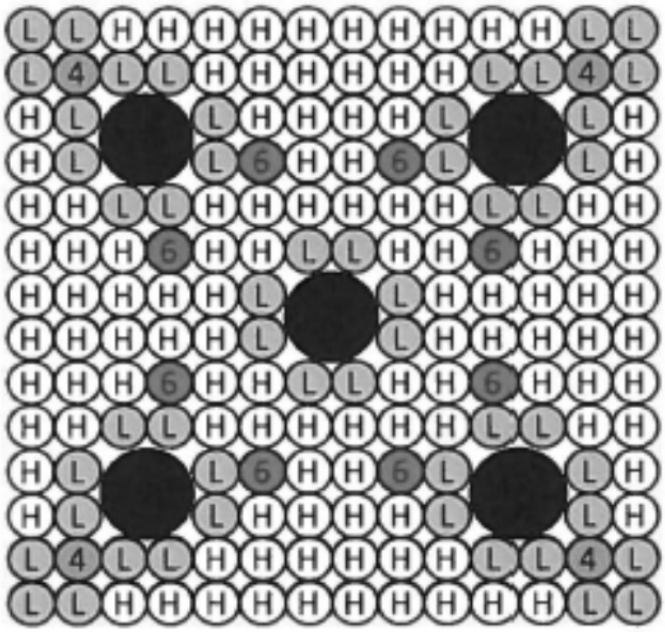

Legend:

H	High Enriched Fuel
L	Low Enriched Fuel
2	2 w/o Gd_2O_3
4	4 w/o Gd_2O_3
6	6 w/o Gd_2O_3
8	8 w/o Gd_2O_3

Bundles: BB4

16 Gd_2O_3 Rods

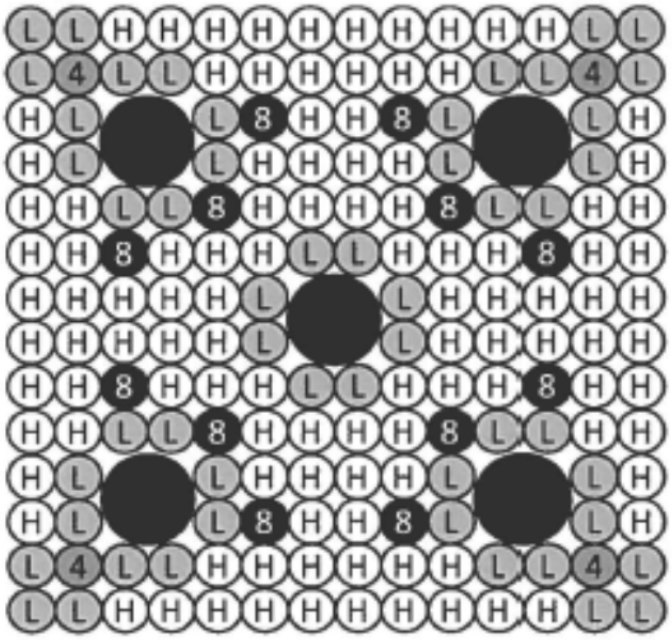

Legend:

H	High Enriched Fuel
L	Low Enriched Fuel
2	2 w/o Gd_2O_3
4	4 w/o Gd_2O_3
6	6 w/o Gd_2O_3
8	8 w/o Gd_2O_3

Bundles: BB5

20 Gd_2O_3 Rods

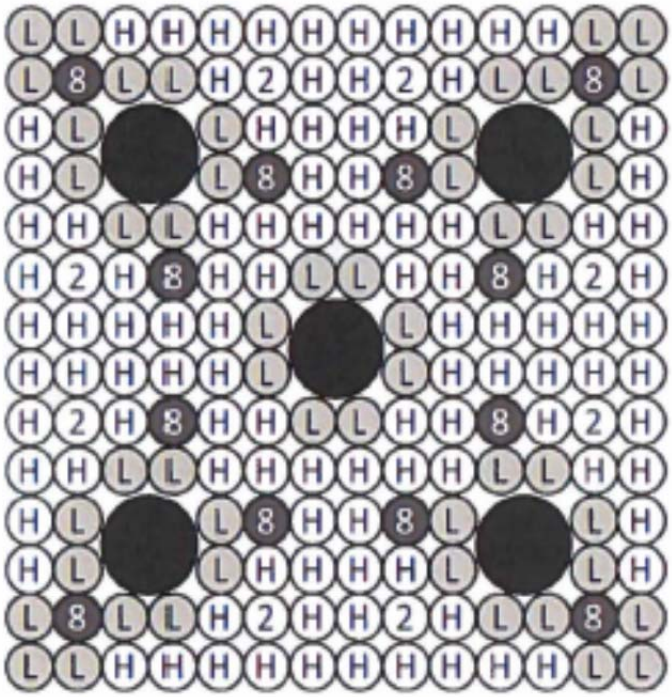

Legend:

H	High Enriched Fuel
L	Low Enriched Fuel
2	2 w/o Gd_2O_3
4	4 w/o Gd_2O_3
6	6 w/o Gd_2O_3
8	8 w/o Gd_2O_3

Calvert Cliffs Nuclear Power Plant	BURNABLE POISON ROD LOCATION Sheet 25	Figure 3.3-4 Revision 48

Bundles: AD1

16 Gd_2O_3 Rods

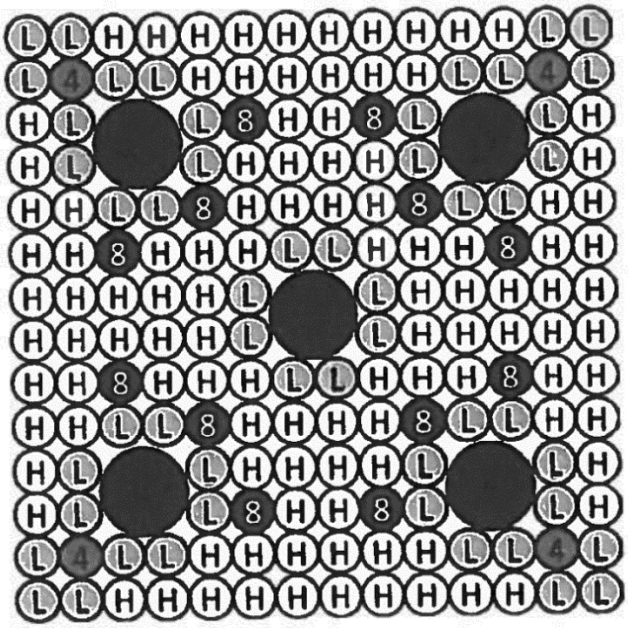

Legend:

H	High Enriched Fuel
L	Low Enriched Fuel
2	2 w/o Gd_2O_3
4	4 w/o Gd_2O_3
6	6 w/o Gd_2O_3
8	8 w/o Gd_2O_3

Bundles: AD2

16 Gd_2O_3 Rods

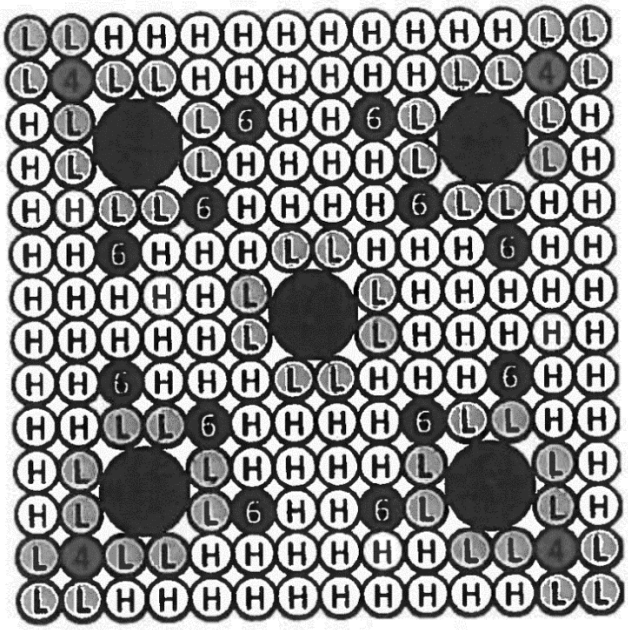

Legend:

H	High Enriched Fuel
L	Low Enriched Fuel
2	2 w/o Gd_2O_3
4	4 w/o Gd_2O_3
6	6 w/o Gd_2O_3
8	8 w/o Gd_2O_3

Bundles: AD3

12 Gd_2O_3 Rods

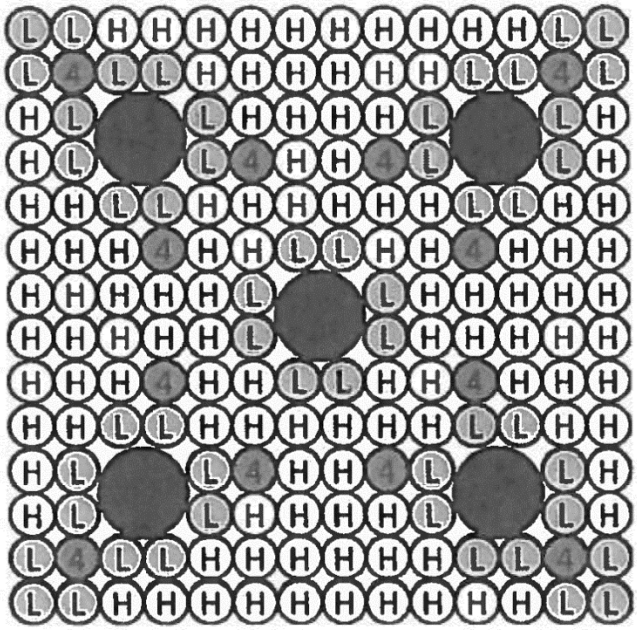

Legend:

H	High Enriched Fuel
L	Low Enriched Fuel
2	2 w/o Gd_2O_3
4	4 w/o Gd_2O_3
6	6 w/o Gd_2O_3
8	8 w/o Gd_2O_3

Bundles: AD4

8 Gd_2O_3 Rods

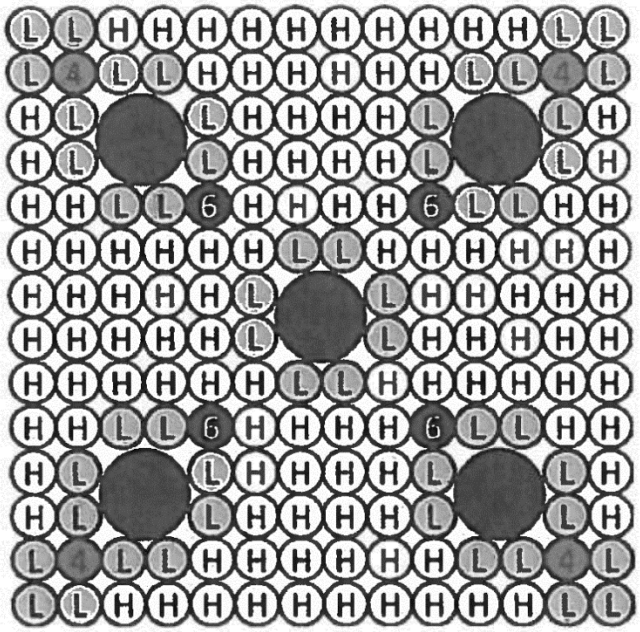

Legend:

H	High Enriched Fuel
L	Low Enriched Fuel
2	2 w/o Gd_2O_3
4	4 w/o Gd_2O_3
6	6 w/o Gd_2O_3
8	8 w/o Gd_2O_3

Bundles: BC1

8 Gd_2O_3 Rods

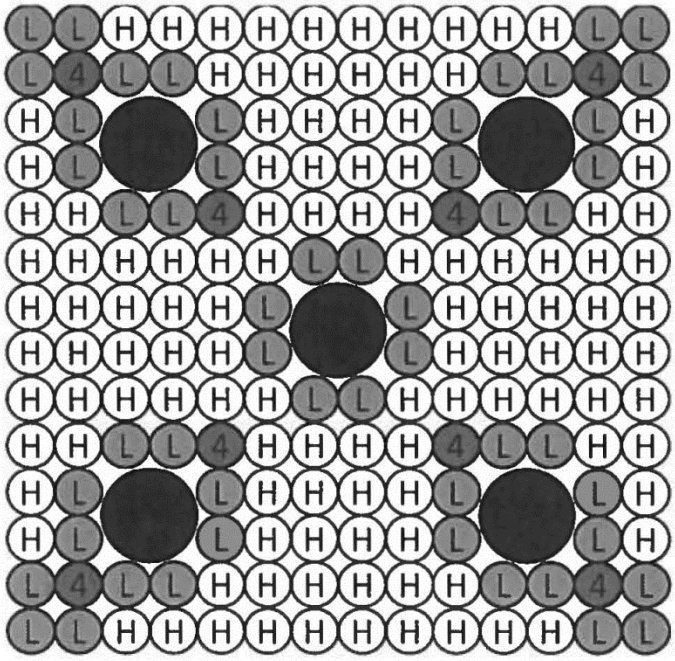

Legend:

H	High Enriched Fuel
L	Low Enriched Fuel
2	2 w/o Gd_2O_3
4	4 w/o Gd_2O_3
6	6 w/o Gd_2O_3
8	8 w/o Gd_2O_3

Bundles: BC2

8 Gd_2O_3 Rods

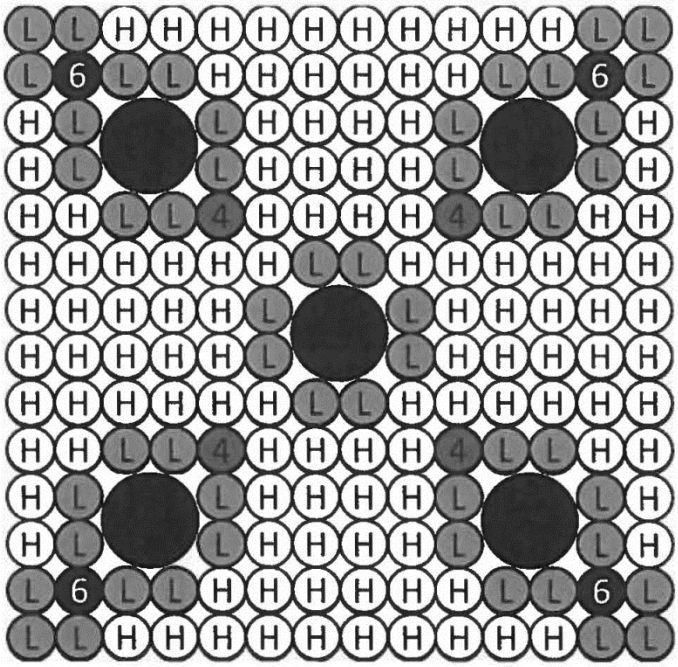

Legend:

H	High Enriched Fuel
L	Low Enriched Fuel
2	2 w/o Gd_2O_3
4	4 w/o Gd_2O_3
6	6 w/o Gd_2O_3
8	8 w/o Gd_2O_3

Bundles: BC3

12 Gd_2O_3 Rods

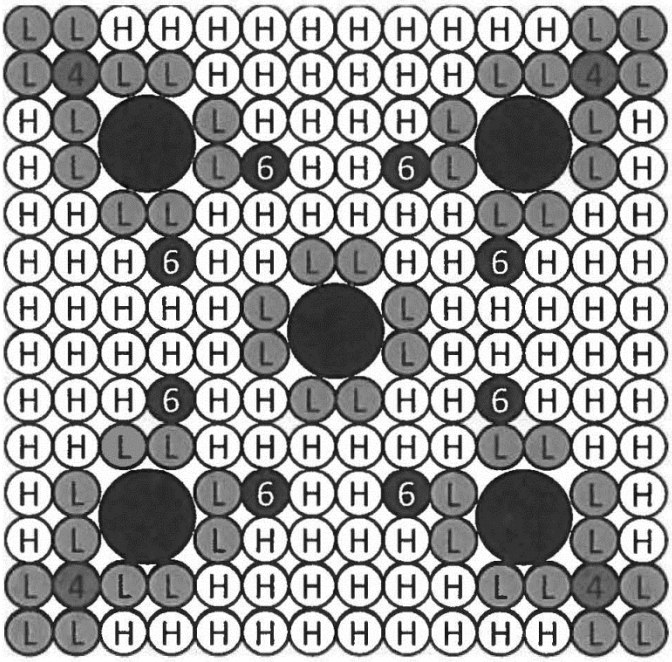

Legend:
- H High Enriched Fuel
- L Low Enriched Fuel
- 2 2 w/o Gd_2O_3
- 4 4 w/o Gd_2O_3
- 6 6 w/o Gd_2O_3
- 8 8 w/o Gd_2O_3

Bundles: BC4

16 Gd_2O_3 Rods

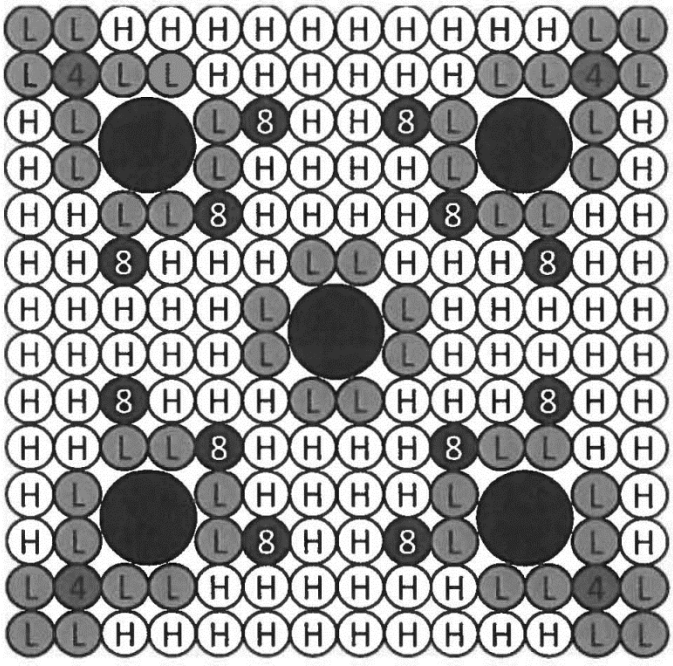

Legend:
- H High Enriched Fuel
- L Low Enriched Fuel
- 2 2 w/o Gd_2O_3
- 4 4 w/o Gd_2O_3
- 6 6 w/o Gd_2O_3
- 8 8 w/o Gd_2O_3

Bundles: BC5

16 Gd_2O_3 Rods

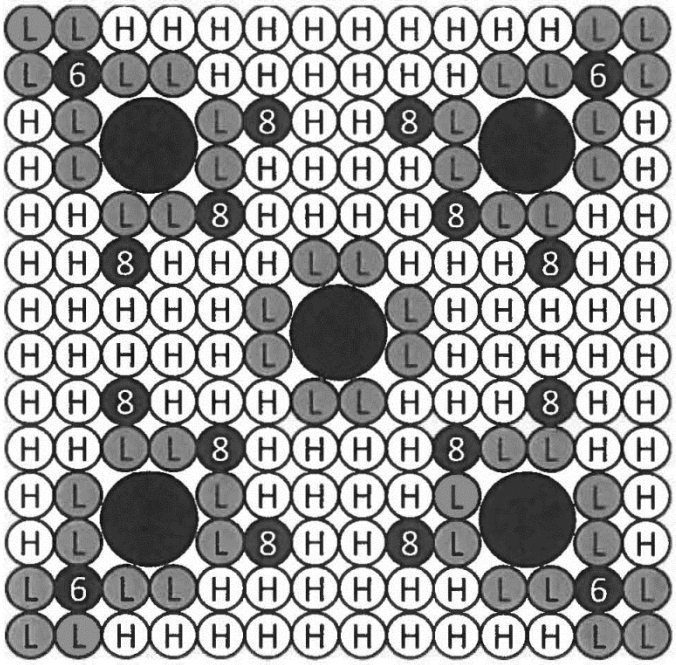

Legend:

H	High Enriched Fuel
L	Low Enriched Fuel
2	2 w/o Gd_2O_3
4	4 w/o Gd_2O_3
6	6 w/o Gd_2O_3
8	8 w/o Gd_2O_3

Calvert Cliffs Nuclear Power Plant	BURNABLE POISON ROD LOCATION SHEET 30	Figure 3-3-4 Revision 49

Bundles: **AE1**

20 Gd_2O_3 Rods

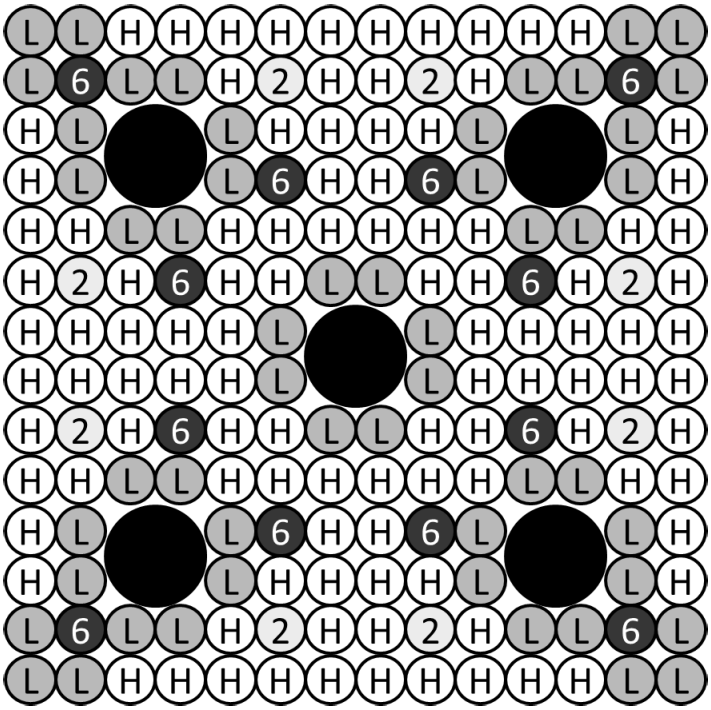

Legend:

H	High Enriched Fuel
L	Low Enriched Fuel
2	2 w/o GD_2O_3
4	4 w/o GD_2O_3
6	6 w/o GD_2O_3
8	8 w/o GD_2O_3

Bundles: **AE2**

16 Gd_2O_3 Rods

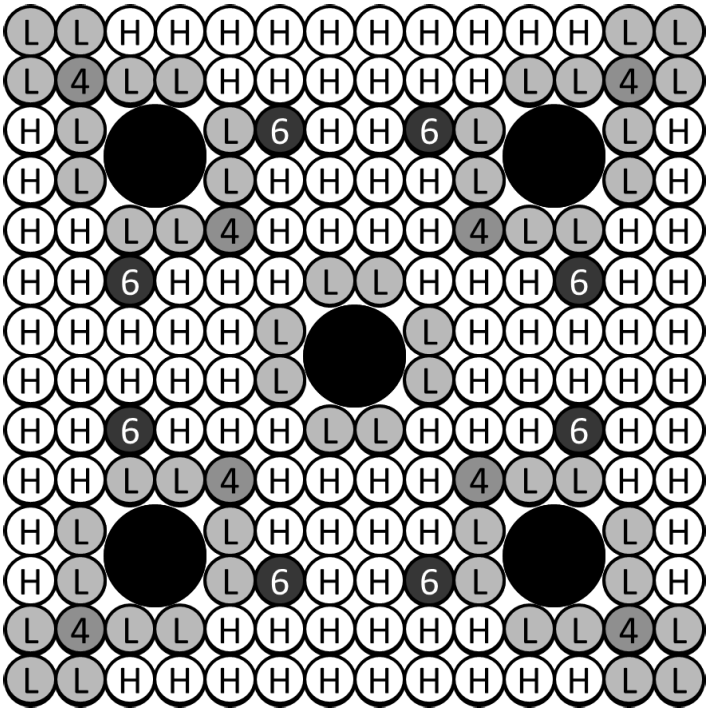

Legend:

H	High Enriched Fuel
L	Low Enriched Fuel
2	2 w/o GD_2O_3
4	4 w/o GD_2O_3
6	6 w/o GD_2O_3
8	8 w/o GD_2O_3

Bundles: **AE3**

12 Gd_2O_3 Rods

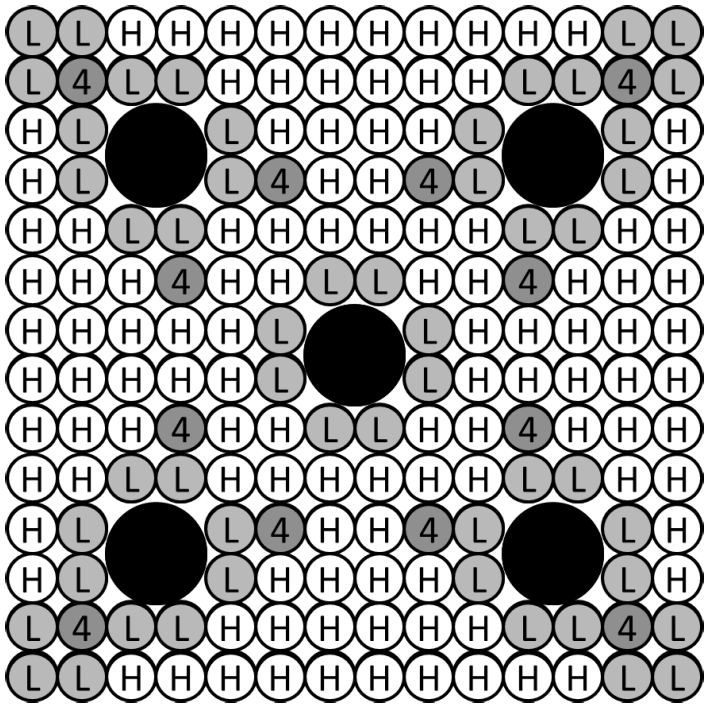

Legend:

H	High Enriched Fuel
L	Low Enriched Fuel
2	2 w/o GD_2O_3
4	4 w/o GD_2O_3
6	6 w/o GD_2O_3
8	8 w/o GD_2O_3

Bundles: **AE4**

8 Gd_2O_3 Rods

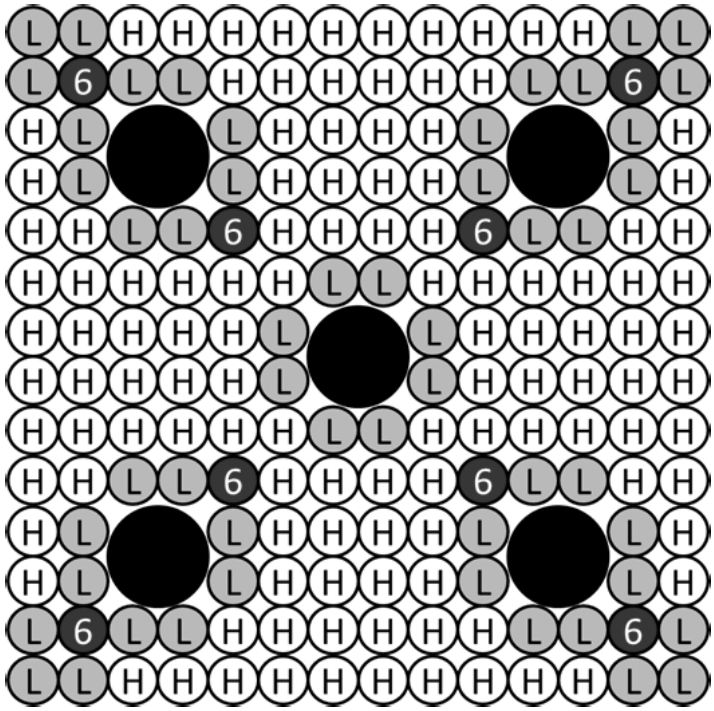

Legend:

H	High Enriched Fuel
L	Low Enriched Fuel
2	2 w/o GD_2O_3
4	4 w/o GD_2O_3
6	6 w/o GD_2O_3
8	8 w/o GD_2O_3

Calvert Cliffs Nuclear Power Plant	BURNABLE POISON ROD LOCATION SHEET 32	Figure 3-3-4 Revision 50

Bundles: **AE5**

8 Gd_2O_3 Rods

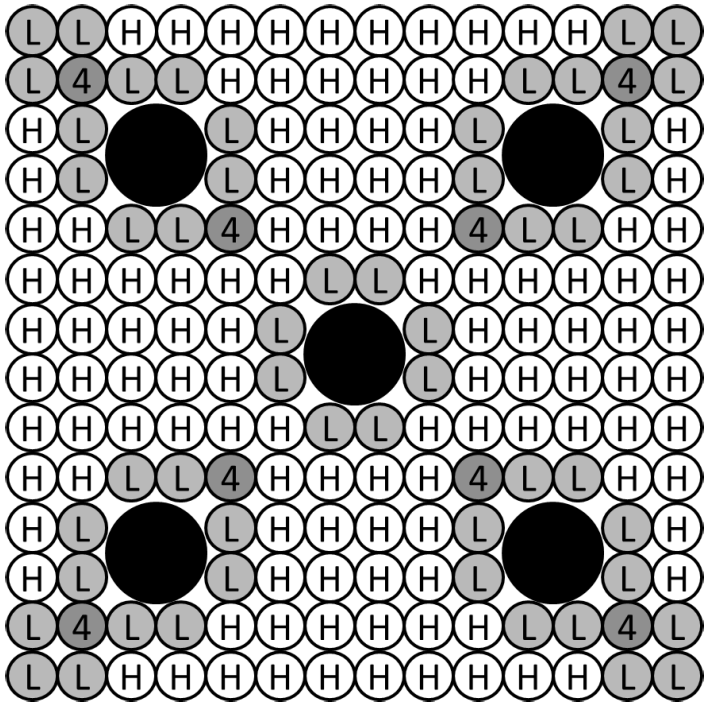

Legend:

H	High Enriched Fuel
L	Low Enriched Fuel
2	2 w/o GD_2O_3
4	4 w/o GD_2O_3
6	6 w/o GD_2O_3
8	8 w/o GD_2O_3

Calvert Cliffs Nuclear Power Plant	BURNABLE POISON ROD LOCATION SHEET 33	Figure 3.3-4 Revision 50

Sub-Batch: BD1

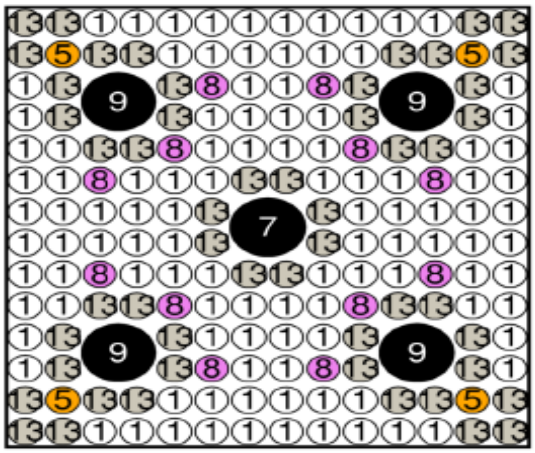

Type	# Rods	U^{235} %	Gd_2O_3 %
1	108	4.91	-
5	4	3.60	5
8	12	2.95	7
13	52	4.33	-

Sub-Batch: BD2

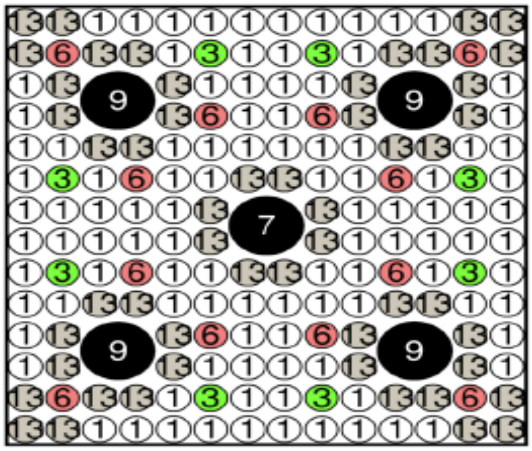

Type	# Rods	U^{235} %	Gd_2O_3 %
1	104	4.91	-
3	8	4.33	2
6	12	2.95	6
13	52	4.33	-

Figure 3-2 Fuel Rod Assembly Lattices

Sub-Batch: BD3

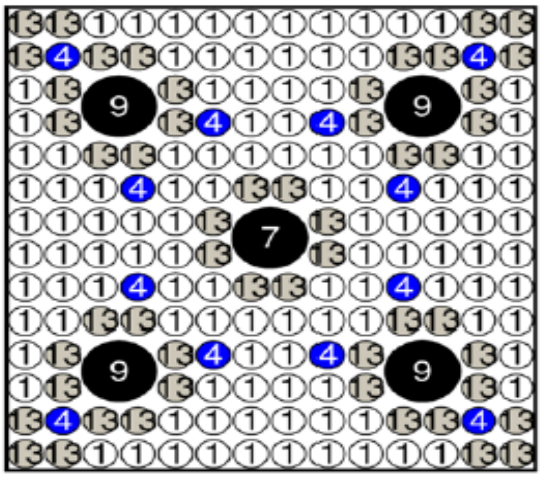

Type	# Rods	U^{235} %	Gd_2O_3 %
1	112	4.91	-
4	12	3.60	4
13	52	4.33	-

Sub-Batch: BD4

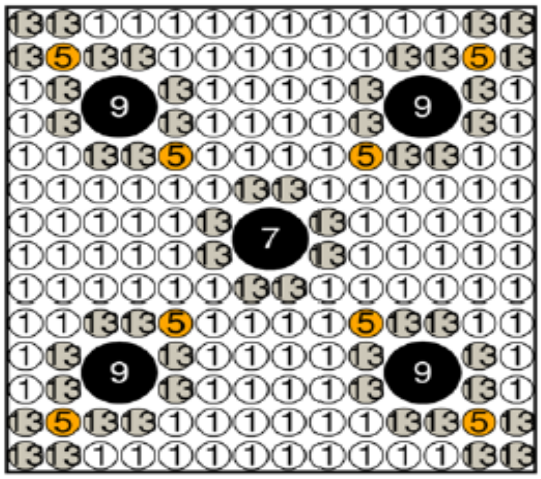

Type	# Rods	U^{235} %	Gd_2O_3 %
1	116	4.91	-
5	8	3.60	5
13	52	4.33	-

Figure 3-2 Fuel Rod Assembly Lattices

Sub-Batch: BD5

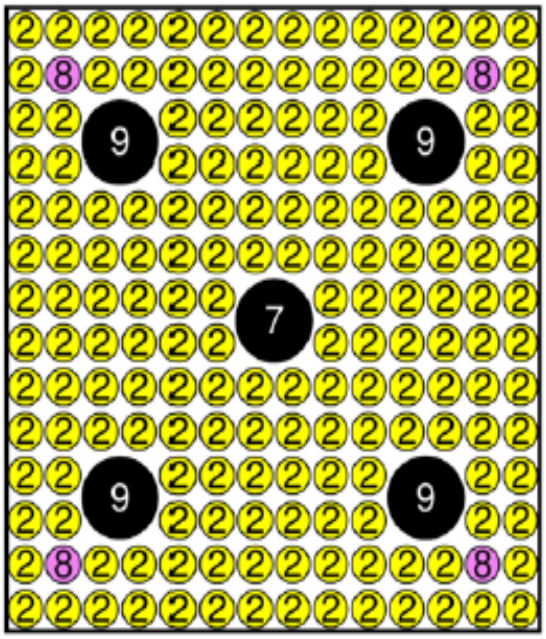

Type	# Rods	U^{235} %	Gd_2O_3 %
2	172	2.95	-
8	4	2.95	7

Figure 3-2 Fuel Rod Assembly Lattices

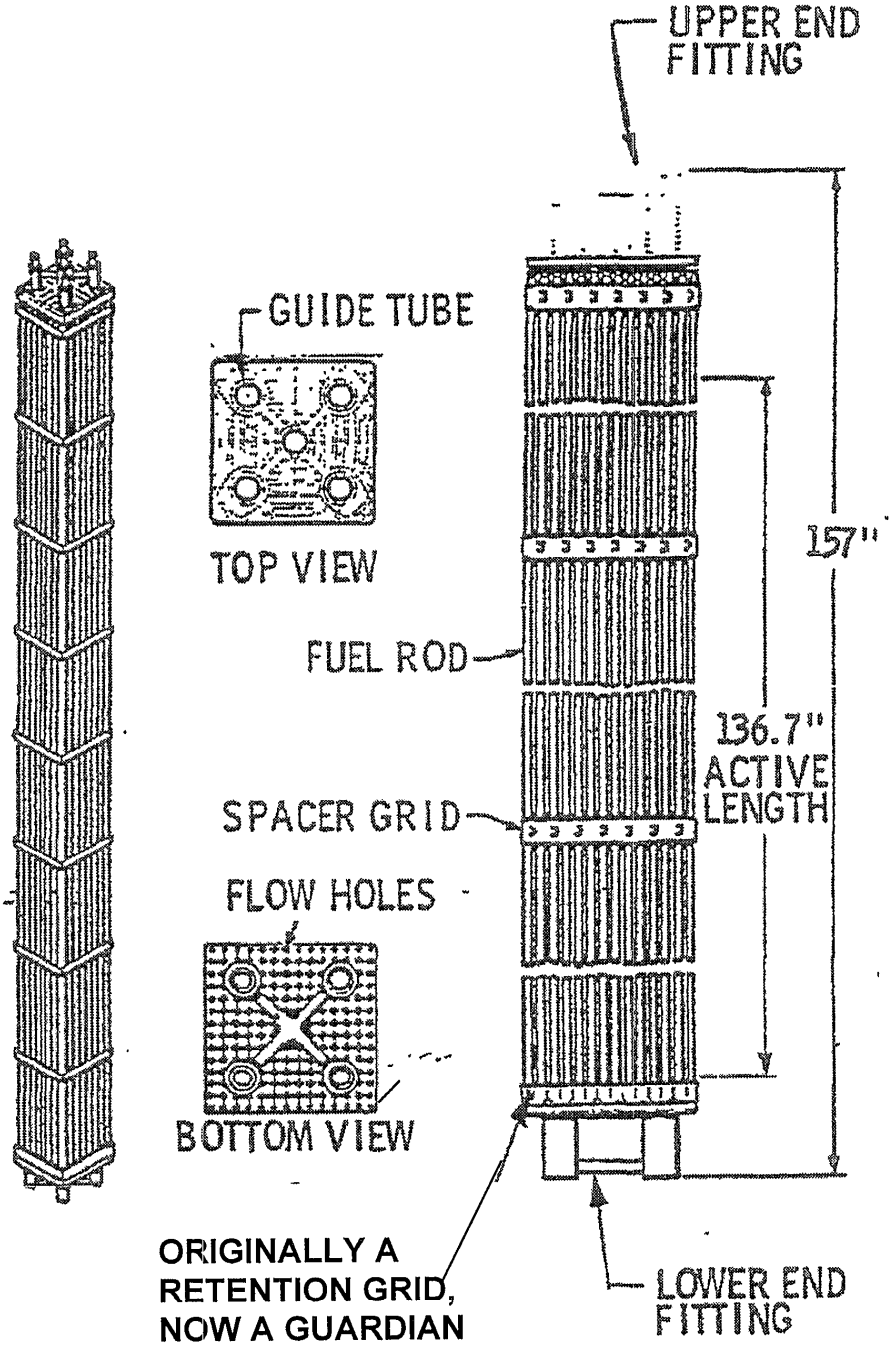

Calvert Cliffs Nuclear Power Plant	FUEL ASSEMBLY	Figure 3.3-5 Revision 43

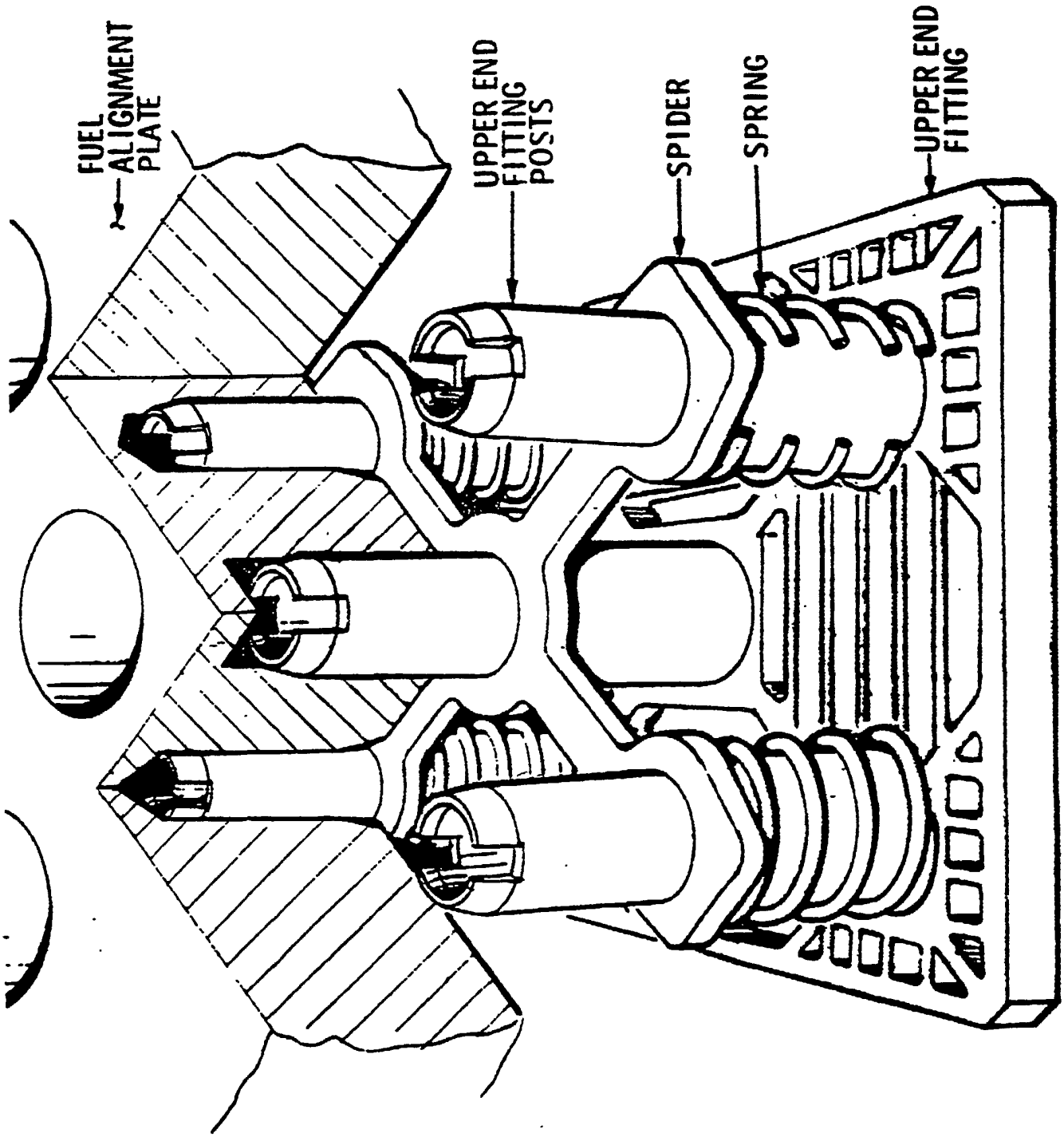

BALTIMORE GAS & ELECTRIC CO. Calvert Cliffs Nuclear Power Plant	Fuel Assembly Hold Down	Figure 3.3-6

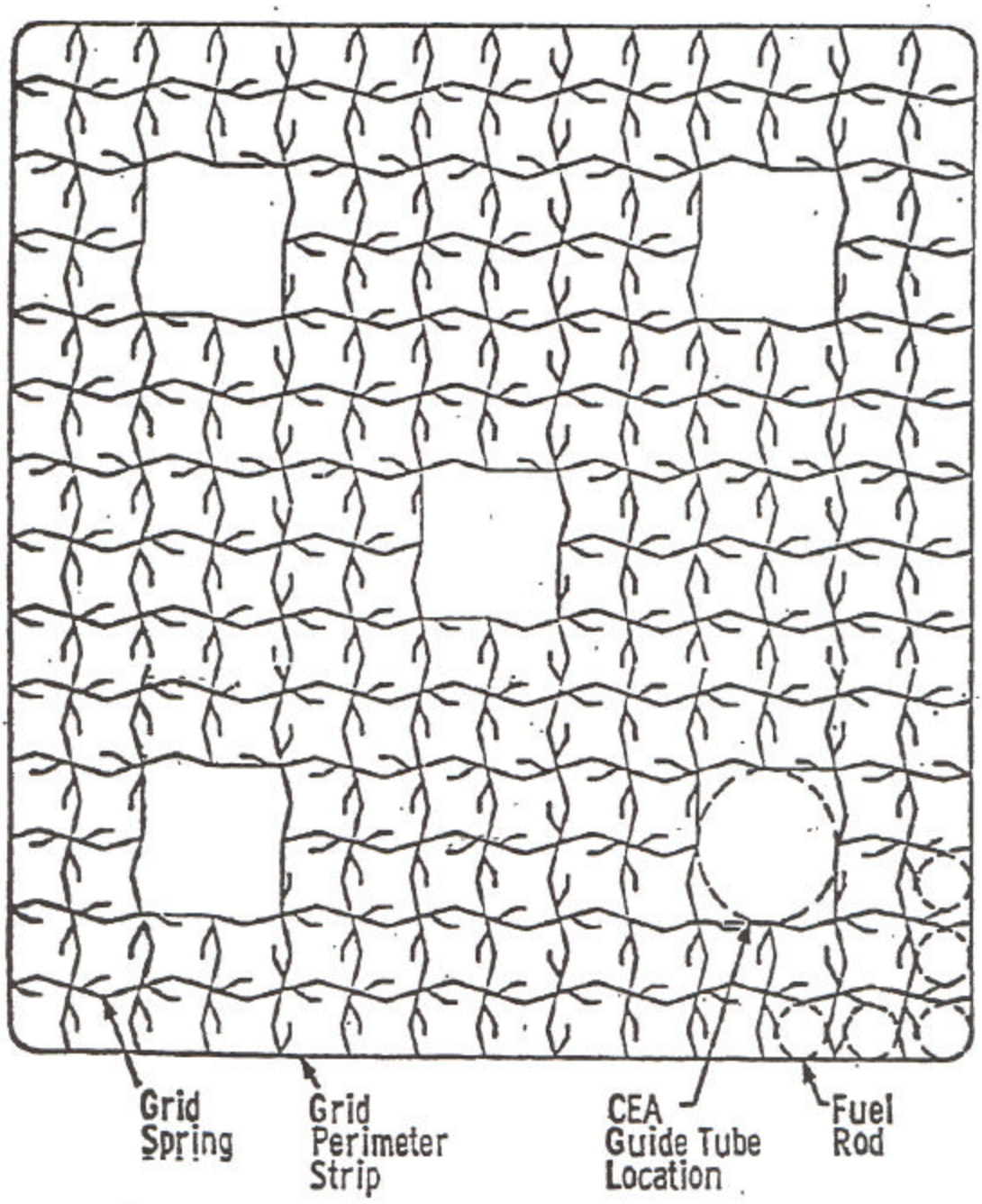

Calvert Cliffs Nuclear Power Plant	CANTILEVER TAB FUEL SPACER GRID	Figure 3.3-7 Revision 32

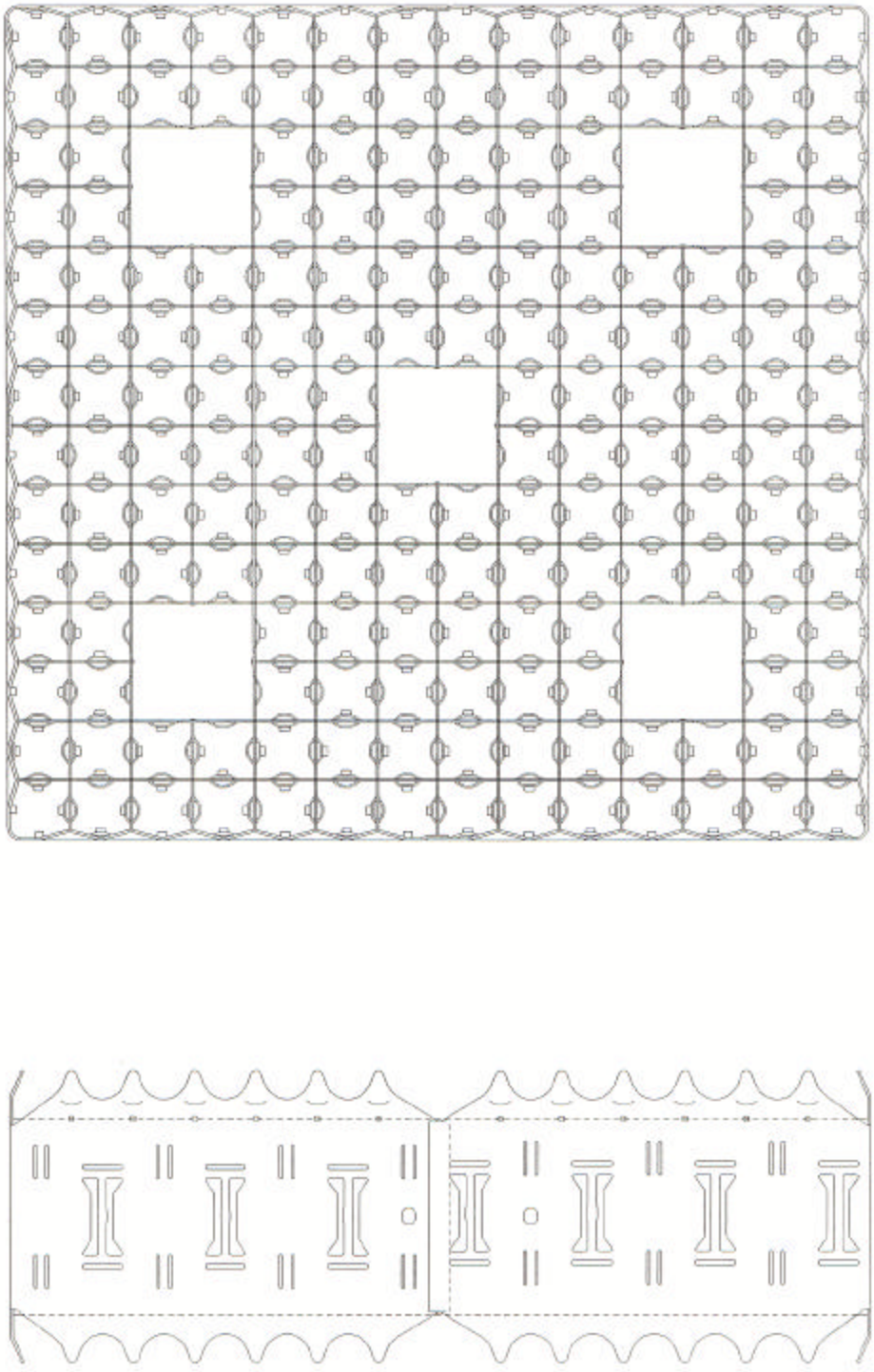

Calvert Cliffs Nuclear Power Plant	I-SPRING UNVANED SPACER GRID (TURBO)	Figure 3.3-7A Revision 32

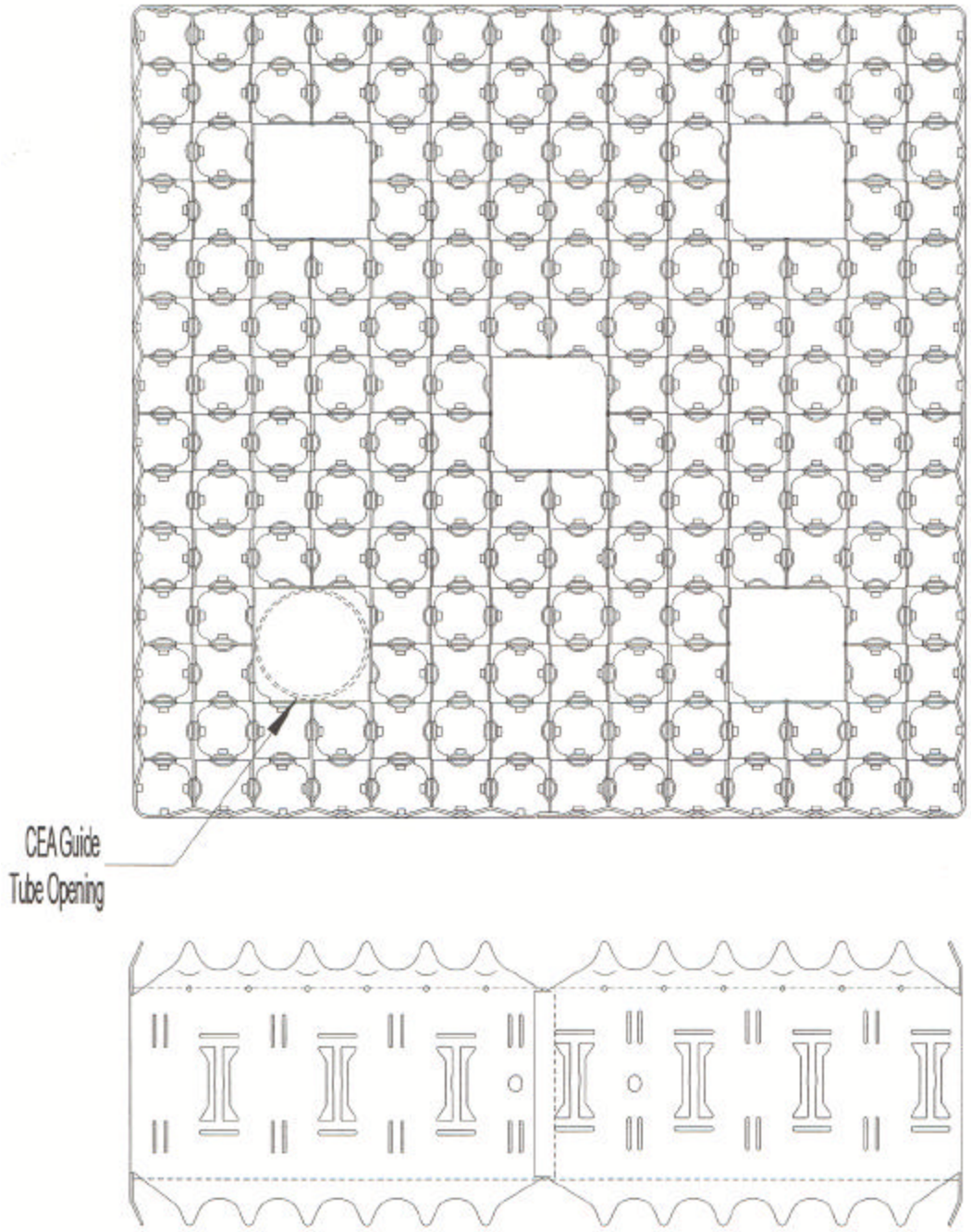

Calvert Cliffs Nuclear Power Plant	I-SPRING VANED SPACER GRID (TURBO)	Figure 3.3-7B Revision 32

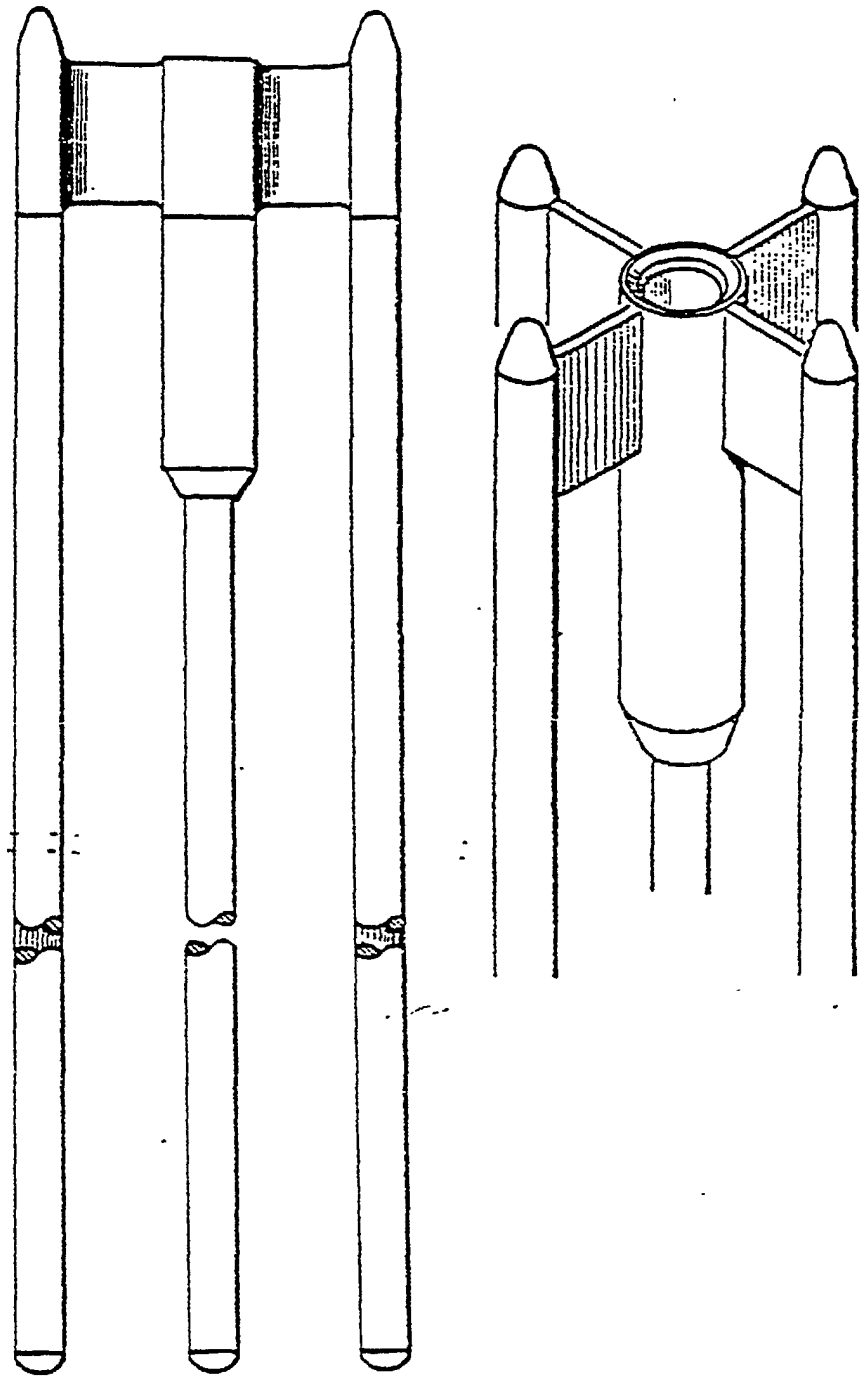

BALTIMORE GAS & ELECTRIC CO. Calvert Cliffs Nuclear Power Plant	CONTROL ELEMENT ASSEMBLY (CEA)	FIGURE 3.3-8 Rev. 0 1/82

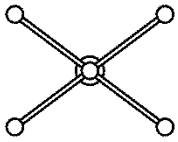

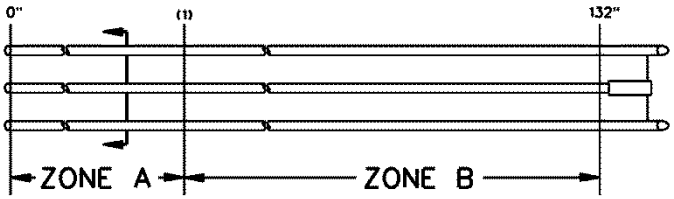

ABBREVIATIONS
FULL LENGTH

MATERIALS[2]

	ZONE A	ZONE B
FLCEA1 (STANDARD)	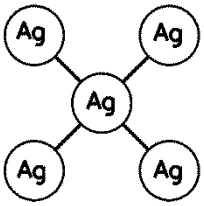	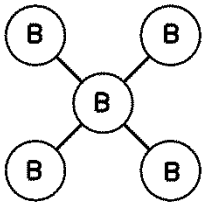
FLCEA2 (RECONSTITUTABLE CORNER FINGERS)	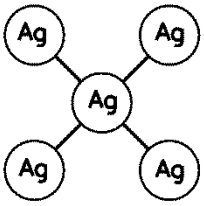	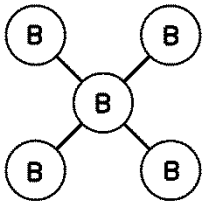
FLCEA8 (NON-RECONSTITUTABLE)	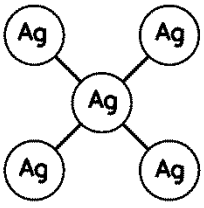	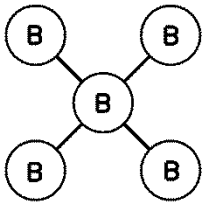
FLCEA7 (NON-RECONSTITUTABLE)	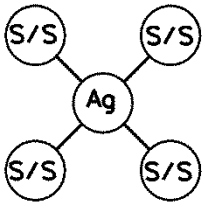	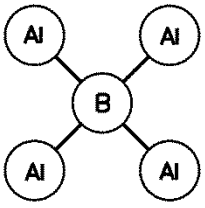

NOTES:
(1) ZONE "A" IS 8" FOR FLCEA1, FLCEA2, AND FLCEA7, AND 12" FOR FLCEA8.
(2) B=B_4C Ag=Ag-In-Cd Al=Al_2O_3 S/S=Stainless Steel

FSAR 3.3-9A.DGN

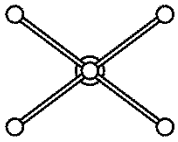

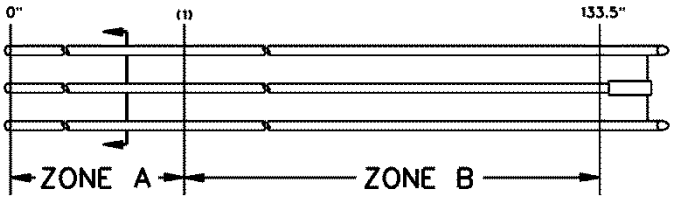

ABBREVIATIONS

FULL LENGTH

MATERIALS[2]

ZONE A

ZONE B[3]

FLCEA10
(AREVA Full Strength)
(Non-Reconstitutable)

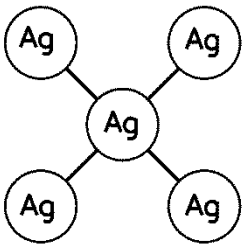

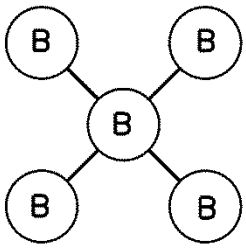

FLCEA9
(AREVA Part Strength)
(Non-Reconstitutable)

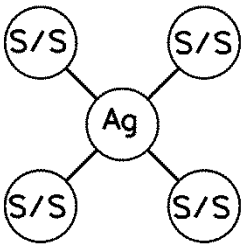

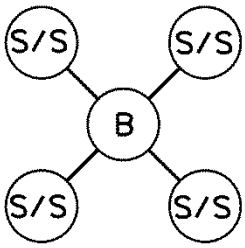

NOTES:

(1) ZONE "A" IS 12.5" FOR FLCEA10 AND FLCEA9

(2) B=B_4C Ag=Ag-In-Cd S/S=Stainless Steel

(3) ZONE "B" STARTS 0.355" ABOVE ZONE "A" FOR ALL FLCEA10 RODS AND ONLY THE CENTER ROD FOR FLCEA9

FSAR 3.3-9B.DGN

Calvert Cliffs Nuclear Power Plant	AREVA /FRAMATOME CONTROL ELEMENT ASSEMBLIES	Figure 3.3-9B Revision 49

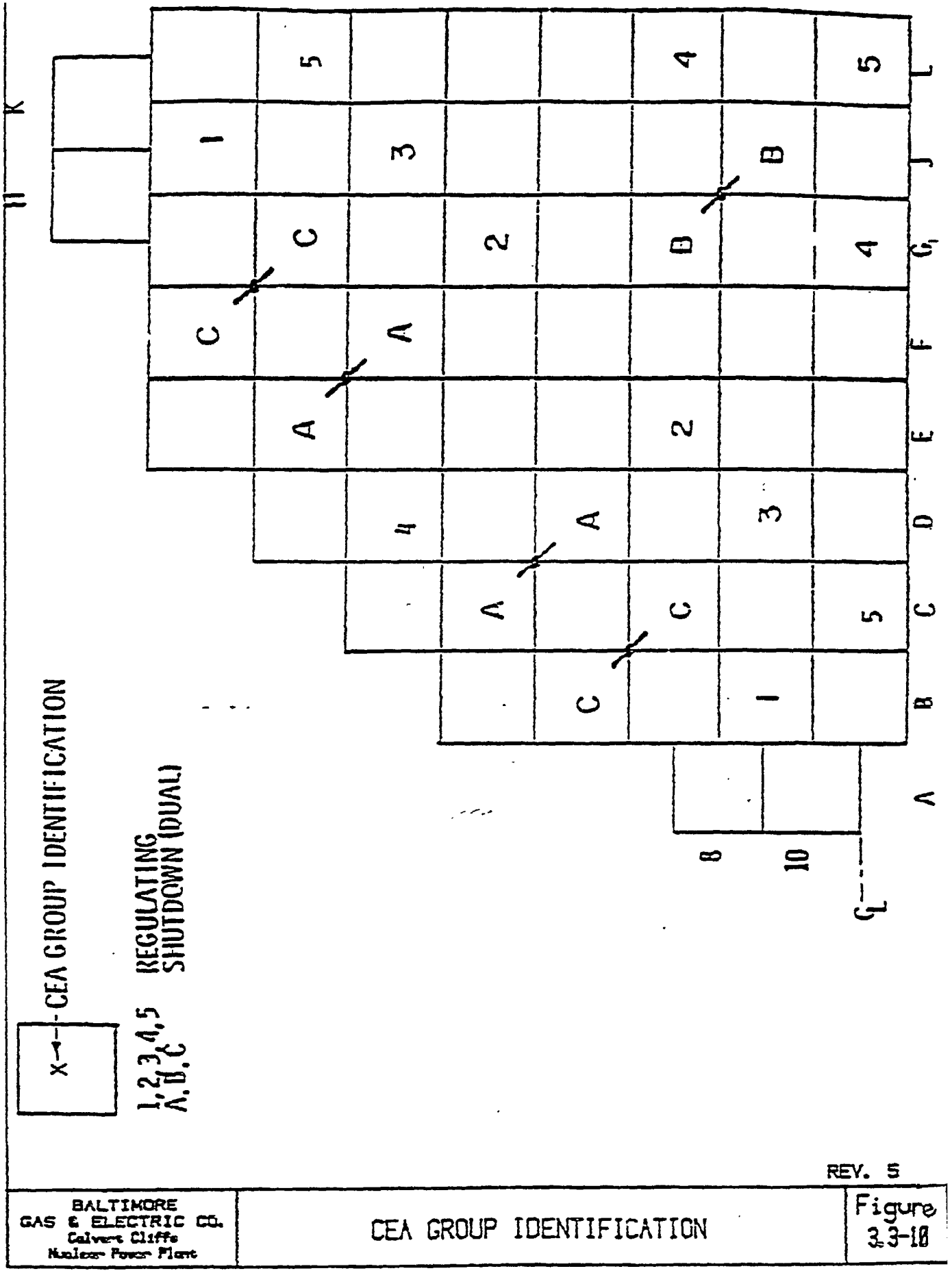
CEA GROUP IDENTIFICATION
REGULATING
SHUTDOWN (DUAL)
1,2,3,4,5
A,B,C
BALTIMORE
GAS & ELECTRIC CO.
Calvert Cliffs
Nuclear Power Plant
CEA GROUP IDENTIFICATION
Figure
3.3-10
REV. 5

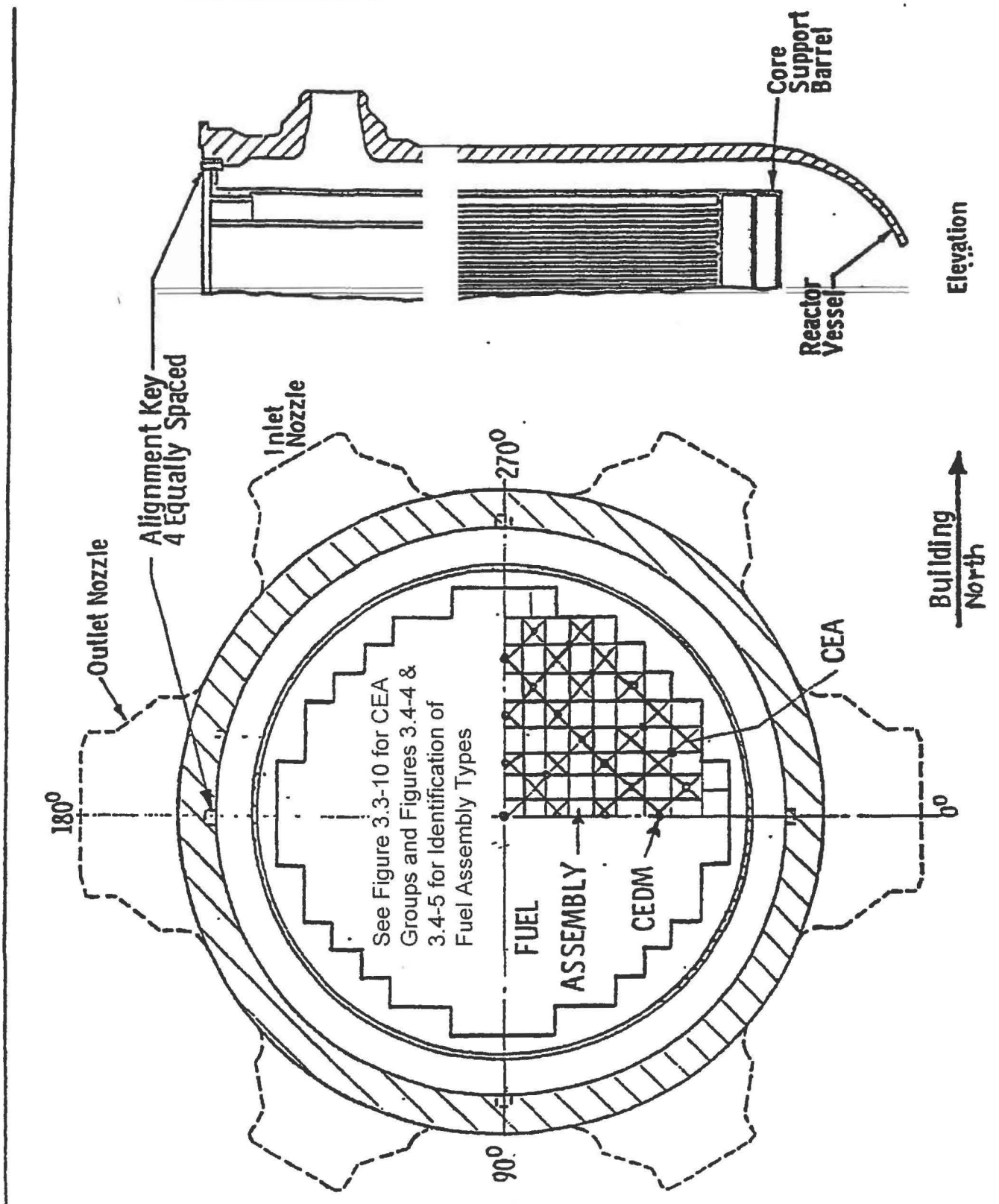

BALTIMORE GAS & ELECTRIC CO. Calvert Cliffs Nuclear Power Plant	Core Orientation	Figure 3.3-11

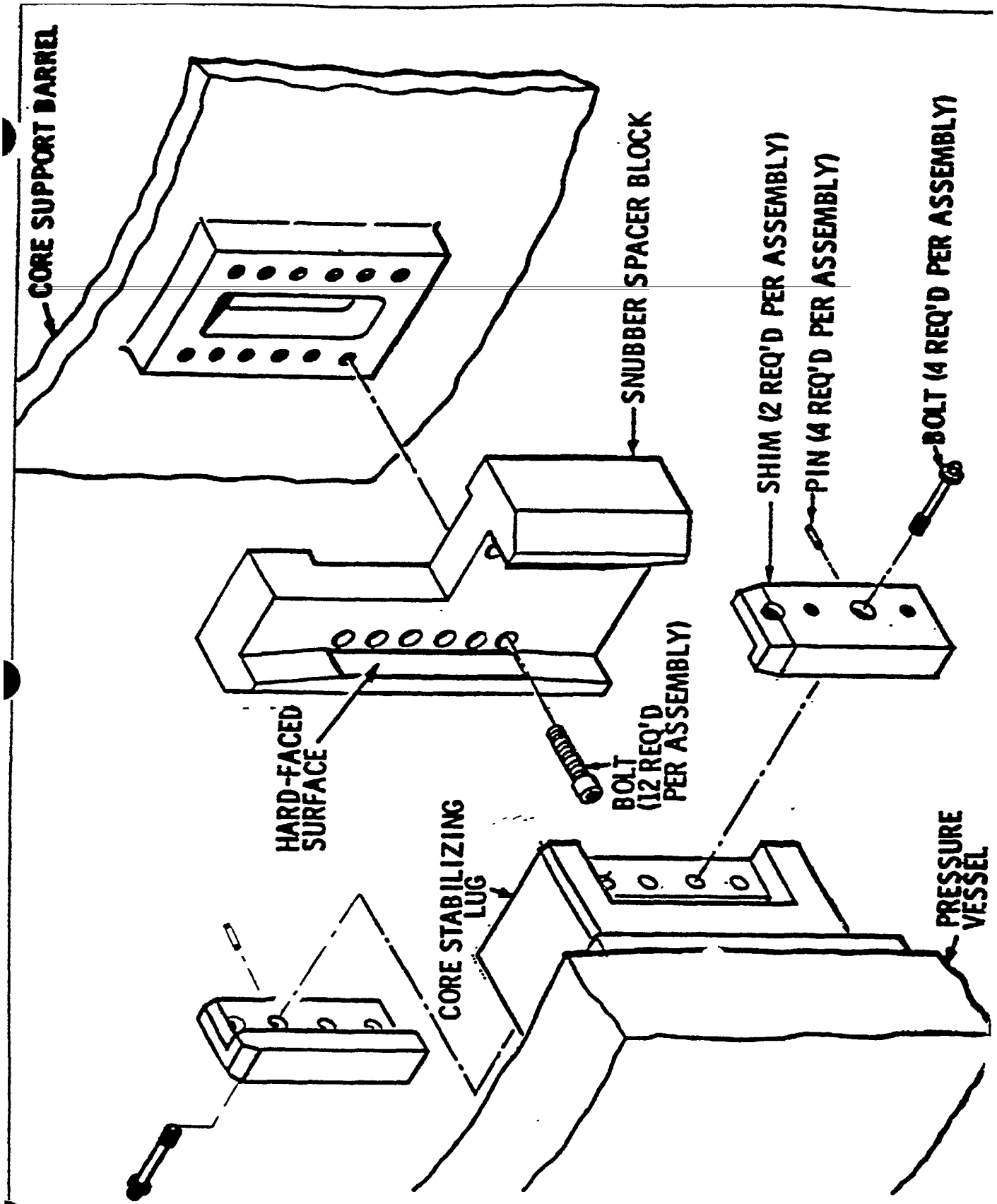

BALTIMORE GAS & ELECTRIC CO. Calvert Cliffs Nuclear Power Plant	Pressure Vessel - Core Support Barrel Snubber Assembly	REV. 11 1/91	Figure 3.3-12

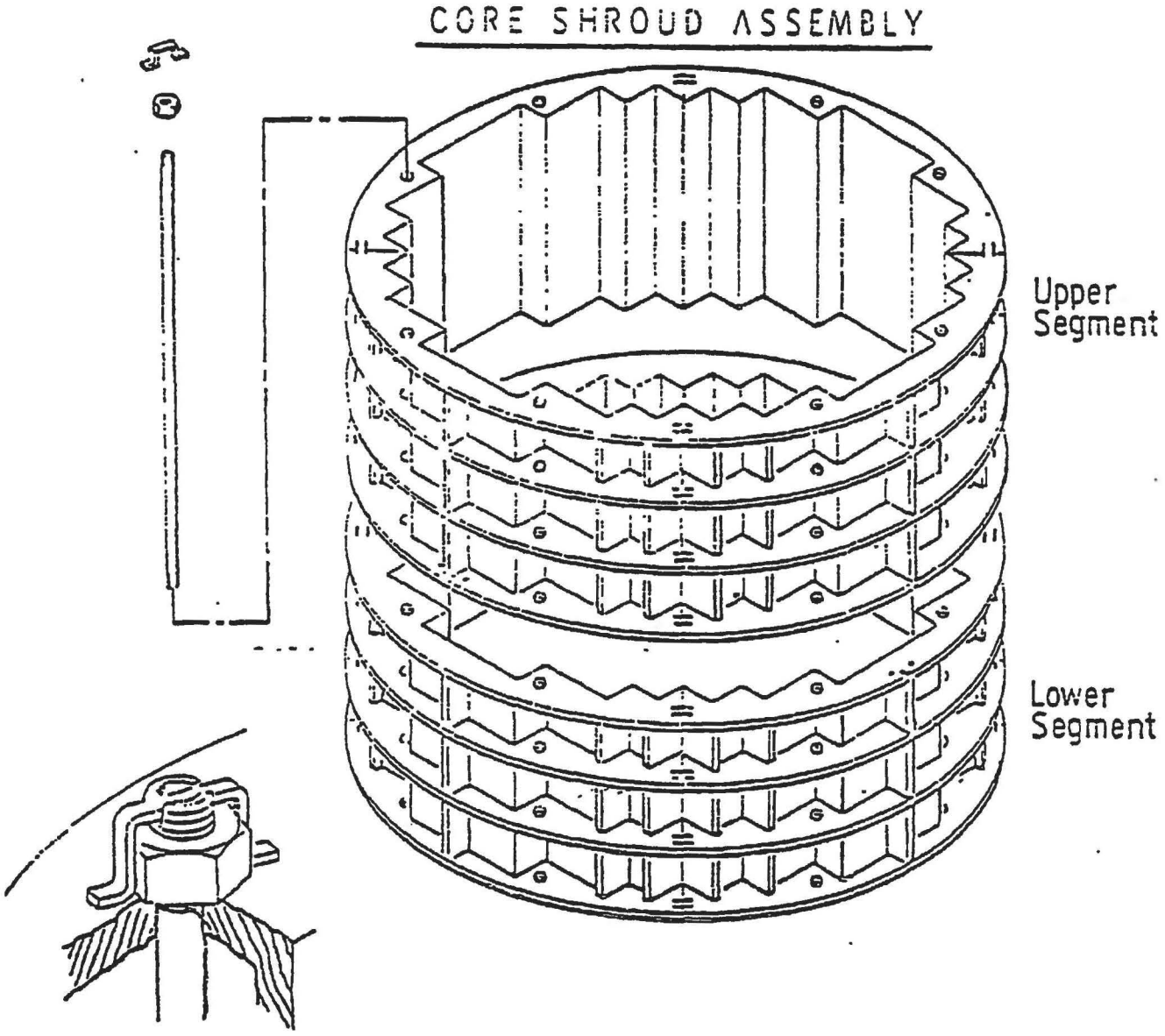

BALTIMORE GAS & ELECTRIC CO.
Calvert Cliffs Nuclear Power Plant

CORE SHROUD ASSEMBLY

Figure 3.3-13

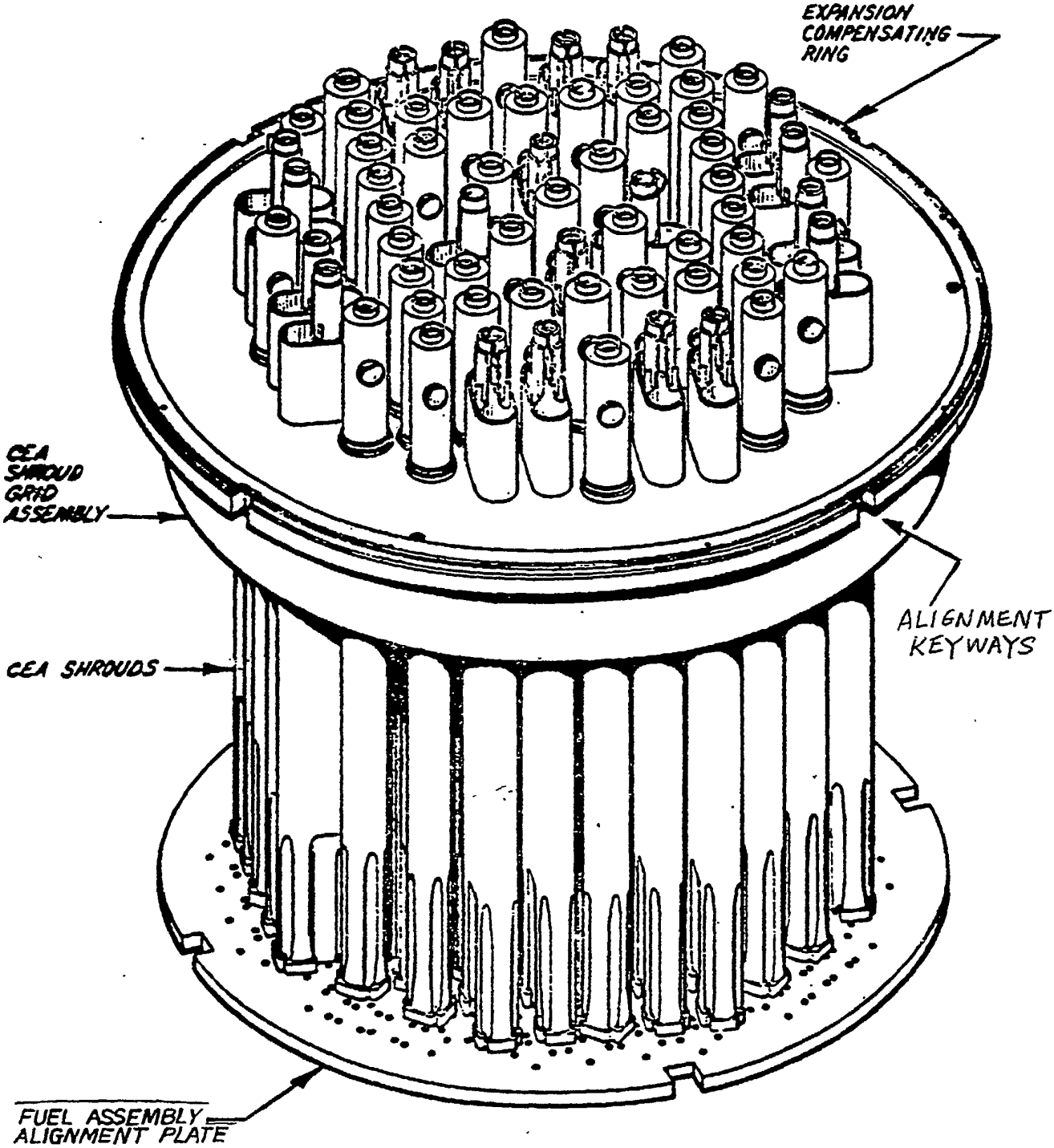

BALTIMORE GAS & ELECTRIC CO. Calvert Cliffs Nuclear Power Plant	UPPER GUIDE STRUCTURE ASSEMBLY	Figure 3.3-14

Revision 21

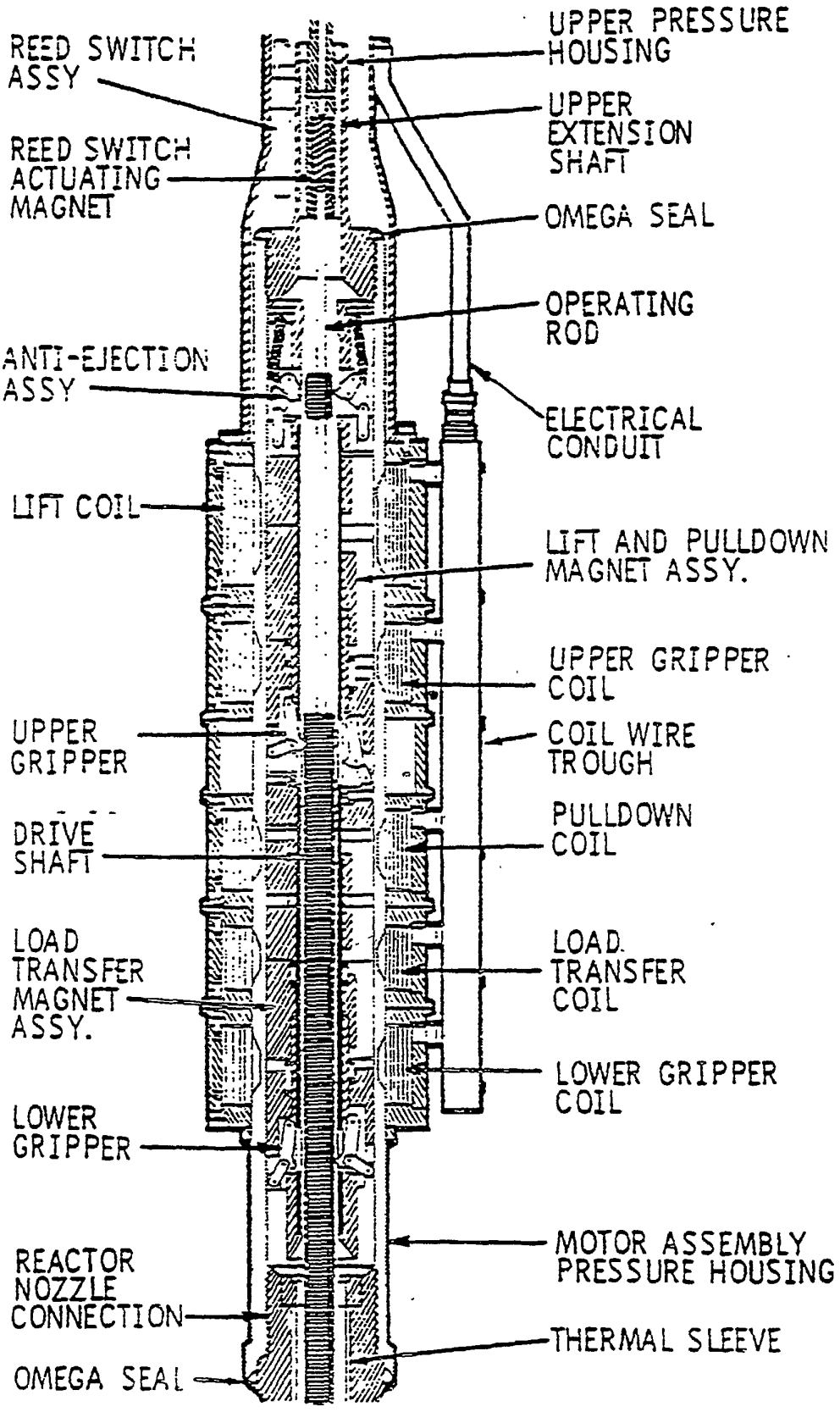

BALTIMORE GAS & ELECTRIC CO. Calvert Cliffs Nuclear Power Plant	CONTROL ELEMENT DRIVE MECHANISM (MAGNETIC JACK)	Figure 3.3-15

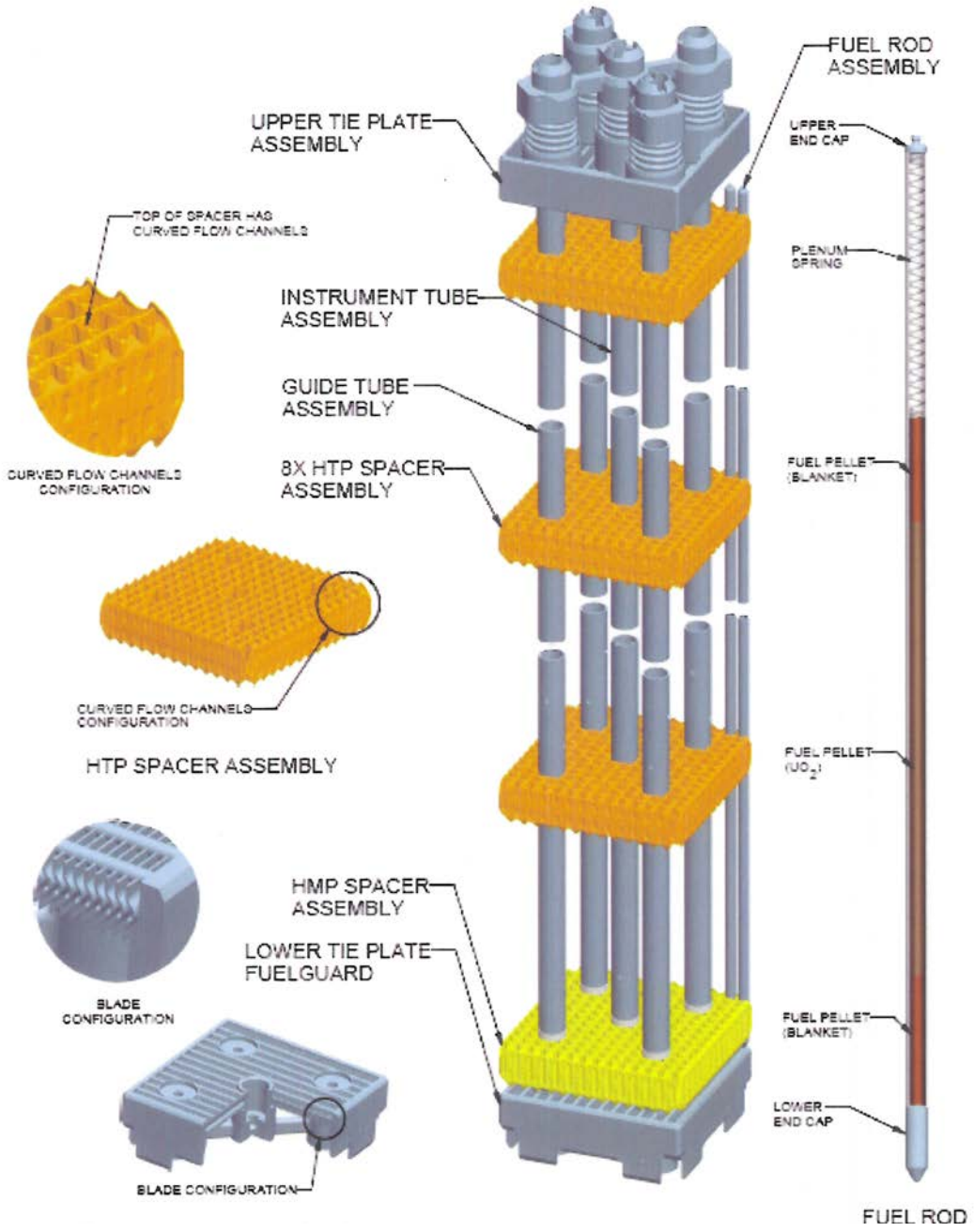

Calvert Cliffs Nuclear Power Plant	AREVA/FRAMATOME HTP FUEL ASSEMBLY, FUEL ROD, AND SPACER GRIDS	Figure 3.3-16 Revision 51

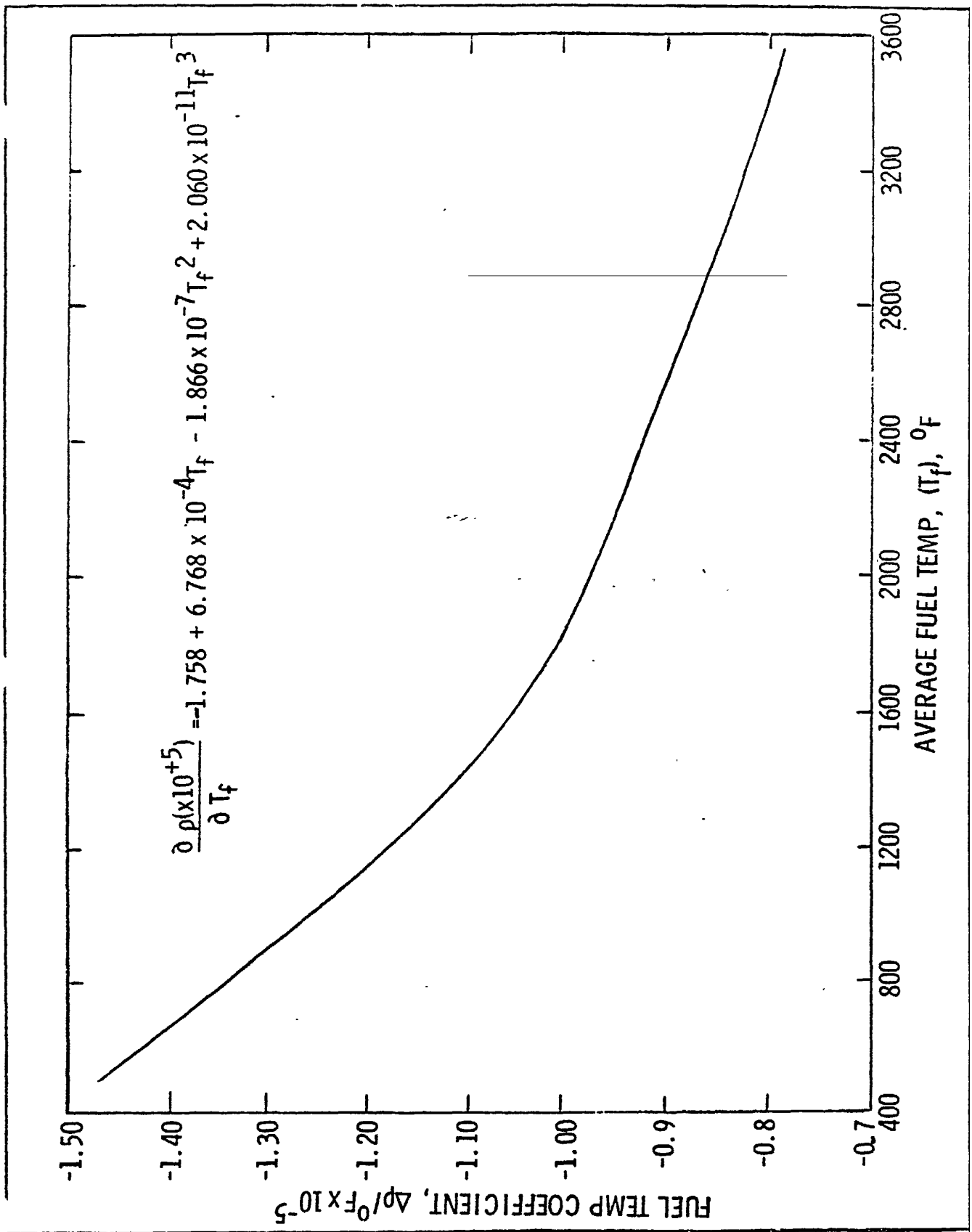

BALTIMORE GAS & ELECTRIC CO. Calvert Cliffs Nuclear Power Plant	CYCLE 1 FUEL TEMPERATURE COEFFICIENT VS AVERAGE FUEL TEMPERATURE	Figure 3.4-1

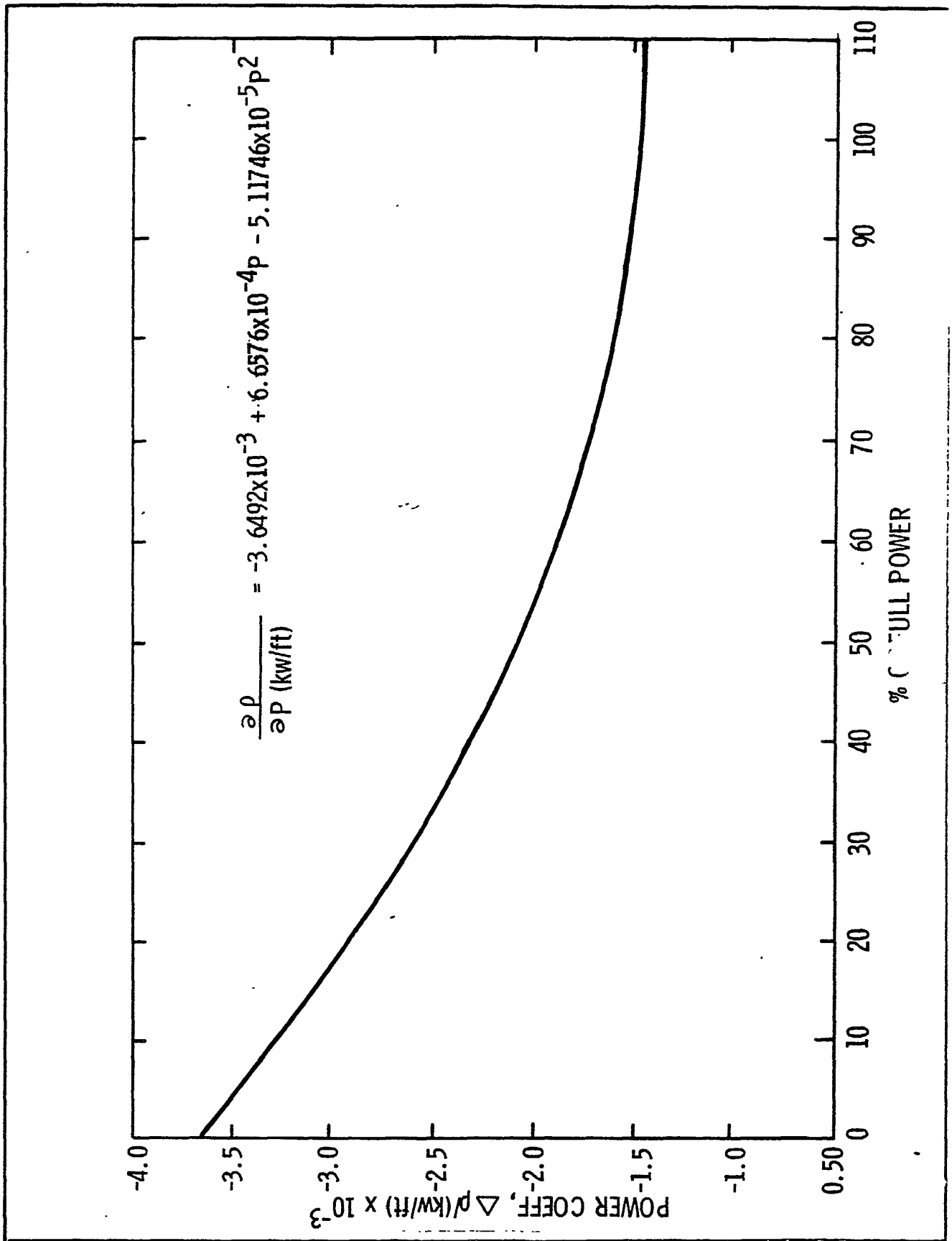

BALTIMORE GAS & ELECTRIC CO. Calvert Cliffs Nuclear Power Plant	CYCLE 1 POWER COEFFICIENT VS PERCENT OF FULL POWER (BEGINNING OF FIRST CYCLE)	Figure 3.4-2

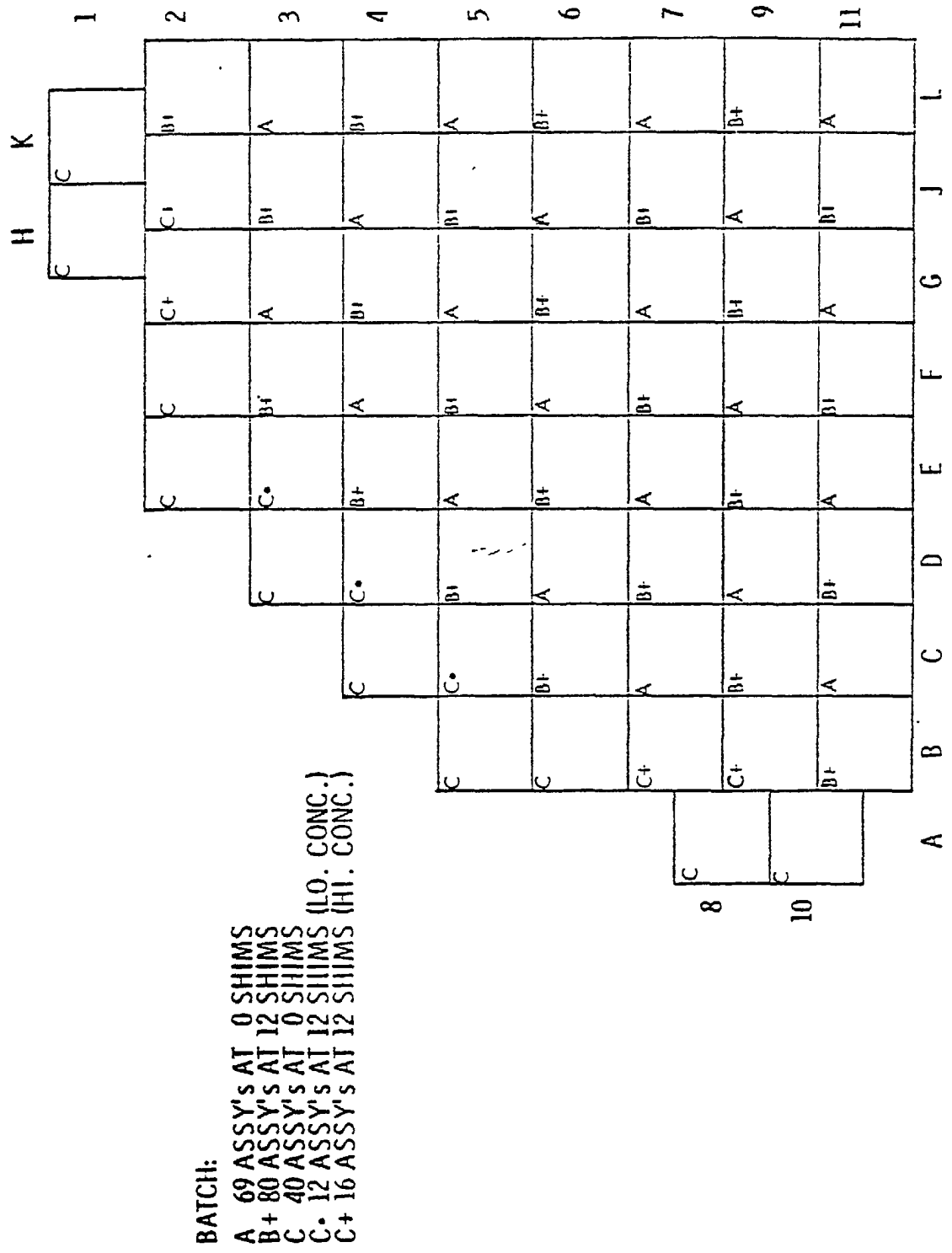

BALTIMORE GAS & ELECTRIC CO. Calvert Cliffs Nuclear Power Plant	FIRST CYCLE FUEL ASSEMBLY IDENTIFICATION BOTH UNITS	FIGURE 3.4-3 Rev. 0 1/82

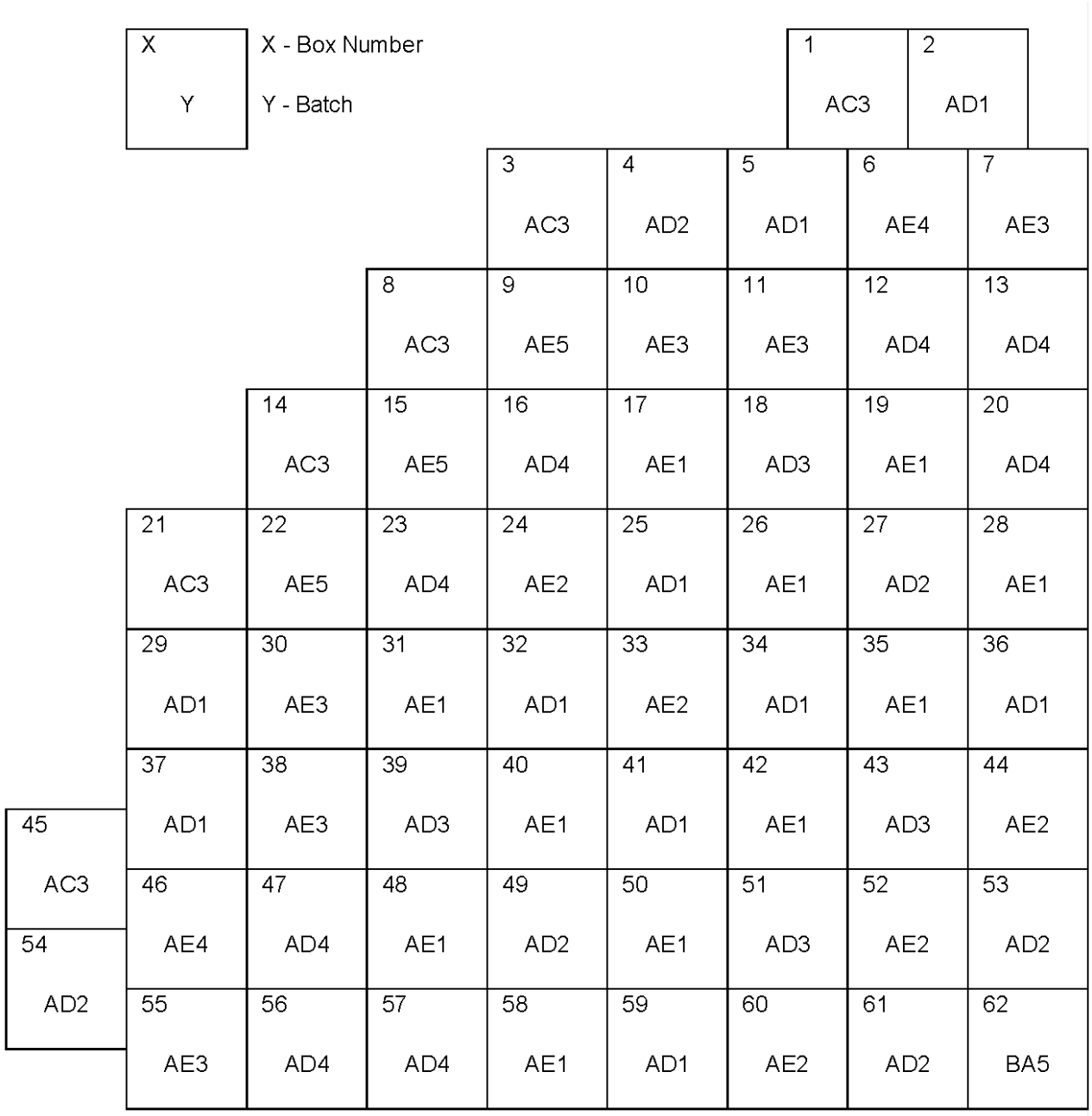

Calvert Cliffs Nuclear Power Plant	UNIT 1 CYCLE 24 CORE MAP	Figure 3.4-4 Revision 50

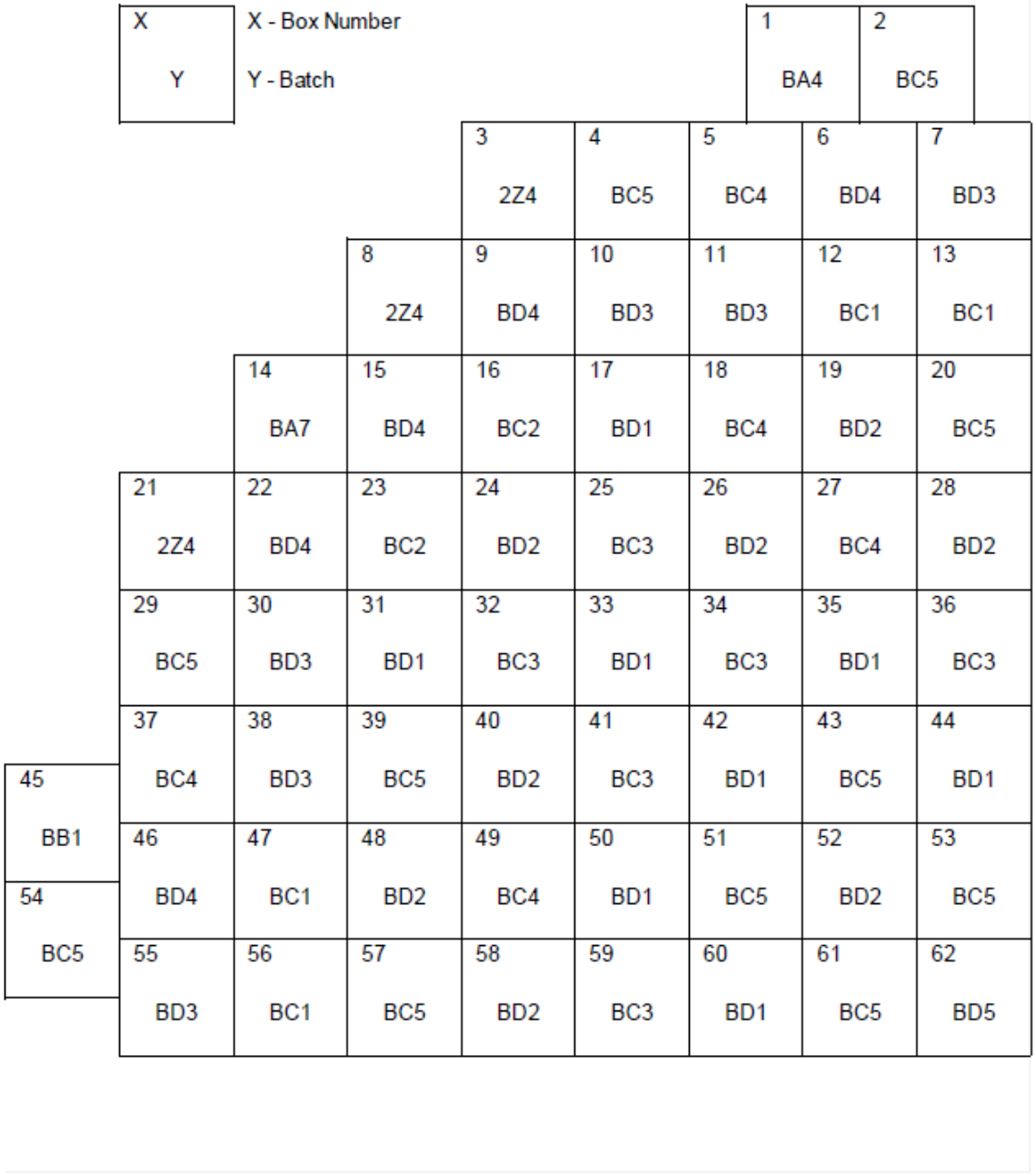

Figure 3-4 Quarter-Core Assembly Map*

* Due to core redesign, Unit 2 Cycle 23 will not be quarter core symmetric.

Calvert Cliffs Nuclear Power Plant	UNIT 2 QUARTER-CORE ASSEMBLY MAP	Figure 3.4-5 Revision 51

X
0.00 ← BOX PEAKING FACTOR 0.00 ← ENTHALPY RISE FACTOR 0.00 ← PIN PEAKING FACTOR

X — ENRICHMENT TYPE

MAXIMA

BOX PEAKING FACTOR 1.29
ENTHALPY RISE FACTOR 1.36
PIN PEAKING FACTOR 1.39

	H	K
1	C 0.57 0.94 0.96	C 0.75 1.03 1.05

	B		D	E	F	G	J	L
2				C 0.54 0.90 0.92	C 0.76 1.05 1.08	C+ 0.91 1.19 1.19	C+ 1.05 1.16 1.19	B+ 0.92 1.04 1.06
3			C 0.63 0.98 1.00	C• 0.94 1.11 1.13	B+ 0.92 1.05 1.07	A 0.99 1.06 1.09	B+ 1.03 1.13 1.15	A 1.02 1.10 1.13
4		C 0.63 0.98 1.00	C• 0.98 1.13 1.16	B+ 0.95 1.07 1.09	A 1.01 1.08 1.12	B+ 1.08 1.18 1.20	A 1.09 1.16 1.20	B+ 1.12 1.20 1.23
5	C 0.54 0.90 0.92	C• 0.94 1.11 1.13	B+ 0.95 1.07 1.09	A 1.02 1.09 1.13	B+ 1.10 1.20 1.22	A 1.12 1.20 1.23	B+ 1.17 1.26 1.28	A 1.16 1.24 1.27
6	C 0.76 1.05 1.08	B+ 0.92 1.05 1.07	A 1.01 1.08 1.12	B+ 1.10 1.20 1.22	A 1.13 1.21 1.25	B+ 1.19 1.29 1.31	A 1.20 1.28 1.32	B+ 1.23 1.31 1.34
7	C+ 0.91 1.19 1.19	A 0.99 1.06 1.09	B+ 1.08 1.18 1.20	A 1.12 1.20 1.23	B+ 1.19 1.29 1.31	A 1.21 1.29 1.33	B+ 1.26 1.34 1.37	A 1.24 1.32 1.36
9	C+ 1.05 1.16 1.19	B+ 1.03 1.13 1.15	A 1.09 1.16 1.20	B+ 1.17 1.26 1.28	A 1.20 1.28 1.32	B+ 1.26 1.34 1.37	A 1.26 1.34 1.38	B+ 1.29 1.36 1.39
11	B+ 0.92 1.04 1.06	A 1.02 1.10 1.13	B+ 1.12 1.20 1.23	A 1.16 1.24 1.27	B+ 1.23 1.31 1.34	A 1.24 1.32 1.36	B+ 1.29 1.36 1.39	A 1.27 1.35 1.39

	A
8	C 0.57 0.94 0.96
10	C 0.75 1.03 1.05

℄

BALTIMORE GAS & ELECTRIC CO. Calvert Cliffs Nuclear Power Plant	CYCLE 1 CORE POWER DISTRIBUTION 2560 MWT (BEGINNING-OF-LIFE) NO XENON	Figure 3.4-6 Rev. 0

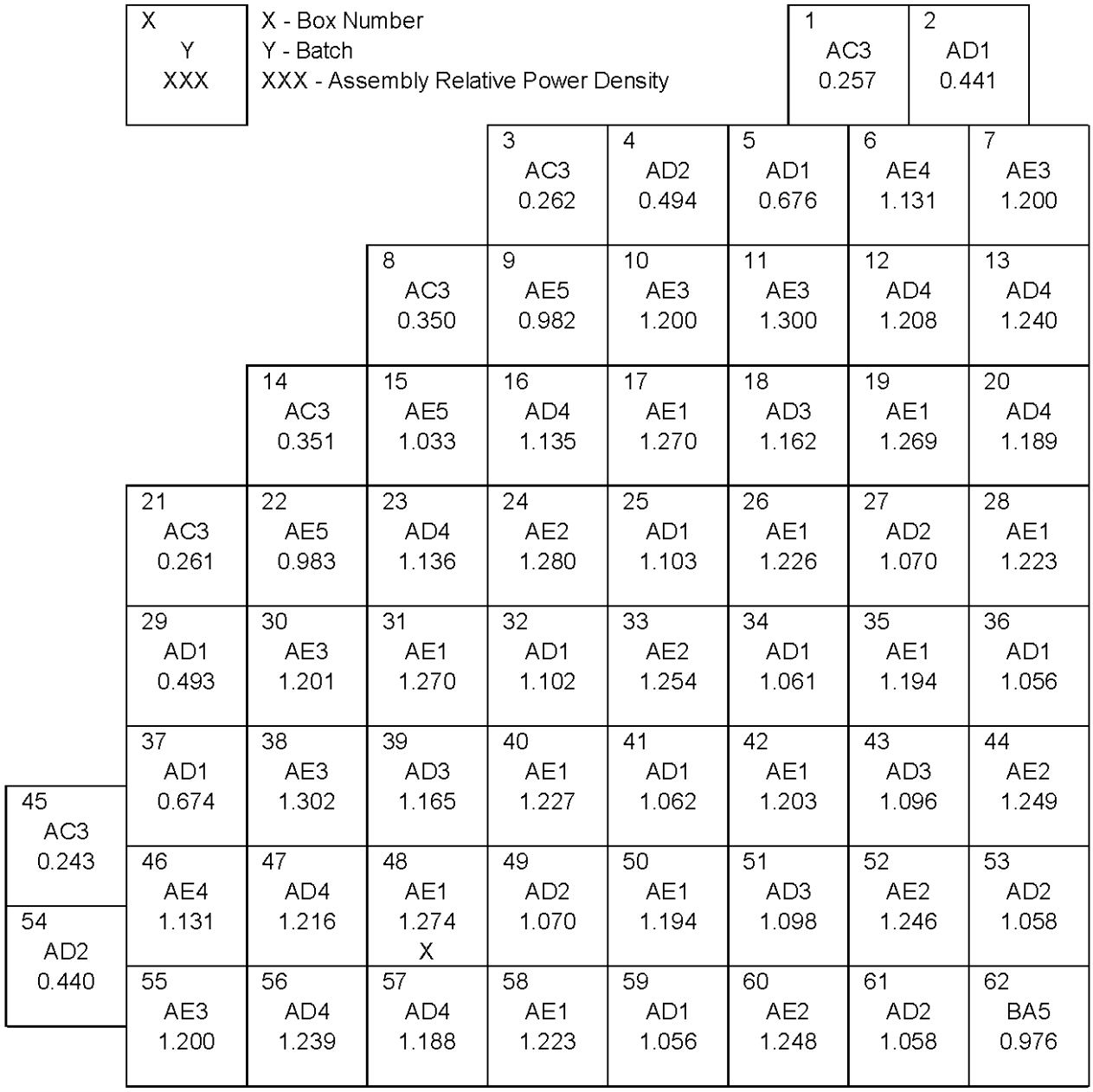

Long N-1 Burnup (21.940 GWd/MTU)

Note: X = Maximum Fr Value = 1.544

Calvert Cliffs Nuclear Power Plant	UNIT 1 CYCLE 24 ASSEMBLY RELATIVE POWER DENSITY AT BOC, HFP, ARO, EQUILIBRIUM XENON	Figure 3.4-7 Revision 50

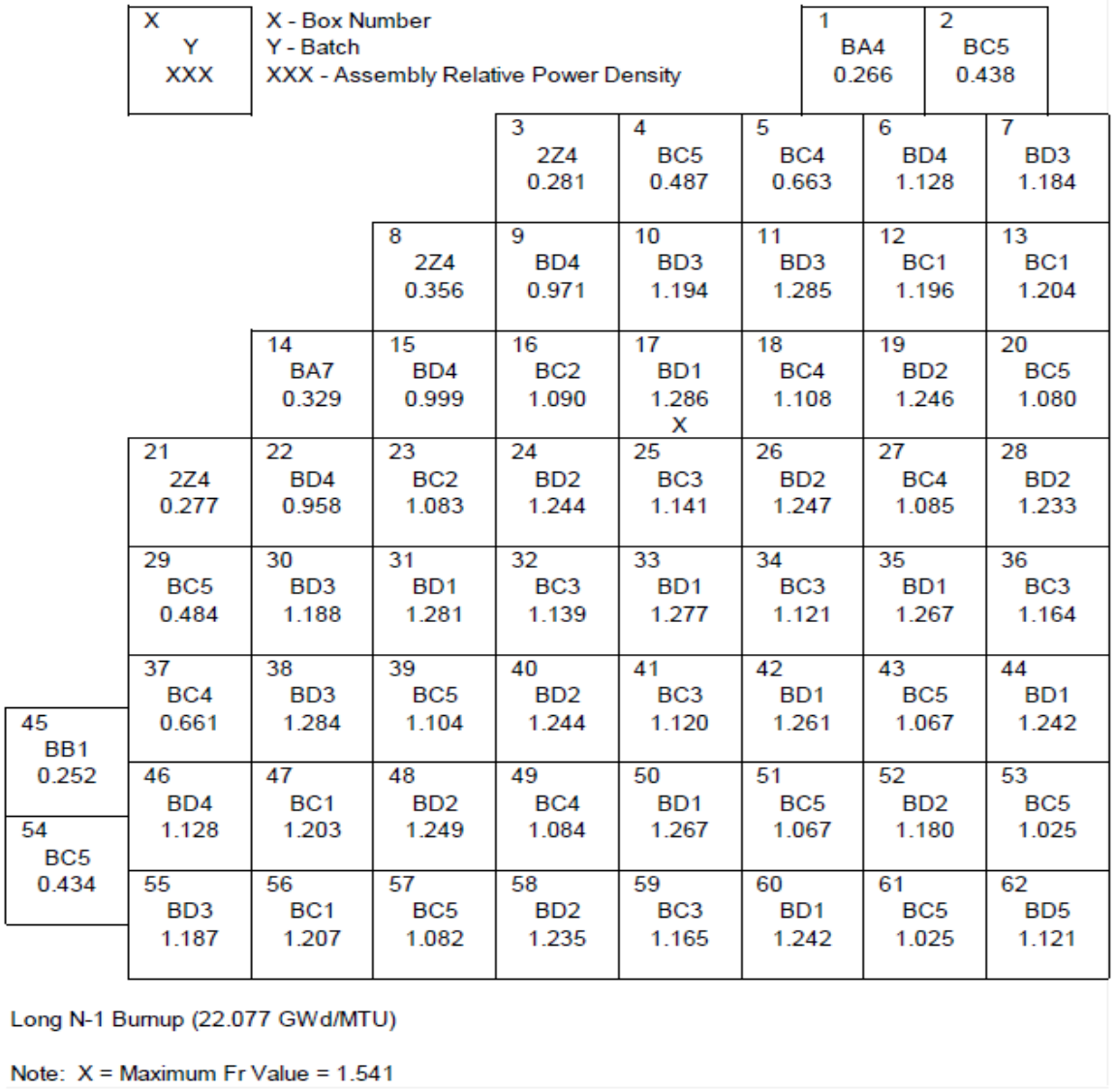

Long N-1 Burnup (22.077 GWd/MTU)

Note: X = Maximum Fr Value = 1.541

Figure 3-5 Assembly Relative Power Density at BOC, HFP, ARO, Equilibrium Xenon*

* Due to core redesign, Unit 2 Cycle 23 will not be quarter core symmetric.

Calvert Cliffs Nuclear Power Plant	UNIT 2 ASSEMBLY RELATIVE POWER DENSITY AT BOC, HFP, ARO, EQUILIBRIUM XENON	Figure 3.4-8 Revision 51

Legend: X = ENRICHMENT TYPE; 0.00 = BOX PEAKING FACTOR; 0.00 = ENTHALPY RISE FACTOR; 0.00 = PIN PEAKING FACTOR

MAXIMA

BOX PEAKING FACTOR 1.31
ENTHALPY RISE FACTOR 1.38
PIN PEAKING FACTOR 1.41

Row	A	B	C	D	E	F	G	H	J	K	L
1								C 0.54 0.90 0.92		C 0.71 0.98 1.00	
2					C 0.53 0.87 0.89	C 0.74 1.02 1.05	C+ 0.89 1.17 1.18		C+ 1.03 1.15 1.18		B+ 0.91 1.03 1.05
3				C 0.61 0.96 0.98	C• 0.93 1.10 1.13	B+ 0.91 1.06 1.07	A 0.98 1.06 1.10		B+ 1.03 1.14 1.16		A 1.02 1.10 1.13
4			C 0.61 0.96 0.98	C• 0.96 1.13 1.16	B+ 0.95 1.08 1.10	A 1.02 1.09 1.13	B+ 1.09 1.19 1.21		A 1.10 1.17 1.21		B+ 1.13 1.22 1.24
5		C 0.53 0.87 0.89	C• 0.93 1.10 1.13	B+ 0.95 1.08 1.10	A 1.03 1.10 1.14	B+ 1.11 1.22 1.24	A 1.14 1.21 1.25		B+ 1.19 1.28 1.30		A 1.17 1.25 1.29
6		C 0.74 1.02 1.05	B+ 0.91 1.06 1.07	A 1.02 1.09 1.13	B+ 1.11 1.22 1.24	A 1.15 1.22 1.26	B+ 1.21 1.31 1.33		A 1.21 1.29 1.33		B+ 1.25 1.33 1.36
7		C+ 0.89 1.17 1.18	A 0.98 1.06 1.10	B+ 1.09 1.19 1.21	A 1.14 1.21 1.25	B+ 1.21 1.31 1.33	A 1.23 1.30 1.34		B+ 1.28 1.36 1.39		A 1.26 1.33 1.37
8	C 0.54 0.90 0.92										
9		C+ 1.03 1.15 1.18	B+ 1.03 1.14 1.16	A 1.10 1.17 1.21	B+ 1.19 1.28 1.30	A 1.21 1.29 1.33	B+ 1.28 1.36 1.39		A 1.27 1.34 1.39		B+ 1.31 1.38 1.41
10	C 0.71 0.98 1.00										
11		B+ 0.91 1.03 1.05	A 1.02 1.10 1.13	B+ 1.13 1.22 1.24	A 1.17 1.25 1.29	B+ 1.25 1.33 1.36	A 1.26 1.33 1.37		B+ 1.31 1.38 1.41		A 1.29 1.36 1.40

℄

BALTIMORE GAS & ELECTRIC CO.
Calvert Cliffs
Nuclear Power Plant

CYCLE 1 CORE POWER DISTRIBUTION
2560 MWT
1000 MWD/MTU, EQUILIBRIUM XENON

FIGURE 3.4-9

Rev. 0 1/82

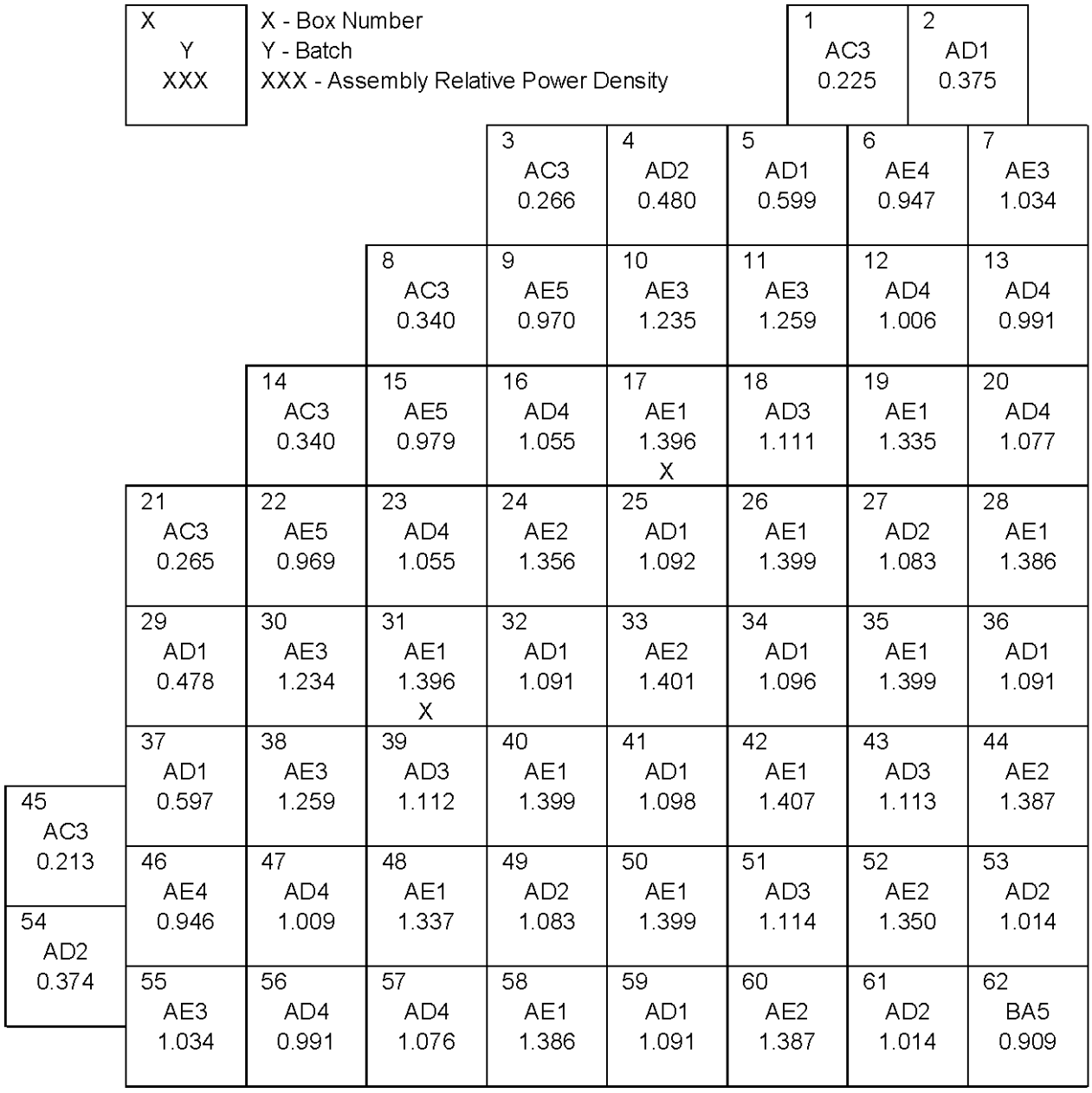

Long N-1 Burnup (21.940 GWd/MTU)

Note: X = Maximum Fr Value = 1.512

Calvert Cliffs Nuclear Power Plant	UNIT 1 CYCLE 24 ASSEMBLY RELATIVE POWER DENSITY AT 10,000 MWd/MTU, HFP, ARO, EQUILIBRIUM XENON	Figure 3.4-10 Revision 50

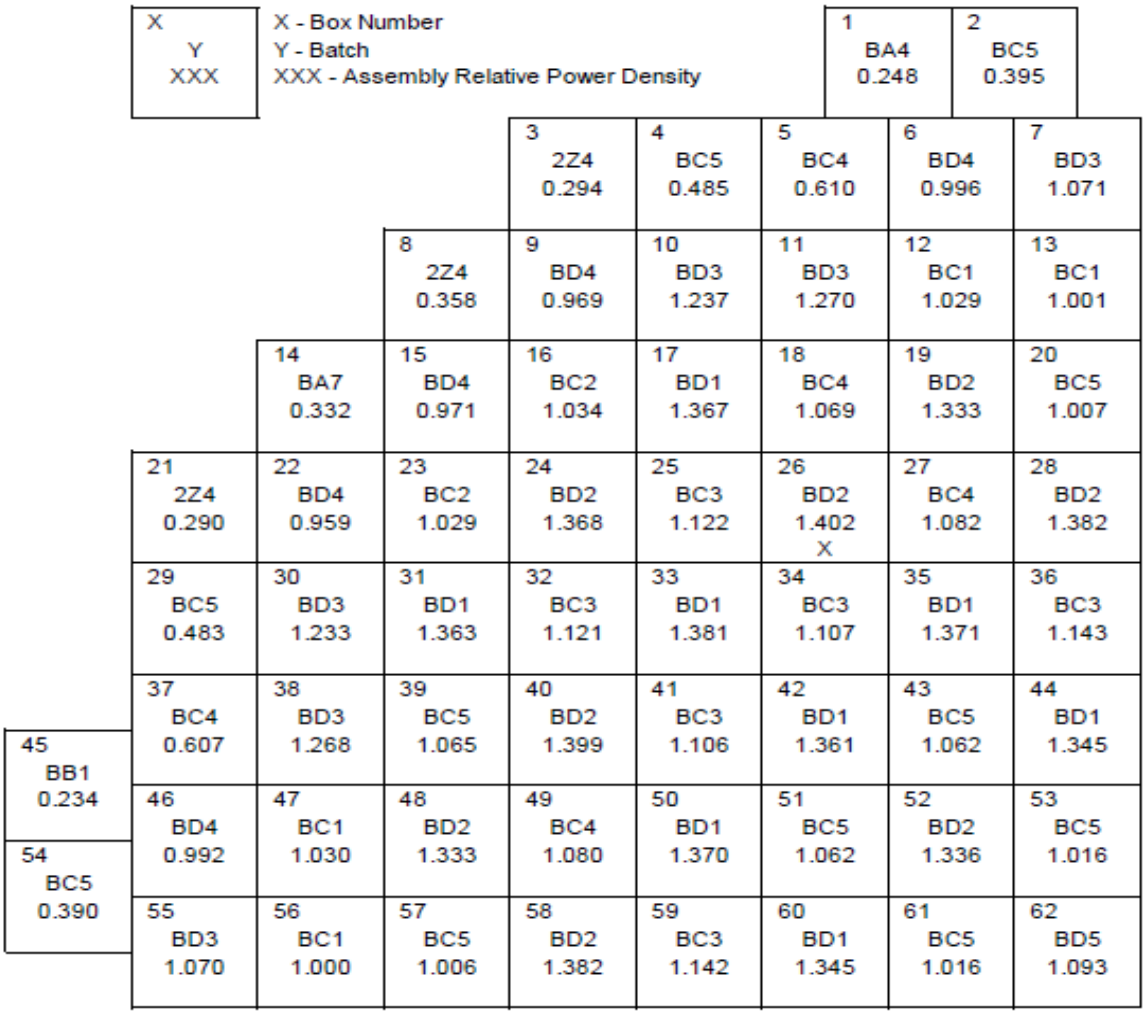

Long N-1 Burnup (22.077 GWd/MTU)

Note: X = Maximum Fr Value = 1.511

Figure 3-6 Assembly Relative Power Density at 10,000 MWd/MTU, HFP, ARO, Equilibrium Xenon*

* Due to core redesign, Unit 2 Cycle 23 will not be quarter core symmetric.

Calvert Cliffs Nuclear Power Plant	UNIT 2 ASSEMBLY RELATIVE POWER DENSITY AT 10,000 MWd/MTU, HFP, ARO, EQUILIBRIUM XENON	Figure 3.4-11 Revision 51

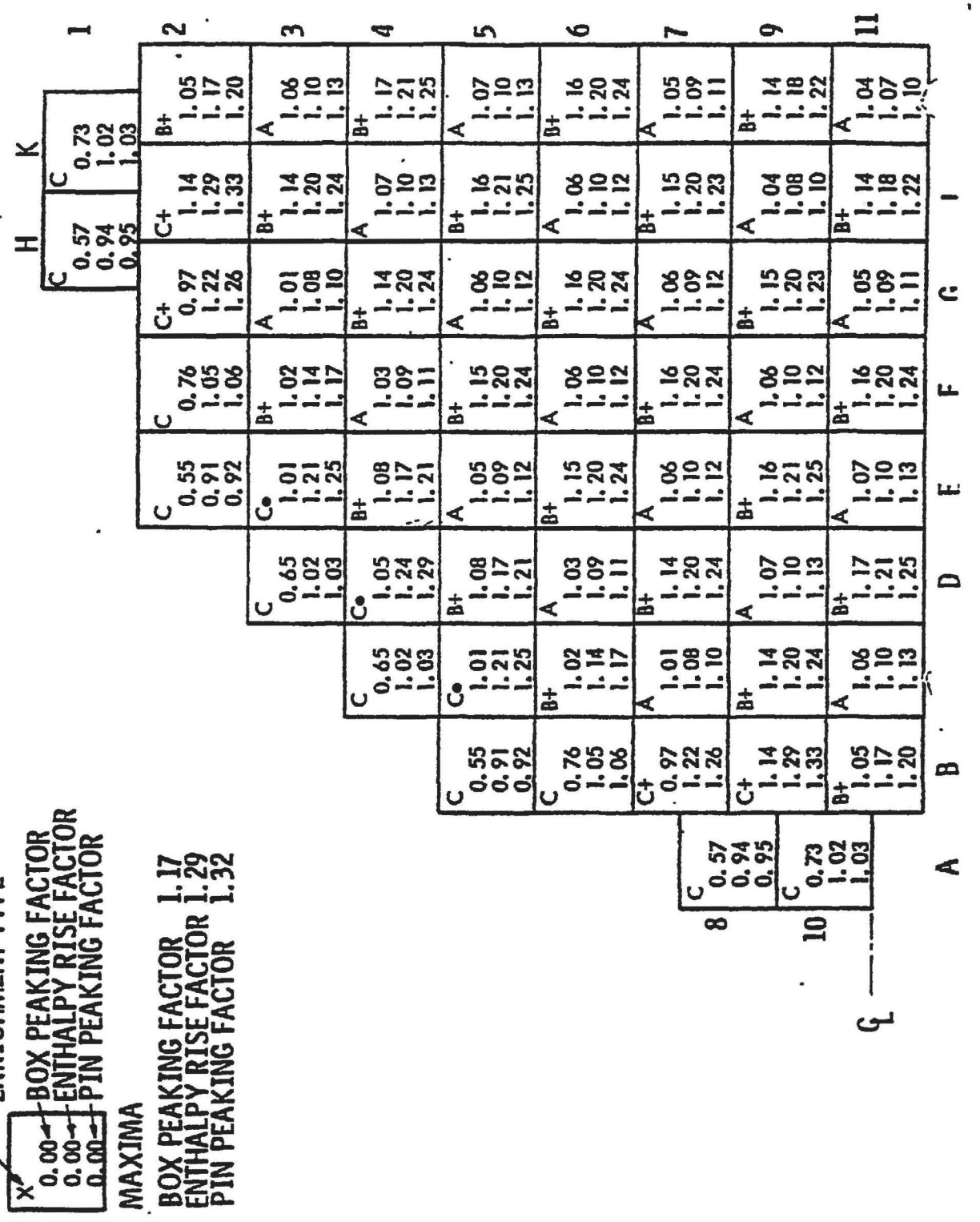

BALTIMORE GAS & ELECTRIC CO. Calvert Cliffs Nuclear Power Plant	CYCLE 1 CORE POWER DISTRIBUTION 2560 MWT END-OF-CYCLE, EQUILIBRIUM XENON	Figure 3.4-12 Rev. 0

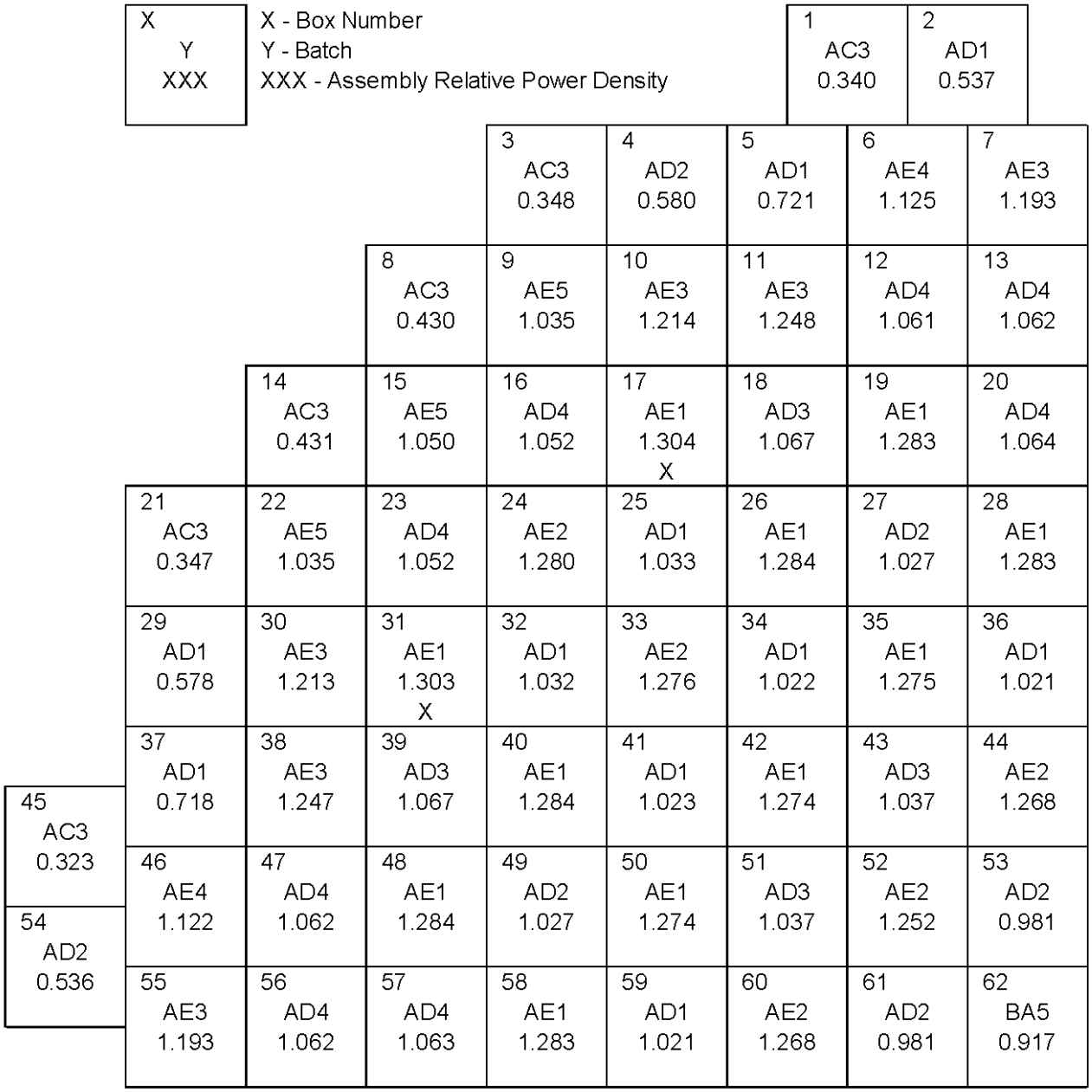

Long N-1 Burnup (21.940 GWd/MTU)

Note: X = Maximum Fr Value = 1.380

Calvert Cliffs Nuclear Power Plant	UNIT 1 CYCLE 24 ASSEMBLY RELATIVE POWER DENSITY AT EOC, HFP, ARO, EQUILIBRIUM XENON	Figure 3.4-13 Revision 50

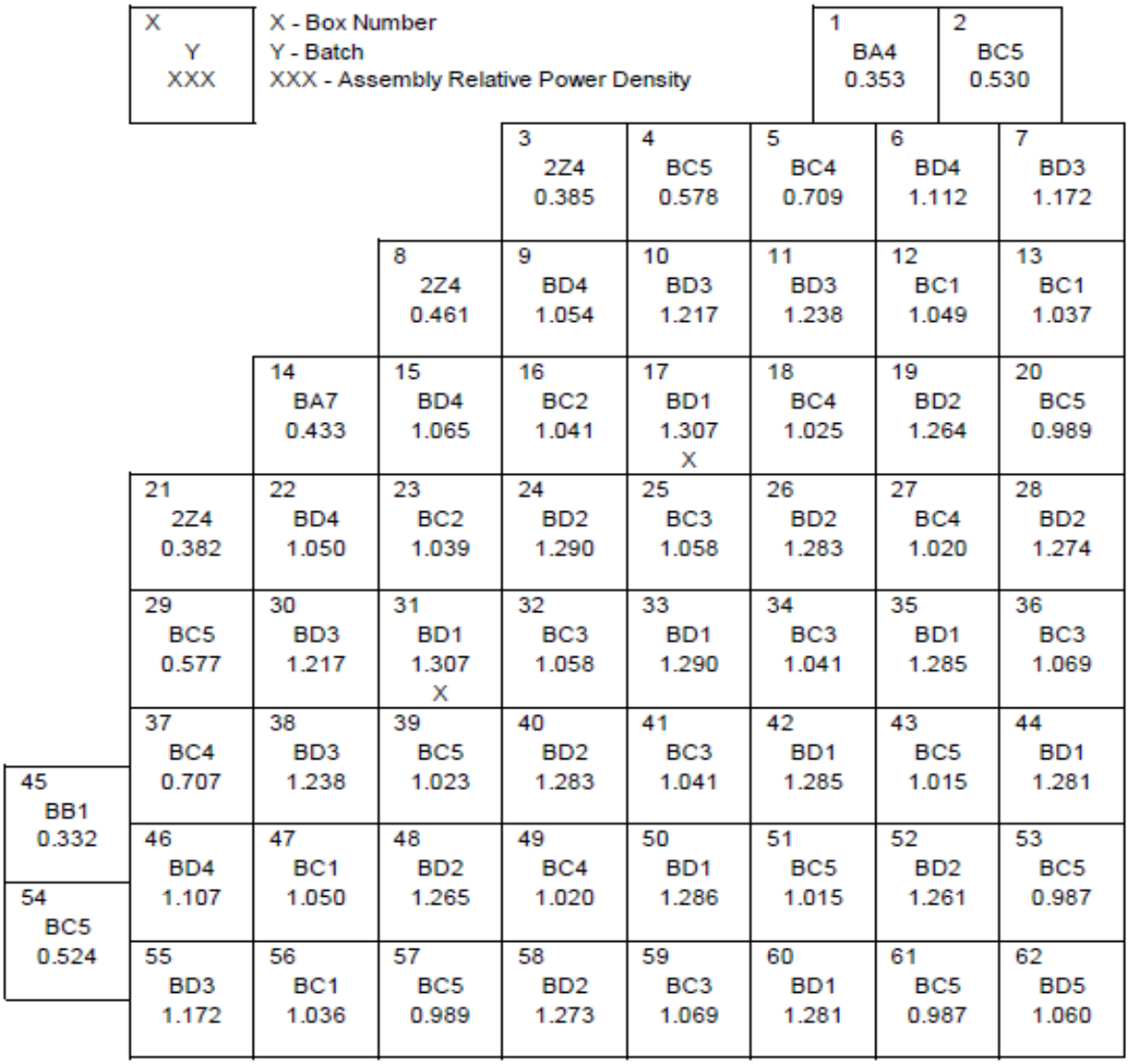

Long N-1 Burnup (22.077 GWd/MTU)

Note: X = Maximum Fr Value = 1.379

Figure 3-7 Assembly Relative Power Density at EOC, HFP, ARO, Equilibrium Xenon*

* Due to core redesign, Unit 2 Cycle 23 will not be quarter core symmetric.

Calvert Cliffs Nuclear Power Plant	UNIT 2 ASSEMBLY RELATIVE POWER DENSITY AT EOC, HFP, ARO, EQUILIBRIUM XENON	Figure 3.4-14 Revision 51

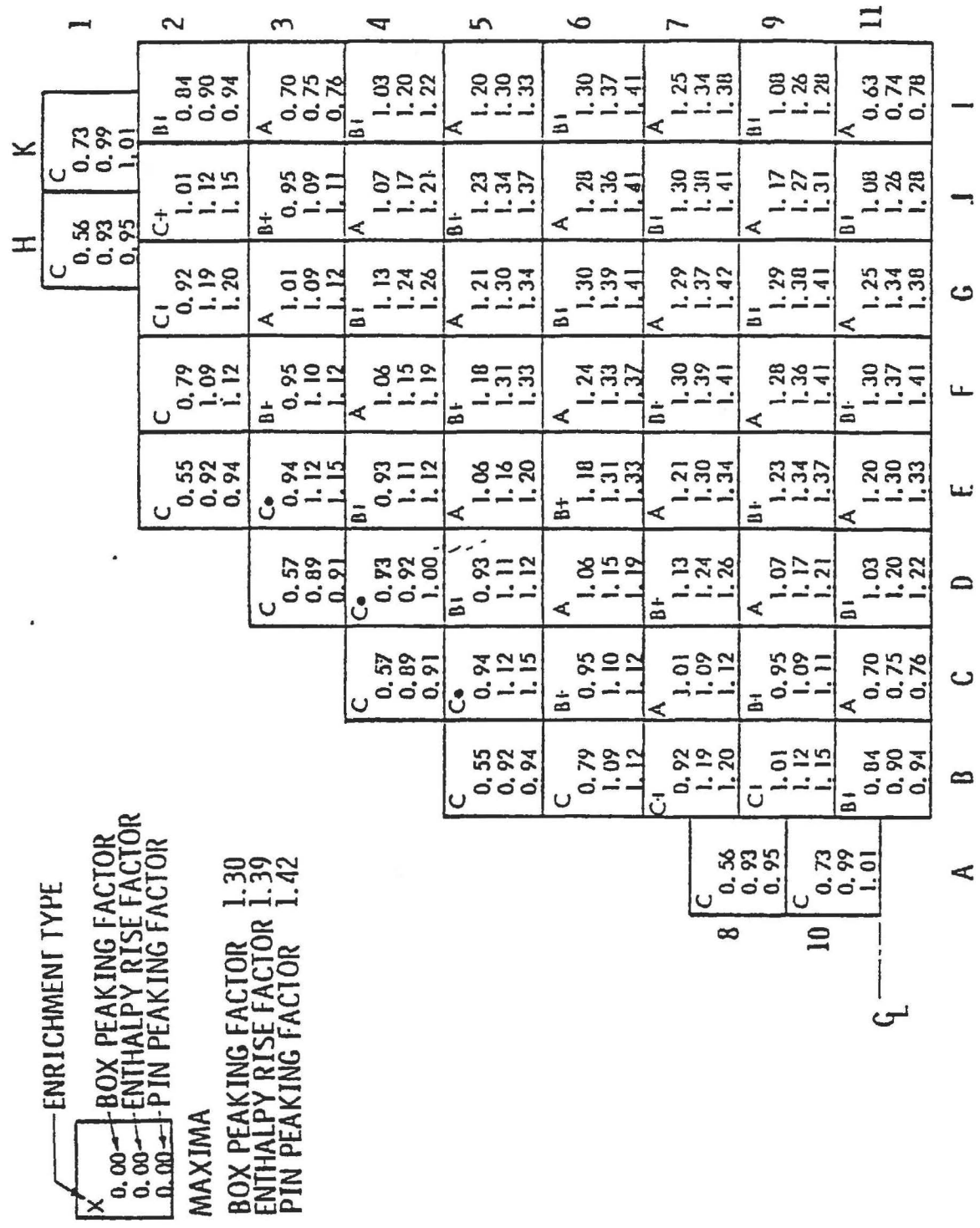

BALTIMORE GAS & ELECTRIC CO. Calvert Cliffs Nuclear Power Plant	CORE POWER DISTRIBUTION - CEA GROUP 5 BEGINNING OF FIRST CYCLE NO XENON	FIGURE 3.4-15 Rev. 0 1/82

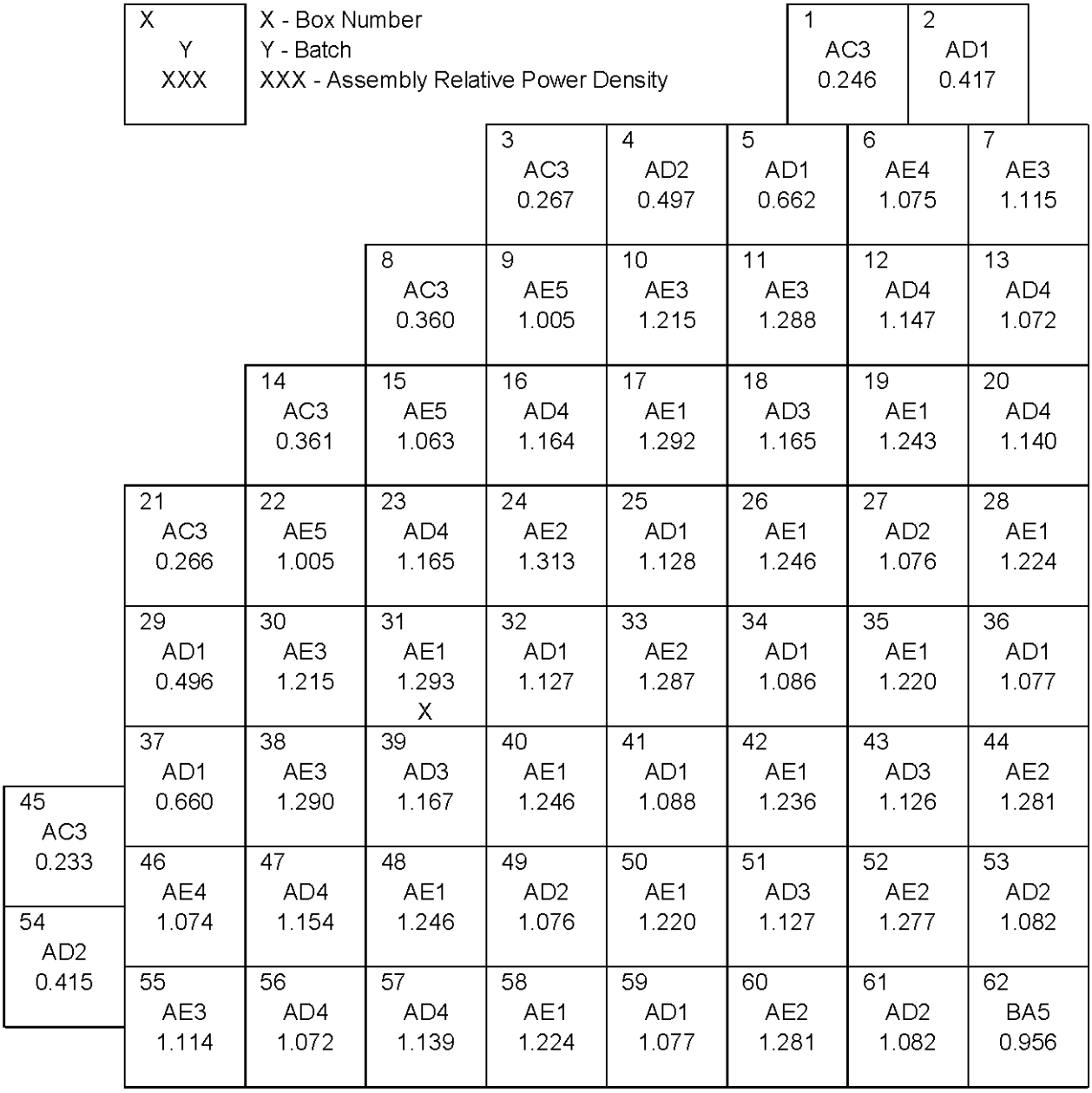

Long N-1 Burnup (21.940 GWd/MTU)

Note: X = Maximum Fr Value = 1.562

Calvert Cliffs Nuclear Power Plant	UNIT 1 CYCLE 24 ASSEMBLY RELATIVE POWER DENSITY WITH BANK 5 INSERTED TO PDIL AT BOC, HFP, EQUILIBRIUM XENON	Figure 3.4-16 Revision 50

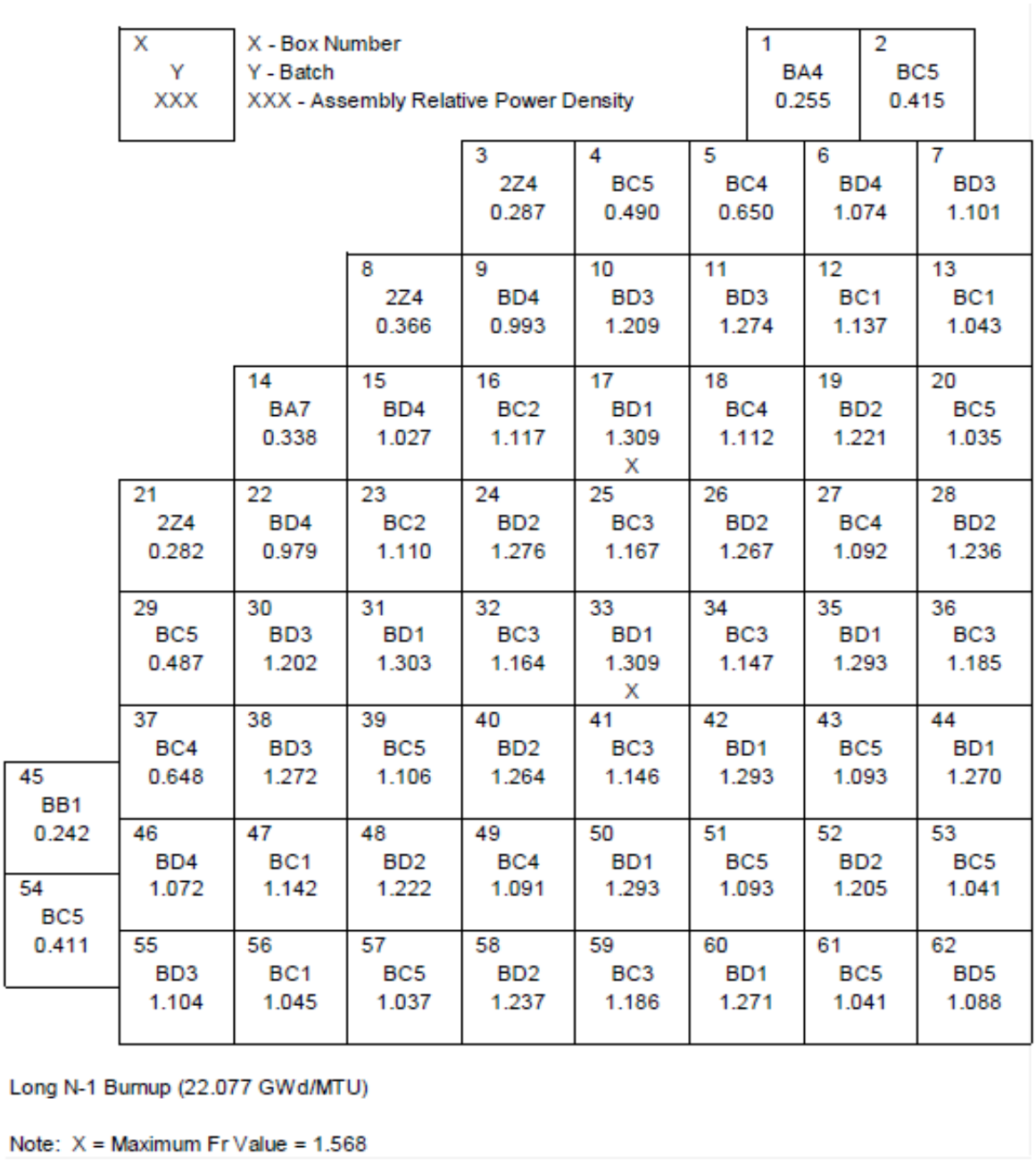

Figure 3-8 Assembly Relative Power Density with Bank 5 Inserted to PDIL at BOC, HFP, Equilibrium Xenon*

* Due to core redesign, Unit 2 Cycle 23 will not be quarter core symmetric.

Calvert Cliffs Nuclear Power Plant	UNIT 2 ASSEMBLY RELATIVE POWER DENSITY AT BANK 5 INSERTED TO PDIL AT BOC, HFP, EQUILIBRIUM XENON	Figure 3.4-17 Revision 51

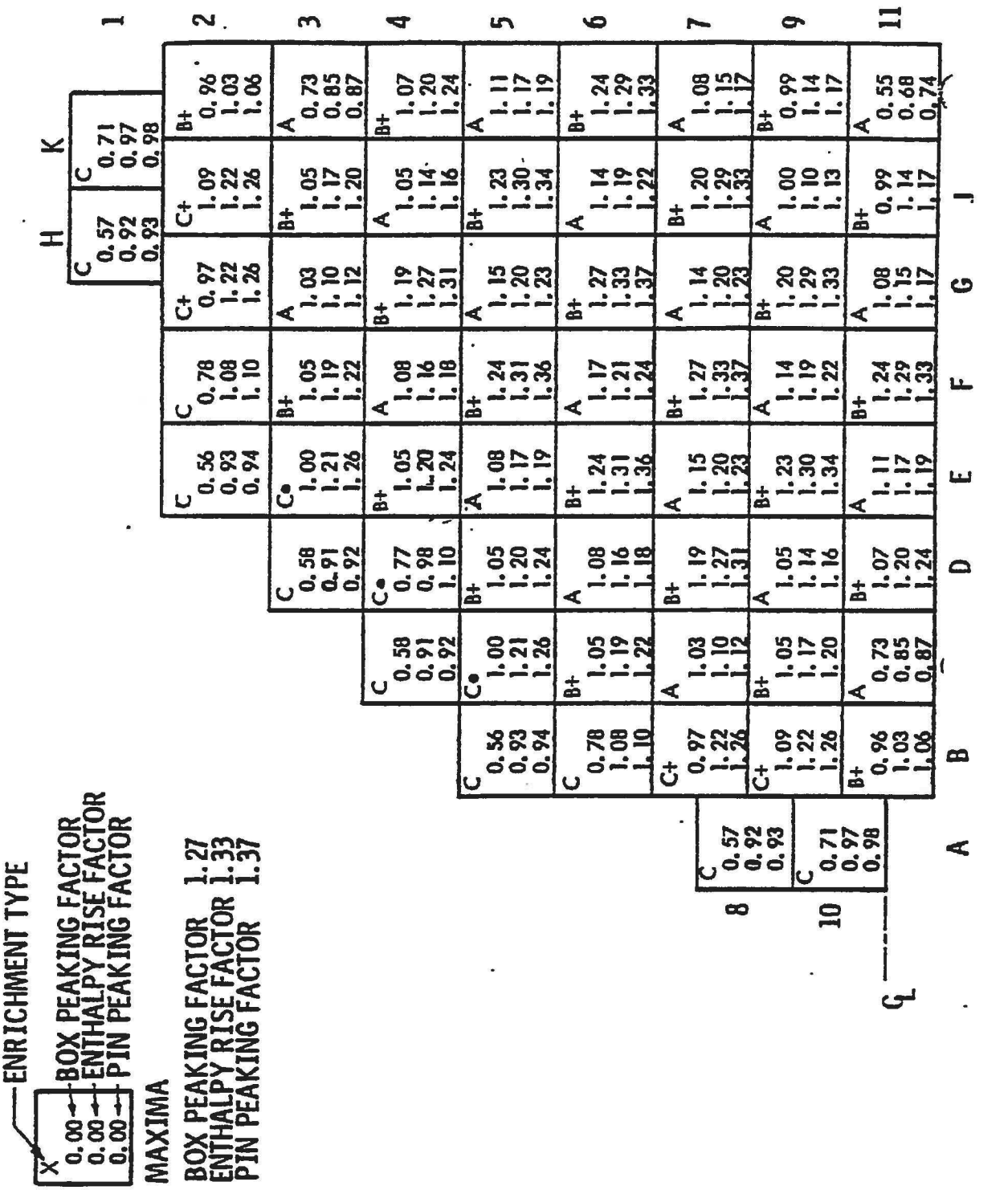

BALTIMORE GAS & ELECTRIC CO. Calvert Cliffs Nuclear Power Plant	CORE POWER DISTRIBUTION - CEA GROUP 5 END-OF-CYCLE 1, EQUILIBRIUM	Figure 3.4-18 Rev. 5

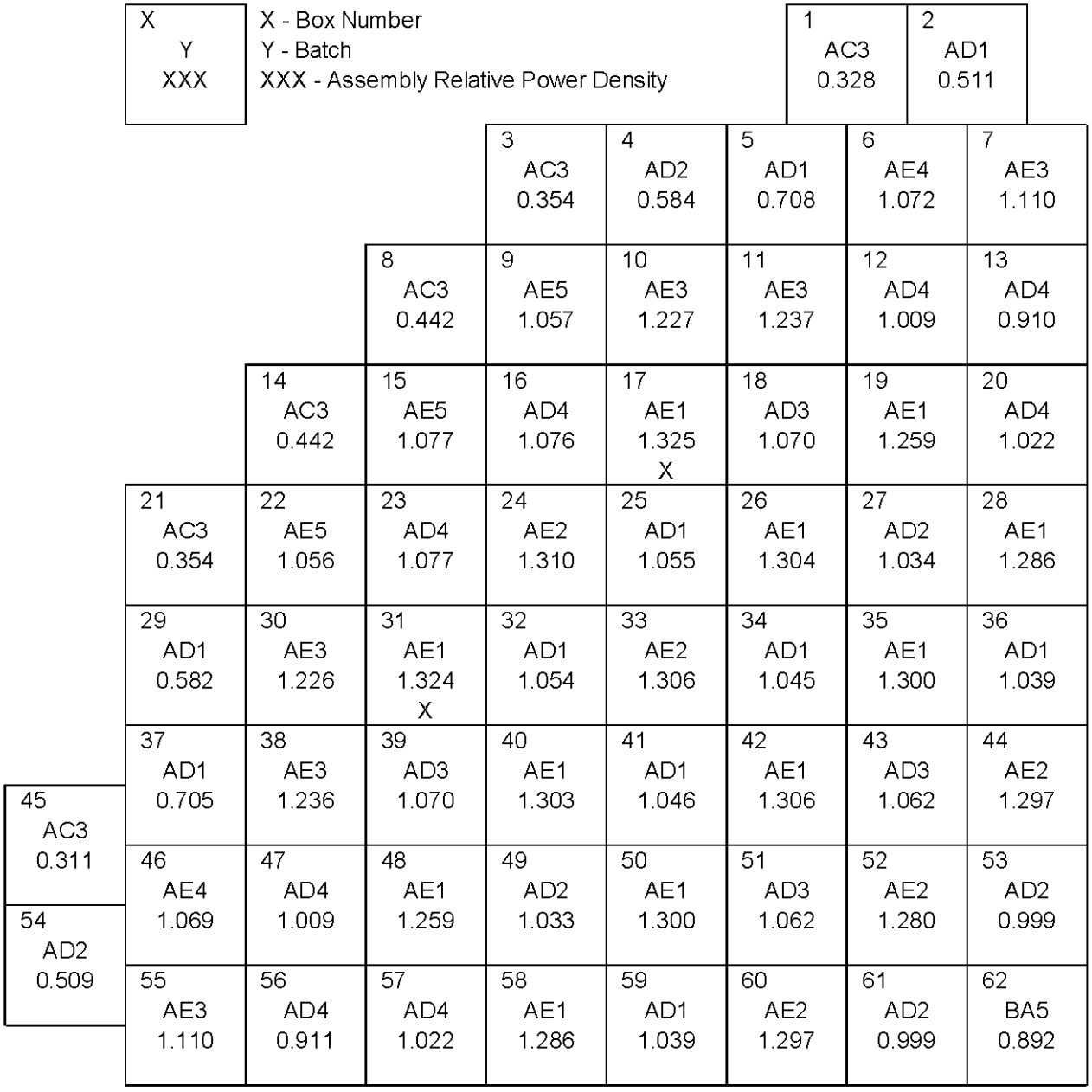

Long N-1 Burnup (21.940 GWd/MTU)

Note: X = Maximum Fr Value = 1.398

Calvert Cliffs Nuclear Power Plant	UNIT 1 CYCLE 24 ASSEMBLY RELATIVE POWER DENSITY WITH BANK 5 INSERTED TO PDIL AT EOC, HFP, EQUILIBRIUM XENON	Figure 3.4-19 Revision 50

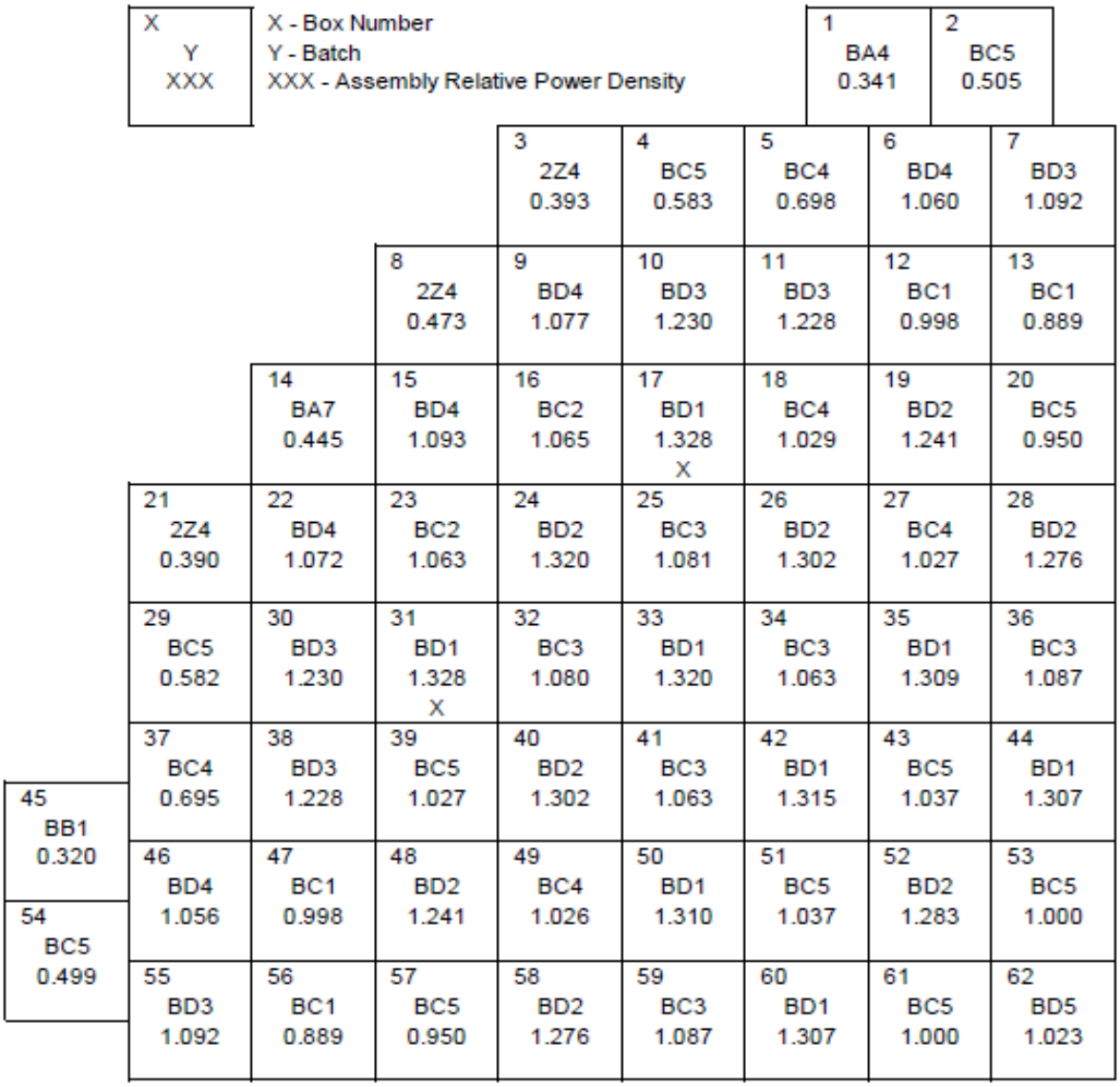

Long N-1 Burnup (22.077 GWd/MTU)

Note: X = Maximum Fr Value = 1.399

Figure 3-9 Assembly Relative Power Density with Bank 5 Inserted to PDIL at EOC, HFP, Equilibrium Xenon*

* Due to core redesign, Unit 2 Cycle 23 will not be quarter core symmetric.

Calvert Cliffs Nuclear Power Plant	UNIT 2 ASSEMBLY RELATIVE POWER DENSITY AT BANK 5 INSERTED TO PDIL AT EOC, HFP, EQUILIBRIUM XENON	Figure 3.4-20 Revision 51

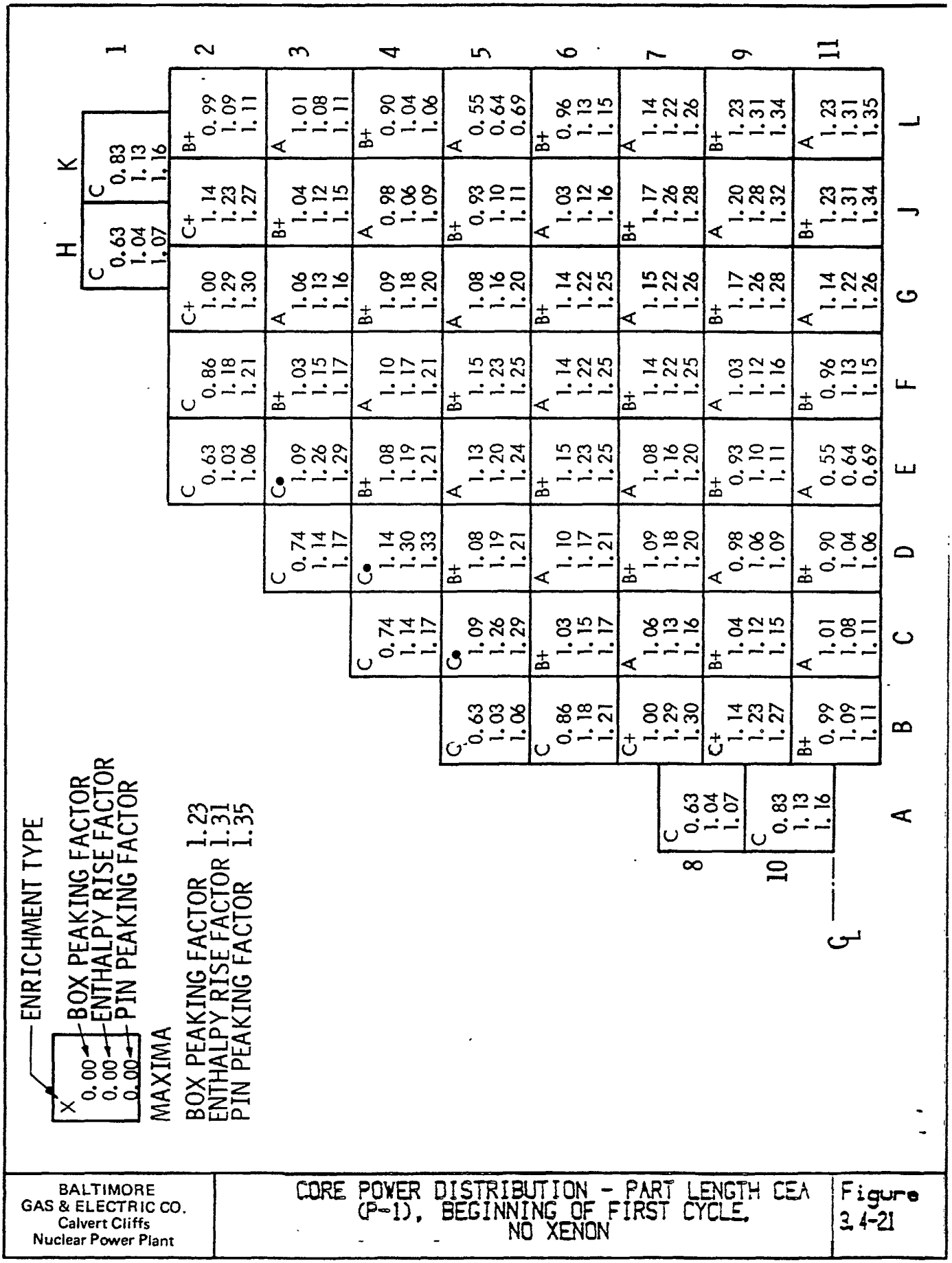

BALTIMORE GAS & ELECTRIC CO. Calvert Cliffs Nuclear Power Plant	CORE POWER DISTRIBUTION - PART LENGTH CEA (P-1), BEGINNING OF FIRST CYCLE, NO XENON	Figure 3.4-21

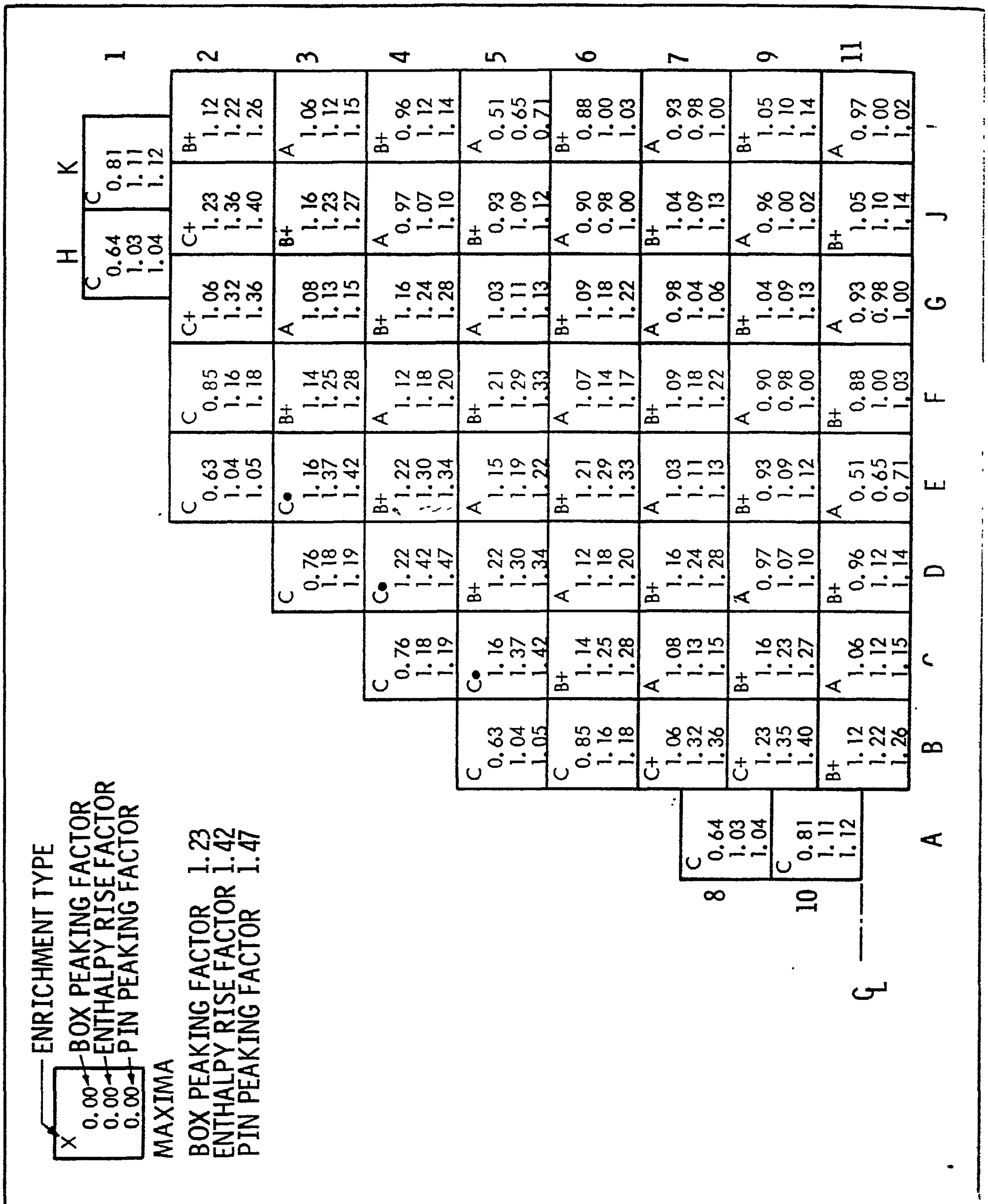

BALTIMORE
GAS & ELECTRIC CO.
Calvert Cliffs
Nuclear Power Plant

CORE POWER DISTRIBUTION - PART LENGTH CEA (P-1), BEGINNING OF FIRST CYCLE, EQUILIBRIUM XENON

Figure 3.4-22

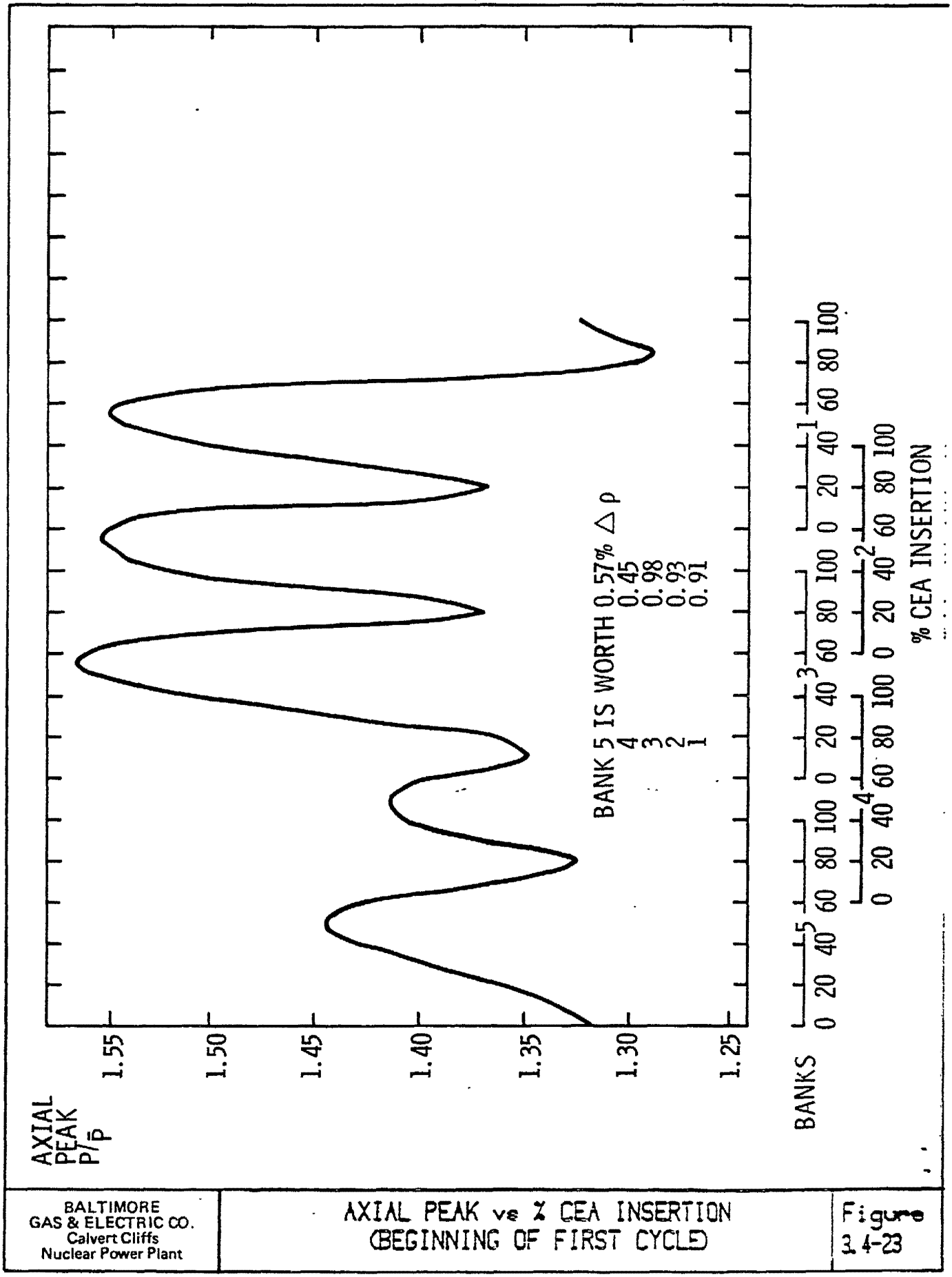

BALTIMORE GAS & ELECTRIC CO. Calvert Cliffs Nuclear Power Plant	AXIAL PEAK vs % CEA INSERTION (BEGINNING OF FIRST CYCLE)	Figure 3.4-23

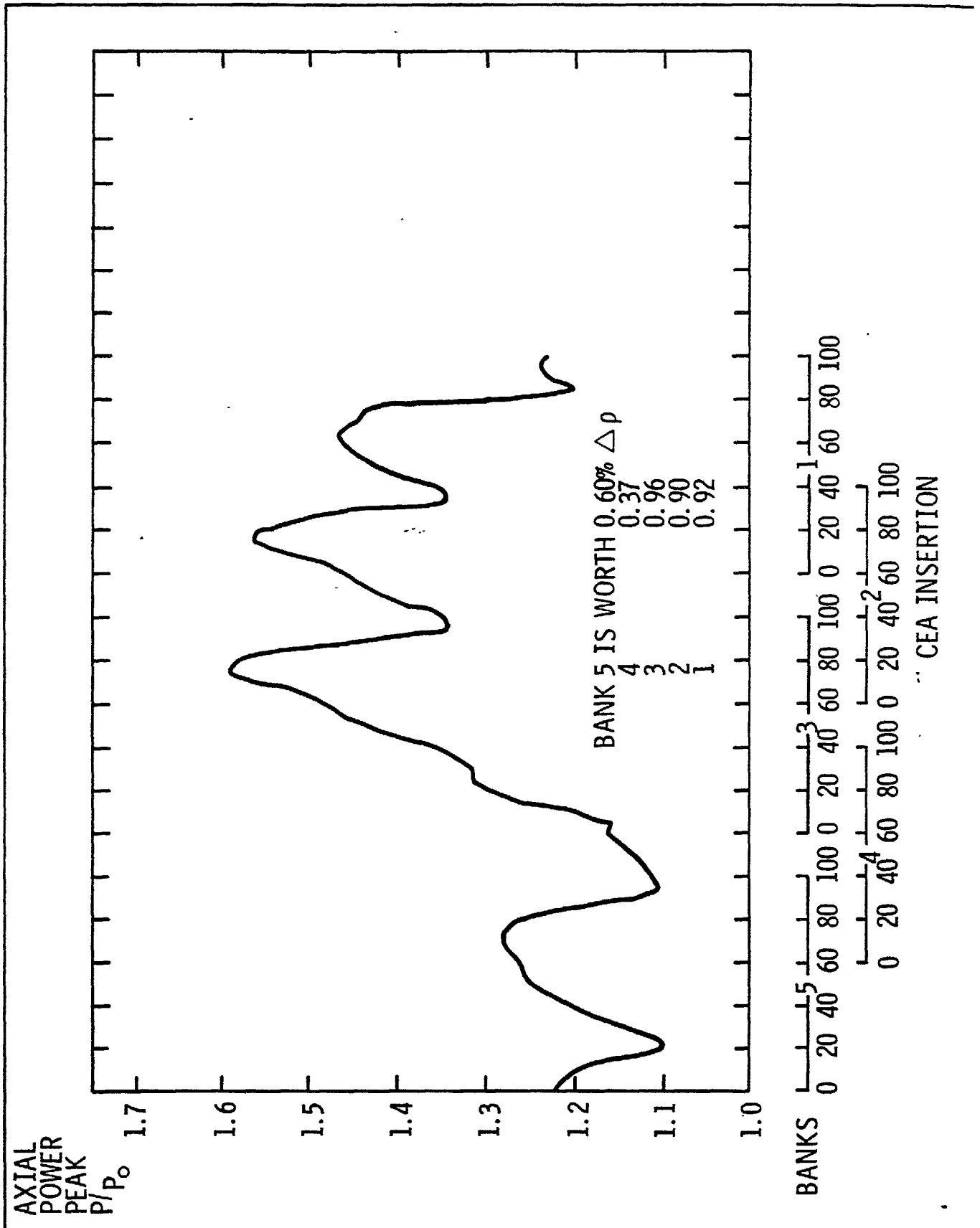

BALTIMORE GAS & ELECTRIC CO. Calvert Cliffs Nuclear Power Plant	AXIAL PEAK vs CEA INSERTION WITH PART LENGTH CEA'S (END OF FIRST CYCLE)	Figure 3.4-24

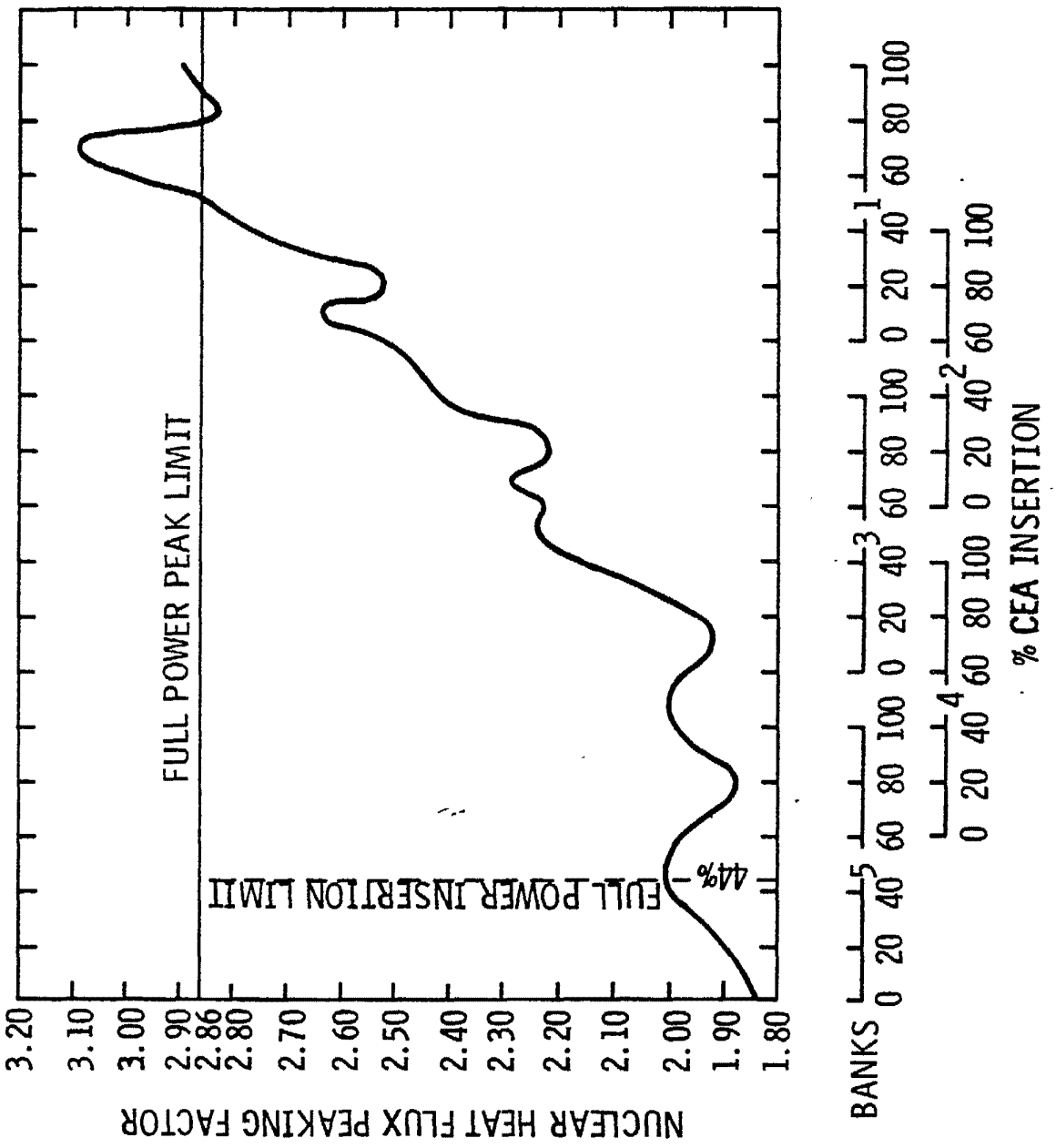

BALTIMORE GAS & ELECTRIC CO. Calvert Cliffs Nuclear Power Plant	NUCLEAR HEAT FLUX PEAK vs CEA INSERTION (BEGINNING OF FIRST CYCLE)	Figure 3.4-25

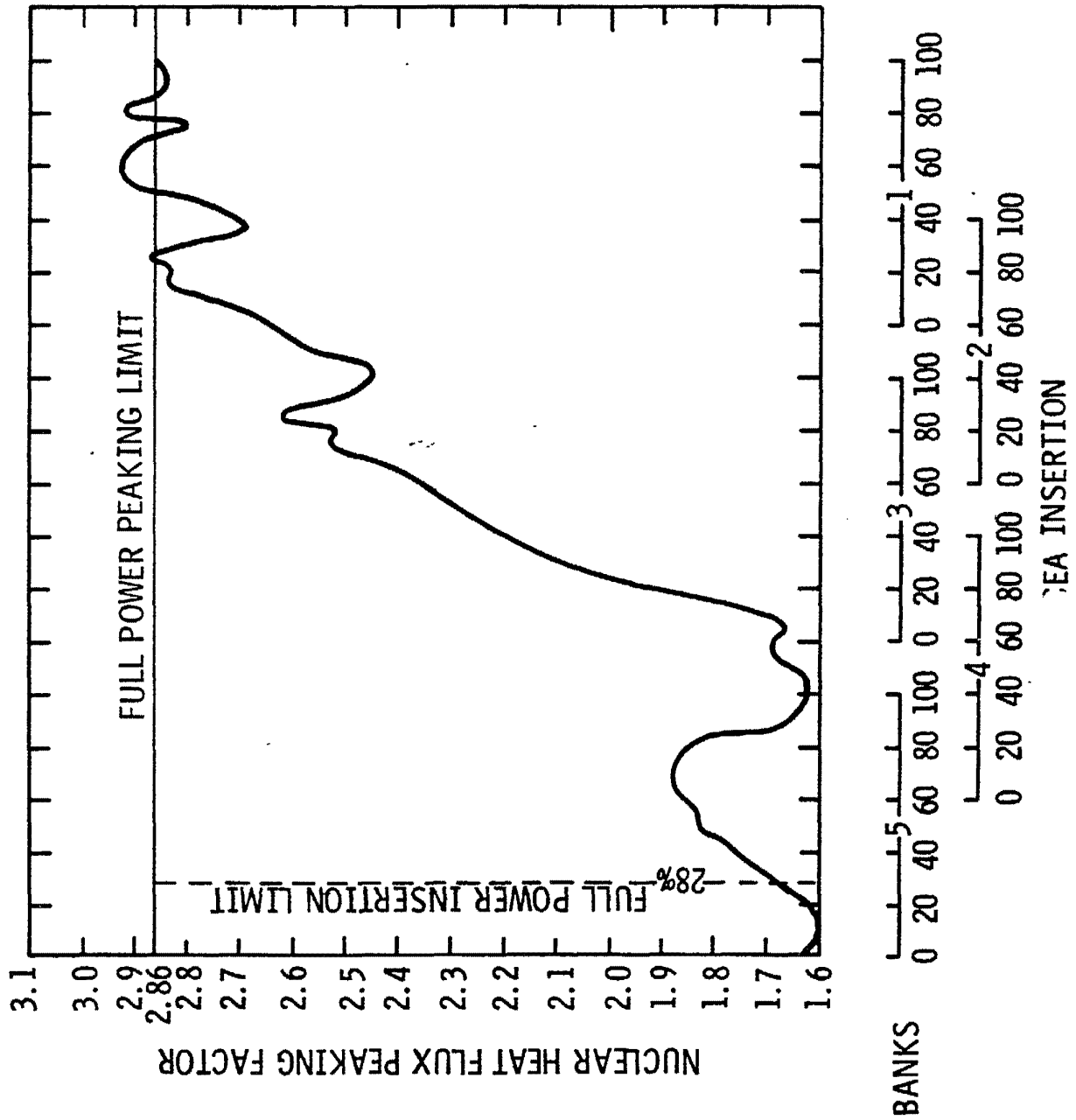

BALTIMORE GAS & ELECTRIC CO. Calvert Cliffs Nuclear Power Plant	NUCLEAR HEAT FLUX PEAK vs CEA INSERTION WITH PART LENGTH CEA'S (END OF FIRST CYCLE)	Figure 3.4-26

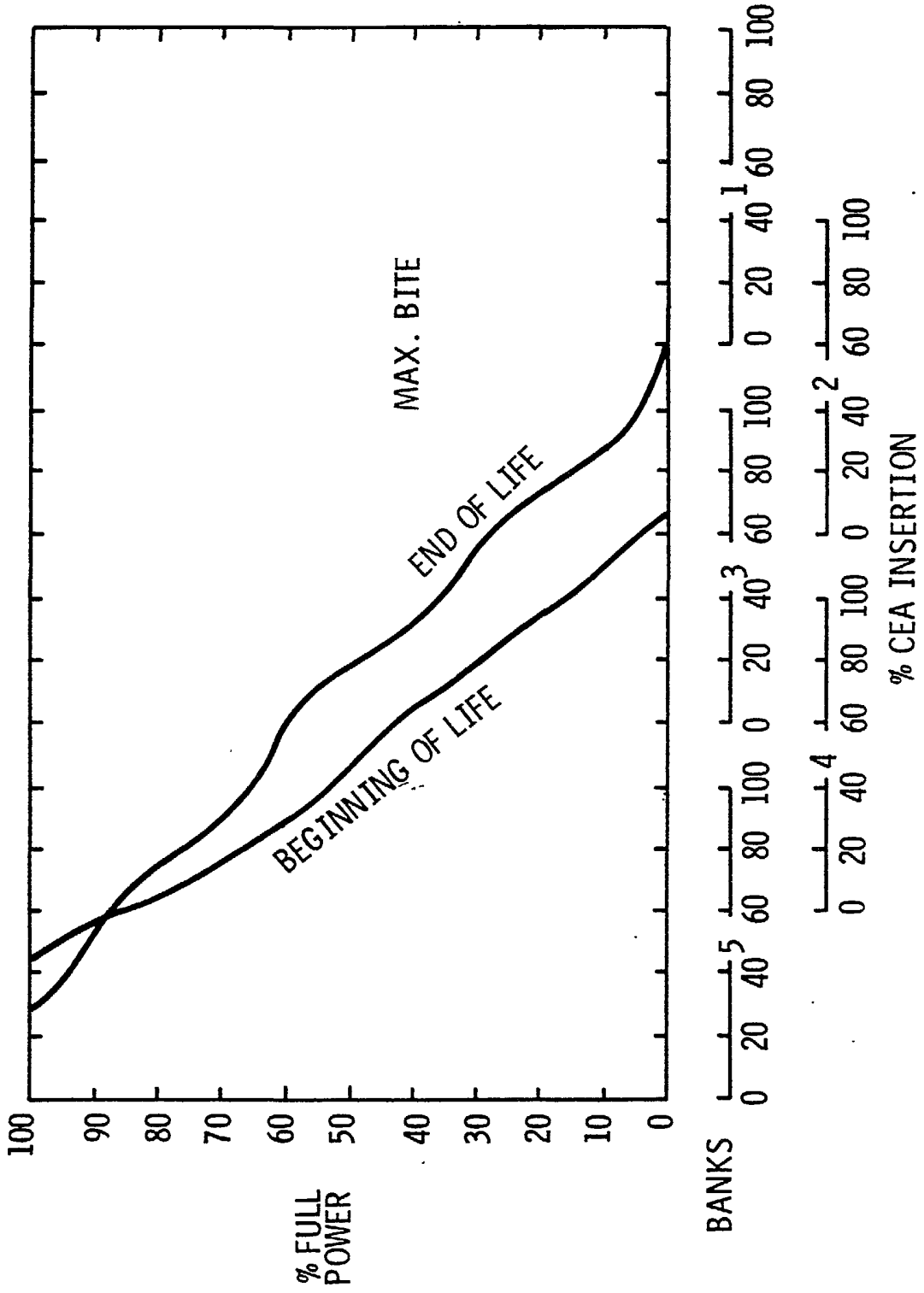

BALTIMORE GAS & ELECTRIC CO. Calvert Cliffs Nuclear Power Plant	FIRST CYCLE POWER DEPENDENT CEA INSERTION LIMITS	Figure 3.4-27

14x14 PWR FUEL BUNDLE

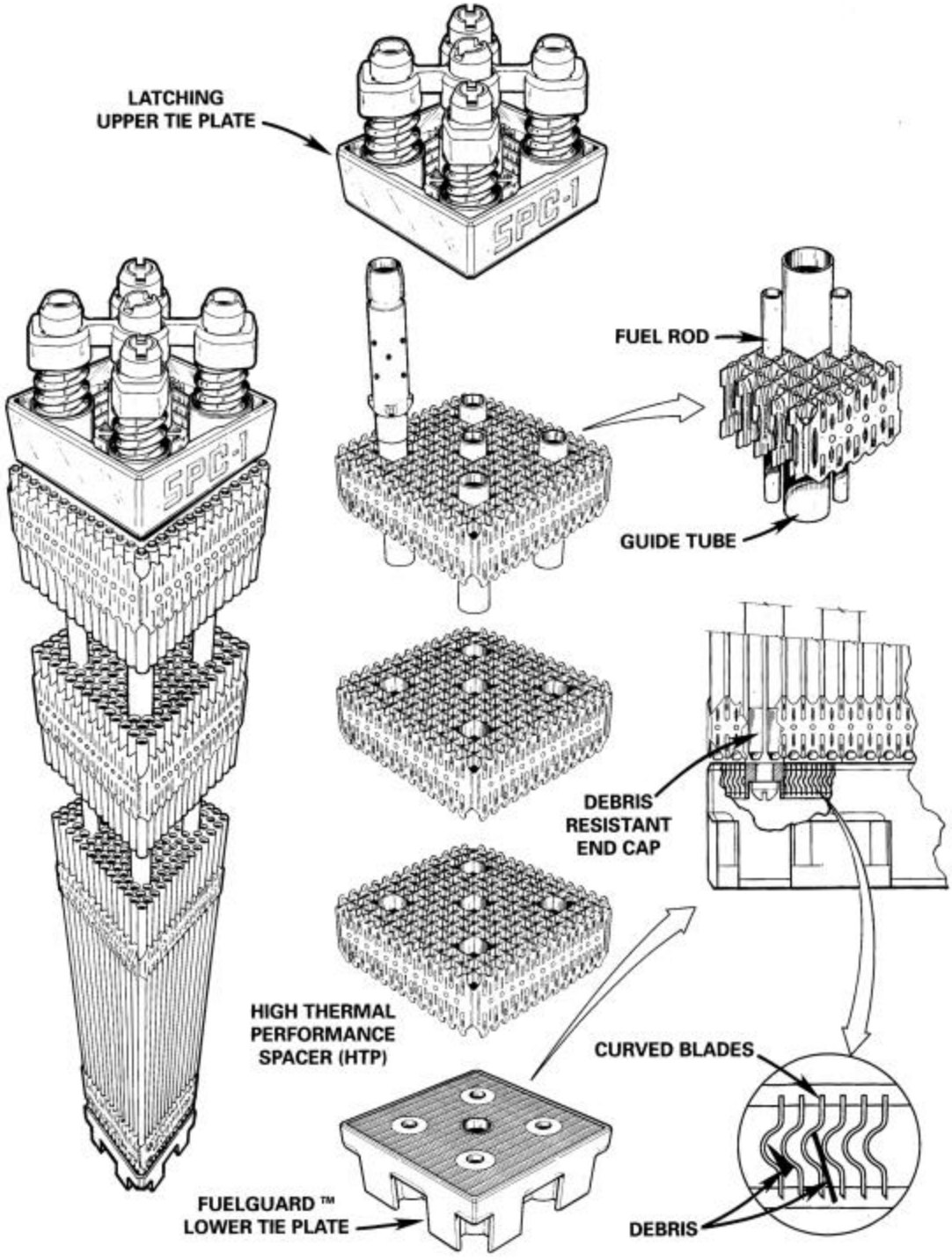

Calvert Cliffs Nuclear Power Plant	Framatome Lead Fuel Assembly	Figure 3.7-1 Revision 33